

1983

Hydrothermal Metamorphism And Ore Genesis At Aljustrel, Portugal

Fernando Jose Barriga

Follow this and additional works at: <https://ir.lib.uwo.ca/digitizedtheses>

Recommended Citation

Barriga, Fernando Jose, "Hydrothermal Metamorphism And Ore Genesis At Aljustrel, Portugal" (1983). *Digitized Theses*. 1289.
<https://ir.lib.uwo.ca/digitizedtheses/1289>

This Dissertation is brought to you for free and open access by the Digitized Special Collections at Scholarship@Western. It has been accepted for inclusion in Digitized Theses by an authorized administrator of Scholarship@Western. For more information, please contact tadam@uwo.ca, wlsadmin@uwo.ca.

The author of this thesis has granted The University of Western Ontario a non-exclusive license to reproduce and distribute copies of this thesis to users of Western Libraries. Copyright remains with the author.

Electronic theses and dissertations available in The University of Western Ontario's institutional repository (Scholarship@Western) are solely for the purpose of private study and research. They may not be copied or reproduced, except as permitted by copyright laws, without written authority of the copyright owner. Any commercial use or publication is strictly prohibited.

The original copyright license attesting to these terms and signed by the author of this thesis may be found in the original print version of the thesis, held by Western Libraries.

The thesis approval page signed by the examining committee may also be found in the original print version of the thesis held in Western Libraries.

Please contact Western Libraries for further information:

E-mail: libadmin@uwo.ca

Telephone: (519) 661-2111 Ext. 84796

Web site: <http://www.lib.uwo.ca/>

CANADIAN THESES ON MICROFICHE

I.S.B.N.

THESES CANADIENNES SUR MICROFICHE



National Library of Canada
Collections Development Branch

Canadian Theses on
Microfiche Service

Ottawa, Canada
K1A 0N4

Bibliothèque nationale du Canada
Direction du développement des collections

Service des thèses canadiennes
sur microfiche

NOTICE

The quality of this microfiche is heavily dependent upon the quality of the original thesis submitted for microfilming. Every effort has been made to ensure the highest quality of reproduction possible.

If pages are missing, contact the university which granted the degree.

Some pages may have indistinct print especially if the original pages were typed with a poor typewriter ribbon or if the university sent us a poor photocopy.

Previously copyrighted materials (journal articles, published tests, etc.) are not filmed.

Reproduction in full or in part of this film is governed by the Canadian Copyright Act, R.S.C. 1970, c. C-30. Please read the authorization forms which accompany this thesis.

**THIS DISSERTATION
HAS BEEN MICROFILMED
EXACTLY AS RECEIVED**

AVIS

La qualité de cette microfiche dépend grandement de la qualité de la thèse soumise au microfilmage. Nous avons tout fait pour assurer une qualité supérieure de reproduction.

S'il manque des pages, veuillez communiquer avec l'université qui a conféré le grade.

La qualité d'impression de certaines pages peut laisser à désirer, surtout si les pages originales ont été dactylographiées à l'aide d'un ruban usé ou si l'université nous a fait parvenir une photocopie de mauvaise qualité.

Les documents qui font déjà l'objet d'un droit d'auteur (articles de revue, examens publiés, etc.) ne sont pas microfilmés.

La reproduction, même partielle, de ce microfilm est soumise à la Loi canadienne sur le droit d'auteur, SRC 1970, c. C-30. Veuillez prendre connaissance des formules d'autorisation qui accompagnent cette thèse.

**LA THÈSE A ÉTÉ
MICROFILMÉE TELLE QU'É
NOUS L'AVONS REÇUE**

HYDROTHERMAL METAMORPHISM AND ORE GENESIS
AT ALJUSTREL, PORTUGAL

by

Fernando Jose Arraiano de Sousa Barriga

Department of Geology

Submitted in partial fulfillment
of the requirements for the degree of
Doctor of Philosophy

Faculty of Graduate Studies
The University of Western Ontario
London, Ontario

June, 1983



Underground at Aljustrel mines. Stope with right rib and back.
Note homogeneity of sulphides.

ABSTRACT

Lower Carboniferous felsic, explosive, submarine volcanism took place at Aljustrel, creating the ores of one of the principal mining centres of the Iberian Pyrite Belt. Some 250 Mt of massive sulphide ore occur near the top of several hundred metres of pyroclastic volcanics which overly a sediment covered continental basement.

Retrographic, mineral chemical, whole rock geochemical and oxygen isotope investigation of the Aljustrel volcanic rocks remote from mineralization shows that their present quartz-keratophytic (felsic spilitic) compositions result from widespread interaction with sea water, at high water/rock ratios and temperatures ranging 0-300°C. Opaque mineralogy and textures show that iron was oxidized in rocks near the sea floor and leached from deeper rocks, with leaching of transition metals. Jaspers and cherts present above the volcanics may have formed concomitantly, through chemical precipitation of silica, forming an impermeable cover.

Investigation of Feitais ore zone rocks suggests that ore formation took place largely in open space, through almost isothermal mixing of sulphur and metal rich waters. There is clear evidence for silica and sulphide precipitation in a feeder stockwork. Cherts and phyllitic sediments covering the ore, show clear evidence of

mineralization and reduction by interaction with the ore-forming fluids. Deformation of such rocks indicates that such mineralization predated regional metamorphism. The presence of a cap rock is also suggested by temperature profiles from oxygen isotope systematics. Thus the Feitais orebody was not exhalative sensu stricto, but formed beneath a thin impermeable cap which in fact may have been floated off on rising fluids.

The ore-forming process postdated sea water alteration of volcanics and involved a second stage convective system with lower water/rock ratios perhaps with a contribution from metamorphic fluids.

The Aljustrel tectonic-thermal setting is clearly one which involves the ideal set of variables producing giant deposits, orders of magnitude larger than those typical of ophiolites.

DEDICATION

This thesis is dedicated to the Portuguese and Canadian peoples. May it in part justify the investment they have made.

ACKNOWLEDGEMENTS

The Government of Ontario, The University of Western Ontario, INIC (Portugal) and the University of Lisbon are thanked for continuing support throughout the course of this project.

I express my sincere gratitude to Pirites Alentejanas, S.A.R.L. for permission to visit and sample the Aljustrel mines, for warm hospitality and access to unpublished files and drillcores. Mine geologists L. Conde and J. C. Leitão and all the geological staff are thanked for the help they granted me. Many of the graduate students, staff and faculty of UWO, Lisbon Geology and the Geological Survey of Portugal are equally gratefully acknowledged. Special mention to J. Starkey for guidance in the use of his high resolution XRD equipment and computing programs, R. Kerrich for the oxygen isotope determinations, R. L. Barnett for keeping his microprobe in top running condition, Barbara Barnett for showing me around in the XRF and wet chemical labs, J.A.S. Barriga, J. Schubert, A. Noon and I. Craig for photolab work, R. Turgeon and B. Damaso for the difficult drafts and Grace McIntyre and Janice Morris for the excellent typing of the manuscript and tables.

Special thanks to J. Munha, D. Carvalho, R. W. Hodder, R. W. Hutchinson (the "devil's advocate" in the capped ore formation idea), R. Kerrich, A. Ribeiro, V. Oliveira, J. T. Oliveira, U. Costa, A. Kishida and M. Ferreira for

valuable criticism and discussion determinant in the development of my ideas on ore genesis and/or the Iberian Pyrite Belt, and also to W. R. Church, A. MacCaig, C.R.B. Lister, A. MacDonald and Z. Haq, who contributed significantly to my knowledge of sea floor rocks and metamorphism.

The selection and definition of my thesis topic resulted from the joint efforts of L. Celestino Silva, R. Quadrado, A. Ribeiro, D. Carvalho and W. S. Fyfe. The latter and C. A. Matos Alves found the means for me to study and research in Canada. They are also thanked for contributing with various forms of essential support, encouragement and enlightening discussions.

Paraphrasing T. LaTour, I am singularly indebted to W. S. Fyfe for providing his unique style of stimulation and imaginative insight throughout the investigation. Many of the interesting points reported in this thesis result at least as much from his thoughts as from my own effort.

My wife Gabriela and my sons Gonçalo and Miguel shared from all the pain involved in the completion of this project and in return enjoyed only part of the rewards. Yet, their understanding and/or tenderness have been inexhaustible.

TABLE OF CONTENTS

CERTIFICATE OF EXAMINATION	ii
ABSTRACT	iv
DEDICATION	vi
ACKNOWLEDGEMENTS	vii
TABLE OF CONTENTS	ix
LIST OF PHOTOGRAPHIC PLATES	xii
LIST OF TABLES	xiv
LIST OF FIGURES	xv
CHAPTER 1 - INTRODUCTION	1
CHAPTER 2 - THE IBERIAN PYRITE BELT AND ITS ORE DEPOSITS	7
2.1 Geology and tectonic evolution	7
2.2 Volcanism in the Iberian Pyrite Belt	25
2.3 Hydrothermal activity and mineralization in the Iberian Belt	36
2.4 Conclusion	46
CHAPTER 3 - GEOLOGY AND ORE DEPOSITS OF THE ALJUSTREL AREA	48
3.1 Introduction	48
3.2 Lithostratigraphy and ore deposits	51
3.3 Structure	53
3.4 Base metal zonation in the Feitais orebody	63
3.5 Concluding remarks	69
CHAPTER 4 - THE ALJUSTREL VOLCANICS	74
4.1 Introduction	74
4.2 Petrography	75
4.2.1 Quartz-eye Tuff	78
4.2.2 Mine Tuff	91
4.2.3 Paraiso Formation Tuffs	98
4.3 Geochemistry	99
4.3.1 Mineral chemistry	99
a) Feldspars	99
b) Fe-Ti oxides and sphene	101
c) Garnet	105
d) Chlorites	107
e) Sericite	110
f) Epidotes	111
g) Stilpnomelane	111
h) Carbonates	111
i) Synopsis of paragenetic relations	111
4.3.2 Whole rock geochemistry	115
a) Major elements	115
b) Immobile trace elements	128
c) Rare earth elements	135
d) Cu, Zn, Pb	139
e) Oxygen isotope compositions	143
4.4 Discussion and conclusions	145

CHAPTER 5 - THE FEITAIS OREBODY OF ALJUSTREL, its associated metalliferous sediments and ore zone hydrothermal alteration.....		152
5.1	Introduction	152
5.2	Petrography	153
5.2.1	Stockwork zone	153
5.2.2	The Feitais massive sulphide deposit	158
5.2.3	Hanging wall siliceous and metalliferous sediments	169
5.3	Geochemistry	178
5.3.1	Mineral chemistry	178
	a) Chlorite	178
	b) Sericite	182
	c) Spessartine garnet	182
	d) Cymrite	185
	e) Carbonates	185
	f) Sphaerite	187
5.3.2	Whole rock geochemistry	189
	a) Stockwork rocks and massive sulphide ore	190
	a1) Major elements	190
	a2) Immobile trace elements	192
	a3) Rare earth element geo- chemistry	197
	b) Hanging wall siliceous and metalliferous sediments	199
	b1) Si/Mn/Fe	199
	b2) Jasper reduction above sulphide ore	202
	b3) Fe/Mn/(Co+Ni+Cu)x10	202
	b4) Thorium abundances	204
	b5) Rare earth element geo- chemistry	204
	b6) Gold abundances	210
	c) Anomalous PS Formation rocks above Feitais	212
	d) Geochemical data on Culm Formation rocks	213
5.3.3	Oxygen isotope geochemistry	216
5.4	Discussion and conclusions	219
CHAPTER 6 - SUMMARY AND CONCLUSIONS		247
6.1	Conclusions	250
6.2	Genetic model	255
6.3	Exploration implications	258

* * *

APPENDIX I.	SUMMARY OF ANALYTICAL TECHNIQUES . . .	260
APPENDIX II.	MINERAL CHEMICAL ANALYSES - ALJUSTREL VOLCANICS	264
APPENDIX III.	WHOLE ROCK ANALYSES - ALJUSTREL VOLCANICS	290
APPENDIX IV.	MINERAL CHEMICAL ANALYSES - FEITAIS ORE ZONE AND OVERLYING SEDIMENTS	297
APPENDIX V.	WHOLE ROCK ANALYSES - FEITAIS ORE ZONE AND ALJUSTREL SEDIMENTS . . .	320
APPENDIX VI.	UNDERGROUND GEOLOGY AND KEY TO SAMPLE LOCATIONS	337
REFERENCES		345
VITA		367

LIST OF PHOTOGRAPHIC PLATES

Plate	Description	Page
1A	Granular tuff matrix (QET)	77
1B	'Dilute greywacke' tuff matrix (MT)	77
1C	Megacryst facies of QET	77
1D	Hydrolised igneous albite phenocryst	77
1E	Chessboard textured albite	77
1F	Poorly developed chessboard albite	77
2A	Relations between feldspars	84
2B	Chessboard albite in K-feldspar	84
2C	Adularia in vein	84
2D	Almandine garnet in lithic fragment	84
2E	Almandine garnet in albite phenocryst	84
2F	Allanite overgrown by epidote	84
3A,B	Opaque phenocrysts in Green facies	89
3C	Opaque phenocrysts in deeper seated facies	89
3D	Accidental lithic fragment	89
3E	Frayed end of cherty lithic fragment	89
3F	Possible former glass shard	89
4A	Breccia at top of Mine Tuff	95
4B	Albite in dilatancy vein	95
4C	Peripheral ore zone alteration in Mine Tuff	95
4D	Outer stockwork rock	95
4E	Stockwork rock	95
4F	Corroded/precipitated zircon in stockwork rock	95
5A	Zoned alteration around stockwork sulphide vein	160
5B	Framboids in sulphide ore	160
5C	Framboids in culm shale	160
5D,E	Polyminerallic sulphide colloform aggregates	160
5F	Pyrite-gangue colloform aggregates	160
6A	Colloform pyrite	162
6B	Colloform radiating pyrite	162
6C	Bed of pyrite cubes adjacent to bed of pyrite framboids	162
6D,E,F	Recrystallized massive sulphide ore	162
7A	Small scale slump fold	165
7B	Allochthonous ore, Tharsis, Spain	165
7C	Albite partly replaced by sulphides	165
7D	Stilpnomelane in unaltered jasper	165

Plate	Description	Page
7E	Stilpnomelane and magnetite in slightly altered jasper	165
7F	Spessartine garnet in chert	165
8	(Colour illustration of reductive alteration in the Feitais hanging wall Jasper unit)	172
8A	Unaltered bright red jasper	172
8B	Incipient vein controlled reduction	172
8C	Breccia pipe-like vein system	172
8D	Advanced alteration of jasper	172
8E	Complete alteration of jasper	172
8F	Post alteration deformation in completely altered jasper	172
9A	Spessartine garnet in metalliferous sediment	176
9B	Hematite + Mn oxide dust in jasper	176
9C	Quartz + carbonate + magnetite in altered jasper	176
9D	Texture of metalliferous sediment	176
9E	Cymrite, porphyroblast	176
9F	Chert domains in metalliferous sediment	176

LIST OF TABLES

Table	Description	Page
3.1	Size and grade of the Aljustrel massive sulphide deposits	52
4.1	Feldspar analyses	100
4.2	Composition of Green facies Fe-Ti oxides	102
4.3	Composition of Fe-Ti rich microphenocrysts in deeper seated Aljustrel Volcanics	103
4.4	Almandine garnet analyses	106
4.5	Chlorite analyses	108
4.6	Stilpnomelane analyses	113
4.7	Paragenetic relations of the minerals in the Aljustrel Volcanics	114
4.8	Ranges and average abundances of major elements in the Aljustrel Volcanics	118
4.9	Original major element composition of the Aljustrel Volcanics	129
4.10	Oxygen isotope composition of the Aljustrel Volcanics	144
5.1	Cymrite analyses	186
5.2	Gold abundances in ore zone rocks	211
5.3	Oxygen isotope composition of rocks and minerals from the Feitais-Estacao ore zone	217

LIST OF FIGURES

Figure	Description	Page
2.1	Paleogeographic and tectonic units in the Iberian Massif	8
2.2	Tentative correlation of main Variscan units in Middle and West Europe	9
2.3	Deep structure of the South Portuguese Zone	13
2.4	General geology of the Iberian Pyrite Belt	15
2.5	Diachronism of flysch and volcanism in the South Portuguese Zone	17
2.6	Zonation of Hercynian regional metamorphism in the South Portuguese Zone	22
2.7	Schematic geologic section of the Tharsis North area (Spain)	33
2.8	Limits of the Iberian Pyrite Belt	37
2.9	Schematic relations between ore, siliceous sediments, ore zone alteration and lithostratigraphy	43
3.1	Location map of Aljustrel	49
3.2	Geology of the Aljustrel area	50
3.3	Lithostratigraphic columns of the Aljustrel area and vicinities	55
3.4a,b	Structure of the Aljustrel area	59, 60
3.5	Schematic lithostratigraphic of the Aljustrel Group	61
3.6a,b,c,d	Abundances of Cu, Zn, Pb and As along drillcores through the Feitais orebody	65-68
3.7	Schematic pre deformation relations between the Aljustrel rocks	72
4.1	X-ray diffraction data for the alkali megacryst feldspars in the Quartz eye Tuff	85

Figure	Description	Page
4.2	Facies in the Quartz eye Tuff	92
4.3	Facies in the Mine Tuff	97
4.4	Compositional variation of the chlorites in the Aljustrel Volcanics	109
4.5	Fe ³⁺ in epidote versus whole rock Fe ratio in the Aljustrel Volcanics	112
4.6	Variation of total iron versus rock Fe ratio in the Aljustrel Volcanics	122
4.7a	Variation in MgO versus rock Fe ratio in the Aljustrel Volcanics	124
4.7b	Variation of MgO versus Loss on Ignition (H ₂ O) in the Aljustrel Volcanics	125
4.8	Variation of scandium versus yttrium in the Aljustrel volcanics	132
4.9	Variation of zirconium/yttrium versus yttrium in the Aljustrel Volcanics	134
4.10	REE patterns in Aljustrel volcanic rocks	136
4.11	REE patterns in chloritized Mine tuffs	137
4.12	Variation of copper versus Fe ratio in the Aljustrel Volcanics	140
4.13	Variation of zinc versus Fe ratio in the Aljustrel Volcanics	142
4.14	Molar water/rock and temperature ranges required to enrich the Aljustrel Volcanics in ¹⁸⁰	147
5.1	Schematic spatial distribution of the various lithotypes constituting and surrounding the Feitais ore zone	155
5.2	Compositional variation of ore zone chlorites	179
5.3	Variation of MnO in ore zone chlorites versus stratigraphic position	181

Figure	Description	Page
5.4	Texture of outer stockwork rock and barium distribution	184
5.5	Dominant cations in ore zone carbonates	188
5.6	Spatial distribution of barium-sericite around the Feitais orebody	191
5.7a	Variation of scandium versus yttrium in the Feitais stockwork	194
5.7b	Variation of zirconium/yttrium versus zirconium in the Feitais stockwork and massive ore	196
5.8	REE patterns in Feitais stockwork rocks	198
5.9	REE patterns in Feitais massive ores	200
5.10	Ratio Si/Fe/Mn in the Feitais siliceous and metalliferous sediments	201
5.11	Schematic spatial distribution of Fe ratios along the Feitais Jasper unit	203
5.12	Ratio Fe/Mn/(Ni+Co+Cu)x10 in the Aljustrel metalliferous and siliceous sediments	205
5.13	Thorium abundances in Jasper unit rocks	206
5.14	REE patterns in jaspers showing little or no alteration	208
5.15	REE patterns in Feitais metalliferous sediments	209
5.16	Variation of Fe/Ti versus Al/Al+Fe+Mn in Paraiso Siliceous Formation rocks	214
5.17	Thorium abundances in Paraiso Siliceous Formation rocks	215
5.18	Representation of the possible mode of access of unmodified sea water to a pond of ore fluid under an impervious blanket	230

Figure	Description	Page
5.19	Water/rock and temperature ranges required to produce high ^{18}O , sea water derived ore fluids	235
5.20	Proposed first stage of sea water hydrothermal metamorphism at Aljustrel	238
5.21	Proposed second stage of sea water hydrothermal metamorphism at Aljustrel	239

CHAPTER 1

INTRODUCTION

The ultimate purpose of the present study is to contribute to the understanding of the genesis of massive sulphide deposits of volcanic association (this subject was recently and thoroughly reviewed by Franklin et al., 1981). Genetic models for this class of deposits have varied widely through time, but currently most authors favour a hydrothermal metamorphic model whereby convective circulation of sea water through permeable footwall rocks, driven with heat from below (magma chambers, intrusions) eventually modifies sea water into a hot, reduced, acidic, mineralized brine which, upon return flow to the ocean and given appropriate conditions at the site of discharge, may

lead to the fast and concentrated precipitation of metal sulphides (Spooner and Fyfe, 1973; Ohmoto and Rye, 1974; Solomon, 1976; Heaton and Sheppard, 1977; Andrews and Fyfe, 1976; Hutchinson et al., 1980). The model was recently confirmed by spectacular findings of hot springs issuing mineralized brines at mid ocean ridges and precipitating sulphides upon contact with sea water (Ballard and Grassle, 1979; Francheteau et al., 1979; Corliss et al., 1979; RISE Project Group, 1980).

Convincing as the sea water convective model may be for the genesis of massive sulphide deposits, several aspects of importance are not yet properly elucidated. Some of these are as follows:

(a) The ability of sea water to leach metals from permeated lithologies has been proven mainly on experimental saline water - rock interaction investigations (Ellis, 1968; Bischoff and Dickson, 1975; Hajash, 1975; Seyfried and Bischoff, 1977; Mottl and Holland, 1978; Mottl et al., 1979; Hajash and Archer, 1980) and in some examinations of naturally altered rocks, not directly related with known massive sulphide deposits (Sigvaldsson, 1959; Wedepohl, 1978; Keays and Scott, 1976; Humphris and Thompson, 1978a,b; Munha and Kerrich, 1980). To the best of our knowledge the only study where the source rock for the metals of an actual massive sulphide deposit was identified is the recent article by MacGeehan and MacLean

(1980) on the Garon Lake mining area of the Canadian Abitibi Belt, where systematic linear decreases of the abundances of several transition metals with increasing silica contents in volcanic rocks from basalt to rhyolite are interpreted as illustrating leaching by sea water.

(b) Sea water convection through permeable volcanic rocks is often pointed as the most plausible mechanism conducive to massive sulphide generation, but the actual hydrodynamic constraints to the process are seldom analysed. A notable exception is Spooner's (1977) thorough analysis of the conditions of deposition of the Cyprus massive sulphide deposits (see also Taylor, 1974).

(c) Despite excellent and conclusive studies on present day sub sea floor hydrothermal activity which prove that sea water convection through oceanic rocks takes place in evolving cellular regimes, as the thermal regimes change (Lister, 1972; Anderson and Skilbeck, 1981), very little research has been directed towards understanding the evolution of convective ore forming processes (Andrews and Fyfe, 1976; Hutchinson et al., 1980).

(d) Massive sulphide deposits throughout the world are often reported to be accompanied by intense footwall Mg metasomatism. Mg is an abundant element in sea water, but experimental studies invariably indicate that Mg is almost quantitatively transferred from the fluid to the rocks in the early stages of interaction, therefore precluding Mg

transport into the environment of ore deposition. Recent hypothesis (Costa, 1980; Hutchinson et al., 1980) explain Mg metasomatism with an ore zone shallow circulation system which would provide an adequate supply of unmodified sea water (rich in Mg) to the footwall rocks in the area of mineralizing fluid ascent. In the course of the present study an alternative possibility became plausible, namely that at least in some cases footwall Mg enrichment may predate mineralization, in the context of evolution of the sea water convective regimes as mentioned in (c).

(e) After the renaissance of syngenetic models for massive sulphide generation in the late fifties (Oftedal, 1958) it became generally accepted that massive sulphide deposition takes place on the sea floor, in direct contact with the water of more or less restricted basins, despite the careful words of most authors admitting formation "at or just below the sea water - rock interface" (Large, 1977). Hanging wall rock alteration is often present above massive sulphide deposits, sometimes with striking development such as at Sullivan, B.C., Canada (Either et al., 1976), and above the Kuroko deposits of Japan (Ijima, 1972), where hanging wall rock alteration extends for hundreds of metres above the orebodies, with formation of alteration assemblages that include "minor mineralization scattered through the clay alteration zones...in the form of veinlets, disseminations, and small massive lenses of

pyrite with or without the other ore minerals" (Lambert and Sato, 1974). Such hanging wall rock alteration must signify that ore related hydrothermal activity persisted after deposition of the altered hanging wall rocks. These facts require interpretation in terms of ore precipitation mechanisms and in terms of hydrothermal fluid pathways.

The Aljustrel area of South Portugal contains extremely large massive sulphide deposits, included in host rocks depicting clear signs of having been affected by the mineralizing agent(s). Also, the Aljustrel area is excellently geologically mapped (Schermerhorn and Stanton, 1969; Freire d'Andrade and Schermerhorn, 1971) and well exposed, not only at the surface, but principally underground, through extensive mine workings and numerous drillholes.

Aljustrel is one of the largest massive sulphide mining centres in the world, with several orebodies with combined reserves of nearly 250 million tonnes (Carvalho et al., 1976b), and it is one of the most important mines in the Iberian Pyrite Belt, Western Europe's most prominent stock of base metals, with global reserves beyond 1000 million tonnes before modern mining started (Strauss et al., 1977).

It is hoped (and believed) that some of the conclusions of the present study may be of interest to

other areas, in the Iberian Pyrite Belt and elsewhere.

CHAPTER 2

THE IBERIAN-PYRITE BELT AND ITS ORE DEPOSITS

2.1 Geology and Tectonic evolution of the South Portuguese Zone with emphasis on its middle sector, the Iberian Pyrite Belt

The Iberian Pyrite Belt is a heterogeneous set of Paleozoic terrains that occurs along an arcuate NW-SE area about 250 kms long and 30 to 60 km wide, extending from near the Atlantic Ocean in South Portugal to Seville in Southwest Spain (Fig. 2.1), and constitutes the intermediate sub-zone of the South Portuguese zone of the Iberian segment of the Hercynian Fold Belt (Lotze, 1945; Carvalho et al., 1971; Ribeiro et al., 1979). The South Portuguese Zone can be correlated (Fig. 2.2) to the

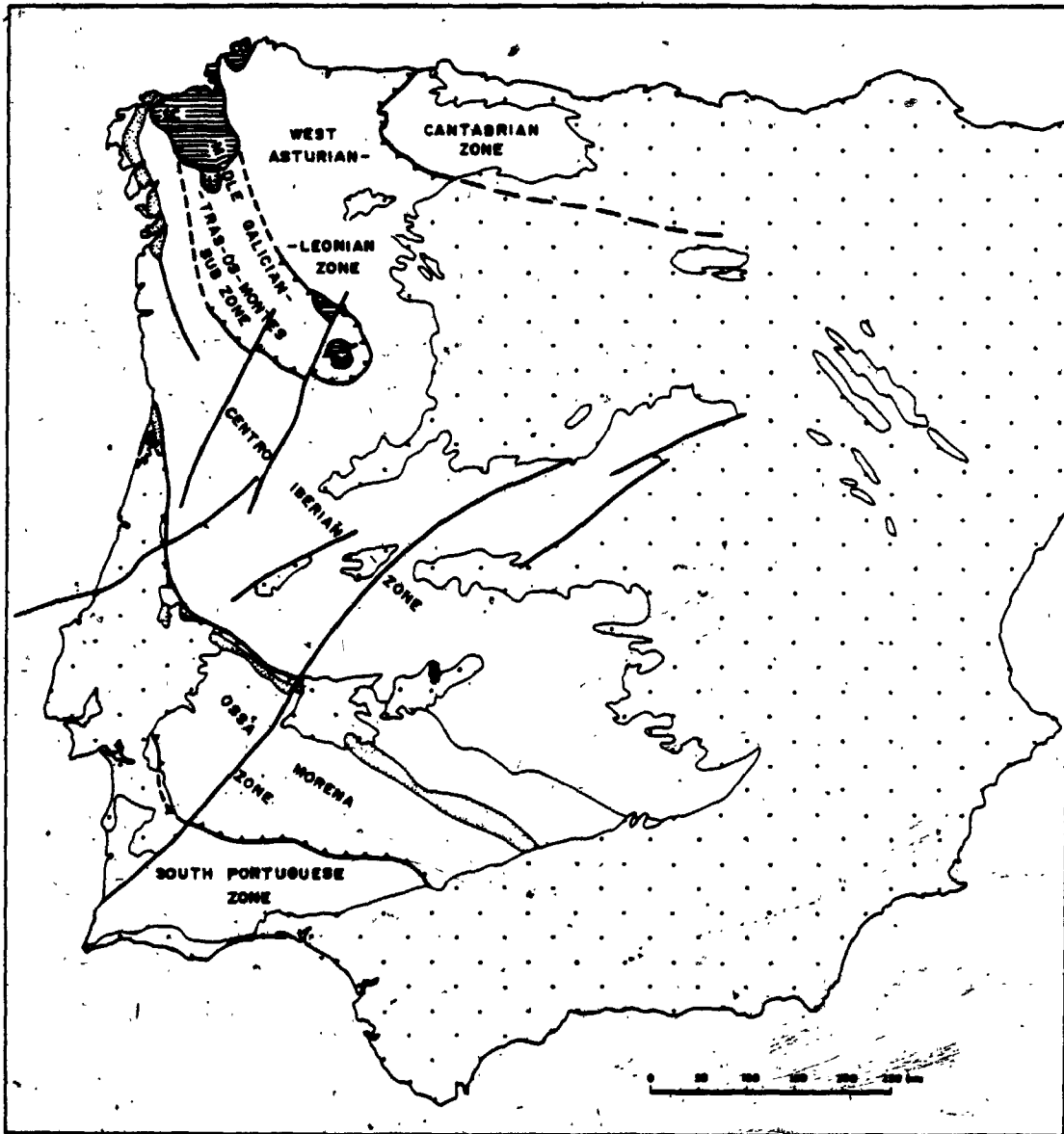


Figure 2.1. Paleogeographic and tectonic units in the Iberian Massif (after Ribeiro et al., 1979). The Iberian Pyrite Belt is the intermediate subzone of the South Portuguese Zone.

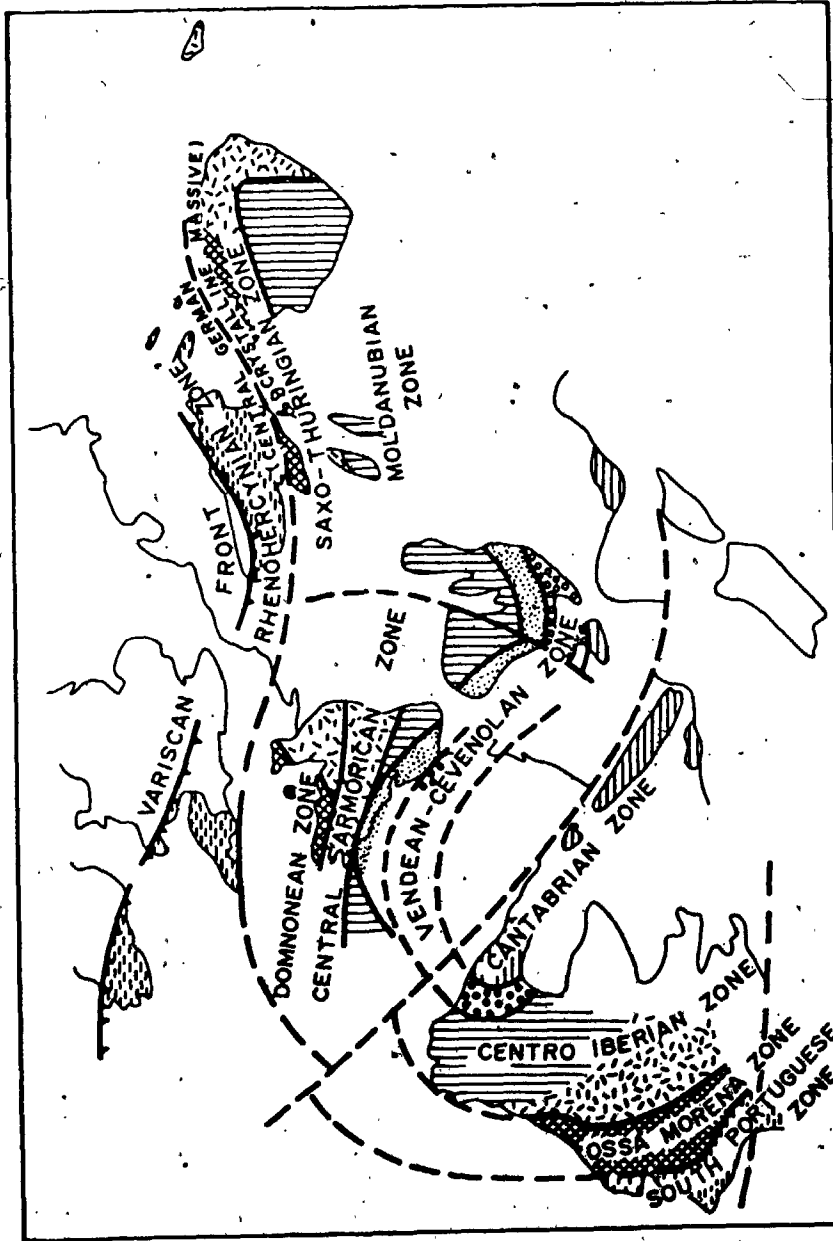


Figure 2.2. Tentative correlation of the main variscan units in Middle and West Europe at the end of hercynian, folding. After Ribeiro et al., 1979.

Devonian and Carboniferous of SW Ireland and England, to the Rhenohercynian Zone and to the Moravio-Silesian Zone of the Hercynian Orogen (Cogne, 1976; Ribeiro et al., 1979; Oliveira et al., 1979). The strongly arcuate belt defined by the above constitutes the External Hercynian Belt, internally bounded by a major thrust beyond which the Internal Hercynian Belt lies. Towards the periphery the External Belt contacts with Caledonian Europe through the Variscan Front in Northern Europe, but not in Southern Iberia, suggesting that the Variscan Front continues in North America, possibly in New Brunswick (Rast and Grant, 1973; Ribeiro et al., 1979).

The South Portuguese Zone is bounded to the SW by the Atlantic Ocean and to the NE by the Ficalho Upthrust (Ribeiro, 1981), that separates it from the adjacent Ossa Morena Zone (part of the Internal Hercynian Belt). The South Portuguese and Ossa Morena Zones depict marked differences with respect to age, lithologies, exposed crustal levels, tectonic style and regional metamorphic facies, raising the possibility that the Ficalho Upthrust (and its continuation in N. Europe) represents the suture from the collision of two continental blocks (Ribeiro et al., in press).

In the Ossa Morena Zone a Precambrian polymetamorphic basement is exposed, followed by a Paleozoic sequence from Cambrian to Permian in age, where Hercynian synorogenic

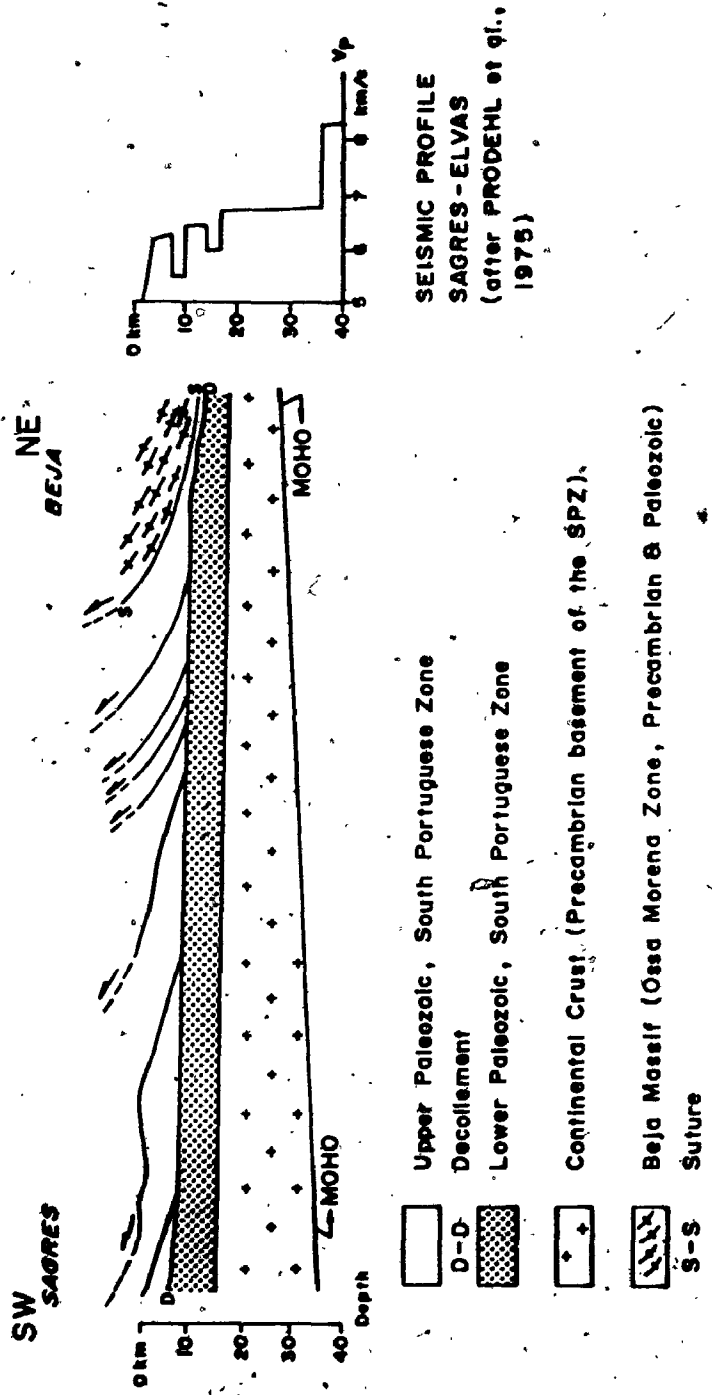
magmatism (dominantly plutonic) is widespread. Several unconformities are present within the sequence. The lower and middle Devonian (platform facies) are separated from an upper Devonian Flysch by a major unconformity that corresponds to the first Hercynian deformation phase (Ribeiro et al., 1979). Tectonically, the Ossa Morena Zone is characterized by an internal blastomylonitic zone, limited by steep faults fanning outwards to the NE and the SW respectively, and separating asymmetric domains of opposite vergences (Ribeiro, 1981). Metamorphism in the Ossa Morena Zone is of uneven grade, attaining medium to high grades along two distinct zones: along the blastomylonitic belt it is of Barrovian type (up to the sillimanite isograd) and probably polymetamorphic, and, further South, in the Evora-Beja-Aracena massif it attained the upper amphibolite facies in a low pressure regime (Bard, 1969; Ribeiro et al., 1979).

In contrast, the oldest exposed beds in the South Portuguese Zone are of alleged Late Devonian age (platform sediments of terrigenous origin), igneous activity is almost exclusively volcanic (in the Pyrite Belt), and diachronous flysch sediments up to several km thick were deposited in a strongly subsiding basin after volcanism. Tectonically the South Portuguese Zone is a thrust belt characterized by the development of an imbricate structure that affects all exposed Paleozoic lithologies. The fact

that even in the larger anticlines all the lithologies postdate the middle Devonian suggests the presence of large scale thrusting at the base of the thrust belt (Ribeiro et al., in press). This hypothesis is supported by deep seismic reflection profiles in the area (Mueller et al., 1973; Prodhel et al., 1975) which show a low velocity channel at the 7-10 km depth, interpreted by Ribeiro et al. as the decollement area (Fig. 2.3). Deformation was accompanied by low grade regional metamorphism that varies from the zeolite facies in the SW to the lower greenschist facies in the NE (Schermerhorn, 1975; Munha, 1976).

The South Portuguese Zone is characterized by pronounced lithostratigraphic anisotropy, with remarkable constancy along subzones roughly parallel to main structural features (NW to SE) and significant facies changes and diachronism across the structures (NE to SW, Fig. 2.1). Three lithostratigraphic groups are present (Fig. 2.4), as follows:

- a lowermost exclusively sedimentary unit (base not seen; top is upper Devonian) of phyllites, quartzites and rare limestones, at least several hundred metres thick, composed (from SW to NE) of the Tercenas Formation, Phyllite-Quartzite Group and Pulo do Lobo Group. Facies are proximal, shelf-like in the SW and more distal to the NE, indicating platform conditions and detrital supply from SW to NE (Ribeiro et al., 1979);



DEEP STRUCTURE OF THE SOUTH PORTUGUESE ZONE

Figure 2.3. After Ribeiro et al., 1982.

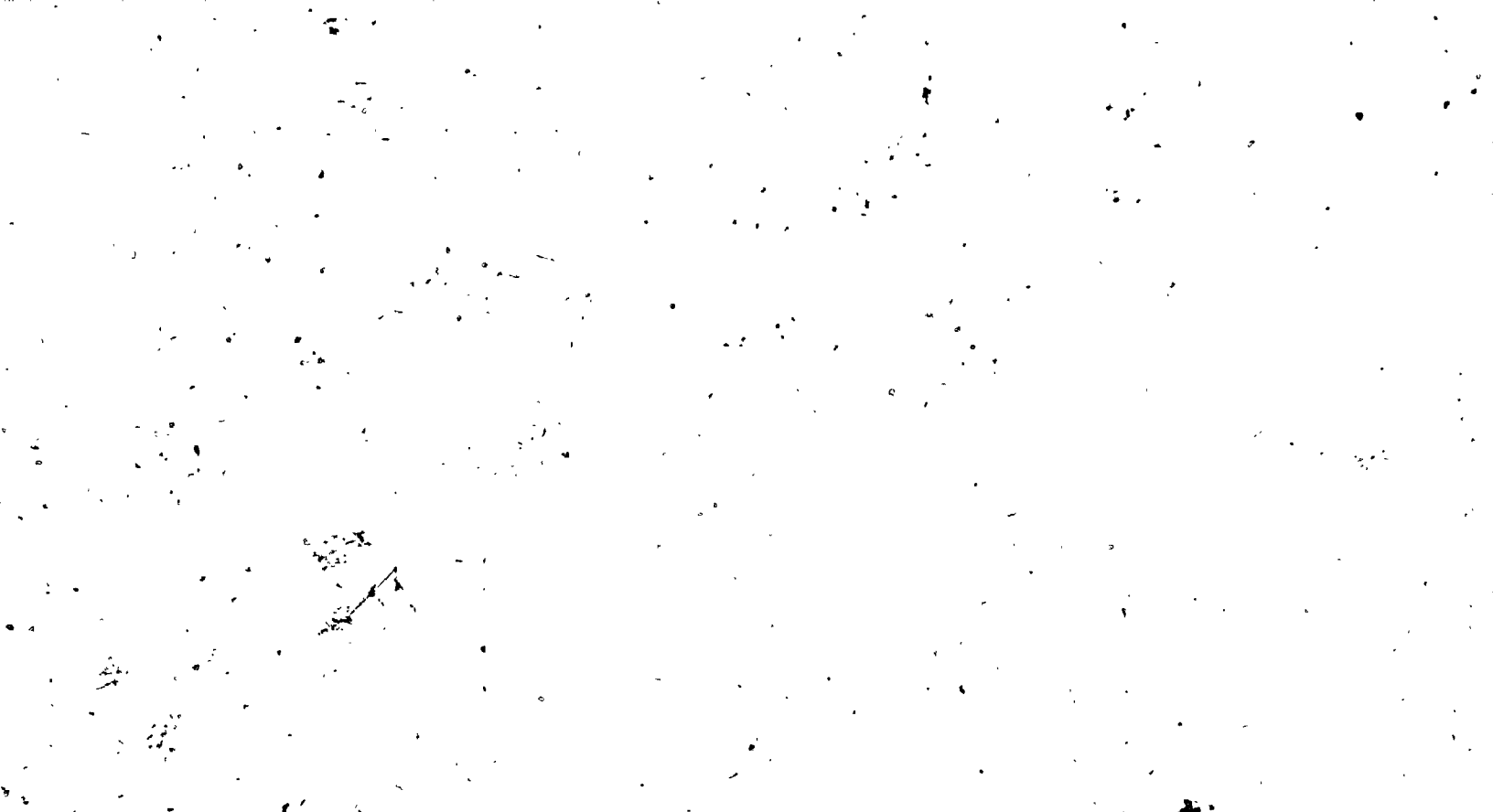


Figure 2.4. General geology of the Iberian Pyrite Belt
(after Carvalho et al., 1976, and Oliveira et
al., 1979).

- an intermediate, very heterogeneous, up to at least 800 m thick, Volcanic-Sedimentary Group (sensu lato) comprising a large spectrum of stratigraphic columns, from solely sedimentary in the SW (Bordalete, Murracao and Quebradas formations) through dominantly volcanic and/or epiclastic in the Pyrite Belt (Volcanic-Sedimentary Group, sensu stricto), to distal volcanic and fine clastic sedimentary to the NE (Ribeira de Limas Formation). According to Carvalho (1976) and Ribeiro et al. (1979) volcanism is significantly diachronous, younging to the NE from upper Fammenian (Strunian) in the Cercal area to Visean close to the Ficalho Upthrust (Fig. 2.5).

Lithologies can seldom be safely correlated in detail from area to area, because of the complications introduced by the volcanic activity. Volcanism is essentially bimodal, composed principally of (dominant) quartz keratophyres and (subordinate) spilites (Schermerhorn, 1970a). Mafic rocks seem to derive from heterogeneous mantle peridotite, and felsic rocks probably resulted from partial melting of continental crust (Munha, 1981). Felsic volcanism was everywhere dominantly explosive, indicating moderate or shallow water depths. Given the subject of this thesis volcanism will be discussed in more detail in section 2.2.

- an uppermost, up to 5 km thick diachronous flysch sequence, the Baixo Alentejo Flysch Group (Oliveira et al., 1979). Its base is Upper Tournaisian to Lower Visean in

the NE (Santa Iria Formation, Carvalho et al., 1976b), Upper Visean in the Pyrite Belt (Mertola Formation, Oliveira et al., i.e. Culm Group, Schermerhorn, 1971) and progressively younger to the SW, attaining lower Westphalian age in the extreme SW (Brejeira Formation; Pfefferkorn, 1968; Oliveira et al., 1979; Ribeiro, in press). Generally speaking, the Baixo Alentejo Flysch becomes progressively more distal from the NE to the SW, and paleocurrent data confirms that the source of detritus was in the Ossa Morena Zone (Boogaard, 1967; Schermerhorn, 1971a; Oliveira et al., 1979). The fact that volcanism in the area was dominantly explosive coupled with the great thickness of the Flysch Group indicates that the South Portuguese lower Carboniferous basin underwent large scale subsidence after volcanism. According to Ribeiro et al. (1979) and Oliveira (in press) subsidence propagated from NE to SW (that is, as expected given the sense of the Flysch diachronism). It should be noted that volcanism progressed in time in the opposite direction (Carvalho, 1976; Ribeiro et al., 1979).

Subsidence was accompanied by major syn sedimentary deformation expressed in pre cleavage overthrusts, slump folds and possibly a major decollement of the whole basin from the pre Upper Devonian basement, as mentioned before (Ribeiro et al., 1979; Ribeiro, 1981). This represents the beginning of the Hercynian Orogeny in the area. Hercynian

tectonic activity evolved essentially continuously from the above early synsedimentary stage into a strongly compressive regime of hard rock deformation responsible for folding of the early overthrust planes (see Schermerhorn and Stanton, 1969), tightening and overturning of the early folds, often accompanied by thrusting of the reverse limbs, and development of widespread, often very penetrative cleavage, not always parallel to the folding planes. All but the least ductile lithologies in the South Portuguese Zone (coarse greywackes, quartzites, cherts, massive lavas and intrusive rocks) exhibit at least one pronounced cleavage. This main cleavage dips steeply to the NE in the NE areas and becomes progressively less steep towards the SW. There is a clear decrease in hard rock deformation from NE to SW, expressed in the interlimb angle of folds: folds are tight or even isoclinal in the NE and get progressively more open to the SW. Also, the stratigraphic thickness of lithologies affected by two cleavages decreases markedly from NE to SW (Caryalho et al., 1976b).

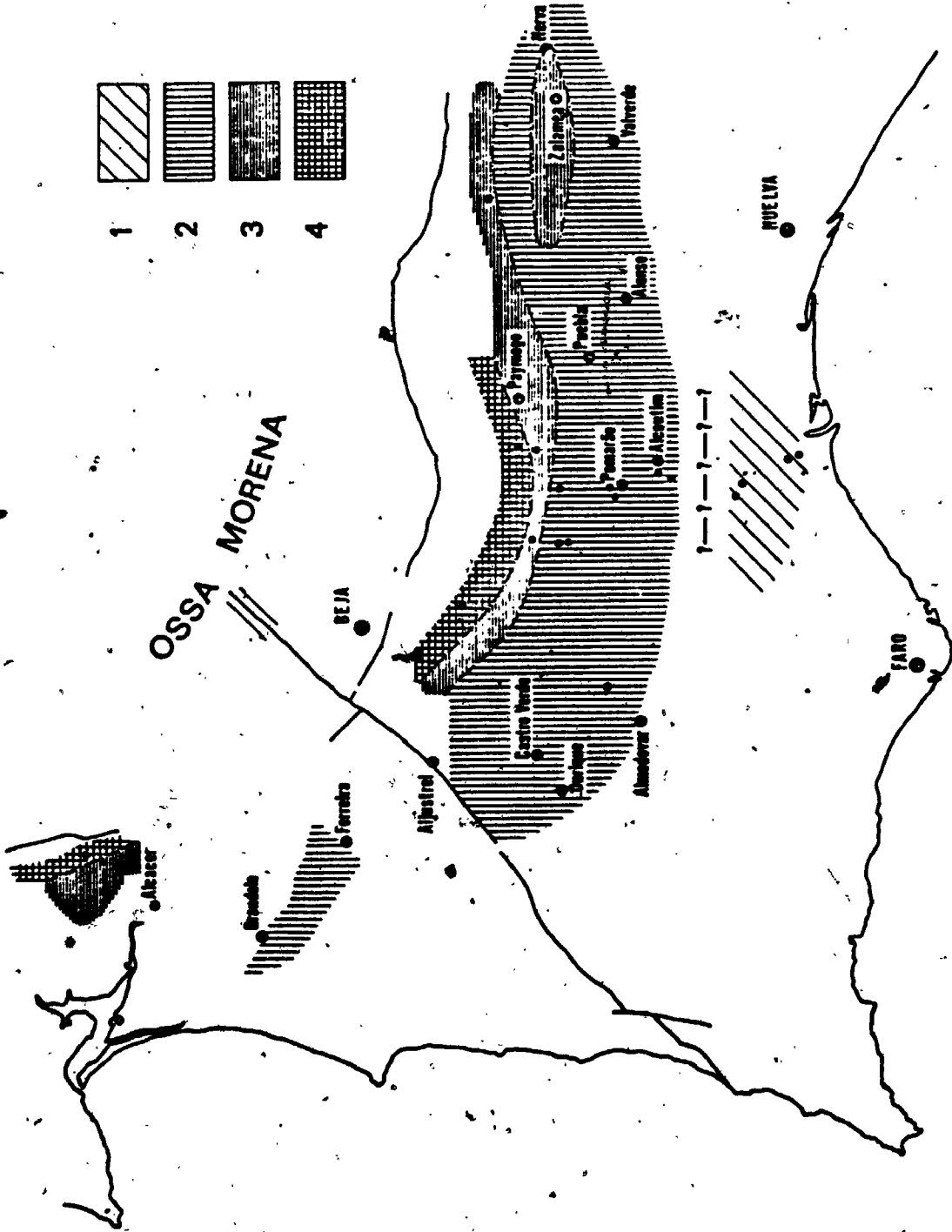
In the intermediate (Pyrite Belt) subzone the net result of early (synsedimentary) and main Hercynian deformation is, at the present level of erosion, the generation of a typical imbricate structure characterized by overturned, often isoclinal folds, with thrust reverse limbs which expose VS lithologies in the anticlines (sometimes PQ also), and Culm flysch in the synclines.





(Ribeiro, 1981). The presence of early overthrusts may in places obscure this simple pattern (see Chapter 3).

Main and late stage Hercynian compression produced numerous wrench faults, trending N, NW and NE in the South Portuguese Zone, with horizontal displacements up to 5 km, both dextral and sinistral, generally related with folding and of relatively shallow nature. The largest of all faults in the area is the Messejana sinistral wrench fault, more than 500 Km long, from the Atlantic Ocean in SW Portugal to near Avila in Spain. It differs from the remaining not only in extent but also in being a much deeper seated dislocation, probably corresponding to a line of major crustal weakness. Lateral displacement along the Messejana Fault is variable around 3 Km, associated with strong drag (Schermerhorn, 1971a; Ribeiro et al., 1979).

Syn and post orogenic metamorphism accompanied deformation, as mentioned before. Munha (1981; in press) defined 4 regional metamorphic zones, from NE and N to S and SW (Fig. 2.6), based on observed mineral assemblages in the mafic metavolcanic rocks and also on illite crystallinity data on other lithologies. Regional metamorphic grade decreases from greenschist facies in the N and NW in the Pulo Formation (metamorphic zone 4), through lower greenschist and prehnite-pumpellyite facies in the Pyrite Belt (zones 3 and 2), to zeolite facies on the extreme South (zone 1). Still according to Munha

Figure 2.6. Zonation of Hercynian regional metamorphism in the Iberian Pyrite Belt. 1-Zeolite facies; 2-Prehnite-pumpellyite facies; 3-Lower greenschist facies; 4-Greenschist facies. After Munha (1981).



- 1 
- 2 
- 3 
- 4 

OSSA MORENA

BEJA

Algeciras

Algeciras

Castro Verde

Zalamea

Huelva

FADO

HUELVA

1-1-1-1-1-1

regional metamorphism was essentially isochemical, took place under low pressure and mineral assemblages are compatible with geothermal gradients in the range of 40 to 50°C/km.

Hercynian deformation eventually stopped flysch deposition, in Westphalian times, through emergence of the area.

The plate tectonic setting of the South Portuguese Zone has been a matter of considerable controversy, perhaps because the nature and significance of the volcanism present therein was not clear. At present time most authors admit that it may correspond to an intracontinental early rift situation, possibly related with back-arc crustal thinning (see Munha, 1981; Oliveira, in press; Ribeiro et al., in press).

Post Hercynian events had relatively minor effects in the South Portuguese Zone. They can be summarized as follows: (see Ribeiro et al., 1979, for a thorough review):

During the Jurassic the Messejana Fault was reactivated under tension, with uprise of tholeiitic magma generating the Messejana Dolerite along that Fault. This is an early manifestation of the opening of the North Atlantic Ocean.

The South Portuguese Zone is bordered to the SE, S and NW by a late Triassic molasse (Gres de Silves) representing the erosion of the Hercynian craton; the Gres de Silves is

in turn covered by Jurassic sediments related with continental subsidence associated with the early stages of opening of the Atlantic Ocean;

During Late Cretaceous times subvolcanic ring complexes were emplaced along an arcuate accident defined by the Monchique, Sines (Fig. 2.4) and Sintra intrusive complexes, possibly related to rotation of the Iberian Peninsula during opening of the Bay of Biscay;

During the Tertiary, Betic compression generated uplift in the Central area of the Iberian Peninsula and concomitant sediment infilling in the Sado and Tagus basins, with accumulation of more than 150 m of clastic and limy sediments which still cover a significant area of the South Portuguese Zone;

Finally, during the Pleistocene several rivers were responsible for up to 20 metres of alluvium along some valleys. Quaternary uplift was responsible for the present ~150 m altitude of the area. Neotectonic activity is expressed in reactivation of faults, sometimes with generation of horsts and grabens, and in rather frequent, generally low magnitude intra plate earthquakes. Neotectonic activity is related with proximity of the plate boundary represented by the Azores-Gibraltar Fault, along which there is intraoceanic subduction to the West and collision of the European and African plates in the vicinity of Gibraltar.

Morphologically, the South Portuguese Zone presently corresponds to an eroded peneplain, plunging gently to the NW and SSE. The climate is mediterranean with atlantic and/or continental influences, characterized by long, dry summers, and short, mild winters. Most of the area is covered by thin soils. Natural rock outcrops are rare and weathered. The main human activities are farming (cereals, cork, olive oil) and mining of massive sulphide deposits.

2.2 Volcanism in the Iberian Pyrite Belt

As mentioned before, sulphide mineralization in the Iberian Pyrite Belt is closely associated with (felsic) volcanism which took place from upper Fammenian (Strunian) to lower Visean times (350 to 335 Ma before present). The volcanic rocks occur as accumulations up to several hundred metres thick in a sedimentary framework of "slates with varying admixtures of coarser terrigenous detritus and biogenic, chemical and volcanic components" (Schermerhorn, 1971a), the ensemble of which constitutes the Volcanic-Sedimentary (or Volcanic-Siliceous) Complex (VS). Discrete volcanic centres occur along major lineaments, particularly well defined in the Western half of the Belt (Portugal), where five such lineaments exist, trending NW-SE. According to Carvalho (1974), the location of the individual volcanic centres is near the intersection of the above structural lineaments with an intersecting, NE-SW old

system of major fractures typified by the Messejana Fault (Fig. 2.1).

Volcanism was markedly bimodal: felsic volcanic rocks constitute about 70% of the known occurrences, most of the remaining are mafic volcanic and shallow intrusive rocks, with only subordinate occurrences of volcanic rocks of intermediate (andesitic) character (Schermerhorn, 1970a; Soler, 1969; Munhá, 1981). Felsic volcanic centres occur throughout the Pyrite Belt, whereas mafic occurrences are dominantly concentrated within two broad domains: the Ourique-Neves lineament of South Portugal and the Eastern area of the Pyrite Belt, in Southwest Spain (Schermerhorn, 1970a; Routhier et al., 1980). Elsewhere mafic igneous activity is either absent or restricted to minor shallow sills or extrusive bodies.

Felsic and mafic igneous activity are well separated, without lithological transitions or alternances, although both types can occur stacked, such as at S. Domingos and Rio Tinto, in which case either felsic or mafic volcanic rocks can be found at the base of VS. VS generally started with felsic volcanism in Portugal and with mafic igneous activity in Spain (Schermerhorn, 1971a). This and the discrete nature of the volcanic centres precludes the existence of a single stratigraphic column for VS applicable to all the Iberian Pyrite Belt (Carvalho et al., 1976). The only large domain where a

well defined stratigraphic sequence can be followed or correlated with certainty over more than a few kilometres is within the Puebla de Guzman anticlinorium area, where the lithostratigraphy established by Boogaard (1967) in the Pomarao area can be traced to near Sotiel, about 60 kms to the East (Carvalho et al., 1976).

The base of the thicker volcanic piles (Aljustrel, Rio Tinto, La Zarza) is generally not exposed or even drilled, which probably explains the otherwise intriguing fact that no volcanic pipes (or other types of volcanic feeder channels) have as yet been found within PQ rocks (Schermerhorn, 1971a; Carvalho et al., 1976).

Volcanism in the Iberian Pyrite Belt was dominantly submarine, as evidenced by the widespread occurrence of pillow lavas with chert-filled interstices, felsic submarine flow tuffs, abundant cherts (radiolarian or not), shales (including black shales), and other subaqueous sediments. However, it is possible that some volcanic episodes were subaerial, because of transient emergence of the top of some of the individual volcanoes (Schermerhorn, 1970b).

Mafic igneous rocks in the Iberian Pyrite Belt consist of lavas, tuffs and shallow intrusive doleritic bodies, usually sills (Strauss, 1965; Rambaud, 1969; Schermerhorn, 1970a), and occur throughout the VS stratigraphic sequences (Schermerhorn, 1975). Munha (1981; see also Munha and Kerrich, 1980) proved that the present spilitic composition

of these mafic igneous rocks, is a consequence of widespread and pervasive hydrothermal metamorphism which took place shortly after emplacement of the rocks, as a consequence of sea water convection through the volcanic piles, driven with heat from within the rocks. Munha (ibid.), in a thorough geochemical investigation of these rocks distinguished primary features from hydrothermal effects, and for the purpose of petrogenetic modelling considered only the least mobile elements under conditions of hydrothermal metamorphism, and primary igneous minerals (mainly pyroxenes), concluding that the mafic igneous rocks of the Iberian Pyrite Belt were originally basaltic, tholeiitic transitional to arc tholeiites at the base of VS, and becoming progressively enriched in incompatible elements towards the top of VS, where they become typical "within plate" alkaline basalts. Munha also concluded that these mafic rocks were produced from different partial melts of heterogeneous mantle, and that such magmas experienced varying degrees of ~~fractionation~~.

Intermediate igneous rocks are generally rare, although they can be locally significant, especially in the northernmost areas of the Iberian Pyrite Belt. They occur both as extrusive accumulations and as shallow intrusive bodies, and are generally feldspar and pyroxene phyrlic (Salpeteur, 1976; Munha, 1981). Munha (1981) concluded that these andesitic rocks did not result from

differentiation of basaltic magmas, and suggested instead "that a suitable source for andesites could be the hydrous equivalent to [the] upper mantle peridotite source of contemporaneous Group 1 [base of VS] basaltic rocks".

Felsic volcanic rocks are the most important type of igneous rocks in the Iberian Pyrite Belt, both volumetrically and because massive sulphide mineralization known to date in the area can invariably be related, more or less intimately, to felsic volcanism (Schermerhorn, 1970b; Carvalho et al., 1971b).

Felsic igneous rocks in the Iberian Belt are at present time ~~unanimously considered to be almost~~ exclusively composed of pyroclastic rocks, from autoclastic explosion breccias to lapilli, ash and dust tuffs (Strauss, 1965; Boogaard, 1967; Schermerhorn and Stanton, 1969; Schermerhorn, 1970b; Carvalho et al., 1971b, 1976; Routhier et al., 1980). Only rarely have minor felsic intrusive occurrences been confirmed, mainly in the Chancá-Paymogo-S. Domingos border zone between Portugal and Spain (Salpêteur, 1976; Carvalho, 1979), mainly as porphyritic dykes and small shallow intrusions producing weak contact metamorphism. Felsic lavas have been reported from several locations, but the cumulative effects of total devitrification, hydrothermal alteration and Hercynian deformation and regional metamorphism may often have obliterated structures and textures beyond recognition of

original characteristics. Welded tuffs have been reported (Lecolle, 1974; L. Conde, personal communication, 1978), on the basis of flattened textures and on the occurrence of prismatic disjunction of some volcanic beds, and interpreted as evidence for subaerial volcanic activity in conflict with several other lines of evidence which leave little room for doubt on the generally submarine, perhaps even pelagic nature of volcanism. Schermerhorn (1970b) reconciled these facts admitting that the uppermost portions of the volcanoes may have emerged, at least transiently. However, the occurrence of welded tuffs is not conclusive evidence of subaerial volcanism, as shown by Fiske and Matsuda (1964) and Yamada (1973); moreover, Sparks et al. (1980) have even proposed that "a subaqueous environment can be more favourable to welding than many subaerial environments".

Thick (hundreds of metres) felsic pyroclastic piles in the Iberian Pyrite Belt generally include coarse breccias and lapilli tuffs, together with the more widespread tuffs and dust tuffs, and must correspond to the areas where isolated or clustered volcanoes existed. These volcanic centres are often elongated, with original areal extents up to tens of kilometres. Given the geologic constraints outlined above detailed reconstructions of the original volcanic edifices are not always possible and often debatable. One of the most successful and complete such

reconstructions is that at Tharsis (Strauss and Madel, 1974; Madel and Lopera, 1976), in the Puebla de Guzman anticlinorium, where three superimposed felsic volcanic cycles are discernible (Fig. 2.7), each with a central domain of proximal volcanic facies (lavas, flow and tuff breccias) grading laterally and symmetrically to flow tuffs which in turn interfinger with distal volcanic and sedimentary lithologies (tuffitic slates, cherts, black slates). Each of these successions (except for the uppermost Gatos volcanic cycle) is capped by a horizon of purple red, tuffitic shales, occasionally with iron rich red jasper (discontinuous) intercalations and small manganese deposits. 2 km North of the volcanic centre (Tharsis mine area) volcanic rocks of the first cycle are restricted to beds of fine grained, well graded tuffs. Similar distal facies of 3 cycles of volcanism can be traced along the strike of the Puebla de Guzman anticline to Pomarao in Portugal (Boogaard, 1967), as mentioned before.

Out of the Puebla de Guzman anticline superimposed volcanic cycles are less well defined. At most other large volcanic centres only one main felsic event took place, despite the occasional presence of distal fine tuffs or tuffites in the sequences, attesting slightly diachronous volcanic activity elsewhere.

Schermerhorn (1970b) proposed that isolated, generally

Figure 2.7. Schematic geologic section of the Tharsis North area (without scale; N-S extension approx. 2 km).

1-Devonian Phyllite-Quartzite Group; 2-Tharsis-I lavas, flow- and tuff-breccias; 3-Black slates, cherts, tuffitic slates; 4-fine to medium grained bedded tuffs of different volcanic phases; 5-Massive sulphide orebodies; 6-Spillitic lavas; 7-Tharsis-II lavas, flow breccias, tuff-breccias, porphyritic tuffs; 8-Manganese formations; 9-Gatos tuff-breccias and tuffs. After Strauss and Madel (1974).

S N

NORTH LODE
OPENCAST

POSITION OF HUECA
PYRITE MINERALIZATION

CERRO GATOS



- 1 [diagonal lines]
- 2 [stippled]
- 3 [wavy lines]
- 4 [white]
- 5 [diagonal lines]
- 6 [diagonal lines]
- 7 [stippled]
- 8 [vertical lines]
- 9 [horizontal lines]

thin occurrences of felsic tuffs within dominantly shaly lithologic sequences must represent "ash flow tuffs laid down by sliding and flowing down volcanoes at the eruptive centres". Schermerhorn invokes low temperature mechanisms such as slides, mudflows and turbidity currents, excluding hot flowage (glowing avalanches; nuees ardentes) as restricted to subaerial volcanism, but we have seen above that this is not necessarily true.

Texturally, most felsic volcanic rocks in the Pyrite Belt are vitric to crystal vitric tuffs of various grain sizes. Lithic fragments are generally present, although subordinate in abundance. Cusped, Y-shaped glass shards are exceedingly rare in these felsic tuffs, although abundant in the mafic tuffs. According to Schermerhorn (1970b) the felsic tuffs display "a 'dilute greywacke' texture made of roughly sand-sized grains of crystals, crystal aggregates and original glass enveloped by a sericitic or sericitic-microfelsitic groundmass (chlorite may also be present), through which are scattered larger and smaller phenocrysts and other fragments".

Phenocrysts in felsic volcanic rocks are euhedral to anhedral (often broken) feldspars, quartz and rarely chloritized biotite and garnet (Schermerhorn, 1976; Lecolle, 1976). In dacitic tuffs feldspar phenocrysts are albitized plagioclase, and clinopyroxene microphenocrysts are sometimes present (Munha, 1981). Rhyolitic tuffs are

largely dominant, however, and display albite and K-feldspar phenocrysts, often after oligoclase-andesine.

Most, if not all volcanic and hypabissal rocks in the Iberian Pyrite Belt were affected by (sea water) hydrothermal metamorphism (Munha, 1979, 1981; Barriga and Kerrich, 1981; this study) which produced marked chemical changes in the rocks. Despite undebatable textural evidence for metasomatism, this fact was not properly accounted for in the past. Most felsic rocks in the area were originally rhyolitic, often highly siliceous (Munha, 1981). Their present composition is mostly quartz-keratophyric to quartz-kalikeratophyric (Schermerhorn, 1970b, 1973), and these rather cumbersome terms obscure the fact that they are simply hydrothermally altered rhyolites (felsic spilites according to Munha et al., 1980).

Munha (1981) concluded that the felsic igneous rocks of the Iberian Pyrite Belt are not linked to the coexisting mafic and intermediate rocks by fractional crystallization, and that they rather result from crustal anatexis of rocks of granitic and/or tonalitic composition, therefore confirming earlier similar hypothesis (Schermerhorn, 1970b, 1975; Priem et al., 1978).

2.3 Hydrothermal activity and mineralization in the Iberian Pyrite Belt

The Iberian Pyrite Belt is the area of the South Portuguese Zone where massive sulphide deposits occur or are likely to be found. This definition corresponds to common usage, based on studies in the Cercal area (Carvalho, 1976) and especially as a consequence of the recent discovery of the outstanding Neves-Corvo deposits (Albouy et al., 1981). Carvalho (1982) recently proposed that the traditional limits of the Iberian Pyrite Belt should be widened significantly to the S and NW, to enclose an area at least twice as large as before (Fig. 2.8).

Two types of mineral deposits are widespread in the Iberian Pyrite Belt: several tens of massive sulphide deposits and several hundred Manganese deposits. Associated metalliferous sediments (Fe-Mn cherts and jaspers and purple slates) are equally important with regard to genetic studies and mining exploration. In this section a brief summary of their more salient features will be presented, condensed essentially from Srauss (1965), Rambaud (1969), Carvalho et al. (1971a, b, 1976), Schermerhorn (1970b, 1971b, 1976), Strauss and Madel (1974), Carvalho (1976, 1979), Strauss et al. (1977) and Routhier et al. (1980).

Massive Sulphide Deposits

The Iberian Pyrite Belt massive sulphide deposits have

been known and exploited since pre Roman times, mainly as gold, silver and copper ores from the supergene enrichment zones of outcropping deposits. It is worth noting that the only deposit discovered to date away from Roman or pre Roman mines is the Salgado deposit (Carvalho, 1976), intersected by drilling in 1976.

About 60 mines operated during the last 100 years or so, and about 280 million metric tonnes (Mt) of massive polymetallic sulphides were extracted in the same period (Strauss and Madel, 1974), mainly for sulphur (average grade 46%), copper (0.7%) and sometimes for iron (40%), although ore nearly always contains appreciable amounts of zinc and lead (combined average 4%, Carvalho et al., 1976), precious metals (0.8 ppm Au, 30 ppm Ag, *ibid.*) and a host of alloy metals such as Sn, Cd, Co, Hg, Bi, Se and many others in concentrations ranging from tens to hundreds of ppm. Many of these metals (including Pb and Zn) are often not recovered because of the fine grained nature of most ores, what in turn is responsible for the expression 'Iberian Pyrite Belt' and for frequent incorrect literature quotations of these orebodies as "barren pyrite" and "pyrite orebodies".

Reserves of massive sulphide ore in the Iberian Pyrite Belt amount to about 700 Mt, essentially concentrated at seven major locations: Aljustrel (250 Mt) and Neves-Corvo (100 Mt) in Portugal and Tharsis (130 Mt), La Zarza (60

Mt), Rio Tinto (55 Mt), Aznalcollar (50 Mt) and Sotiel (40 Mt) in Spain. Exhausted or nearly exhausted other mines which were important in the past include S. Domingos (30 Mt) and Lousal (20 Mt?). A very large part of these reserves (which do not include stockwork type ores) was discovered after the early 1960's, as a consequence of widespread acceptance of the exhalative-sedimentary theory of ore genesis (Øftedal, 1958), originally advocated by Klockman (1894), eloquently illustrating the importance of correct geologic understanding and models in mineral exploration (Strauss et al., 1977; Carvalho, 1979).

As a result of high quality geologic studies during the last two decades, under the light of the "new" exhalative-sedimentary theory several important aspects concerning the origin of the orebodies are presently well established, namely that they are syngenetic (sensu lato), as evidenced by the well defined horizons where they occur, the common sedimentary features they depict and also because they experienced the same tectonic and metamorphic history of the rocks that host them; volcanogenic in the sense that they formed in close association with the waning stages of (felsic) volcanism; exhalative, that is, resulted from metalliferous aqueous solutions that raised through the footwall rocks, as shown by chemical zonation, the presence of underlying stockwork zones and by prominent hydrothermal alteration of the host lithologies in the

vicinity of autochthonous orebodies; and submarine from the submarine lithologies and facies that host them (mostly submarine felsic tuffs, cherts, jaspers) and from the subaqueous textures of the ores themselves.

The Iberian Pyrite Belt massive sulphide deposits occur invariably in stratigraphic horizons that correspond to the waning stages of felsic volcanism at each specific volcanic centre, or, if stacked felsic volcanic cycles occur, to the end of one or more of the volcanic periods. They can occur at or near the top of thick felsic piles, or anywhere along strike, in laterally equivalent positions, both on more distal volcanic facies or even mainly on sedimentary sequences (shales, black shales) again laterally equivalent to the volcanic rocks, as schematically illustrated in Figure 2.8. As a consequence of this range of host lithologies the orebodies can be found anywhere from near the base to almost at the top of VS, as they are hosted in sediments or at the top of thick felsic pyroclastic piles, respectively.

Sulphide orebodies lying on thick pyroclastic piles are invariably underlain by stockworks of stringer and disseminated mineralization in highly altered host lithologies, whereas such stockworks are generally not found under orebodies hosted in sediments or on distal volcanic facies. Also, soft sediment deformation structures such as slumping, scour and fill,

syndimentary breccias and even "turbidite" textures are ubiquitous in orebodies not associated with stockworks and rare or absent in orebodies rooted in stockworks.

The above facts suggest that massive sulphide deposits in the Iberian Pyrite Belt formed from metalliferous aqueous solutions rising through the footwall rocks, and precipitating sulphides at or near the coeval sea floor. Slope instability and thixotropic behaviour of the sulphide "muds" precipitated on the hydrothermal vents may in some cases have induced sliding down volcano flanks with redeposition in deeper waters, among distal volcanic beds or even within sediments (Schermerhorn, 1970b, 1971b). Much in the same way as Carvalho (1979) we will use autochthonous to describe massive sulphide deposits rooted in stockworks and allochthonous or redeposited for sulphide accumulations on unaltered footwalls and depicting evidence of significant soft sediment deformation, hence avoiding the confusing "proximal" and "distal" denominations (see Large, 1979; Jambor, 1979). Clear cut examples of autochthonous orebodies are Rio Tinto and Perrunal-La Zarza in Spain and Feliz-Estacao (Aljustrel) in Portugal. Good examples of allochthonous orebodies are Filon Norte and S. Guillermo (Tharsis) in Spain and Lousal (Portugal). The Salgadoinho disseminated deposit, hosted in felsic tuffs depicting stockwork type alteration (Carvalho, 1976; Plimer and Carvalho, 1982) probably represents the roots of an ore

forming system, and massive mineralization (not yet found in the area) may have moved downslope from its top. It is interesting to note that this ore deposit was found partly as result of alteration studies (Carvalho, 1976). The relations between the various types of sulphide deposits, siliceous sediments, ore zone alteration and lithostratigraphy are schematically illustrated in Figure 2.9.

Hydrothermal alteration

Apart from the already mentioned regional, widespread sea water hydrothermal alteration responsible for the present spilitic and quartz-keratophytic compositions of most igneous rocks in the Iberian Pyrite Belt, stockwork mineralization in the area is hosted in rocks that are intensely hydrothermally altered, often to such extreme degrees that the original texture and mineralogy are lost, and the rocks become aggregates of exclusively alteration minerals, usually quartz, chlorite and sulphides (chalcopyrite, pyrite, minor pyrrhotite and sphalerite), sometimes with significant sericite and/or carbonates. Oxygen isotope determinations in minerals from the stockworks of several sulphide deposits in the Pyrite Belt (Rio Tinto, Chanca, Salgadinho and Feitais-Estacao, Barriga and Kerrich, 1981; Munha and Kerrich, 1981) indicate that ore fluids were generally isotopically similar to sea water ($00/00 \delta^{18}O$ SMOW), although significantly ^{18}O enriched

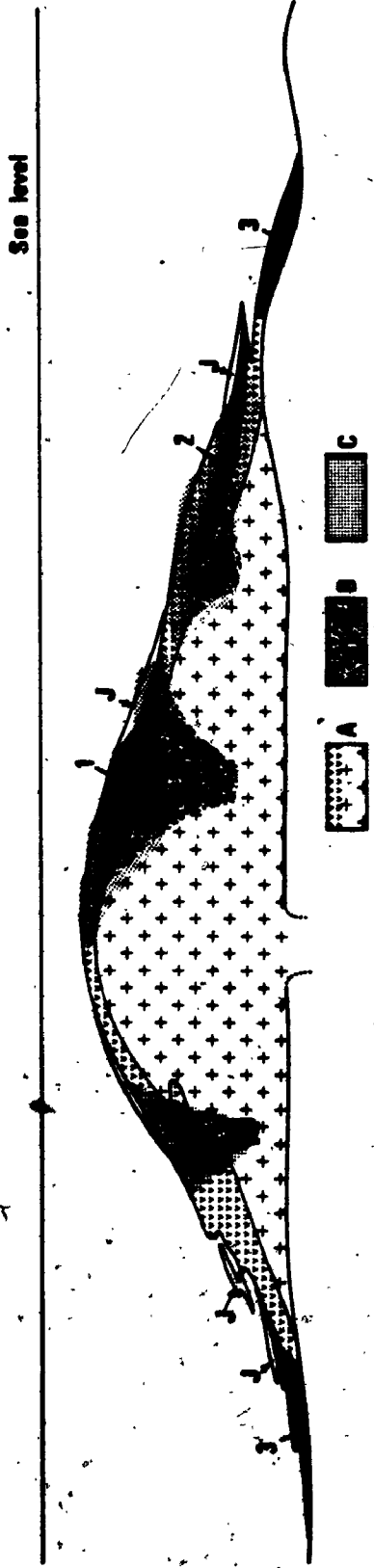


Figure 2.9. Schematic representation of the relations between sulphide ores, siliceous sediments, ore zone alteration and lithostratigraphy. 1 - Autochthonous type sulphide ore; 2 - Transitional type ore; 3 - redeposited type ore; J - Jasper; A - felsic volcanic rocks; B - strong chloritic alteration and cupriferous stockwork; C - strong sericitic alteration. After Carvalho (1979), slightly modified.

fluids were detected at Salgadoinho and Feitais-Estacao. The study of hydrothermal alteration associated with the Feitais-Estacao orebody of Aljustrel is a significant part of the present thesis.

Manganese deposits and other metalliferous sediments

Hundreds of small manganese deposits are known from within the VS Complex of the Iberian Pyrite Belt, and were object of minor mining operations in the past. They occur within various lithologies, namely tuffites, siliceous slates (often red or purple, hematitic), and cherts and jaspers. The ensemble of Mn concentrations and their immediate host lithologies constitute mappable units, and ~~invariably lie on volcanic rocks, both mafic and felsic, or on their lateral equivalents.~~ In the field, they constitute good evidence of a late or post volcanic environment, but cannot be considered true "marker horizons" in exploration for massive sulphide deposits, as they occur associated with both productive and non productive volcanic episodes (at least as far as is known). Notwithstanding with this limitation, the occurrence of Fe-Mn formations can be an indication of ore proximity, as some such Fe-Mn rich horizons are indeed related with massive sulphide deposition (Strauss, 1965; Strauss and Madel, 1974; Carvalho et al., 1976). Jaspers are particularly significant. According to Carvalho (1979) "...jaspers are perhaps the most typical rocks of the

Iberian Pyrite Belt. Several types are known, which can occur at one or more levels of the volcanic sequences. The facies more closely related with sulphide mineralization stands out as it is generally light grey and contains scattered pyrite crystals. At Feitais [Aljustrel] these jaspers contact directly with the sulphide orebody. They grade laterally into another type of jaspers, predominantly red, with hematite and manganese oxides" (translated from Portuguese).

Munha (1981) analysed Fe and Mn rich cherts from one of the Pyrite Belt Manganese mines (Lagoas do Paco, Portugal) and, on the basis of their Lanthanide element patterns and on their low minor metals (Ni, Co, Cu) contents concluded that they resemble present day sea floor hydrothermal metalliferous deposits (Bonatti, 1981; Fyfe and Lonsdale, 1981).

If the present is still the key to the past ancient sea floor surfaces now recorded in the Iberian Pyrite Belt metalliferous sedimentary horizons should represent hydrothermal metalliferous deposits near ancient hydrothermal vents and hydrogenous metalliferous concentrations away from such sites (i.e., away from stockwork sulphide mineralization and alteration). In the course of the present work we will try to elucidate this aspect as well.

2.4 Conclusion

The Iberian Pyrite Belt is located in South Portugal and Southwest Spain, and constitutes Western Europe's most prominent stock of base metals. Extremely large massive sulphide deposits occur associated with the waning stages of (felsic) explosive volcanism which took place in early Carboniferous times, on a Phyllite-Quartzite, shelf facies, conformable basement. Subordinate mafic volcanism accompanied the felsic volcanic activity, producing a bimodal association in which the two types of igneous rocks are not related by magmatic differentiation; basaltic rocks seem to derive from heterogeneous mantle peridotite and felsic rocks resulted from partial melting of crustal material. Volcanic rocks were affected by widespread sea water hydrothermal metamorphism responsible for the present spilitic and quartz-keratophytic (felsic spilitic) compositions of the rocks, for the massive sulphide deposits and also for abundant volcanogenic sediments such as manganese accumulations, Fe-Mn cherts, purple and red slates genetically equivalent to present day sea floor Fe-Mn hydrothermal and hydrogenous metalliferous concentrations.

Volcanism took place along lineaments of discrete volcanic centres in a framework of detrital, biogenic and chemical sediments, generating a widely variable (ore hosting) Volcanic-Sedimentary Complex. After volcanism the

area experienced pronounced subsidence, with deposition of a conformable, several km thick Flysch Group (base Viséan to Westphalian). During the time of Flysch deposition large scale synsedimentary deformation took place, enhanced by probably continuous, subsequent tectonic compression, generating a complex imbricate structure of tight folds and folded overthrusts where VS anticlines are exposed between, and often thrust on, Flysch synclines. Deformation was accompanied (and followed) by low grade (zeolite-lower greenschist) and low pressure regional metamorphism of essentially isochemical nature. On the basis of the above we favour that the plate tectonic setting of the Iberian Pyrite Belt probably corresponds to an early continental rifting situation, or to a back arc basin associated with subduction further North, in which case the Flysch phase of the basin and the tectonic activity would be related to closure of an adjacent ocean and continental collision.

Aljustrel is one of the main mining centres of the Iberian Pyrite Belt.

CHAPTER 3

GEOLOGY AND ORE DEPOSITS OF THE ALJUSTREL AREA

3.1 Introduction

Aljustrel is located in the Beja district of South Portugal (Fig. 3.1). The geology of the Aljustrel area (Fig. 3.2) has been described by Schermerhorn and Stanton (1969), Freire d'Andrade and Schermerhorn (1971) and Carvalho et al. (1976). Ribeiro et al. (1982) recently commented on the structural evolution of the area and the geological staff of Pirites Alentejanas, S.A.R.L., the Aljustrel mining company, produced a number of detailed geologic cross sections of the area (unpublished mine reports, 1978, 1979; L. Conde, J. C. Leitão, personal communications, 1978, 1979, 1980). Pirites Alentejanas,

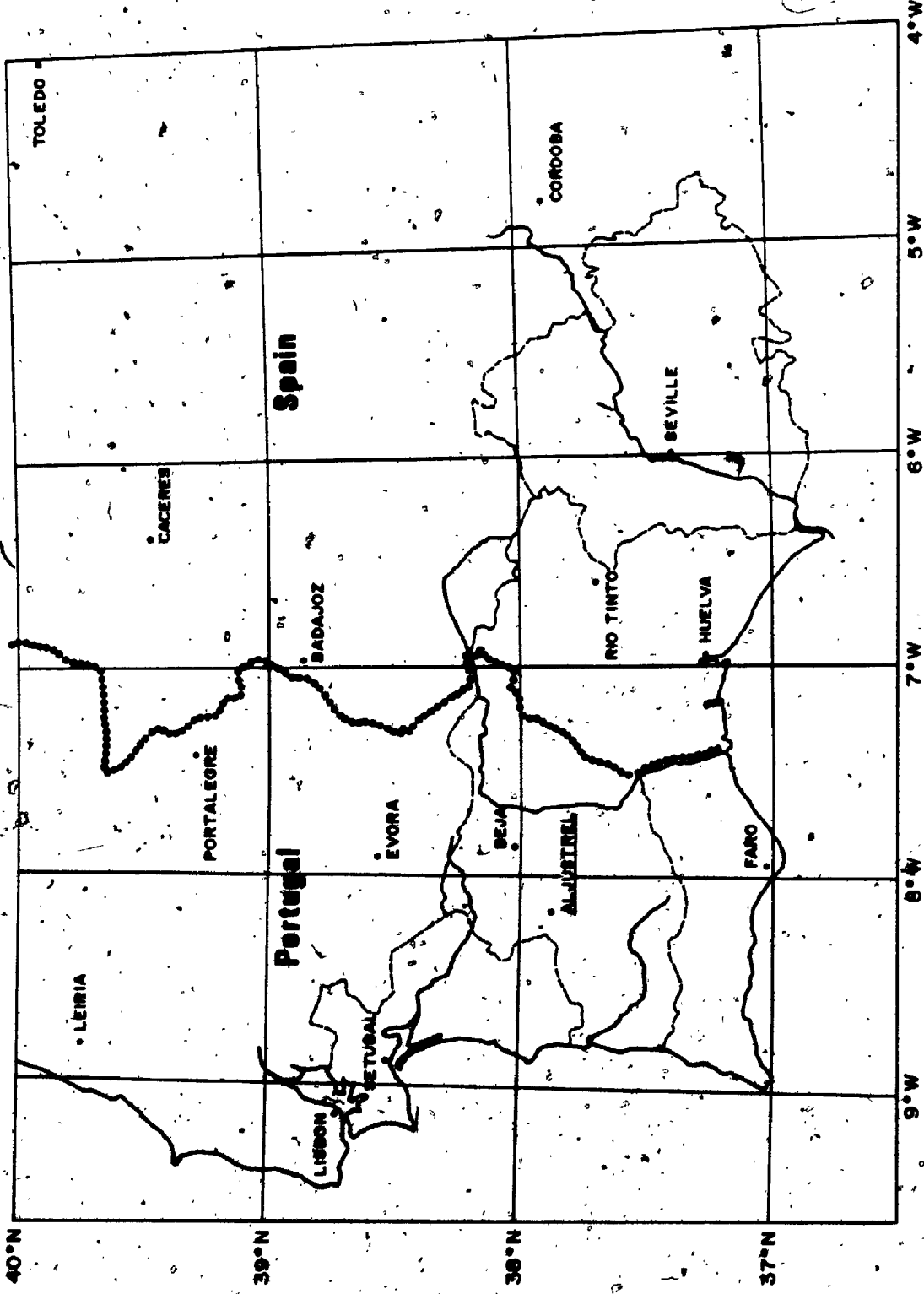


Figure 3.1. Location map of Aljustrel.

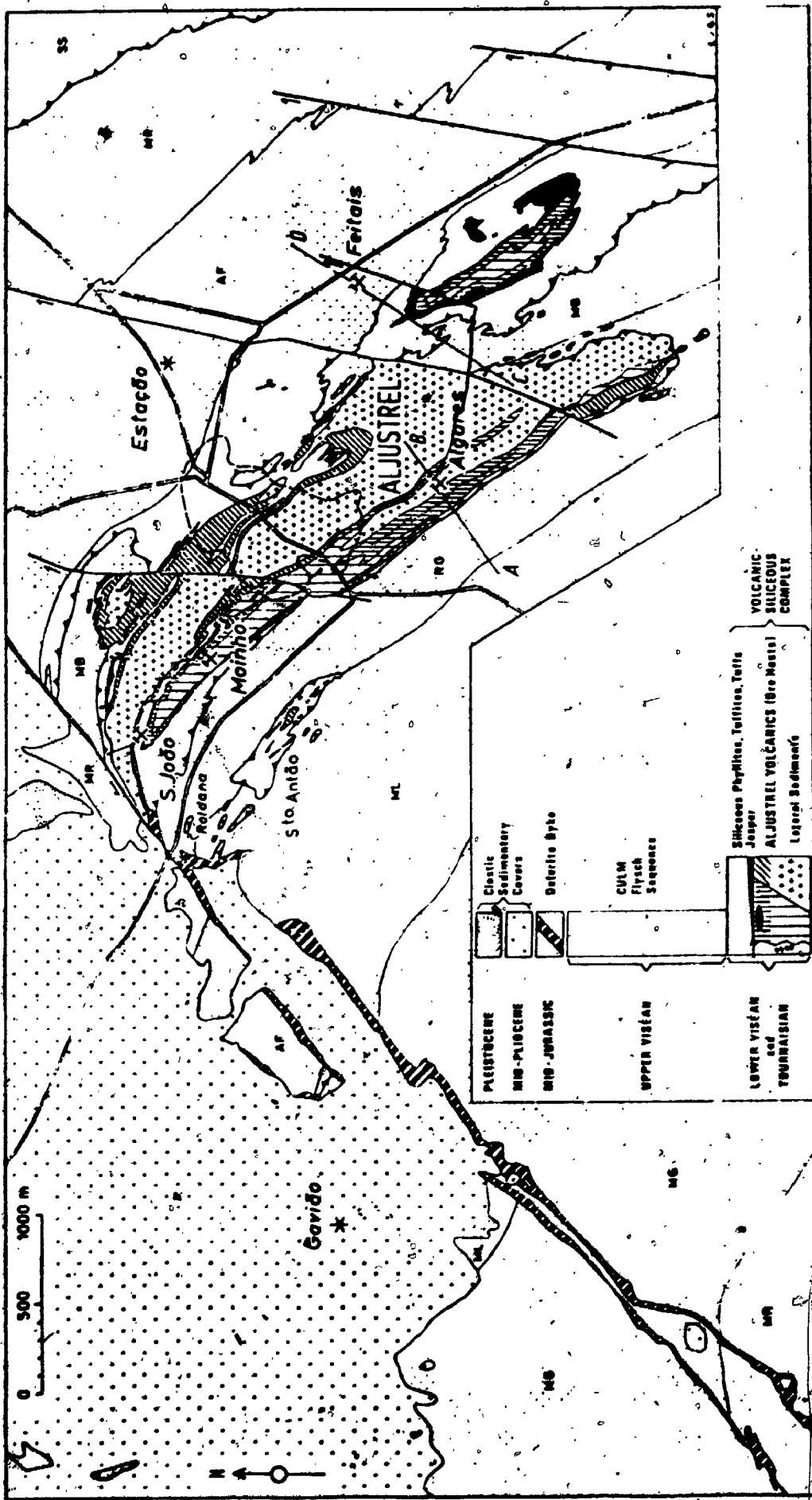


Figure 3.2. Geology of the Aljustrel area. After Schermerhorn and Stanton (1969) and Freire d'Andrade and Scheimerhorn (1971). For Culm Group lithostratigraphy see Figure 3.3.

S.A.R.L. is owned by the Portuguese Government (93%) and by Belgian private interests (7%).

3.2 Lithostratigraphy and ore deposits

At Aljustrel the base of the ore bearing VS Group is not seen, nor does the regionally underlying PQ Group outcrop. VS (locally named Aljustrel Group) is composed of a thick (>250 m - base not seen) succession of felsic pyroclastic rocks (Aljustrel Volcanics) conformably overlain by a ~50 m thick unit of siliceous sediments, tuffites and rare tuffs (Paraiso Siliceous Formation, PS). At or near the contact between the Aljustrel Volcanics and PS several massive sulphide deposits occur, totalling nearly 250 Mt (Table 3.1), accompanied by prominent lenses and strata of chert and jasper and several small manganese deposits.

Aljustrel Group rocks outcrop within an elongated, ~1.5 by 5 km area (Fig. 3.2), surrounded by Upper Viséan turbidites (Culm Group, up to 3000 m thick), except to the NW, where the Aljustrel Group is truncated by a major accident, the Messejana Fault, beyond which Paleozoic formations are buried under 60 to 100 m of Tertiary clastic and limy sediments (Sado Basin Formation) filling a major graben limited in the area by the Messejana Fault. The contact between Aljustrel Group and Culm Group rocks is conformable along the NE boundary of the latter (Feltais

Table 3.1. Quantities and compositions of the Aljustrel massive sulphide deposits, not including stockwork type ores. Tentative compilation after Freire d'Andrade (1967), Freire d'Andrade and Schermerhorn (1971), Carvalho et al. (1976), Montes and Silva (1979) and unpublished data from Pirites Alentejanas, S.A.R.L. Other elements present in potentially recoverable quantities include Au (0.7 ppm), Ag (35 ppm), Sb (1000 ppm), Hg (95 ppm), Bi (150 ppm), Cd (60 ppm), Se (35 ppm), Te (50 ppm), Co (200 ppm) and Mo (35 ppm). Significant stockworks are known at Feltais and Moinho.

	Quantities of massive ore (10 ⁶ metric tonnes)			Composition (%)				
	Mined to date	Proven	RESERVES Indicated+Infer.	S	Fe	Cu	Zn	Pb
Algares		-	<5	} 45 } to } 47 }	} 38 } to } 41 }	} 0.55 } to } 1.7 }	} 3.5 } }	} 1.2 } }
Moinho	6	16	45					
S. Joao		3	15					
Gaviao	-	16	15					
Feltais	1	30	50					
Estacao	-	-	40					0.3

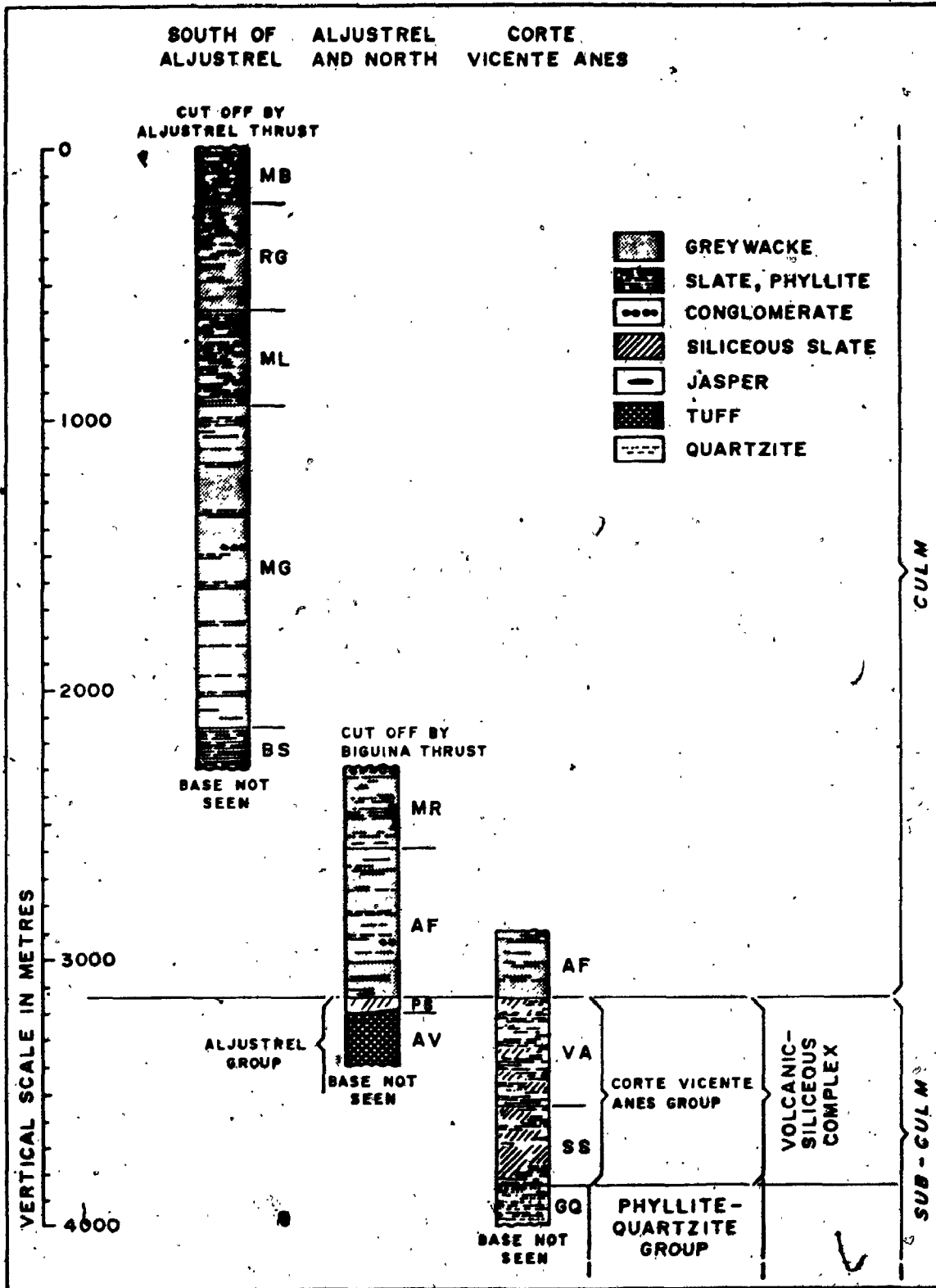
anticline). Elsewhere this contact is tectonic, through generally low angle thrust planes (Schermerhorn and Stanton, 1969; Ribefro et al., 1982).

To the South and Southwest vicinities of Aljustrel VS Group rocks do not outcrop. 5 km Northeast of Aljustrel, near Corte Vicente Anes, VS is again exposed, this time conformably overlain by PQ rocks, as a ~700 m thick sedimentary and distal volcanic sequence (dust tuffs, tuffites). The Aljustrel and Corte Vicente Anes lithostratigraphic columns are represented in Figure 3.3. To the Northwest the Aljustrel Group continues under the Sado Basin cover (~3 km offset by the Messejana Fault) for another 2 km, until it interfingers with fine grained slates and dust tuffs (Gaviao Formation) and also with mafic pillow lavas and diabase sills related with a mafic volcanic centre near Milhouros, 7 km NW of Aljustrel.

3.3 Structure

Aljustrel Group rocks occur as a series of tight to isoclinal anticlines trending NW-SE, separated by intervening synclines and/or thrust faults. Axial planes dip steeply to the NE. From NE to SW the anticlines are named the Feitais Anticline, Central Anticline and Southwest Anticline, with the much smaller, Santo Antao Anticline still further SW (Fig. 3.2). In each it can be seen that the Aljustrel Volcanics are conformably overlain

Figure 3.3. Columnar sections showing lithostratigraphic divisions of the Paleozoic of the Aljustrel area. GC, Gomes Quartzite; AV, Aljustrel Volcanics; PS, Paraiso Siliceous Formation; SS, Seixo Siliceous Formation; VA, Vale de Agua Formation; AF, Agua Forte Greywackes; MR, Monte Ruas Slates; BS, Brunheiras Slates; MG, Maroicos Greywackes; ML, Mau Ladrão Slates; RG, Represa Greywackes; MB, Monte da Broca Slates. After Schermerhorn and Stanton (1969).



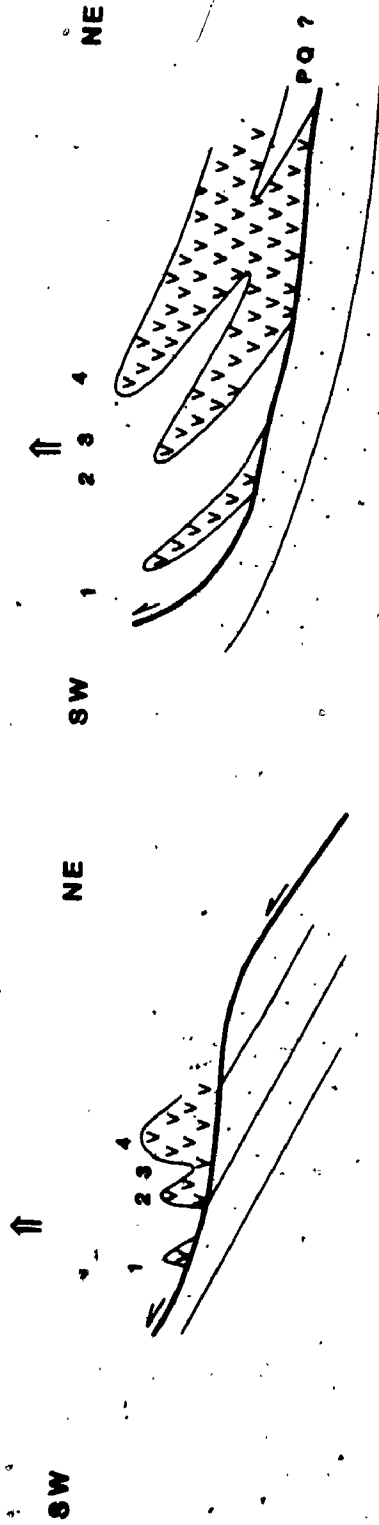
by the PS Formation. All but the least ductile Aljustrel Group rocks (cherts, massive felsites) display strong schistosity (main cleavage) striking NNW, at a small angle with the axial planes of the folds, with vertical or steep-NE dips. According to published reports, two major low angle overthrusts brought the Aljustrel Group and Corte Vicente Anes Group rocks to rest on a several hundred metre thick monoclinical sequence of Culm rocks, implying lateral displacements (NW to SE) of the order of many kilometres. These are respectively the Aljustrel and Biguina overthrusts, active at the onset of the Hercynian Orogeny, and representing the earliest deformation events in the area. Movement along these thrust planes took place prior to the development of cleavage, and generated gentle, open folds. The Aljustrel and Biguina overthrusts were therefore probably synsedimentary thrusts (Ribeiro et al., 1979; Ribeiro, 1981; see Chapter 2).

The main phase of Hercynian compression followed the above early deformation stage, and was approximately coaxial with it, tightening all structures, and folding the early overthrust planes (Schermerhorn and Stanton, 1969), or produced later thrusting of the inverse flanks of the now overturned anticlines (Ribeiro et al., 1982). The final result of these two main successive phases of (probably continuous) deformation is that the Central, Southwest and Santo Antao anticlines are believed to float

on many hundred metres of (younger) Culm rocks which constitute a monoclinial sequence. The Feitais Anticline is in conformable contact with Culm, and its core (not seen) could still rest on a VS "basement" (Fig. 3.4a). Aljustrel mine geologists defend a substantially different interpretation (Fig. 3.4b), essentially based on their own Culm Group stratigraphy and style of deformation. The main point of immediate concern to the present report is that the Feitais Anticline is the least deformed structure in the Aljustrel area (Figs. 3.2 and 3.4), and was therefore selected as the more favourable area for field work and sampling.

The Central Anticline (or anticlinorium) is occupied by a thick (>250 m - base not seen) sequence of coarse, quartz and feldspar phyrlic tuffs, the Megacryst tuff (AV₁-M, below, >200 m thick) and the Green tuff (AV₂-gt, above, 0-50 m thick). The SW, Santo Antao and Feitais Anticlines contain a mutually equivalent but different pyroclastic sequence, of finer grained tuffs consistently devoid of quartz phenocrysts, the felsitic facies tuffs (AV₁-ff, below) and the mine tuffs (AV₂-mt, above). The massive sulphide deposits occur as two lineaments within the SW and Feitais anticlines, at or near the top of the mine tuffs. The spatial relationship between the different tuff facies has been observed at various locations, and is schematically illustrated in Figure 3.5. AV₂-gt and AV₂-mt

Figure 3.4a. Structure of the Aljustrel area. Early overthrusting of Aljustrel Group rocks on a monoclinial sequence of younger Culm turbites (lower sections), followed by folding of the overthrust plane (S, Schermerhorn and Stanton, 1969) or, alternatively, development of tectonic thrusting (R, Ribeiro et al., 1982). After Ribeiro et al. (1982).



-  Culm
-  Paraiso effluvous FM
-  Ajuastrel volcanics

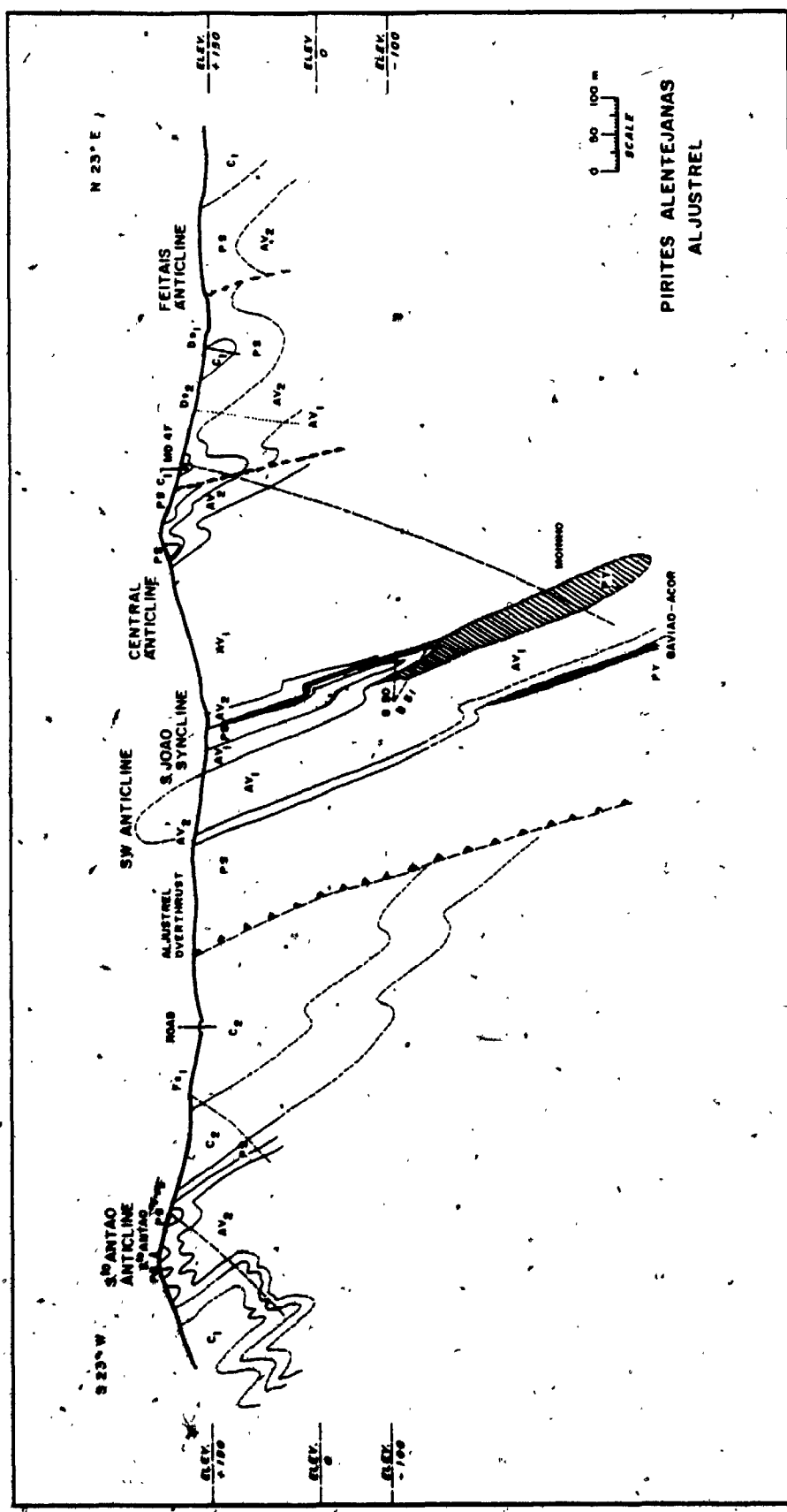


Figure 3.4b). Structure of the Aljustrel area according to Pirites Alentejanas (unpublished). Used with permission. (L. Conde, 1983).

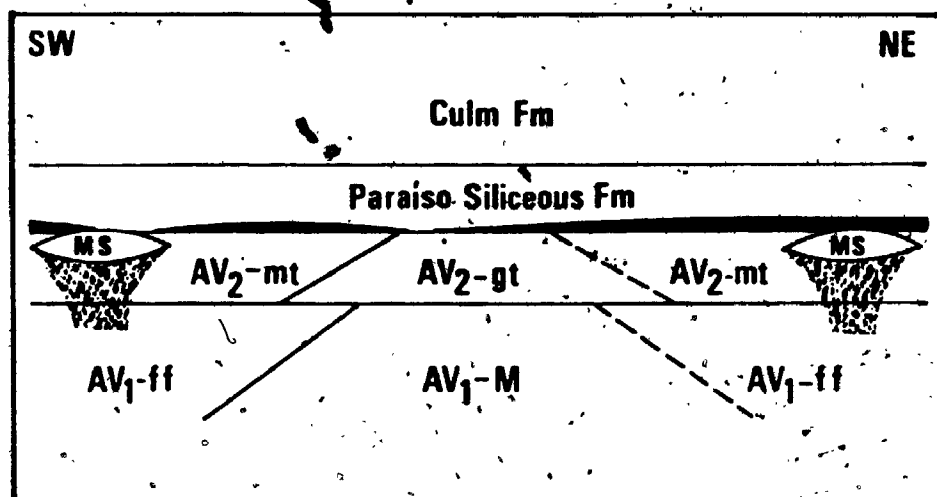


Figure 3.5. Schematic lithostratigraphy of the Aljustrel Group (overlying Culm Group also shown). AV, Aljustrel Volcanics. MS, massive sulphide deposits. Jasper unit shown in black. AV₁-M+AV₂-gt: Quartz-eye Tuff Formation (this study). AV₁-ff+AV₂-mt: Mine Tuff Formation (Caryalho et al., 1976). Modified after Freire d'Andrade and Schermerhorn (1971).

are laterally equivalent, whereas AV₁-M and AV₁-ff are partly so; AV₁-M has been found under AV₂-ff at several locations. AV₂-mt and AV₁-ff interfinger peripherally with the Gaviao (SW) and Seixo (NE) Formations, which are dominantly sedimentary with minor dust tuffs and tuffites.

The SW Anticline is an isoclinal, asymmetric structure, linked to the Central Anticline through an equally tight syncline, the S. Joao Syncline.

Mineralization (Algares, Moinho, S. Joao do Deserto and Gaviao) extends for about 4 500 m in the SE-NW direction of the structures, with an 800 m gap between Algares and Moinho. Elsewhere along this lineament mineralization is essentially continuous, occurring on both flanks of the S. Joao syncline; intense deformation folded the sulphide lenticular bodies. Their original peripheral areas are presently close together, as subparallel vein like bodies dipping steeply to the NE and coalescing at depth. Hanging wall rocks are markedly tectonically displaced and thinned. This SW lineament of orebodies is therefore not appropriate for detailed genetic studies.

In contrast, the Feitais Anticline contains an elongated, once continuous ore zone nearly 1 700 m long (minimum length), the Feitais and Estacao orebodies lying on the normal, NE flank of the anticline, on top of a thick succession (~200 m, base not seen) of Mine Tuff, overlain by prominent bedded cherts and jaspers in turn overlain by

the PS phyllites and tuffites.

3.4 Base metal zonation in the Feltais orebody

The Feltais massive and stockwork sulphide orebody and its associated lithologies will be described in detail in Chapter 5 of this thesis; Figures 3.6 a to d illustrate the Cu, Zn, Pb and As abundances along 4 drillholes which transect the deposit (data from unpublished drillhole logs, Pyrites Alentejanas, 1963 to 1971). It is apparent that metal abundances vary widely, and that high grade domains are frequently intercalated in essentially massive pyrite. Zn and Pb are strongly covariant, Zn + Pb concentrations frequently exceed 15%, especially near the stratigraphic top of the massive orebody. Cu is generally low within massive ore, although locally abundant (as ore shoots) near its base, and especially within the footwall stockwork zone, where drillholes have often intersected many tens of metres of disseminated and stringer mineralization containing 3% Cu, intercalated in equally long barren domains. Stockwork Cu rich mineralization is invariably hosted in chlorite - quartz or chlorite - quartz - sericite rock, and the unmineralized intercalated sections are occupied by islands of volcanic rocks (Mine Tuff) indistinguishable from those occurring away from the sulphide orebody.

The data briefly outlined above shows that the

Figure 3.6a to d. Diagrams illustrating the variation of Cu, Zn, Pb and As abundances along drillholes transecting massive and stockwork ore, nearly at right angles with the massive ore lens. Zones where only Cu is reported are stockwork. Feitais orebody.

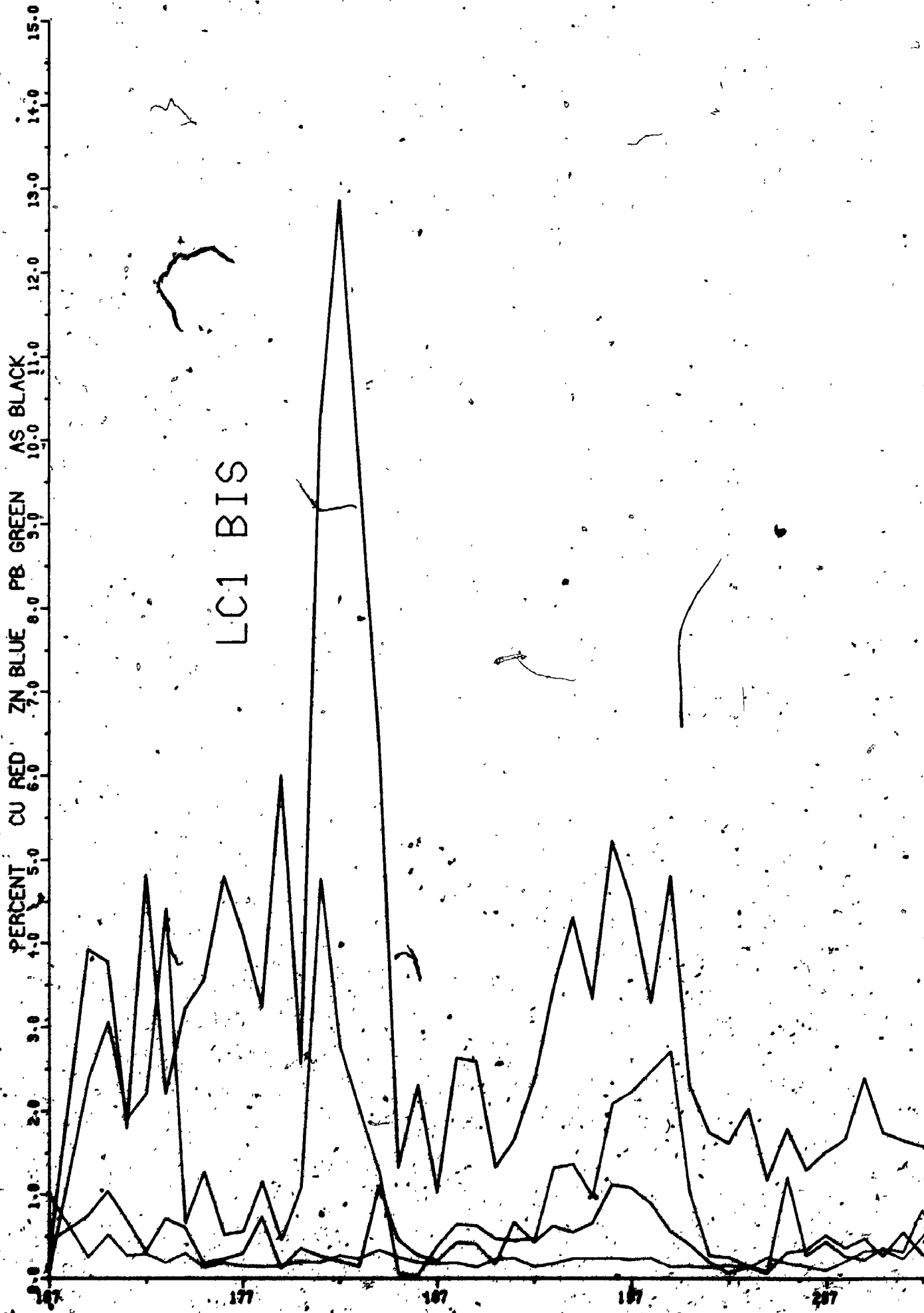
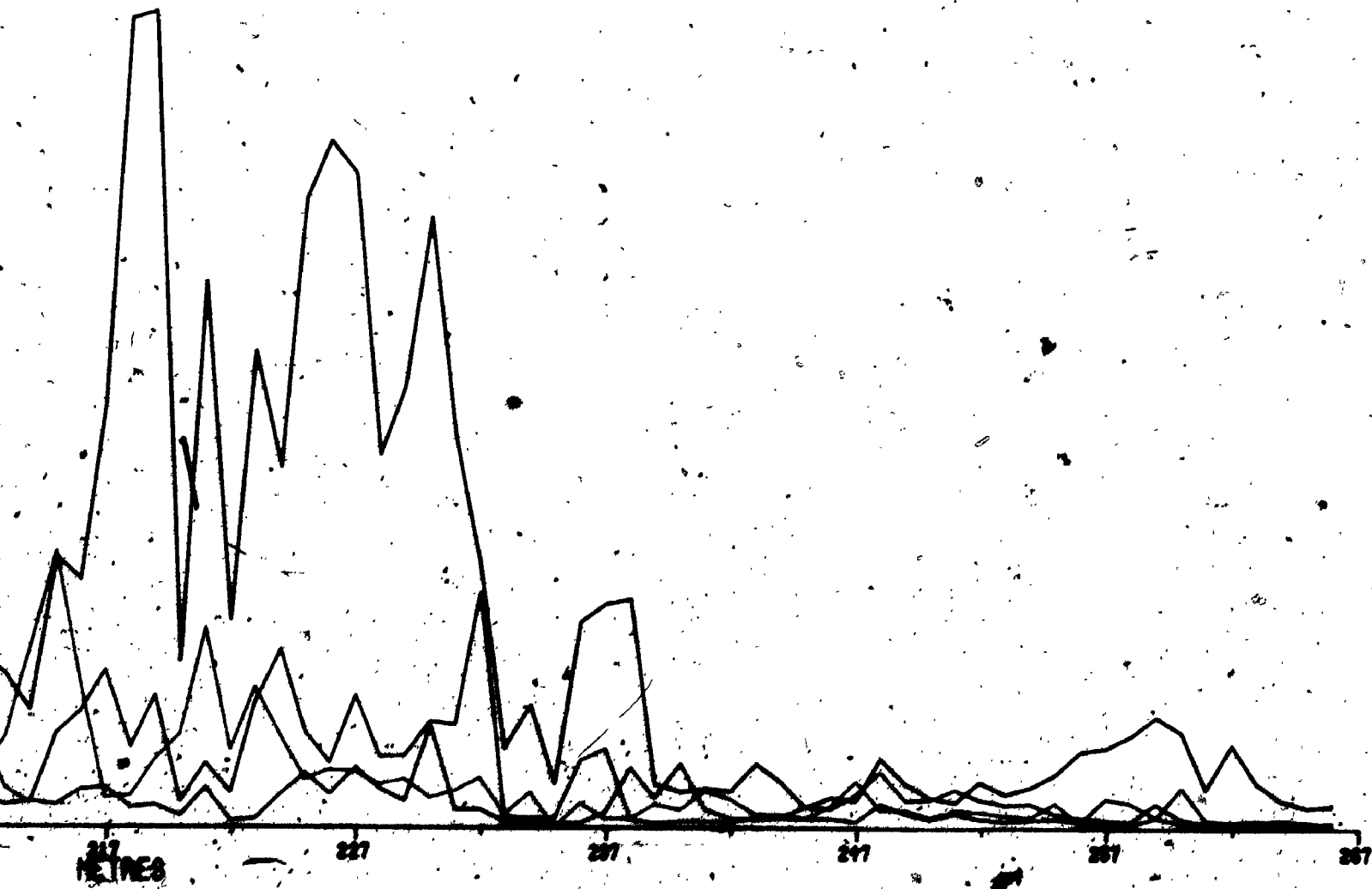
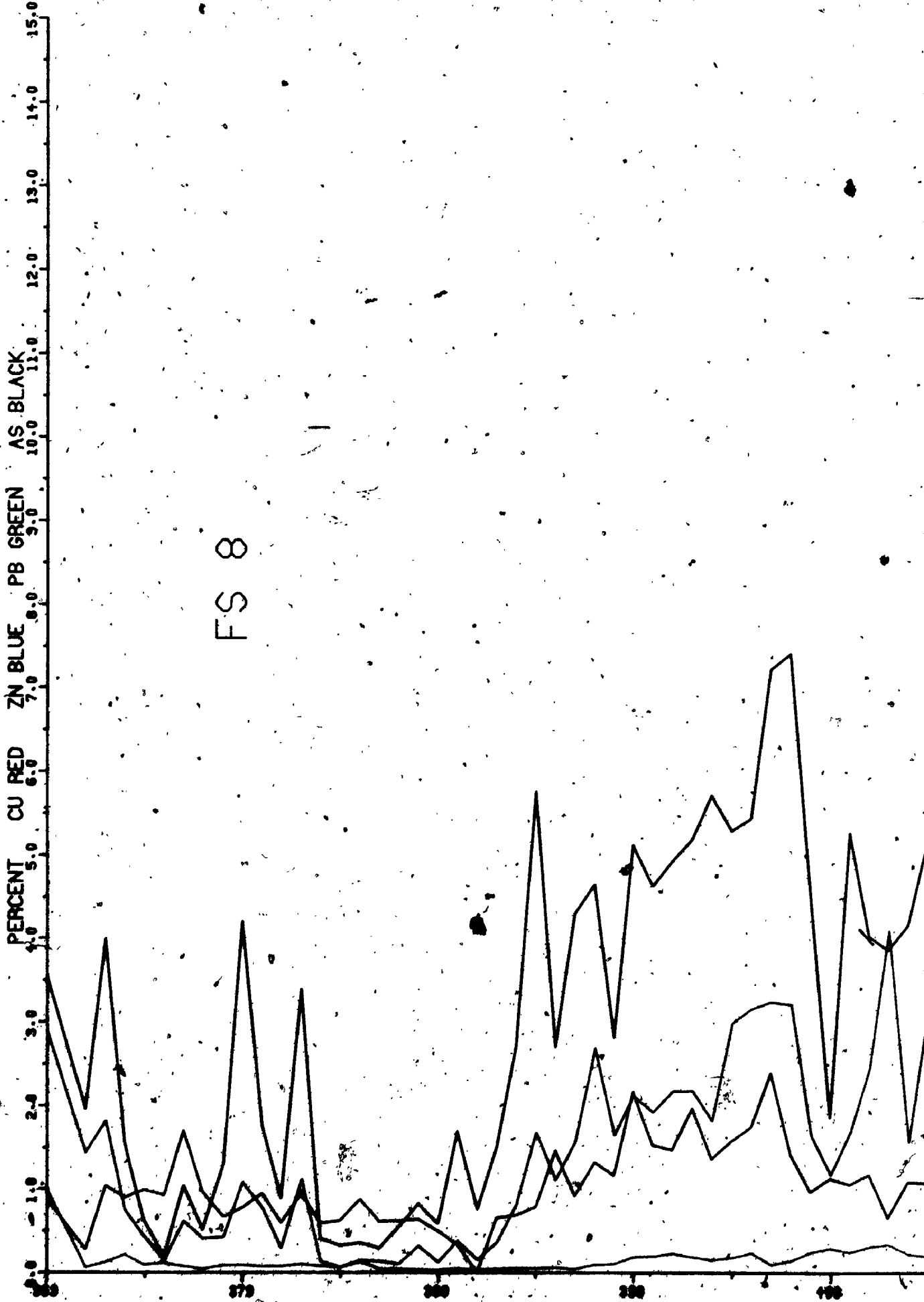


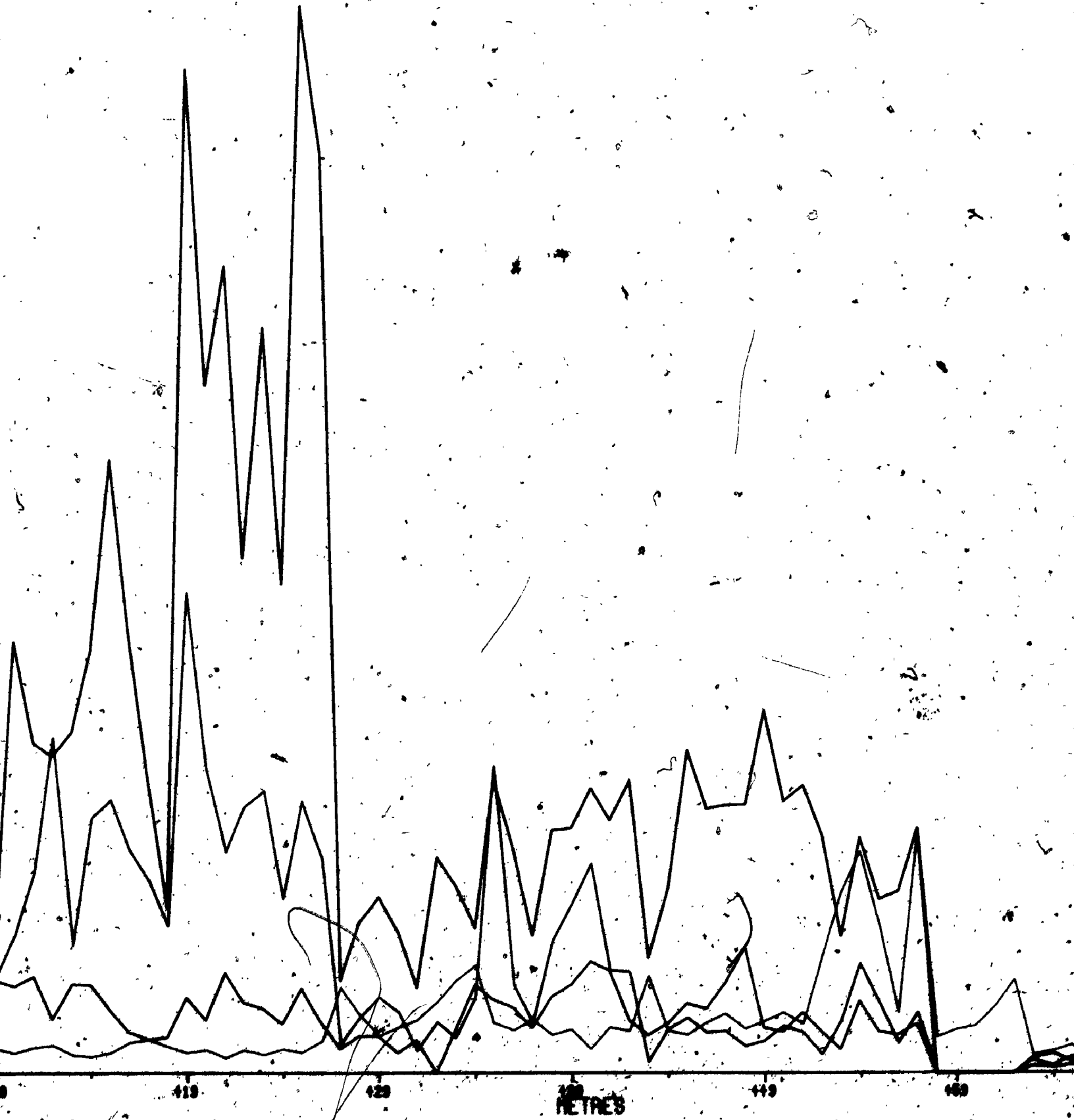
FIGURE 3 6 A



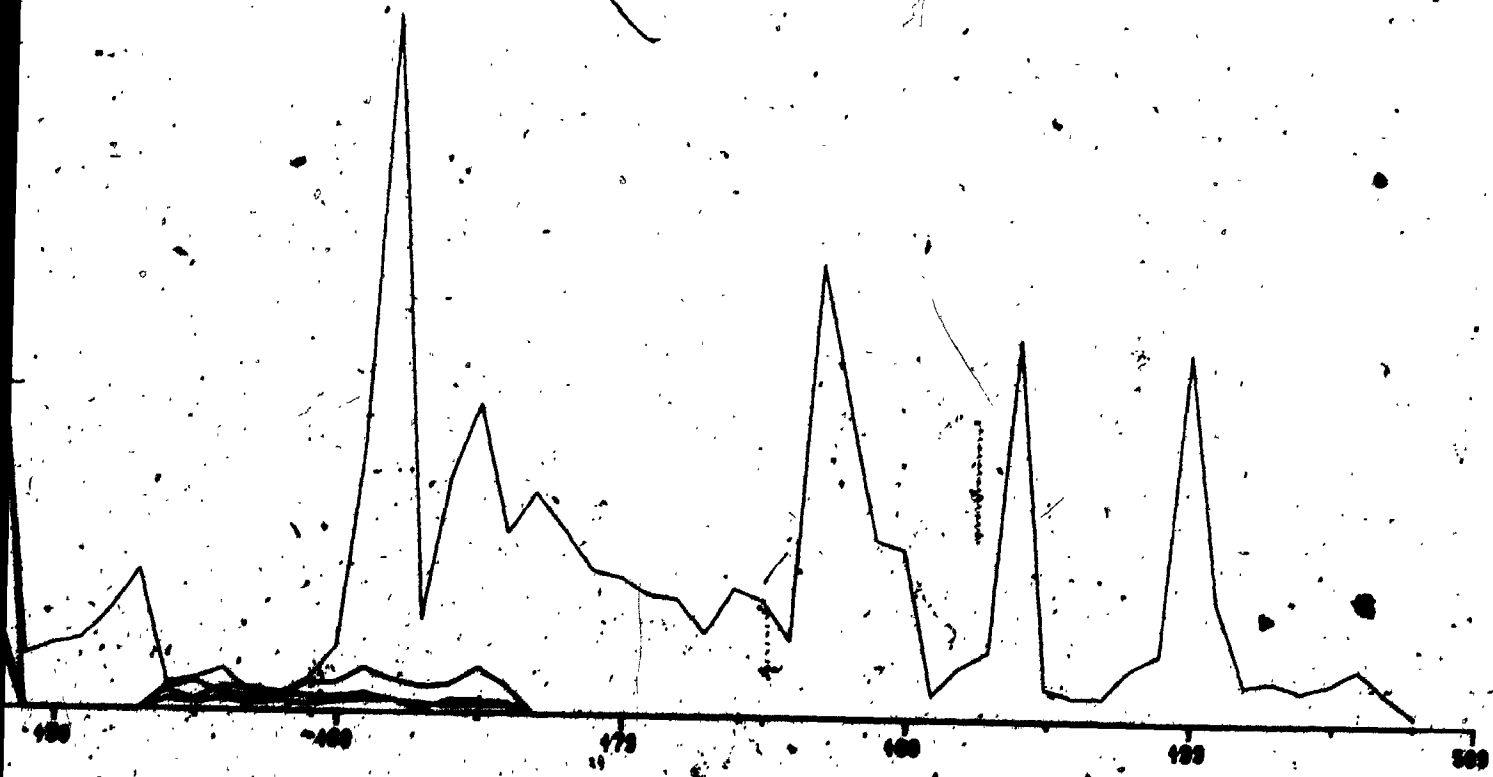
12 of 2



101 | FIGURE 3 6 B



120%



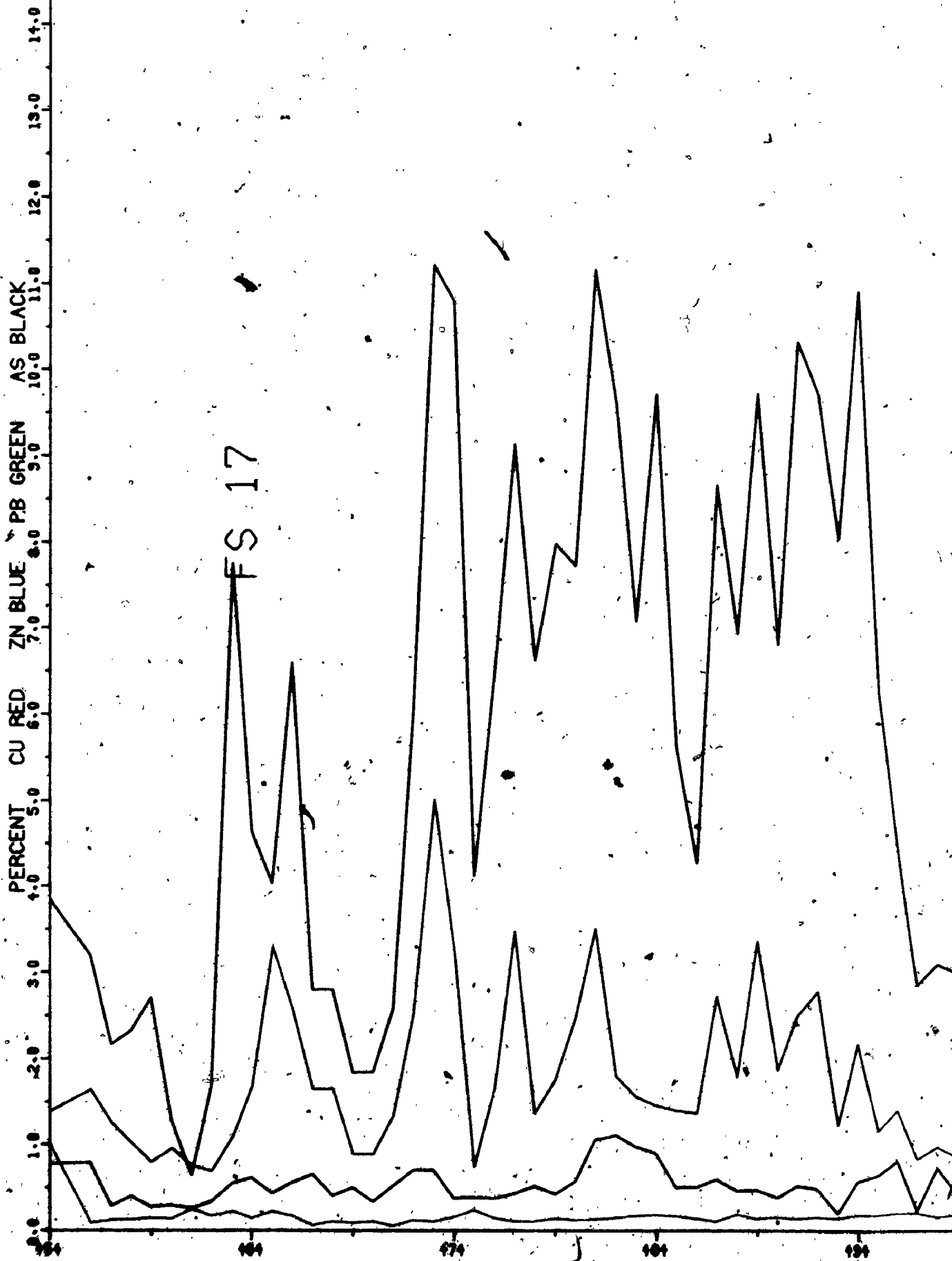
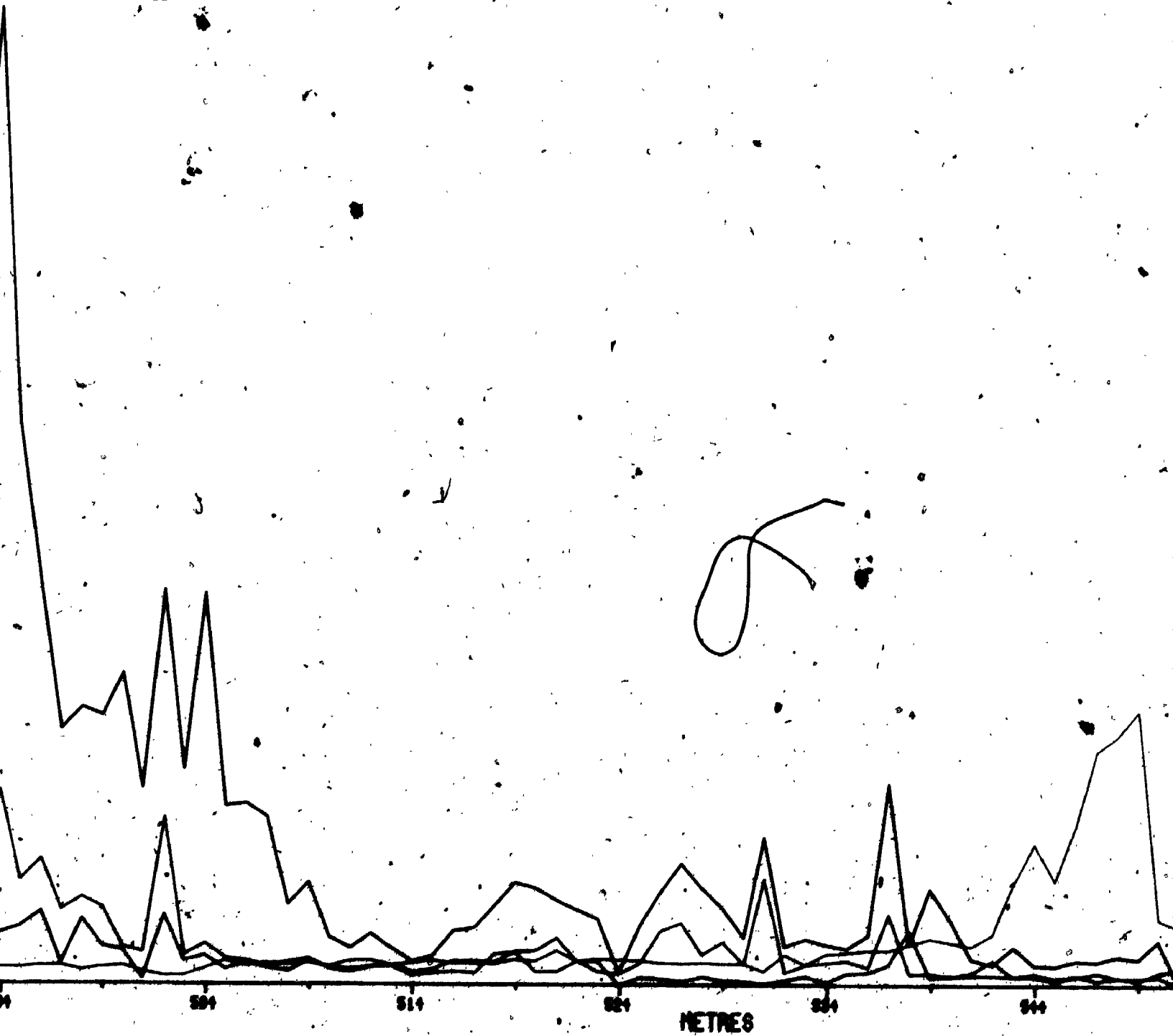
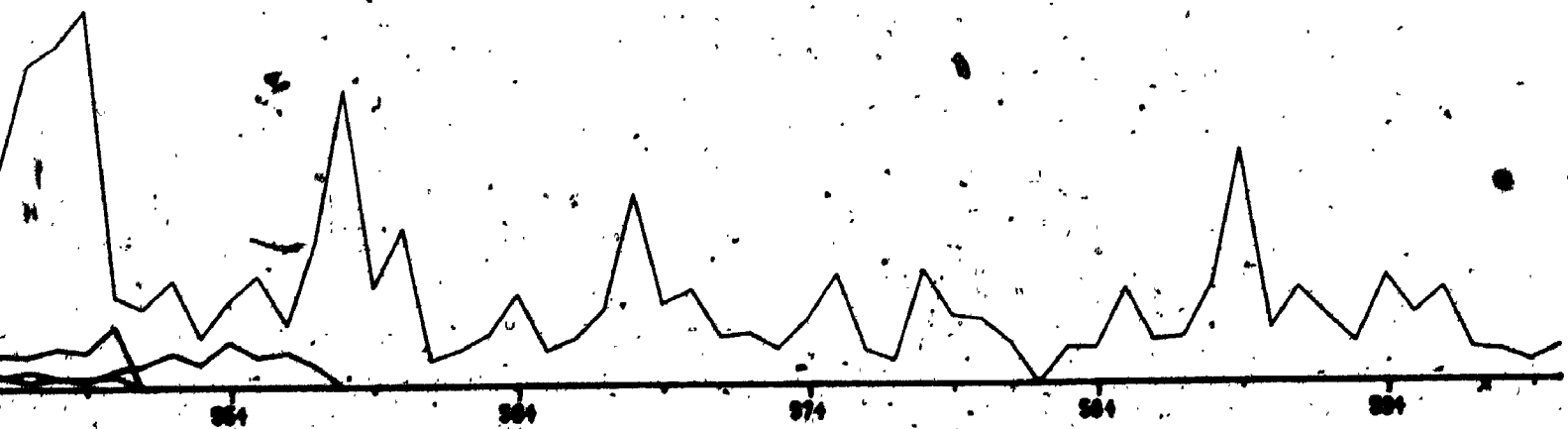


FIGURE 3 6 C

1/2



1207



| 3 of 3

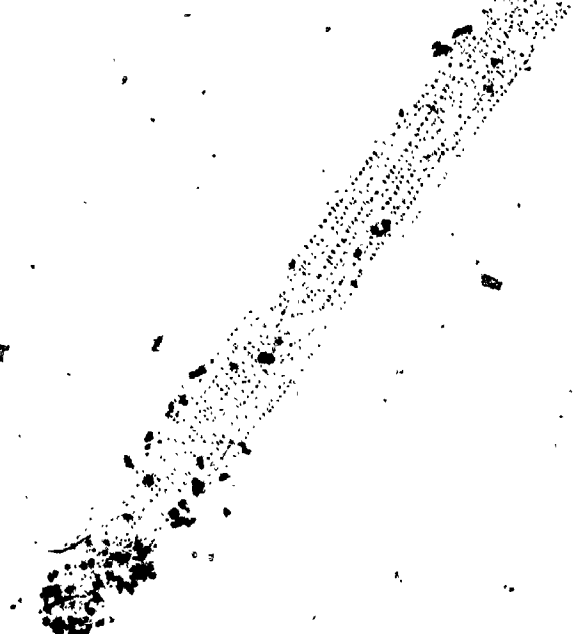
PERCENT CU RED ZN BLUE PB GREEN AS BLACK

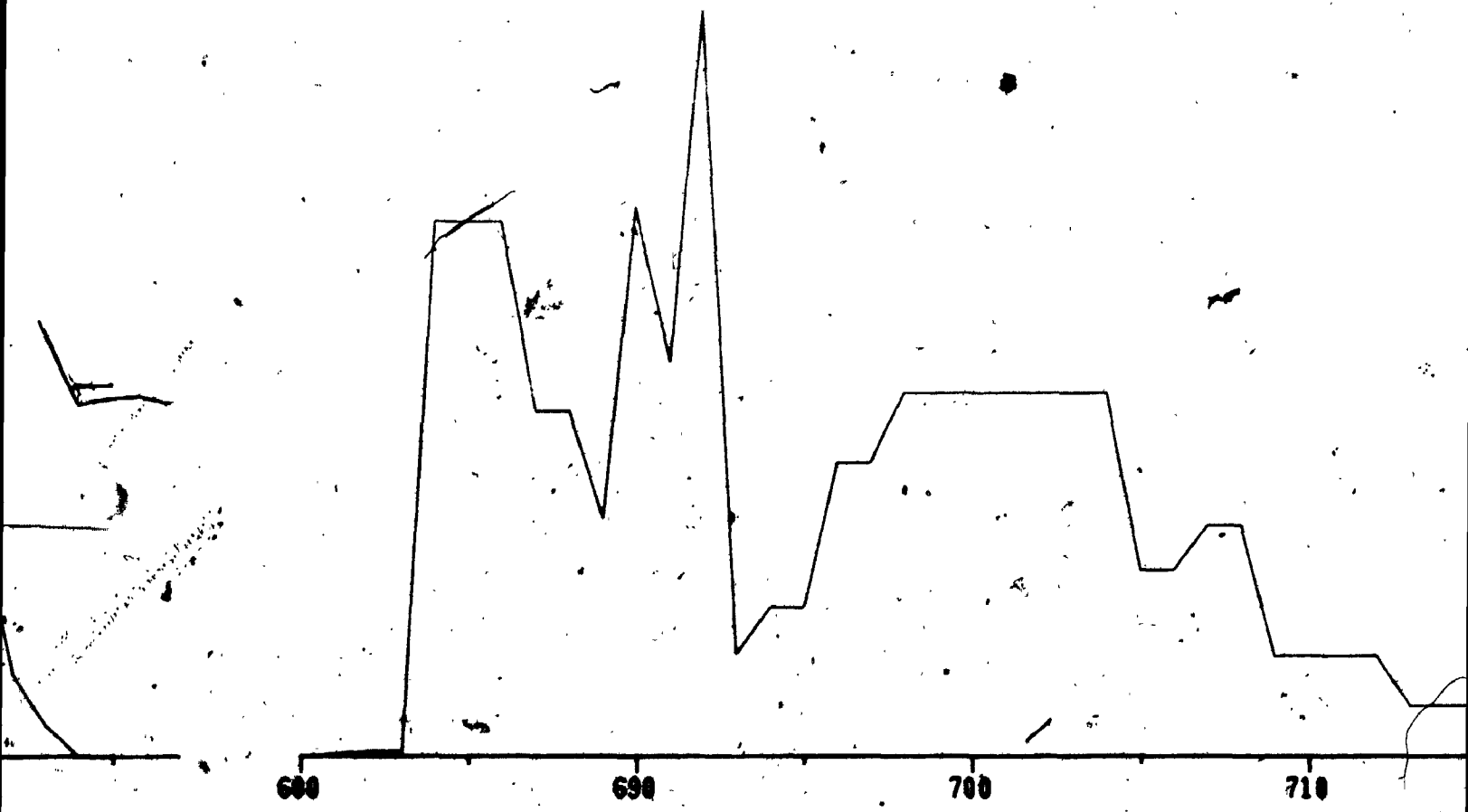
0.0 1.0 2.0 3.0 4.0 5.0 6.0 7.0 8.0 9.0 10.0 11.0

FS 22

500 510 520

FIGURE 3 6 D





1901

80

720
METRES

730

740

750

3 of 3

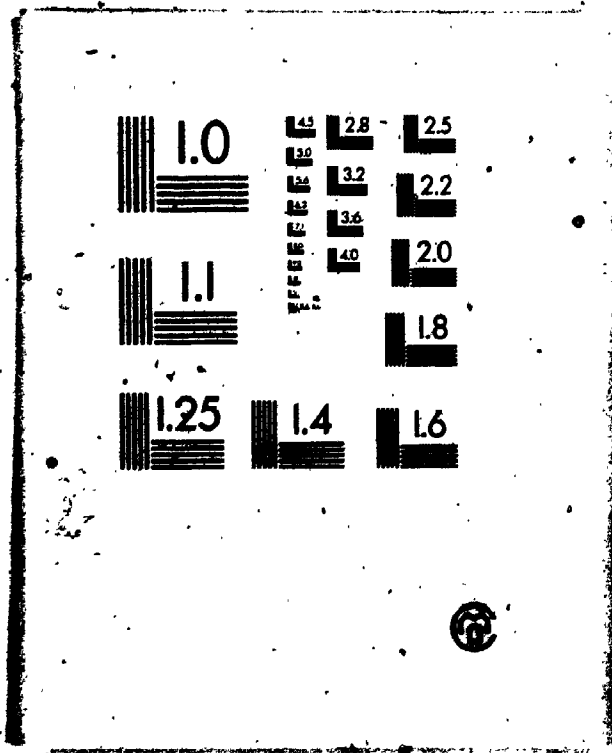
relatively low base metal grades listed in Table 3.1 are a consequence of averaging medium and even high base metal grades with the low base metal contents of vast pyritic domains of the sulphide deposit, which would not be considered ore in most other metallogenic provinces. Regarding the Cu rich stockwork zone, it is located mainly 400 to 700 metres below surface (see Appendix VI), and at the present time is not properly surveyed with regard to size and grade.

The prominent base metal zonation outlined above compares well to similar features of many other massive sulphide deposits (Hutchinson, 1973; Franklin et al., 1981) and is of particular interest to this study, as it shows that the metals were deposited along well defined physico-chemical gradients (see Chapter 5).

3.5 Concluding remarks

The Aljustrel Group rocks (including ores) were formed in the course of felsic, submarine, explosive volcanism which took place in Visean times and produced $>10^1$ km³ of pyroclastic rocks. These can be grouped as follows: a central unit of coarse quartz-eye tuffs (Megacryst Tuff and Green Tuff), flanked on either side by finer grained felsic tuffs devoid of quartz phenocrysts (felsitic, and feldspar phyric tuffs, named Felsitic facies and Mine tuff, and together Mine Tuff Formation). At the waning stages of

2



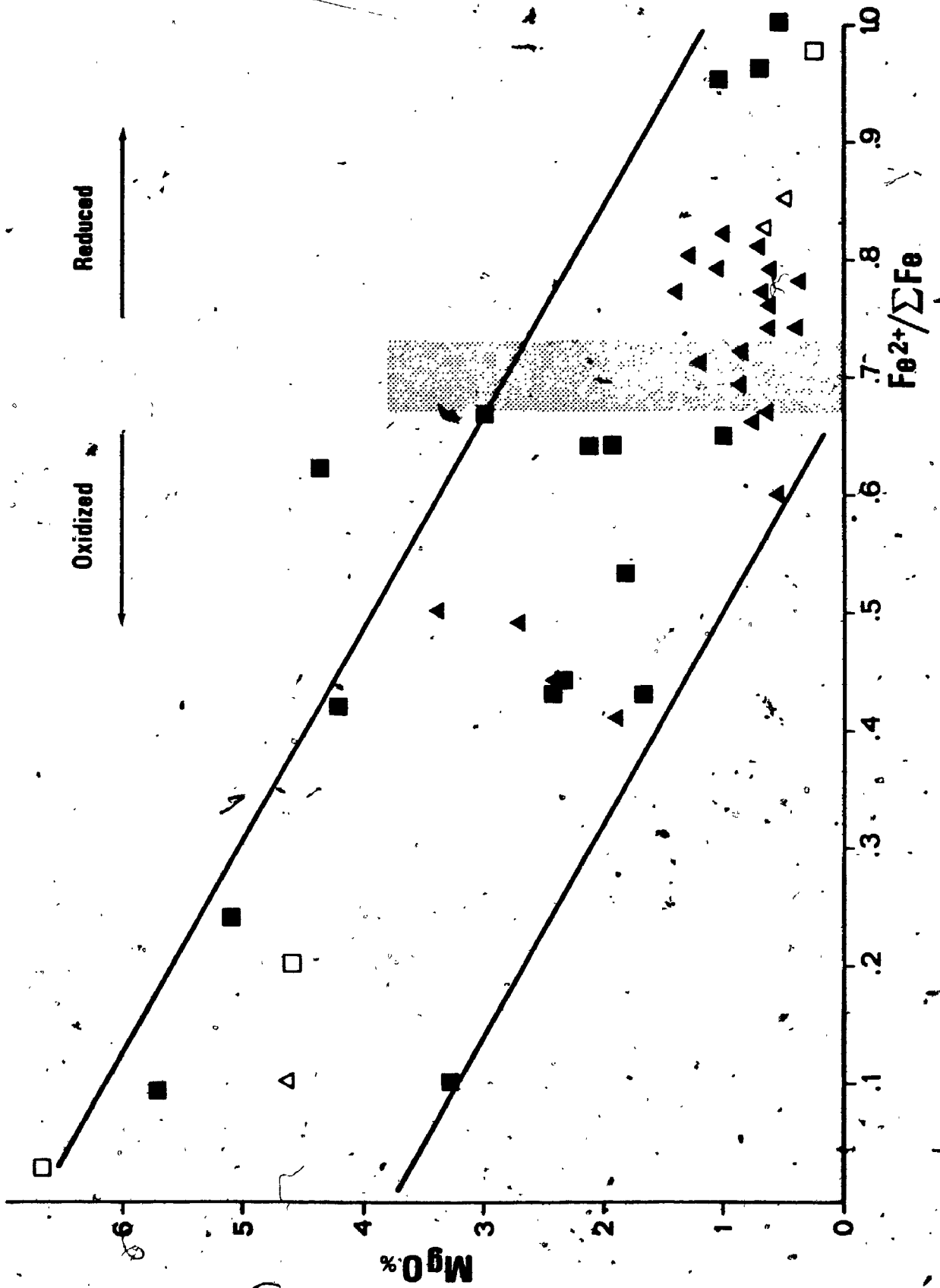
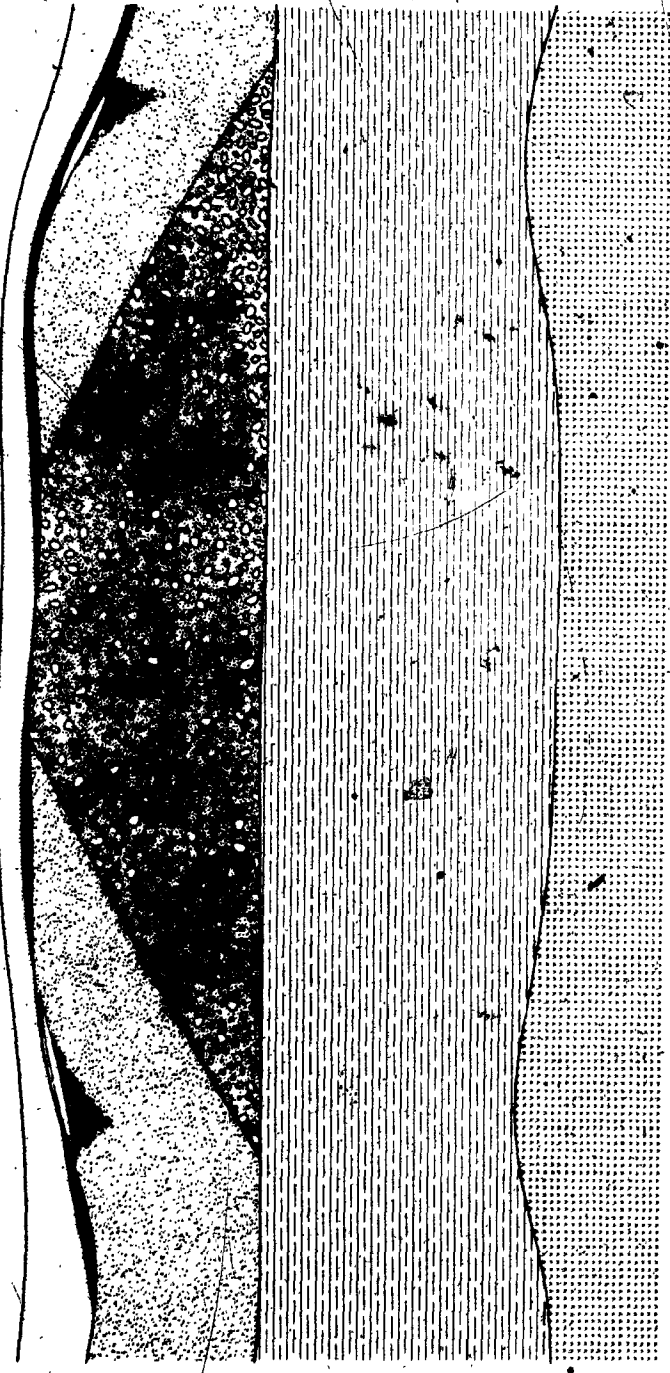


Figure 3.7. Schematic representation of the possible pre deformation relations between the various Aljustrel rocks. Magma chamber and Phyllite-Quartzite Group not seen.

3 - 5 Mins between orebodies

CULM GROUP
VOLCANIC-SILICEOUS COMPLEX
PHYLLITE-QUARTZITE GROUP
MAGMA CHAMBER



VS COMPLEX

Phyllites and tuffites | PS Fm
 Jasper and chert
 Massive sulphide ore
 Stockwork
 Mine Tuff
 Aljustrel Volcanics

restricted to one of the symmetrical halves of the system, given the structural differences previously outlined. For the sake of clarity Aljustrel volcanic rocks markedly affected by ore forming fluids will be described as part of the ore system (Chapter 5).

CHAPTER 4

THE ALJUSTREL VOLCANICS

4.1 Introduction

The main purpose of the present study of the Aljustrel Volcanic rocks was to find out whether or not had they been affected by sea water hydrothermal metamorphism and, if so, to evaluate the nature and extent of such phenomena and to delineate the history of the possible Aljustrel paleo hydrothermal system. In the course of work it became clear that the Aljustrel volcanic rocks had been far more metasomatized than anticipated. Part of the diversity detected by previous work in the area (see Chapter 3) does not reflect primary differences, it rather derives from large scale interaction with convectively circulated sea

water through the highly permeable submarine pyroclastic rocks. The data reported here supports a model for the origin and relations of the various Aljustrel Volcanic facies which is more detailed and somewhat different than those proposed by earlier authors, although rooted in their excellent geologic observations.

4.2 Petrography

The Aljustrel volcanic rocks are mostly composed of granular tuffs (Schermerhorn, 1975, 1976), characterized by a fragmental matrix composed of felsitic grains enclosed in an almost submicroscopic framework of sericite and felsitic matter + chlorite (Plate 1A, 1B). Felsitic grains vary in size (mostly 0.05 to 1 mm), shape (more or less rounded or lensoid) and composition (generally quartz-feldspar, sometimes feldspar + sericite), and can be closely packed together with only minor interstitial sericitic-felsitic "cement", or inversely this cement can predominate, generating a "dilute greywacke" texture (Schermerhorn, 1970b). Sericite in the cement depicts marked preferred orientation, parallel to the main cleavage (invariably present except in massive felsites). Recognizable cusped shards are rare.

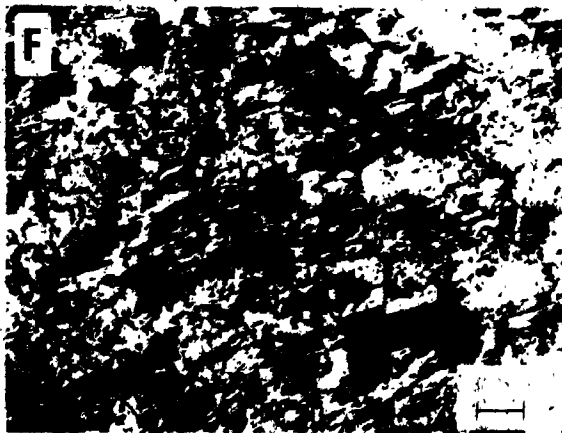
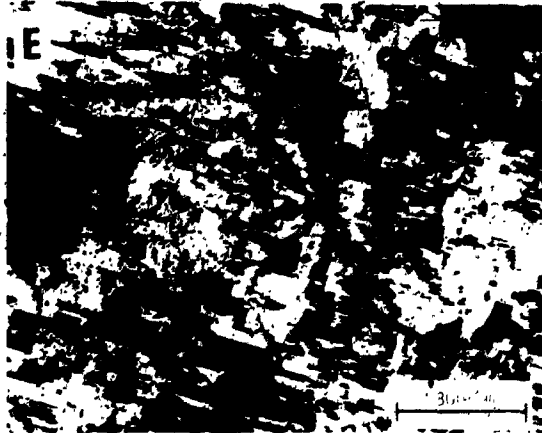
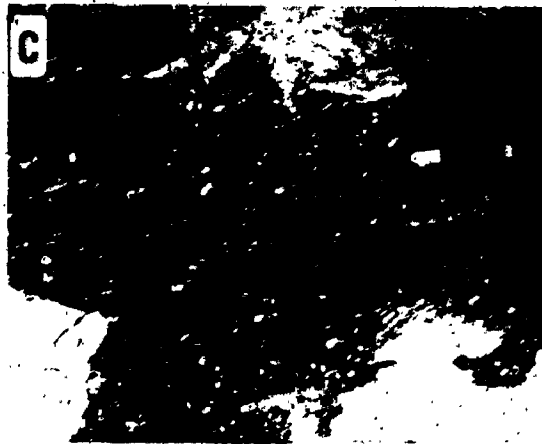
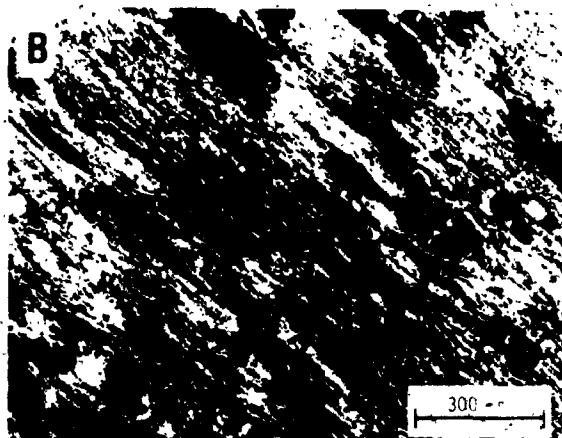
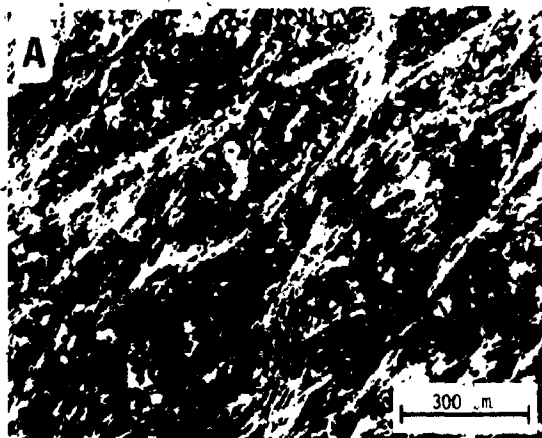
The granular matrix described above usually contains variable amounts of crystals and crystal fragments of several minerals, lithic fragments and larger devitrified

PLATE 1

(all scale bars 300 μ m)

- A. Tuff matrix (Quartz-eye tuff) dominated by grains of felsitic matter cemented by sericite. Crossed nicols.
- B. "Dilute greywacke" texture in tuff matrix (Mine tuff), dominated by a sericite-quartz-feldspar cement with sparse grains of felsitic matter. Crossed nicols.
- C. Megacryst facies of Quartz eye Tuff. Note preferred orientation of alkali feldspar megacrysts. Pen is 15 cm. long.
- D. Igneous albite phenocryst, intensely hydrolised into sericite and minor calcite, surrounded by metasomatic chessboard albite (QET). Crossed nicols.
- E. Chessboard textured albite (QET). Crossed nicols.
- F. Poorly developed crystal of chessboard albite, at the expense of tuff matrix. Green facies of QET. Crossed nicols.

PLATE 1



glass fragments. Variations in the nature, size and relative abundance of all these components distinguish the various Aljustrel tuffs. Carvalho et al. (1976) and Schermerhorn (1976) grouped the Aljustrel Volcanics in two main divisions, the Megacryst Tuff and Green Tuff "sequence" and the Mine Tuff Formation. We propose the designation "Quartz-eye Tuff (QET) Formation" to the former "sequence", and will use the designation Mine Tuff (MT) Formation in the same sense as those authors.

4.2.1 Quartz-eye Tuff

Quartz-eye tuffs are known to occur at Aljustrel in the Central Anticline, and under the Mine Tuff Formation rocks in the S. Joao Syncline and SW anticline (see Chapter 3), occupying a minimum volume of 2 km³. Schermerhorn (1976) described the petrography of these tuffs (Megacryst Tuff and Green Tuff), which are grouped here in view of their marked similarities, and on the conviction that many of the differences between the two main types (Megacryst Tuff and Green Tuff) are not primary igneous (see below).

Quartz-eye tuffs from Aljustrel are characterized by the invariable presence of abundant, randomly distributed quartz phenocrysts in a relatively coarse granular matrix (felsitic grains averaging 0.5 mm). These Quartz-eye tuffs always contain crystals of other minerals as well, especially alkali and plagioclase feldspars, but these

occur also in the Mine Tuff rocks, whereas quartz phenocrysts are rare or absent in Mine tuffs.

Quartz phenocrysts are subhedral to rounded, often broken, and attain 6 mm in diameter. In hand specimen they are somewhat bluish, and under the microscope they generally depict undulose extinction, deformation bands or even subgrains which do not affect the continuity of frequent fluid inclusion rows. Another prominent feature of these quartz phenocrysts is that they frequently contain corrosion embayments filled with microcrystalline quartz and felsitic matter. Quartz phenocrysts in the top layers of the QET (Green Facies, see below) often show partial replacement by chlorite and chlorite-sericite aggregates.

Feldspar crystals of various sizes, habits and compositions are also very frequent in Quartz-eye Tuff rocks. Some are true phenocrysts formed at the magmatic stage of the history of the rocks, but others are believed to have formed after emplacement of the rocks, during metasomatic, subsolidus events. We diverge from Schermerhorn (1976), who suggested that K feldspar megacrysts in the Quartz-eye tuffs of Aljustrel are an intratelluric phase.

Feldspar phenocrysts include Albite and/or Carlsbad twinned albite up to 8 mm in size, and less frequent (sometimes perthitic), microcline crystals, seldom larger than 2 mm. Feldspar phenocrysts are very often fragments

of euhedral crystals, and are nearly always mottled with unoriented or mosaic sericite inclusions; sometimes epidote (+ carbonate) inclusions are present, with or instead of sericite. Feldspar phenocrysts are often completely replaced by sericite flakes.

Alkali feldspar megacrysts are a frequent and striking feature of the Aljustrel Quartz-eye tuffs, as they can attain 4 cm in length and occur only a few cms apart from each other, with weak preferred orientation, often parallel or subparallel to rock cleavage (Plate 1C). Larger megacrysts are nearly always euhedral, and no isolated megacryst fragments were found; when disrupted by brittle deformation the resulting fragments lie close together. Smaller (down to a few millimetres) alkali feldspar megacrysts are usually more or less rounded, or globular elongated. They are composed of invariably fresh (apart from sporadic late stage replacement by coarse crystalline calcite) albite, K-feldspar, or both.

Alkali feldspar megacrysts often contain inclusions, of both tuff matrix and igneous phenocrysts. Tuff matrix inclusions vary in shape: they can be elongated, globular or irregular. Albite (igneous) phenocrysts included in alkali-feldspar megacrysts are invariably sericitized, and/or epidotized, with or without accompanying calcite (Plate 1D). Albite megacrysts are crystal-clear, frequently chessboard textured (Plate 1E). According to

Smith (1974, Vol. II, p. 278). "Chessboard albite is characterized by crystals containing many Albite twins whose lamellae consist of short plates on (010) which either wedge out or are abruptly truncated by (010). The plates are not of equal size and are not stacked in a lattice array. Nevertheless the parallelism of the (010) faces and the elongation along c tend to produce a rudimentary pattern which led to the name of chessboard albite". There is considerable controversy regarding the origin of chessboard albites (see Smith, op. cit.). Our observations suggest that chessboard albite megacrysts in the Aljustrel Quartz-eye tuffs are due to hydrothermal porphyroblastic growth, much in the same way as proposed by Battey (1955) for the chessboard albites in the New Zealand keratophyres. Plate 1F illustrates the development of chessboard albite from isolated patches of a full crystal, with remnants of tuff matrix left within the chessboard albite. Albite megacrysts not depicting chessboard textures (i.e., apparently untwinned) also occur. It is not known whether the lack of chessboard texture is real or simply hidden by orientation (sections parallel to 010).

Equivalent K-feldspar megacrysts also occur in the Quartz-eye Tuff, although they are much less abundant than albite megacrysts. They are morphologically indistinguishable from their albite counterparts, and under

the microscope they can easily be mistaken for non-chessboard albite, and vice-versa. In the course of the present study 43 samples of Quartz-eye tuffs including about 50 alkali feldspar megacrysts were studied under the optical microscope and extensively analysed by electron microprobe (see below). About 70% of the megacrysts are albite, 20% K-feldspar and only 4 samples contain intergrowths of both. At the scale of hand specimen these three types were never seen to coexist, and intergrowths in different crystals from the same sample, when present, contain approximately constant proportions of albite and K-feldspar. Intergrowths are due to replacement, K-feldspar replaces albite (Plate 2A), although the inverse cannot be ruled out (Plate 2B). Some of these replacement textures resemble patchy perthites. No true perthites were seen. Adularia (in the textural sense of the word) is sometimes present, both within veinlets and scattered in the tuff matrix (Plate 2C).

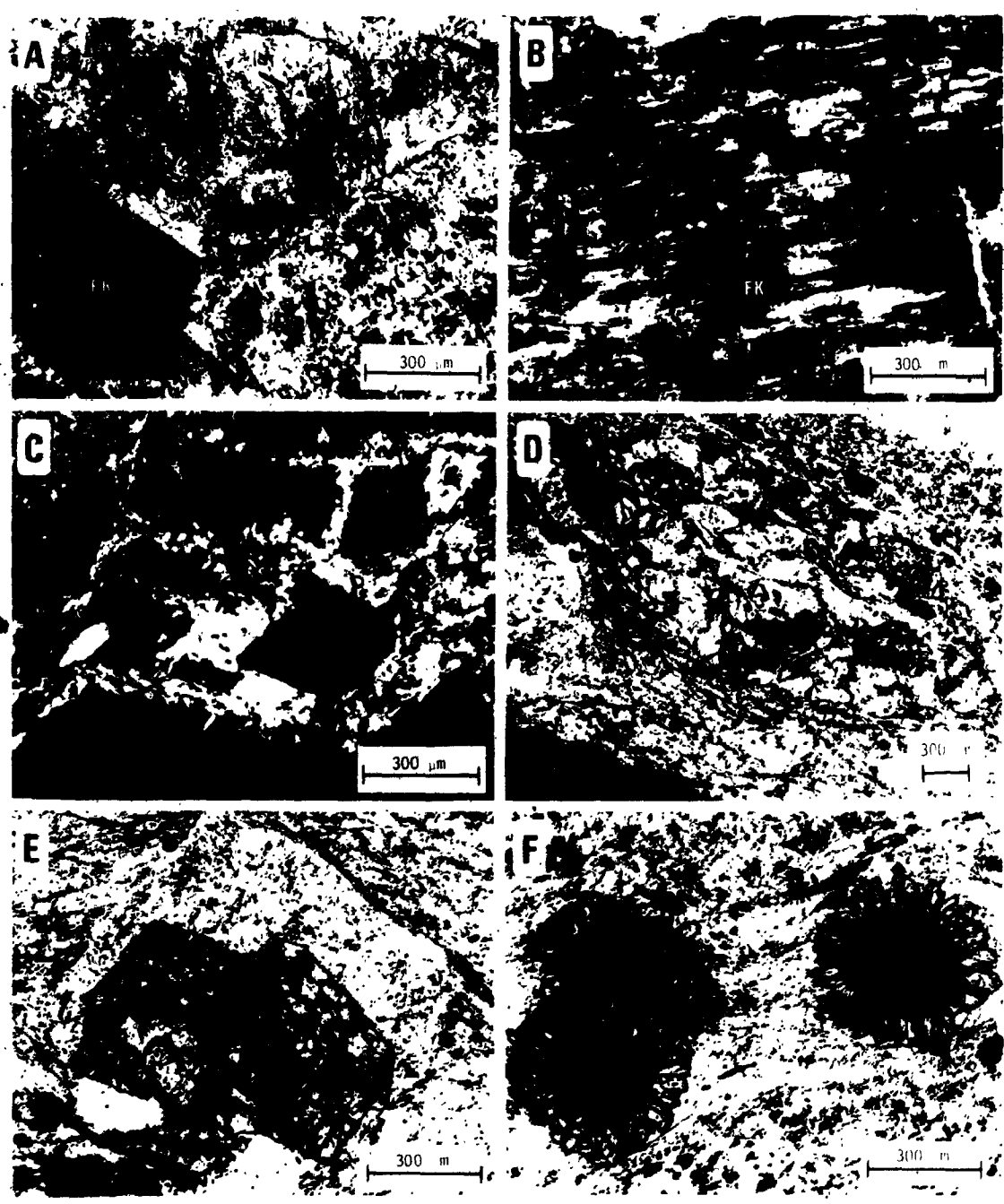
Alkali feldspar megacrysts were also studied by the 3 peak X-ray diffraction method (Wright and Stewart, 1968; Wright, 1968). Results are plotted in Figure 4.1, and show that the alkali feldspar megacrysts are composed of low albite and maximum microcline end members, in good agreement with the textural evidence for (hydrothermal) metasomatic origin. The paragenetic relations among the various feldspars are as follows:

PLATE 2

(all scale bars 300 μ m)

- A. Deeply altered igneous albite (lower right) surrounded by hydrothermal albite (AB) in turn partly replaced by K-feldspar (FK). QET. ~~Crossed nicols.~~
- B. "Islands" of chessboard textured albite in K-feldspar megacryst (FK). QET. Crossed nicols.
- C. Adularia (black) in vein in QET. Same sample as A. Crossed nicols.
- D. Almandine garnet-bearing lithic fragment in QET. One nicol only.
- E. Euhedral almandine garnet (partly replaced by chlorite) hosted in albite (igneous) phenocryst (QET). One nicol only.
- F. Allanite (dark) overgrown by clear radiating epidote. Green facies of QET, one nicol only.

PLATE 2



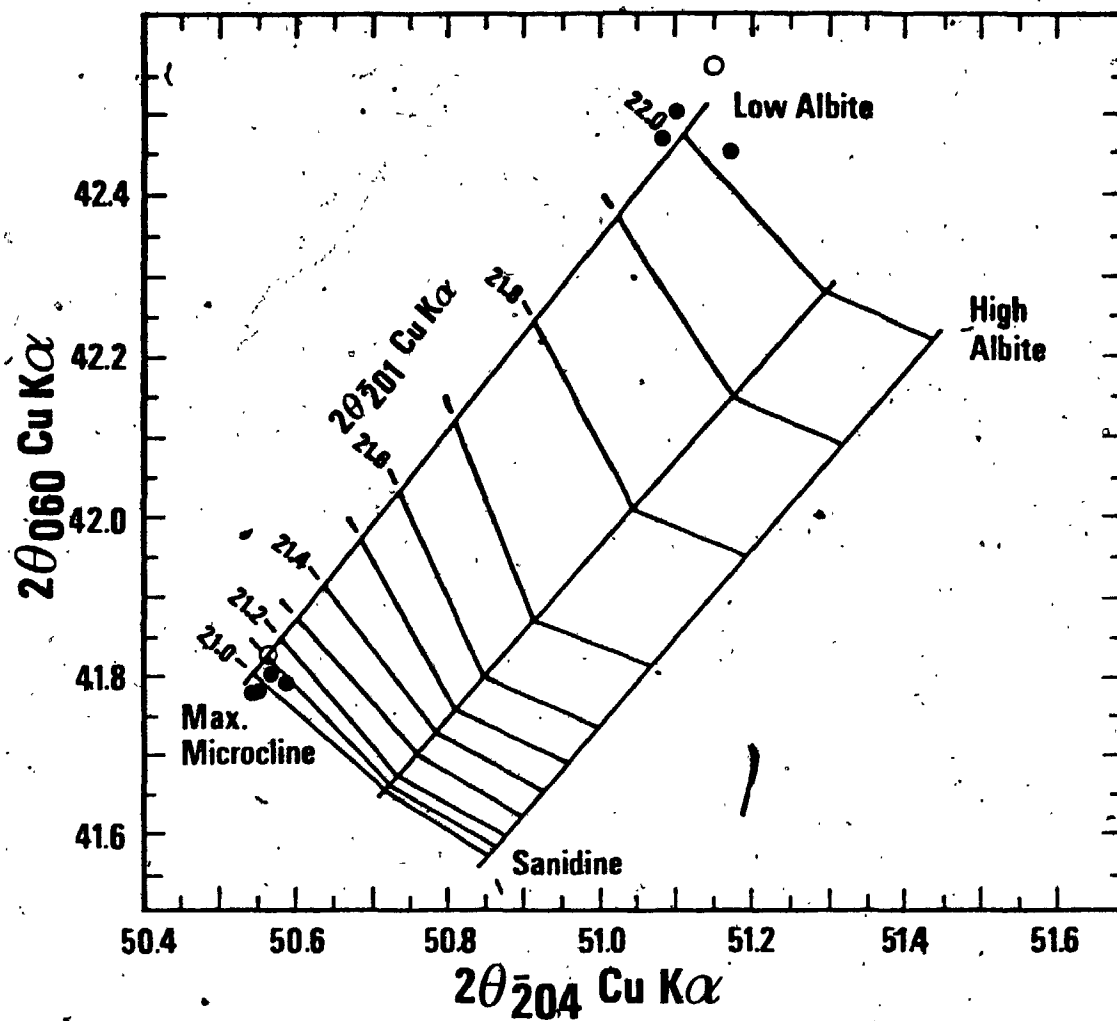


Figure 4.1. X-ray diffraction data for alkali-megacryst feldspars in the QET, illustrating that these are low temperature feldspars. Solid circles, coexisting albite and K-feldspar; open circles, one feldspar only in megacrysts.

Original (igneous)

Abundant albite phenocrysts

Minor microcline phenocrysts

Abundant albite and (?) K-feldspar in the matrix (or their glassy precursors)

Metasomatic

Early alteration of igneous albite (sericite, epidote, calcite)

Subsequent formation of metasomatic albite

Subsequent formation of metasomatic K-feldspar

Much smaller and scarcer crystals of biotite (?), garnet, zircon, apatite, allanite and Fe-Ti oxides. (containing sphene) also occur, as well as interstitial, poikilitic and overgrown secondary sericite, chlorite, epidote, calcite in often important amounts and very rare greenish brown stilpnomelane, sphene, pyrite, chalcopryrite and sphalerite. Fluorite occurs sporadically, especially as millimetric veins particularly abundant within the stratigraphic top of the Quartz-eye Tuff formation (vein spacings in the order of tens of metres).

Biotite (?) microcrysts are rare and completely altered into anomalous, mottled chlorite and opaque dust. Infrequent microcrysts of garnet occur mostly in lithic fragments (Plate 2D) and are totally or partially replaced by chlorite; fracture controlled partial replacement leaves angular fragments of completely fresh garnet (Plate 2E).

Allanite occurs as rounded or irregular rare microphenocrysts up to 0.7 mm in size, often overgrown by post tectonic euhedral radiating epidote (Plate 2F). Euhedral apatite (up to 0.5 mm long) and zircon are also frequent in QET rocks.

Fe-Ti oxides are also frequent accessories, both as microphenocrysts and as Ti-hematite minute scattered flakes. Their distribution varies strikingly from top to bottom in the Quartz-eye Tuff Formation, being one of the main causes of chemical zonation in the unit (see below). Thus in the uppermost tens of metres of the QET Formation (Green Tuff of previous authors) Fe-Ti rich phases occur as Ti-hematite + leucoxene + pseudobrookite microphenocrysts and also as abundant minute Ti-hematite flakes. Deeper seated QET rocks do not contain Fe-oxide flakes, and microphenocrysts do not include Ti-hematite or magnetite; instead, they are composed of ilmenite + sphene + leucoxene. Magnetite was not found in any Quartz-eye tuff, despite extensive, electron microprobe assisted searches.

Textural relations of the various Fe-Ti minerals in the QET are illustrated in Plate 3A, B and C. They are interpreted as representing primary igneous exsolution of Ti-magnetite, ilmenite and rutile, followed by oxidation in the top layers of the QET and Fe leaching in deeper seated domains, perhaps with recrystallization of immobile Ti as sphene through reaction with Ca and Si either directly from

PLATE 3

A,B. Opaque microphenocrysts found exclusively in Green facies rocks (uppermost QET and MT): ultra fine grained intergrown Ti-hematite + leucoxene + pseudobrookite ($Fe_2O_3.TiO_2$) rimmed by Ti-hematite. Note also minute flakes of Ti-hematite scattered in tuff matrix. It is believed that these minerals represent oxidation of primary igneous Ti-magnetite, rutile and ilmenite. QET, reflected light (oil immersion), one nicol only. Scale bars 100 μm .

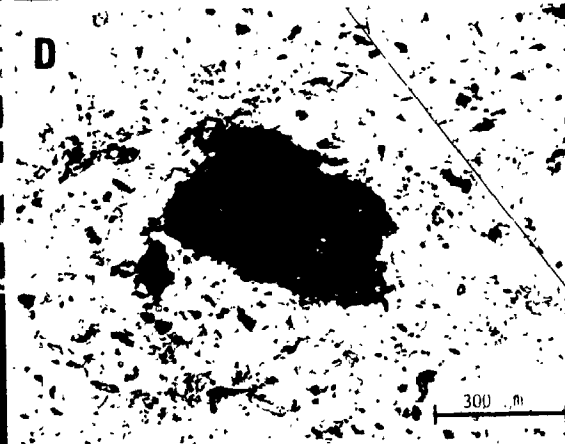
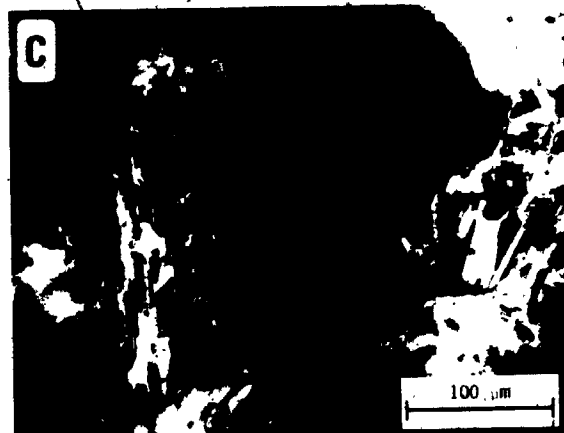
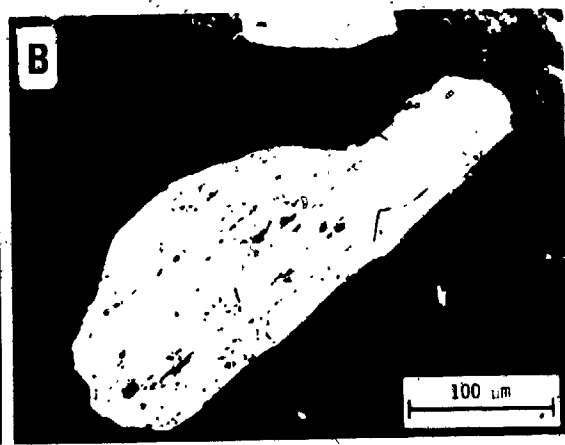
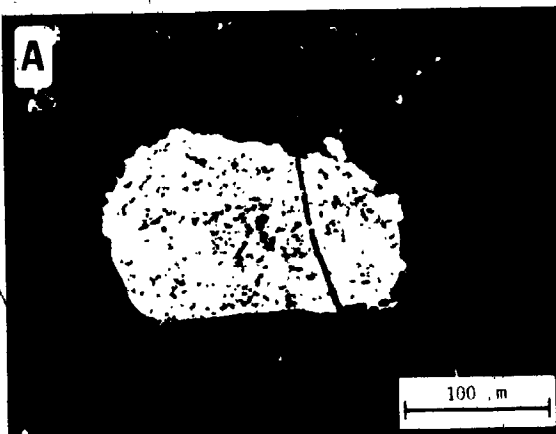
C. Typical opaque microphenocrysts occurring in Aljustrel volcanic rocks other than Green facies (deeper seated): leucoxene (white) + ilmenite (light grey) + sphene (dark grey). Note also the absence of opaque flakes in matrix. It is believed that this assemblage was obtained through Fe leaching of original igneous opaques identical to those of Green facies rocks. QET, reflected light (oil immersion), one nicol only. Scale bar 100 μm .

D. Accidental lithic fragment composed of finely banded quartz and hematite QET, one nicol only. Scale bar 300 μm .

E. Frayed end of "cherty quartz" lithic fragment, possibly formerly pumice. QET, one nicol only. Scale bar 300 μm .

F. Sericite (+ minor chlorite, medium grey) inclusion in QET, possibly a flattened former cusped glass shard. Subhedral white crystals are apatite. One nicol only. Scale bar 300 μm .

PLATE 3



solution or from neighbouring mineral phases. These changes can be summarized as follows:

Quartz-eye tuffs: Opaque Mineralogy

Top (Green facies, oxidized)	Original	Deep zones (reduced)
Ti-Hem flakes	Ti-Mag flakes	(Leached out)
Ti-hem + lcx + pseudobr intergrowths	Ilm + Ti-Mag + Rut intergrowths (Pyrite?)	Ilm + Sph + Lcx intergrowths Pyrite (sea water sulphur fixation) Fe oxides totally absent

Lithic fragments of sizes up to 10 cm are of frequent occurrence. They are mostly volcanic, although red chert fragments are also present. Finely banded quartz-Ti-hematite fragments of unknown origin were found in several samples (Plate 3D; compare with Ross and Smith, 1961, figure 87). Locally abundant irregularly lens shaped "cherty quartz" inclusions up to 5 cms long may correspond to former pumice fragments (Plate 3E; note frayed ends). Rarely some sericite-chlorite-felsitic matter aggregates stand out from the granular matrix of the tuffs, and resemble cusped glass shards (Plate 3F).

Megascopic zonation in the Quartz-eye Tuff Formation

Three varieties of Quartz-eye tuffs exist, defined essentially on the proportion of sericite + chlorite in the matrix and on the abundance of alkali-feldspar megacrysts. One of these varieties, the Green facies, could even be mapped separately from the remaining Quartz-eye tuffs (Schermerhorn and Stanton, 1969; Freire d'Andrade and Schermerhorn, 1971; See Figure 3.2) as its occurrence is restricted to a 0-50 m thick layer at the stratigraphic top of the Quartz-eye Tuff Formation.

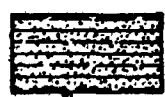
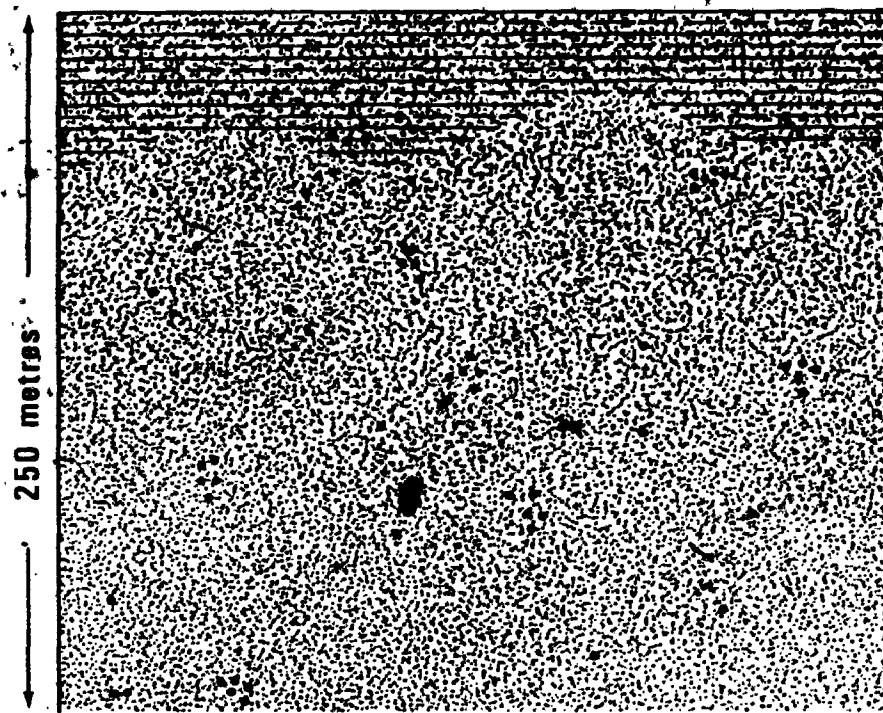
The Green facies is characterized by very abundant sericite and chlorite in the tuff matrix, and by the presence of scattered minute flakes of Ti-hematite. It may or may not contain feldspar megacrysts.

The Megacryst facies is characterized by a dominantly felsitic matrix and by the occurrence of abundant alkali-feldspar megacrysts. Ti-hematite flakes are absent. A third variety (unnamed) corresponds to the same rock as the Megacryst tuff when alkali feldspar megacrysts are absent. These two latter varieties occur intimately mixed. The spatial relationships of the various facies in the Quartz-eye Tuff Formation are schematically illustrated in Figure 4.2.

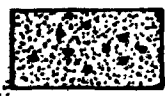
4.2.2 Mine Tuff Formation

Mine Tuff Formation rocks occur as two mutually

Quartz-eye Tuff



Green Facies



Megacryst Facies

Figure 4.2. Schematic representation of the spatial relations between facies in the Quartz eye Tuff.

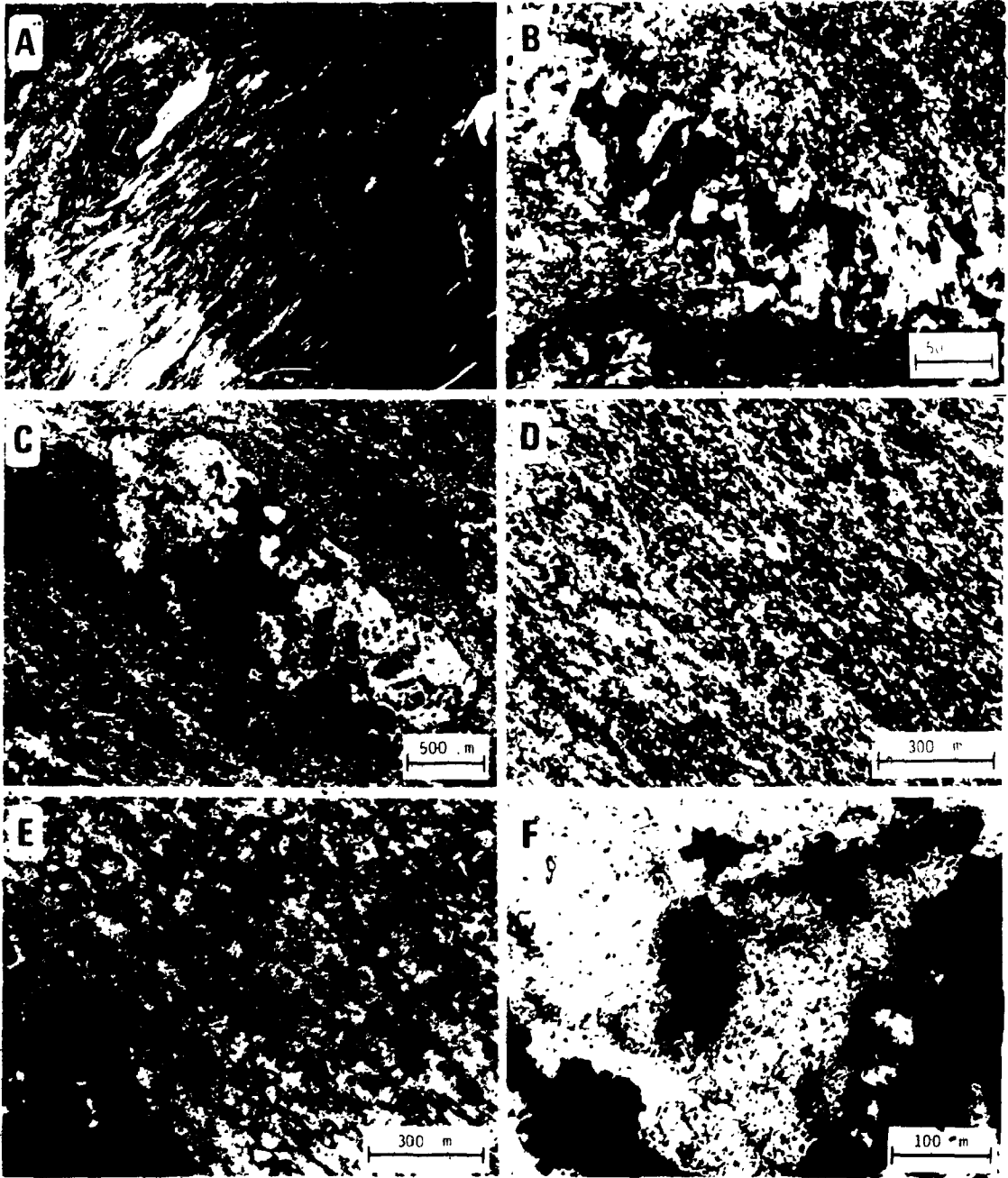
equivalent units flanking the Quartz-eye Tuff symmetrically to the SW and to the NE (see Chapter 3). Study of the Mine tuffs is complicated by the presence of the massive sulphide pre systems, with their striking and voluminous haloes of ore zone hydrothermal alteration, which extend far beyond the limits of sulphide mineralization itself. Ore zone hydrothermal effects are superimposed on earlier metasomatism markedly similar to that affecting Quartz-eye tuffs, and will be described separately (Chapter 5).

Large (metasomatic) alkali-feldspar megacrysts are also absent, although non-sericitized chessboard albite crystals (up to 0.5 cm) are sometimes present in Mine tuffs also. Furthermore, the granular matrix of Mine tuffs is generally finer grained than that of Quartz-eye tuffs and, probably as a consequence, the main cleavage is far more penetrative in Mine tuffs than in Quartz-eye tuffs (sometimes a second crenulation cleavage is also present in Mine tuffs). The Mine Tuff Formation is often well bedded, and includes layers (up to ~3 m thick) of massive felsites and felsophyres intercalated in the highly schistose, largely dominant granular tuffs. Bed thicknesses lie normally in the range of 0.5 to a few metres, but vary from a few centimetres to > 20 m. Graded bedding was not observed. Thin horizons of slabby breccias are known from near the top of the Formation (Plate 4A). Phenocrysts in Mine tuffs are essentially restricted to feldspar minerals,

PLATE 4

- A.. "Slabby" breccia at the top of the Mine Tuff (Feitais mine).
- B. Tectonic dilatancy vein filled with albite crystals, elongated normal to the vein walls. MT, crossed nicols. Scale bar 500 μm .
- C. Peripheral ore zone alteration in Mine tuff. Phenocryst is albite. Note high degree of alteration. There is abundant sericite both in phenocryst and in matrix, replacing formerly felsitic matter grains. One nicol only. Scale bar 500 μm .
- D.. Outer stockwork rock, composed of sericite + quartz + sulphides (feldspar completely absent). Crossed nicols. Scale bar 300 μm .
- E. Stockwork rock, composed of chlorite + quartz + sulphides. Note chalcopyrite (black)-quartz-chlorite vein (lower left). One nicol only. Scale bar 300 μm .
- F. Zircon surrounded by pleochroic haloes in chlorite. Both euhedral and anhedral (as an aggregate of extremely small individual grains) zircon is visible. Stockwork rock, one nicol only, scale bar 100 μm .

PLATE 4



dominantly albite with sporadic K-feldspar, always non-perthitic. Albite is often Albite and/or Carlsbad twinned, and almost invariably highly sericitized or epidotized, except when it occurs within tectonic dilatancy veins (Plate 4B), where it is believed to have reprecipitated after local diffusion of its components through pore fluids in the course of syntectonic pressure-solution.

Microphenocrysts and accessory small intratelluric crystals include Fe-Ti oxides, allanite and zircon, rather similar to those occurring in Quartz-eye tuffs (section 4.2.1). Fe-Ti oxides are markedly less abundant than in Quartz-eye tuffs. Biotite, garnet and apatite were not observed. Scattered and vein fluorite is present in lesser amounts than in the Quartz-eye Tuff.

Lithic fragments are restricted to ubiquitous small (from 2 cm down to matrix size) lenses of "cherty" quartz (probably former pumice), and to sporadic large (up to 20 cm) slabby fragments of Mine tuff cemented by Mine tuff itself, forming thin (up to 1 m) autobreccias (Plate 4A) which may have formed through disruption of the top of ash-flow beds caused by slope instability movements. Accidental lithic fragments were not observed.

Zonation in the Mine Tuff Formation

Two zonation patterns can be distinguished in the Mine Tuff Formation (Fig. 4.3): lateral zonation caused by the

Mine Tuff

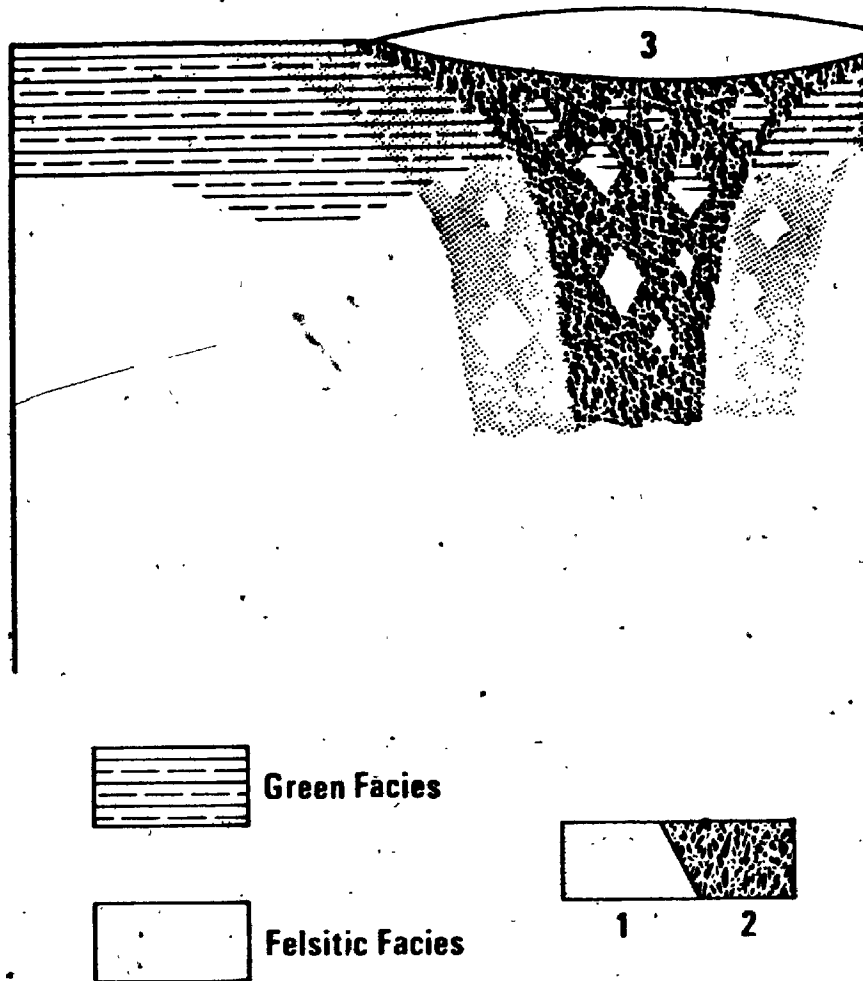


Figure 4.3. Schematic representation of the spatial relations between facies in the Mine Tuff.

sulphide ore systems (Chapter 5), and an earlier vertical zonation strikingly similar to that previously described in the Quartz-eye Tuff Formation, with an upper Green facies of Mine Tuffs approximately 0-50 m thick, also characterized by extremely abundant sericite and chlorite in the matrix of the tuffs. The Mine Tuff Green facies (the mine tuff rock of previous authors) is laterally equivalent to the Quartz-eye Tuff Green facies, and the two rock types are often closely similar, except for the absence or presence of quartz phenocrysts. Deeper seated Mine tuffs, however, are not strictly lateral equivalent to corresponding Quartz-eye tuffs, as Quartz-eye tuffs are frequently found stratigraphically under the Mine Tuff.

4.2.3 Paraiso Formation tuffs

Rare felsic and intermediate pyroclastic rocks are sometimes found intercalated within the (dominant) phyllites and tuffites, as discontinuous metric horizons. Apart from a few whole rock analysis (Appendix V-3), they were not studied in detail. Their occurrence indicates that weak proximal volcanic activity at Aljustrel persisted until PS times. The intermediate (andesitic) nature of some of these last erupted, volumetrically insignificant volcanic rocks probably reflects the development of important compositional zoning within the magma chamber (see Cox et al., 1979).

4.3 Geochemistry

4.3.1 Mineral chemistry

Comprehensive tables of representative electron microprobe analyses of the minerals discussed in this section are presented in Appendix II; selected analyses or averages are presented within the text.

a) Feldspars (Table 4.1)

Igneous phenocrysts are composed of albite with significant calcium contents (An 3-8 mole %), whereas (metasomatic) albite megacrysts are invariably almost pure albite (generally 0-1 An %), in good agreement with the textural and X-ray diffraction data indicative of different origins for each type. Matrix albite is generally very similar in composition to albite phenocrysts, suggesting that it may derive from glass devitrification.

K-feldspars replacing albite megacrysts or forming its own megacrysts are chemically indistinguishable and very similar also to typical vein adularia (of sporadic occurrence), or from (rare) matrix K-feldspar. BaO contents are generally significant, up to ~5 Celsian mole % (hyalophane).

The evidence presented here indicates that both albite and K-feldspar "megacrysts" are metasomatic porphyroblasts. The designation "megacrysts" is maintained, however, in view of the fact that it has been widely used in the Iberian Pyrite Belt literature to identify the

Table 4.1. Selected analyses of feldspars (see also Appendix I).

Unit Sample no.	QET 2-GF-87 1	QET GF-A 2	QET 4-GF-W 3	QET 4-GF-17 4	QET 4-GF-W 5	QET 4-GF-W 6	QET 2-FS-87 7
SiO ₂	66.90	67.07	68.68	63.86	63.37	64.60	64.57
Al ₂ O ₃	20.25	20.83	19.64	18.28	18.45	18.89	17.62
FeO	0.00	0.24	0.00	0.00	0.01	0.04	0.04
CaO	1.74	1.34	0.09	0.04	0.03	0.05	0.00
BaO	0.05	0.07	0.14	0.28	2.79	2.77	0.21
Na ₂ O	10.91	10.50	11.24	0.12	0.32	0.30	0.20
K ₂ O	0.07	0.08	0.14	16.39	14.99	14.93	16.93
TOTAL	99.92	100.14	99.86	98.96	99.96	101.67	99.57
Ions on the basis of 32 Oxygens							
Si	11.755	11.737	11.999	11.969	11.902	11.898	12.055
Al	4.194	4.296	4.044	4.035	4.082	4.121	3.877
Fe	0.000	0.035	0.000	0.000	0.004	0.004	0.006
Ca	0.328	0.251	0.017	0.008	0.008	0.012	0.000
Ba	0.003	0.005	0.010	0.020	0.207	0.199	0.015
Na	3.717	3.562	3.807	0.043	0.117	0.109	0.072
K	0.006	0.018	0.013	3.918	3.590	3.508	4.032
Σ	20.012	19.904	19.890	19.992	19.910	19.852	20.058
An%	8.09	6.54	0.44	0.20	0.20	0.31	0.00
Cs%	0.07	0.05	0.26	0.50	5.28	5.20	0.36
Ab%	91.69	92.86	98.96	1.08	2.98	2.85	1.75
Or%	0.15	0.47	0.34	98.22	91.53	91.64	97.89

1: Igneous Albite phenocryst. 2: Igneous Albite in tuff matrix. 3.: Chessboard Albite megacryst (hydrothermal). 4: K-feldspar megacryst. 5: Barium rich K-feldspar megacryst (hyalophane). 6: Coexisting Ba-rich vein adularia. 7: Vein adularia.

alkali feldspar porphyroblasts of the Quartz-eye Tuff Formation.

b) Fe-Ti Oxides and Sphene

Microphenocrysts composed of various Ti and/or Fe oxide minerals with or without closely associated sphene are of widespread occurrence within the Aljustrel Volcanic rocks (see section 4.2), being particularly abundant in Quartz-eye tuffs. A detailed electron microprobe investigation of these microphenocrysts was undertaken in order to clarify the reason for the marked whole rock variations in iron abundances and the remarkable constancy of TiO_2 within each of the Quartz-eye Tuff and Mine Tuff (see section 4.4).

Representative electron microprobe analyses of Fe-Ti oxides (+ Sphene) are presented in Tables 4.2, 4.3 and Appendix II-3.

Ti-hematite occurs exclusively in Green Facies rocks, both as scattered minute flakes and as part of microphenocrysts, with the latter intergrown with leucoxene and possibly with pseudobrookite ($Fe_2O_3 \cdot TiO_2$), and also rimming these intergrowths. Ti-hematite + leucoxene + pseudobrookite intergrowths are so fine grained that it was not possible to obtain electron microprobe analyses of any of the phases alone (typical electron beam diameter 5-10 μm). However, summations of the analyses of composite material approximate 100% when Fe is expressed as Fe_2O_3 ,

Table 4.2. Composition of Green Facies Fe-Ti Oxides. See Plate 3A, B, and Appendix II-3.

Sample No.	(a) PMTV-1	(a) PMTV-1	(a) PMTV-1	(b) PMTV-1
SiO ₂	0.50	0.76	0.57	1.05
TiO ₂	44.84	51.29	60.02	7.24
Al ₂ O ₃	0.17	0.32	0.08	0.56
Cr ₂ O ₃	0.08	0.24	0.05	0.04
Fe ₂ O ₃ ^{tot}	53.42	45.32	37.62	89.33
MnO	0.00	0.15	0.00	0.02
MgO	0.02	0.01	0.04	0.05
CaO	0.00	0.06	0.00	0.03
TOTAL	99.03	98.15	98.38	98.32
				ions on the basis of 3 oxygens
Si				0.027
Ti				0.142
Al				0.017
Cr				0.000
Fe ³⁺				1.755
Mn				0.000
Mg				0.002
Ca				0.001
Σ				1.945

(a) Ultra fine grained Ti-hematite + leucoxene
+ pseudobrookite

(b) Ti-hematite

Table 4.3. Representative composition of Ti-Fe rich microphenocrysts in Aljustrel Volcanic rocks (excluding Green facies). The analyses were obtained from the crystal in Plate 3C.

Sample no.	3-GF 1	3-GF 2	3-GF 3
SiO ₂	29.12	0.64	0.50
TiO ₂	33.60	52.60	99.13
Al ₂ O ₃	3.41	0.01	0.20
Cr ₂ O ₃	0.00	0.11	0.07
Fe ₀ ^{tot}	1.97	43.36	0.00
MnO	0.00	3.59	0.00
MgO	0.07	0.09	0.04
CaO	28.27	0.57	0.19
TOTAL	96.45	100.97	100.14
Ions on the basis of	4 Si	3 oxyg.	2 oxyg.
Si	(4)	0.016	0.007
Ti	3.471	0.984	0.989
Al	0.552	0.000	0.003
Cr	0.000	0.002	0.000
Fe ²⁺	0.226	0.902	0.000
Mn	0.000	0.076	0.000
Mg	0.014	0.003	0.001
Ca	4.161	0.015	0.003
		1.999	1.003

(1) Sphene; (2) Mn-Ilmenite; (3) Leucoxene

strongly suggesting that essentially all Fe present in these intergrowths is Fe^{3+} , in good agreement with the fact that Green Facies rocks are invariably characterized by low whole rock $\text{Fe}^{2+}/\Sigma\text{Fe}$ ratios (section 4.4).

In Aljustrel Volcanic rocks other than those belonging to the Green facies (i.e., all but the uppermost tens of metres of the Aljustrel Volcanics) there is no counterpart to the Ti-hematite dust scattered within the matrix of Green facies rocks, and Ti-rich microphenocrysts, morphologically indistinguishable from their Green facies counterparts are composed of leucoxene, Mn-ilmenite and/or sphene (Table 4.3). The internal texture of these microphenocrysts is more varied than that found in Green Facies tuffs, and lamellar, coarser exsolution textures are often found; this difference (if real: most rocks studied are not Green Facies tuffs) may be due to quenching of the upper levels of volcanic rocks.

MnO contents in ilmenite are remarkably high, up to 13.46 (see Appendix II-3). Sphene shows considerable substitution of Ti by Fe and especially Al, up to ~30% Al occupancy of the Ti structural sites. The chemistry of the Aljustrel sphenes is similar to that of sphenes from mafic volcanic rocks elsewhere in the Iberian Pyrite Belt (Munha, 1981), and their occurrence is also similar, both replacing Fe-Ti oxides microphenocrysts and as anhedral, often vein contained aggregates. Regarding "leucoxene", it is not

known which TiO_2 polymorphs are actually present. The occurrence of leucoxene + sphene (without Fe rich phases) totally replacing former Fe-Ti oxides microphenocrysts suggest that leucoxene in these rocks may result from Fe leaching, and reprecipitation of immobile Ti as sphene and leucoxene (perhaps directly from rutile). Finally, it is noteworthy that, despite much effort magnetite was not found in any Aljustrel volcanic rocks (except when related to sulphide mineralization).

c) Garnet (Table 4.4 and Appendix II-4)

Garnet relicts occurring in Quartz-eye tuffs are rather constant in composition: they are almandines with 10-15% pyrope mole % and minor amounts of spessartine and grossular. Structural formulas were calculated taking into consideration that $M^{4+} = 3/2 M^{3+} = M^{2+}$. This procedure suggests that all Fe is present as Fe^{2+} . The occasional introduction of small amounts of H_4 is probably not real, rather reflecting the possible presence of small quantities of Ti (not analysed). End member molecules were subsequently computed following the procedures of Rickwood (1968).

The composition of these garnets is compatible with either an igneous or high grade metamorphic origin (see Meagher, 1980). No high grade (amphibolite or granulite facies) metamorphic event affected the Aljustrel Volcanics, but the almandine garnet may have survived the partial

Table 4.4. Averages of analyses of closely similar almandine garnets from Quartz eye tuffs.

Sample no. of analyses	GF-15.8 7	3-GF 9	4-GFW 6
SiO ₂	36.95	36.93	36.77
Al ₂ O ₃	20.99	21.26	21.35
FeO	36.67	35.33	36.34
MnO	1.72	1.12	1.68
MgO	2.27	3.69	2.32
CaO	0.99	1.06	1.02
TOTAL	99.59	99.39	99.48
Ions on the basis of 24 Oxygens.			
Si	6.009	5.931	5.954
H ₄ (calc.)	0.000	0.069	0.046
Al	4.023	4.024	4.075
Fe ³⁺	0.000	0.000	0.000
Fe ²⁺	4.987	4.745	4.921
Mn	0.237	0.152	0.230
Mg	0.550	0.883	0.560
Ca	0.173	0.182	0.177
Σ	15.979	15.988	15.963
Pyrope %	9.36	15.05	9.41
Spess.	3.94	2.43	3.96
Hydrogros.	0.00	0.97	0.99
Grossular	2.96	1.94	1.98
Almandine	83.74	79.61	83.66
% Cati. allocated	99.33	99.46	98.50

melting event that probably generated the Aljustrel magmas (see below). This hypothesis is somewhat supported by the occurrence of the almandine crystals within lithic fragments.

d) Chlorites

Electron microprobe analyses of the chlorite minerals from the Aljustrel volcanic rocks are presented in Table 4.5 and Appendix II-5 and plotted in Fig. 4.4. They are almost exclusively ripidolites, as a consequence of relatively constant Si and Al contents. Fe-Mg variations are much more pronounced, with FeO contents ranging from nearly 41 to 18 wt % and MgO contents varying correspondingly from less than 5 to more than 19 wt %. Despite the fact that individual chlorite analyses were performed in grains from the matrix, and replacing garnet, feldspars and biotite, no significant compositional variations were found at the scale of the hand specimen.

Green facies rocks of both the Quartz-eye Tuff and the Mine Tuff invariably contain the more magnesian chlorites analysed. Thus Mg in chlorite is generally proportional to the abundance of chlorite in the rocks (section 4.2) and to the whole rock absolute abundances of both Mg and Fe, and also to the relative abundance of Fe^{3+} in the rocks (see section 4.3.2). No obvious primary igneous petrologic reasons exist for this stratigraphically controlled systematic variation in the Fe-Mg ratio in chlorites. The

Table 4.5. Averages of the compositions of closely similar chlorites from representative Aljustrel Volcanics (see also Appendix II-5).

Unit Sample no. of anal.	Green facies						
	QET 2-GF-87 3	QET 6-GF-17 3	QET GFA 3	QET MD4F 4	QET PMTV-1 6	MT bis-330 6	MT bis-341.8 4
SiO ₂	23.54	23.06	24.08	24.36	26.51	27.68	27.93
TiO ₂	0.02	0.01	0.00	0.00	0.00	0.00	0.00
Al ₂ O ₃	19.87	20.75	19.87	21.26	21.74	19.61	19.07
FeO	40.74	37.22	35.64	30.69	18.03	20.14	20.17
MnO	0.38	0.29	0.27	0.43	0.16	0.40	0.71
MgO	4.71	5.54	7.87	10.37	19.12	19.30	19.38
CaO	0.02	0.06	0.02	0.02	0.00	0.02	0.00
BaO	0.04	0.05	0.05	0.00	0.00	-	0.06
Na ₂ O	0.06	0.00	0.01	0.00	0.03	0.00	0.00
K ₂ O	0.00	0.00	0.00	0.00	0.01	0.01	0.00
TOTAL	89.38	86.98	87.81	87.13	85.60	87.16	97.32
Ions per 14 Oxygens							
Si	2.663	2.653	2.695	2.668	2.745	2.849	2.876
Al	1.337	1.347	1.305	1.332	1.255	1.151	1.124
Al	1.312	1.447	1.316	1.413	1.398	1.228	1.190
Ti	0.002	0.001	0.000	0.000	0.000	0.000	0.000
Fe	3.855	3.556	3.336	2.811	1.561	1.734	1.737
Mn	0.036	0.028	0.026	0.040	0.014	0.035	0.062
Mg	0.794	0.943	1.313	1.693	2.951	2.961	2.975
Ca	0.002	0.007	0.000	0.002	0.000	0.002	0.000
Ba	0.002	0.002	0.002	0.000	0.000	-	0.002
Na	0.013	0.000	0.002	0.000	0.006	0.000	0.000
K	0.000	0.000	0.000	0.000	0.001	0.001	0.000
Σ	10.017	9.967	9.995	9.959	9.932	9.962	9.967

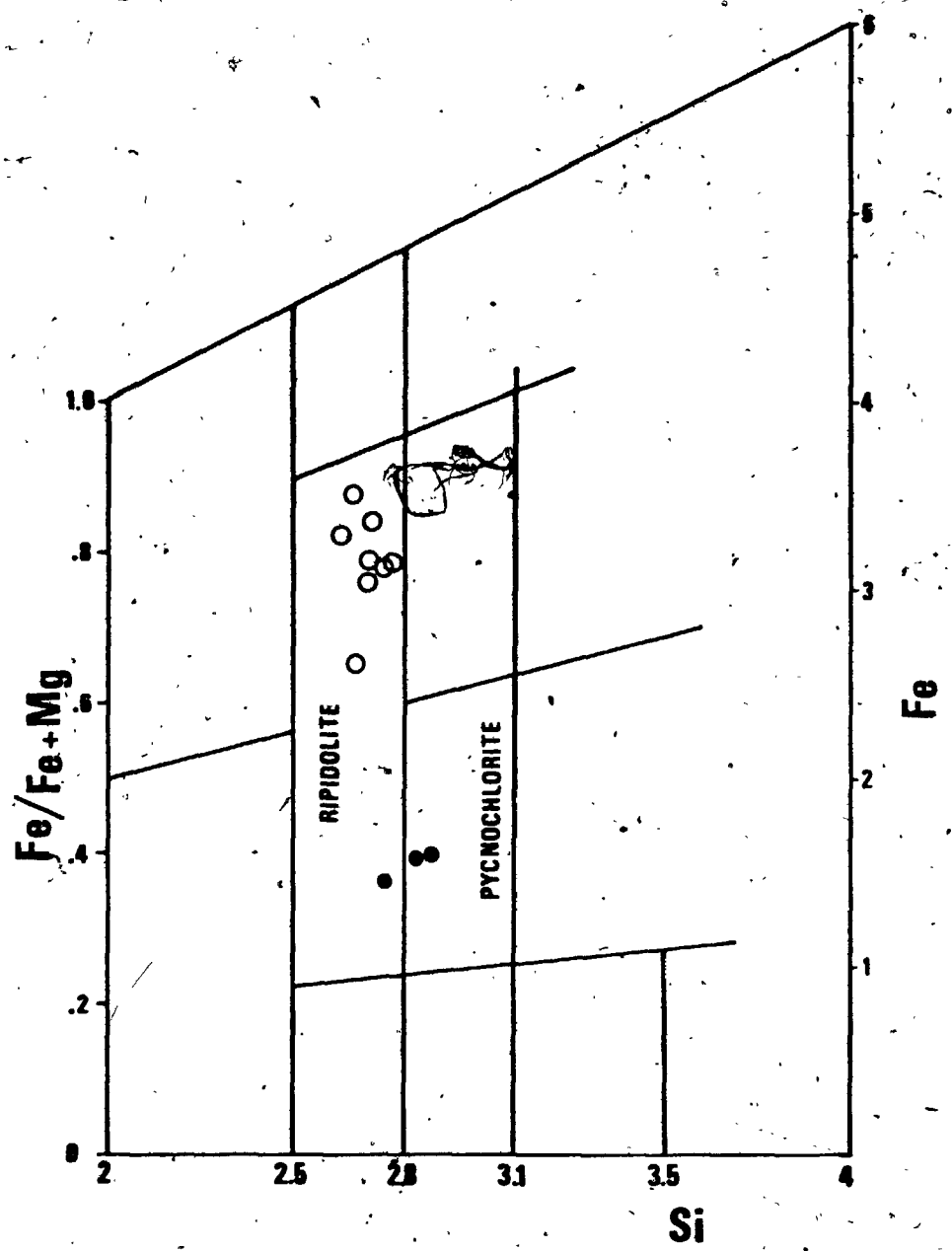


Figure 4.4. Diagram illustrating the compositional variation of the chlorites from the Aljustrel Volcanics. Solid circles, Green facies; open circles, deeper seated rocks.

only magnesian igneous mineral actually known to have been present in the Aljustrel Volcanics is biotite, in minute amounts, and there is nothing to suggest that biotite might have been particularly abundant at the stratigraphic top of the Aljustrel Volcanics. Moreover, the fact that chlorites replacing various phenocrystic minerals or occurring in the tuff matrix are chemically indistinguishable at the scale of the hand specimen also contraindicate a primary igneous cause for the megascopic compositional zonation of chlorites.

e) Sericite

Electron microprobe analyses of sericites (i.e. K-rich phyllosilicates) from the Aljustrel Volcanics are presented in Appendix II-6. Most analyses obtained from matrix sericites depict high Fe contents (up to 6 wt % FeO). It is not known whether all the iron reported in the analyses is actually in illite or muscovite structures, or some corresponds to submicroscopic amounts of other minerals, given the extremely fine grained nature of matrix sericites (individual crystals are often less than 1 micron wide). Sericite replacing igneous albite phenocrysts typically contains only about 1 wt % FeO. MgO contents in sericite usually range from 1 to 2 wt %. Small amounts of Ba were occasionally detected (up to 0.35% BaO), especially in samples containing Ba-rich K-feldspars.

f) Epidotes

Analyses of (igneous) allanite and of (hydrothermal and regional) metamorphic epidotes (*sensu stricto*) are presented in Appendix II-7. The main chemical variation among the latter is the pronounced substitution of Al by Fe³⁺, ranging from 0.366 to 0.750 Fe³⁺ ions per formula (12.5 O). This substitution correlates well with whole rock Fe²⁺/Fe (Fig. 4.5), suggesting that Fe³⁺ accommodation in the epidote structure may be controlled by oxygen fugacity (Liou, 1973), as already observed for other Pyrite Belt metamorphic rocks (Munha, 1981).

g) Stilpnomelane

Analyses of stilpnomelane from one Quartz-eye tuff sample are presented in Table 4.6. They correspond to low Mg, Ba-bearing stilpnomelane. The Ba content is higher than that of coexisting K-feldspar (0.75 against 0.25 BaO wt %, respectively).

h) Carbonates

The only carbonates analysed in Aljustrel Volcanic rocks (except for ore zone carbonates) are those occasionally found replacing alkali-feldspar megacrysts and phenocrysts in the Quartz-eye Tuff. They are mostly pure calcite, occasionally ferroan-calcite (up to 6% FeCO₃; see Appendix II-8).

i) Synopsis of paragenetic relations

Petrographic observations, X-ray diffraction and

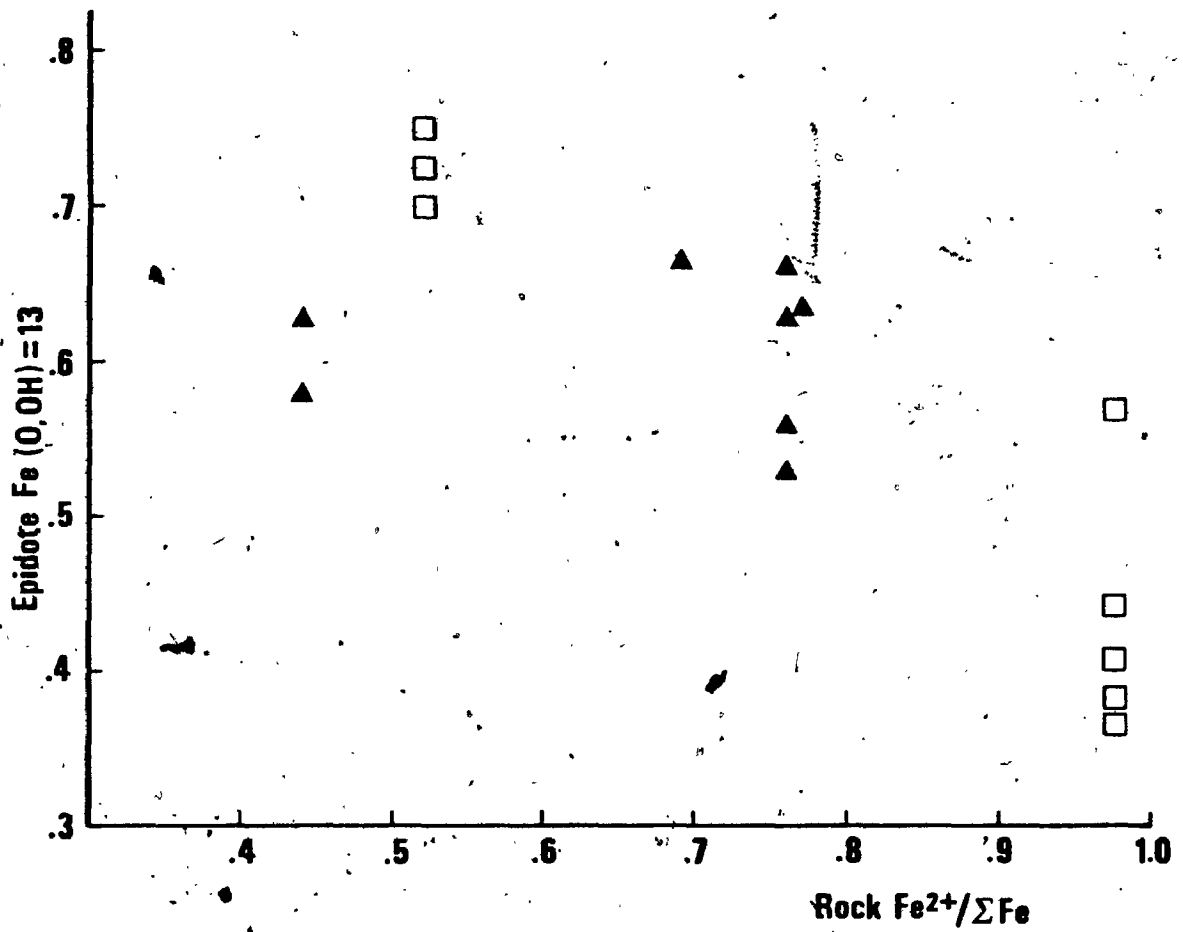


Figure 4.5. Diagram illustrating the variation of Fe^{3+} in epidote versus the oxidation state of the host rock. Triangles, QET; squares, MT.


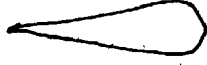
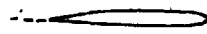
Table 4.6. Analyses of stilpnomelane from the Quartz-eye Tuff formation.

Unit Sample Analysis no.	QET 2-GF-87				
	24	25	35	36	37
SiO ₂	44.93	45.02	45.15	45.23	44.78
Al ₂ O ₃	6.55	6.50	6.68	6.77	6.47
Cr ₂ O ₃	0.00	0.00	0.04	0.01	0.07
FeO	33.00	33.92	35.68	34.53	34.33
MgO	1.61	1.70	1.70	1.70	1.74
MnO	2.39	2.52	2.63	2.33	2.28
CaO	0.16	0.11	0.05	0.04	0.05
BaO	0.63	0.75	0.82	0.66	0.81
Na ₂ O	0.31	0.35	0.44	0.72	0.57
K ₂ O	1.01	0.78	1.53	0.57	0.85
TOTAL	90.60	91.66	94.77	92.57	91.96

Number of ions per 7.5 (Si+Al+Cr+Fe+Mg+Mn)

Si	3.978	3.936	3.861	3.915	3.917
Al	0.684	0.670	0.673	0.691	0.667
Cr	0.000	0.000	0.003	0.001	0.005
Fe	2.444	2.480	2.552	2.500	2.511
Mg	0.212	0.222	0.217	0.219	0.227
Mn	0.179	0.187	0.190	0.171	0.169
Ca	0.015	0.010	0.005	0.004	0.005
Ba	0.022	0.026	0.027	0.022	0.028
Na	0.053	0.059	0.073	0.121	0.097
K	0.114	0.087	0.167	0.063	0.095

Table 4.7. Paragenetic relations of the minerals in the Aljustrel Volcanics.

	Primary Igneous	Hydrothermal Metasomatic		Regional Metamorphic
		Early	Late	
Matrix albite	X (a)			
Matrix K-feldspar	X (a)			
Matrix quartz	X (a)			
Sericite			Low-grade	→ X
Chlorite			phyllosilicates	→ X
Ti-hematite flakes (Ti-magnetite)		→	X	
Albite (An ₈) phenocrysts	X			
Poikilitic sericite, epidote, calcite			X	→ ?
Albite (An ₀₋₃) megacrysts				
K-feldspar megacrysts				
vein K-feldspar (adularia)				
Fe-Ti microphenocrysts	Ti-hematite (Ti-magnetite)	→	X	
	Leucoxene (rutile)	→	X	
	Pseudobrookite(?) (ilmenite)	→	X	
	Sphene		X	X ?
Ilmenite	X			
Zircon, apatite, almandine garnet, biotite, allanite	X			
Vein epidote, sphene			X	X
Fluorite	X ?		X ?	
Stilpnomelane				X

(a) Products of devitrification of volcanic glass

mineral chemistry suggest that the minerals presently found in the Aljustrel Volcanic rocks were formed in three main successive stages (Table 4.7), in good agreement with the geologic history of the Iberian Pyrite Belt (Chapter 2).

4.3.2 Whole rock Geochemistry

Whole rock analytical data pertaining to 47 Aljustrel Volcanic rocks is presented in Appendix III. Samples are representative of all the variations detected in both the Quartz-eye Tuff and the Mine Tuff. Mine Tuff samples were collected mostly in the Feitais Anticline (for the reasons outlined in Chapter 3), and do not include rocks markedly affected by ore fluids (Chapter 5). Appendix III-1 and III-2 contain the abundances of major elements, 16 selected trace elements and, for some samples (15), lanthanide element concentrations in Quartz-eye Tuffs and Mine Tuffs, respectively. The results of 13 whole rock oxygen isotopic analyses of Aljustrel Volcanic rocks are presented in Table 4.10.

a) Major elements

Inspection of major element abundances in the Aljustrel Volcanics shows that these rocks constitute a typical quartz-keratophytic suite (see Schermerhorn, 1973) in which variability is perhaps the most prominent feature. From the petrologic and mineral chemical data presented in previous sections there can be little doubt

that major post depositional⁴ metasomatism affected the Aljustrel Volcanics. Thus major element abundances do not represent solely primary igneous compositions but rather (and principally) the results of major mass transfer of several components and the apparent changes in other elements which stem from such transfers.

An important aspect of the apparent changes produced by metasomatism in immobile elements is that their percentual abundances will be changed proportionally to their relative abundances, e.g. 3 wt % hydration of 100 g of a rock initially with 70% SiO₂, 15% Al₂O₃ and 0.50% TiO₂ will produce 103 g of a rock containing 67.96% SiO₂, 14.55% Al₂O₃ and 0.49 TiO₂. This factor, too often disregarded when metasomatized rocks are studied, constitutes a problem that has been obviated by several methods of mass balance evaluation, among which "the general metasomatic equation derived by Gresens (1967) supersedes all others because of its general applicability to all conditions of metasomatism and through its introduction of corrections for differences between specific gravities of samples and for volume changes during alteration" (Appleyard, 1980). Gresens (and all other) mass balance computations are a means of estimating the gains and losses necessary to obtain a metasomatized rock composition from a parental rock composition.

Unfortunately, data indicates that formal mass balance

calculations cannot be performed on the Aljustrel Volcanics with realistic results, because no unaltered, parental rocks exist. Furthermore, Hercynian deformation is likely to have produced significant porosity reduction in the rocks, easily in the order of 10%, given that the Aljustrel Volcanics were originally submarine felsic pyroclastic rocks, probably similar to coarse sand (see Bear, 1972). Under these conditions the mass balance considerations presented here are essentially qualitative and oriented towards elucidation of parental compositions from metasomatized rocks that show textural, mineral chemical and whole rock geochemical evidence for various, often opposite geochemical gains and losses.

The ranges of variation and some averages of the abundances of major elements in the Aljustrel Volcanics are presented in Table 4.8. The Quartz-eye Tuff (QET) and Mine Tuff (MT) formations are chemically very similar, differing essentially in their TiO_2 , Fe and P_2O_5 contents (higher in the QET), and in generally higher SiO_2 values in MT. These differences are in good agreement with petrographic characteristics, with Fe-Ti oxide (+ sphene) microphenocrysts more abundant in QET rocks, apatite occurrence restricted to QET and the QET quartz phenocrysts compensated by a much more quartz rich matrix in MT.

Ti and Al are generally immobile elements (on a scale of cms) in most metasomatic processes, given the narrow

Table 4.8. Ranges and some averages (bracketed) of the abundances of major elements in the Aljustrel Volcanics.

	Quartz-eye Tuff	Mine Tuff	Remarks
SiO ₂	65-73(70.8)	60-79(72)	(dry basis)
TiO ₂	0.44-0.73(0.51)	0.10-0.32(0.19)	variations believed to reflect to a large extent losses and gains in other components
Al ₂ O ₃	12-20(15.5)		
Fe	1.5-5	0.5-3	Higher values in Green facies
Fe ²⁺ /ΣFe	0.09-1.00		Green facies strongly oxidized
MnO	0.02-0.17(0.04)		
MgO	0.37-4.62*	0.56-5.81	Strongly enriched in Green Facies
CaO	0-3.9		
BaO	0.03-0.38		
Na ₂ O	1.2-4.5	0-6.5	
K ₂ O	1.5-6.8	0.2-6.8	
P ₂ O ₅	0.07-1.25(0.26)	<0.02	
LOI	0.81-7.41		Strongly enriched in Green Facies

LOI (Loss on ignition) is mainly H₂O, as indicated by petrography.

(*) MgO content of the QET Green facies analysis in Schermerhorn (1976).

limits of their solubility under normal physicochemical conditions (see Garrels and Christ, 1965; Ferry, 1979). In both the QET and the MT rocks Ti and Al are markedly covariant (correlation coefficients 0.79 and 0.73, respectively) and their variations (especially Al) far more pronounced than those found in recent, unaltered zoned felsitic tuffs (see Hildreth, 1979, 1981). A significant proportion of the Ti and Al variations in the Aljustrel Volcanics must simply reflect pronounced metasomatic losses and gains of other elements.

Total Fe variations show markedly good correlation with the Fe-Ti oxide mineralogy, being higher in rocks containing Ti-hematite + leucoxene \pm pseudobrookite (the Green Facies rocks of both QET and MT), and decreasing progressively as opaque grains and microphenocrysts are partially replaced by sphene, with removal of a significant proportion of the iron originally present. The higher Fe concentrations are compatible with Fe-rich rhyolitic and high silica rhyolitic original compositions of QET and MT, respectively.

Variations of the oxidation state of iron in altered rocks are often a sensitive indicator of both the degree of alteration and the nature of the intervening fluid or fluids (Spooner, 1977; Fyfe et al., 1978). The Aljustrel Volcanic rocks show almost as large as possible variation in $Fe^{2+}/\Sigma Fe$ (Fe ratio), from 0.09 to 1.00. Green facies

rocks are invariably oxidized, whereas deeper seated rocks get progressively relatively enriched in Fe^{2+} , despite the concomitant decrease in Fe, as illustrated in Fig. 4.6. Mn shows identical general behaviour, but most MnO determinations (0.01 to 0.06 Mn %) are too close to detection limit to be reliable. Higher MnO values (0.17%) were found in two highly oxidized samples (Appendix III-2).

Not surprisingly, LOI (i.e., H_2O) covaries with the Fe ratio, strongly suggesting that at least part of the vertical zonation of the Aljustrel Volcanics is due to oxidation and hydration at the top layers by an aqueous, oxidized fluid. Deeper seated rocks are much less hydrated, not oxidized (often markedly reduced) and Fe depleted. These facts are readily explained considering downflow of an originally oxidized fluid which becomes progressively reduced upon reaction with rocks.

The variations in the Mg abundances of the Aljustrel volcanic rocks are particularly striking. Fig. 4.7 shows unequivocally that Mg abundances are strongly covariant with both LOI and the oxidation state of iron, a feature that cannot be likely explained either by magmatic processes or by numerical artifices. Mg in the Aljustrel Volcanics occurs mostly in chlorite (scattered within the matrix and replacing various minerals, including phenocrystic quartz in the QET, see section 4.2). If the oxidized fluid that may have been responsible for the Fe

Figure 4.6. Total iron versus whole rock Fe ratio in the Aljustrel Volcanics. Triangles QET; squares MT. Open symbols correspond to analyses in Schermerhorn (1976). Mineralogy and textures indicate that the higher iron contents correspond to original abundances (see text).

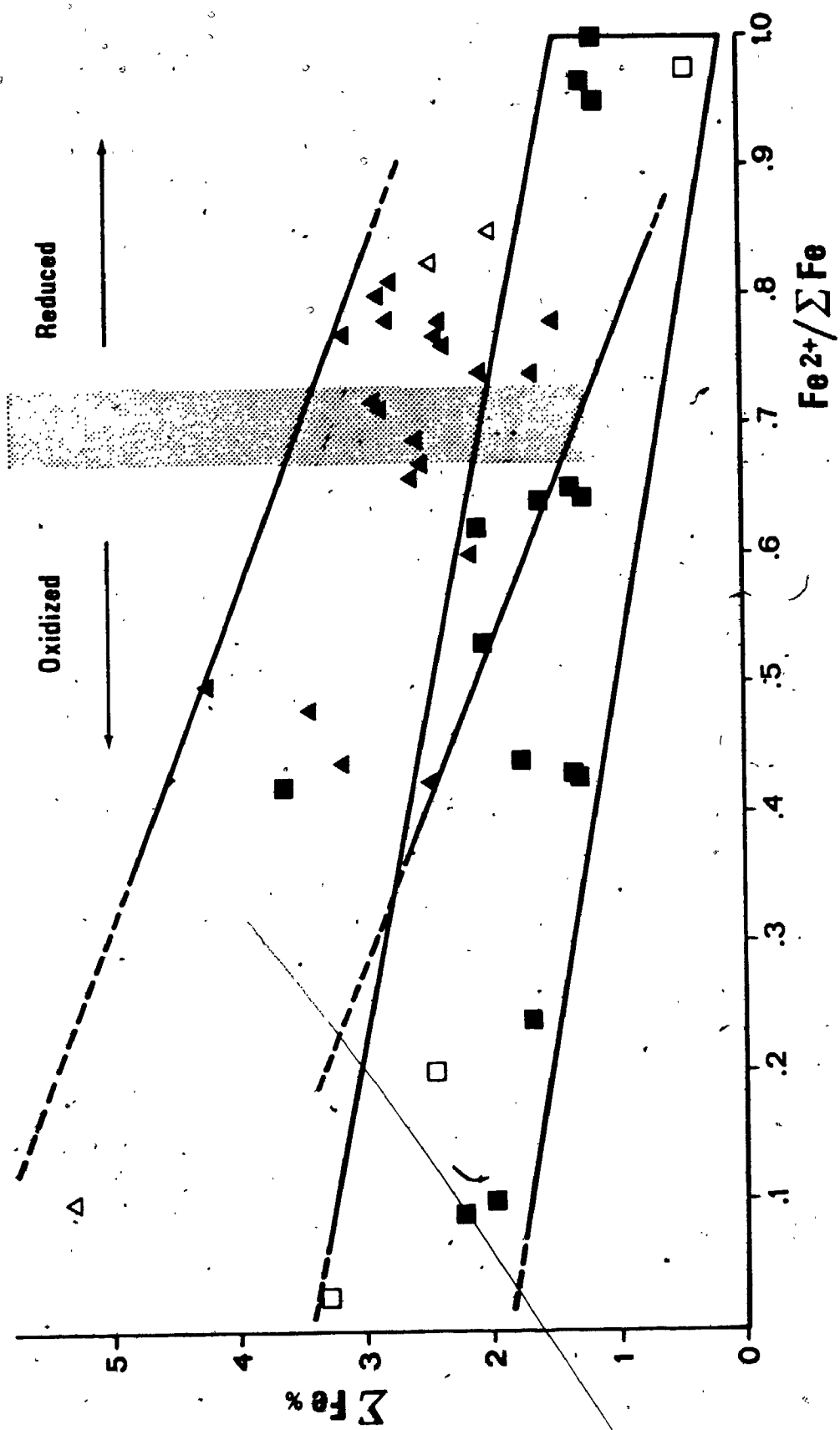
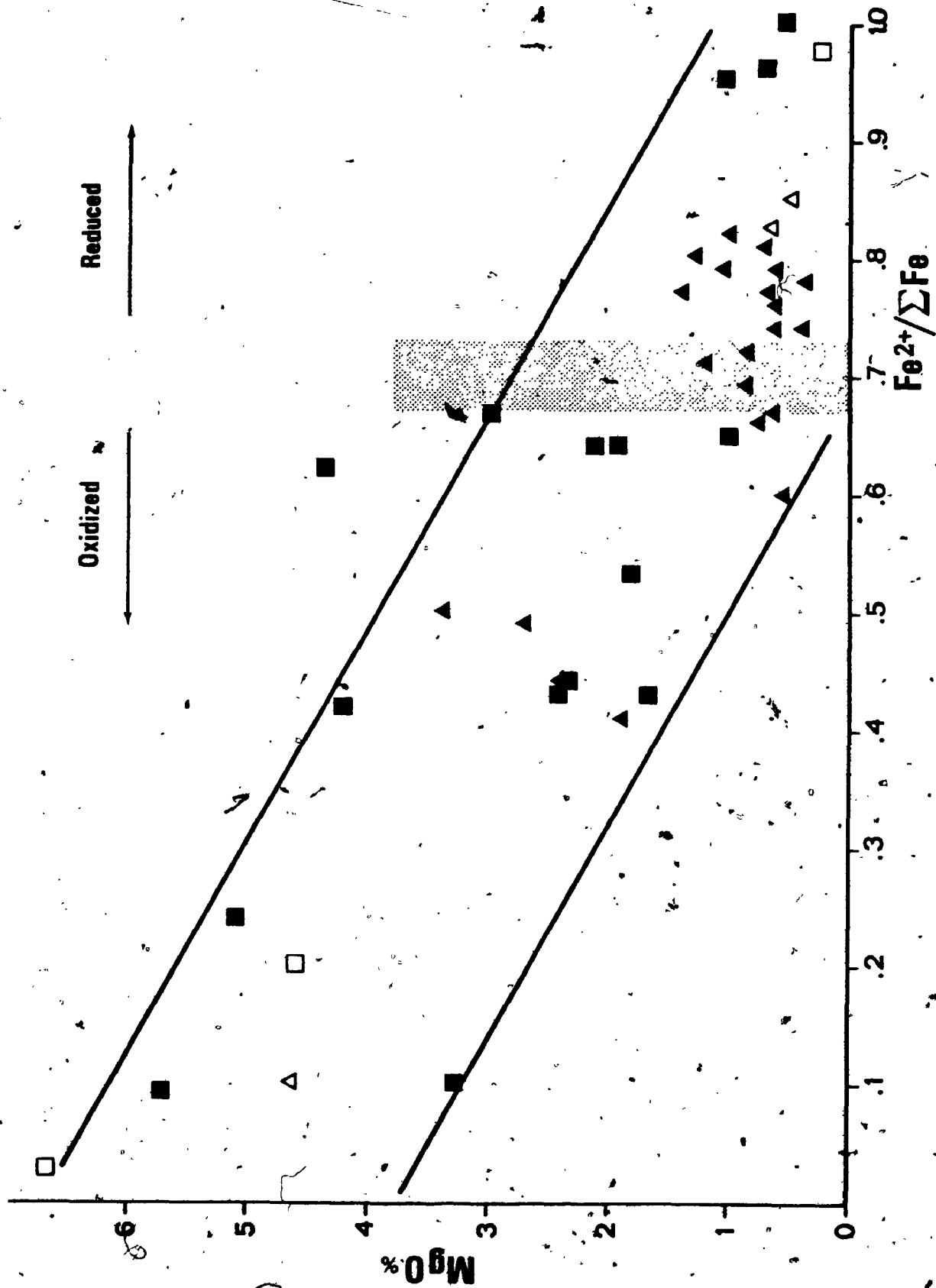


Figure 4.7a. Diagram illustrating the variation of MgO versus Fe ratio in the Aljustrel Volcanics. Symbols as in Fig. 4.6. It is believed that the variation corresponds to fixation of sea water Mg (see text).



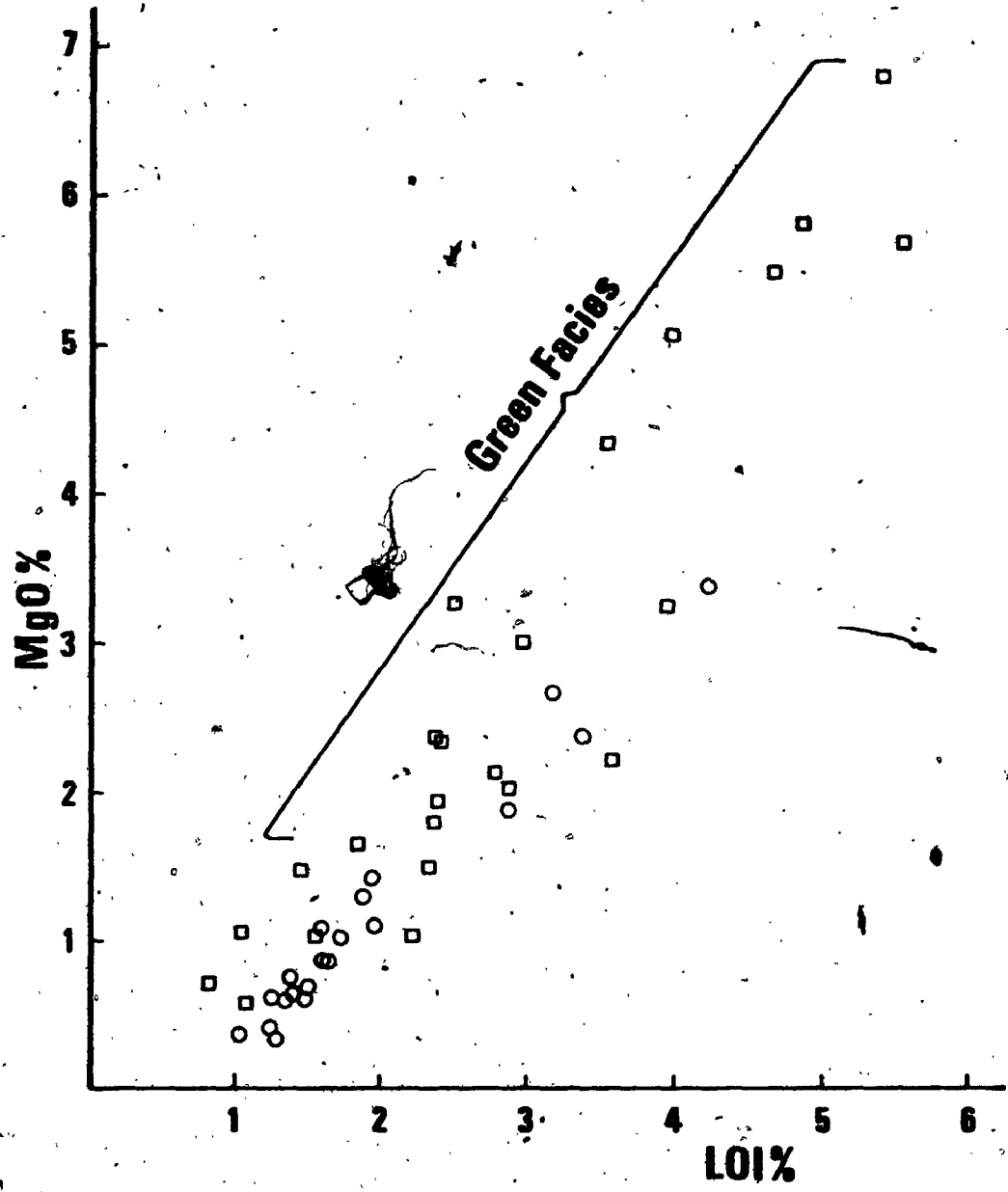


Figure 4.7b. Diagram illustrating the variation of MgO versus LOI (essentially H₂O: one carbonate rich sample excluded). Circles, QET; squares, MT.

and Fe ratio variations in these rocks was also Mg-rich, its Mg would be transferred to solid phases upon initial interaction with rocks, as shown by all experimental sea water (1300 ppm Mg^{2+})-rock interaction studies (Bischoff and Dickson, 1975; Hajash, 1975; Mottl, 1976; Hajash and Archer, 1980; Mottl and Seyfried, 1980). Furthermore, the composition of the sea water derived hydrothermal fluids exiting from the Iceland geothermal systems are also very Mg depleted (Bjornsson et al., 1972).

Variations in alkalis are another striking feature of the Aljustrel Volcanics. Textural, X-ray diffraction and mineral chemical data presented before indicates complex and evolving behaviour of the alkalis, eloquently reflected in the whole rock abundances. No defined megascopic zonation on the occurrence of the alkalis was detected. Given that K_2O occurs in sericite, matrix K^+ feldspar (primary?), vein adularia and in metasomatic megacrysts (in QET), data is not conclusive with respect to the initial K abundances in the Aljustrel Volcanics. Munha et al. (1980) have shown that the Cercal rhyolites (Iberian Pyrite Belt, see also Carvalho, 1976 and Chapter 2) are strongly depleted in Na and enriched in K, forming adularia that was seen replacing plagioclase, and attributed adularia formation to high water/rock interaction of the Cercal rhyolites with sea water, at temperatures below $150^{\circ}C$ (see also Munha, 1981).

Data presented so far in this study proves that the

Aljustrel Volcanics were affected by major post-depositional metasomatism which requires interaction with an oxidized, Mg rich fluid. The only likely available fluid reservoir with these characteristics is sea water, given that the Aljustrel Volcanics are submarine rocks.

As outlined in Chapter 2, Munha (1981; see also Munha and Kerrich, 1980) also concluded that sea water was responsible for major spilitization of the mafic igneous rocks of the Iberian Pyrite Belt. Under such circumstances the highly variable alkali abundances in the Aljustrel Volcanics are interpreted as reflecting marked variations in temperature and water/rock of the metasomatic events. Textural evidence (section 4.2) clearly indicates that the physicochemical conditions responsible for the various stages of feldspar formation did not remain constant during metasomatism, rather indicating complex and evolving behaviour of the alkalis. According to the conclusions of Munha et al. (1980), temperatures both above and below 150°C may have prevailed during alkali metasomatism of the Aljustrel Volcanics.

From the above discussion it is obvious that a significant proportion of the variation in the percentage abundances in SiO₂ in the Aljustrel Volcanics simply reflects variation in other species, namely H₂O, Fe, Mg and alkalis. However, some of the samples depicting lower SiO₂ abundances are also high in Al₂O₃ and TiO₂, indicating

that large scale silica removal may have taken place locally, as sporadically confirmed by textural data. Some of this silica removal may have taken place concomitantly with the major metasomatic episode, as will be seen later, but it is also likely that some of the low silica samples reflect late tectonic, pressure-solution removal of SiO_2 , as indicated by the frequent occurrence of syn and late tectonic quartz (+ calcite) veins within the Aljustrel Volcanics; these can be locally > 2 m wide.

Table 4.9 is a tentative compilation of the likely primary compositions of the Aljustrel Volcanics, based on the above considerations. The Quartz-eye Tuff would have been originally a high iron rhyolitic unit, whereas the Mine Tuff seems to have been a high silica rhyolite. These presumed original major element compositions are sufficiently similar to suggest that the Aljustrel Volcanics may derive from a common source.

b) Immobile trace elements

Widely scattered trace element concentrations (particularly those of LILE, see Appendix III-1 and III-2) further confirm the high degree of metasomatism experienced by the Aljustrel volcanic rocks. Some high field-strength elements (Sc, Y, Zr, Hf and Nb) do show, however, relatively constant abundance ratios within each of the QET and MT formations, in accordance to their normally immobile behaviour during alteration processes affecting volcanic

Table 4.9. Probable original major element composition of the Aljustrel Volcanics (see text).

	Quartz-eye Tuff	Mine Tuff	Remarks
SiO ₂	70-73	71-75	Actual averages
TiO ₂	0.50	0.20	
Al ₂ O ₃	13-15	12-14	Probably lower on MT given sample representativity considerations
Fe ₂ O ₃	1.80	1.00	Based on Fe ~4.5 and ~2.5 and on Fe ²⁺ /ΣFe ~0.7 (see Fig. 4.6)
FeO	4.20	2.30	
MnO	?	?	
MgO	<0.5	<0.5	See Figure 4.7
CaO	1?	1?	Given the low An component in igneous albite (section 4.3)
Na ₂ O	3-5	3-5	
K ₂ O	3-5	3-5	
P ₂ O ₅	0.25	<0.02	
H ₂ O	0-1.5	0-1.5	

rocks (see Alderton et al., 1980).

Figures 4.8 and 4.9 represent the variations of Sc against Y and Zr/Y against Zr for the analysed rock samples. On both diagrams there is a clearly defined discrimination between the QET and MT formations, with lower Sc abundances and Zr/Y in the MT.

Although aware of the difficulties met when attempting to model quantitatively igneous processes in high-silica volcanic rocks (see Mahood and Hildreth, 1983) it seems that at least some of the observed compositional variations could be accommodated by variable degrees of partial melting of a common garnet-bearing source followed by varying degrees of shallow level crystal fractionation (compare Pearce and Norry, 1979). Moreover, some of the geochemical characteristics of the MT formation are closely similar to those of modern high-silica rhyolites (Bacon et al., 1981; Hildreth, 1981; Smith and Johnson, 1981). It thus seems possible that the MT formation could represent a somewhat more evolved stage (with respect to the QET) on the differentiation history of the magma chamber feeding the Aljustrel volcanic centre.

The above hypothesis is compatible with field relations, as the QET apparently erupted slightly earlier than the MT. However, it does not properly explain the marked bilateral symmetry of the Aljustrel Volcanics (Fig. 3.6), nor the absence of Green facies Quartz-eye tuffs at

Figure 4.8. Diagram illustrating the variation of Sc versus Y in the Aljustrel Volcanics.
Triangles, QET; squares, MT.

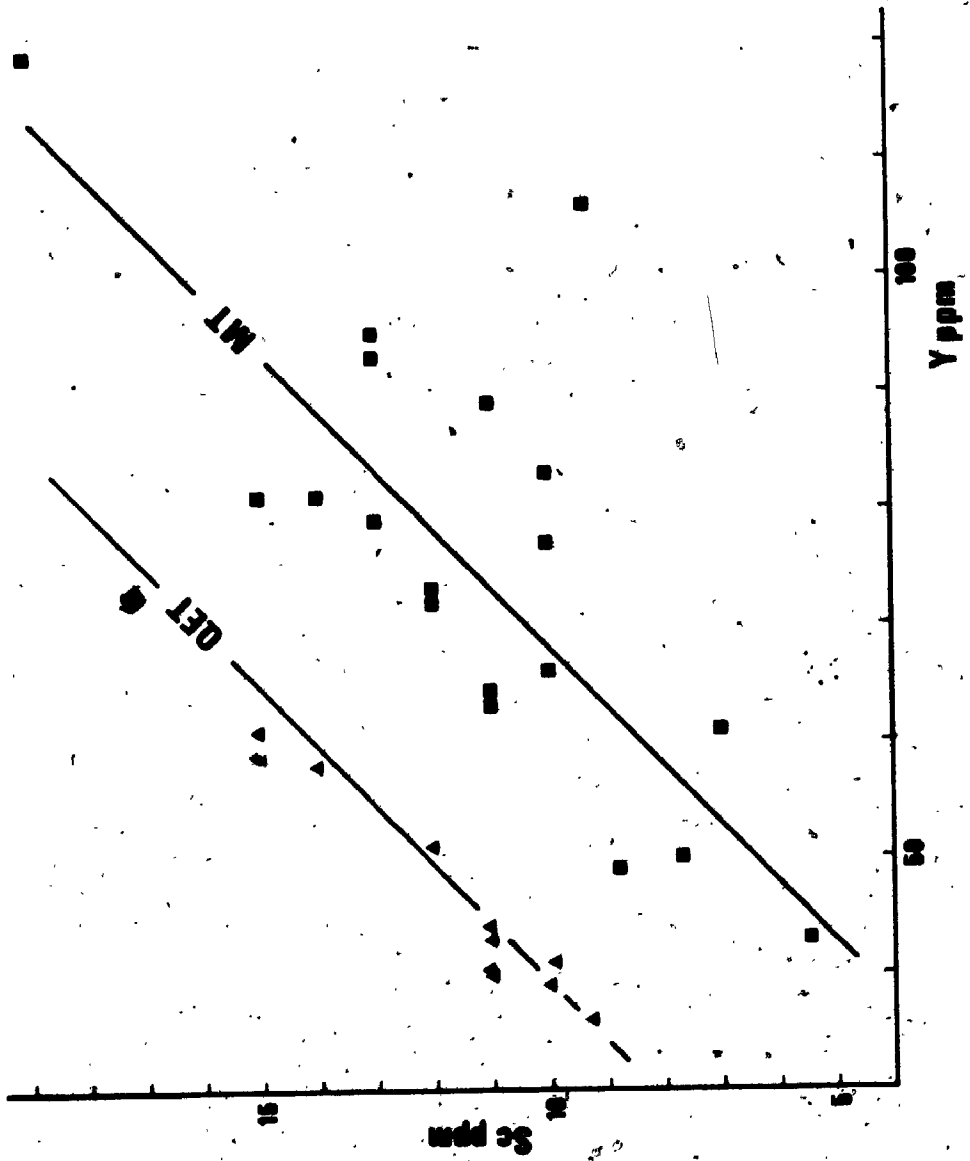
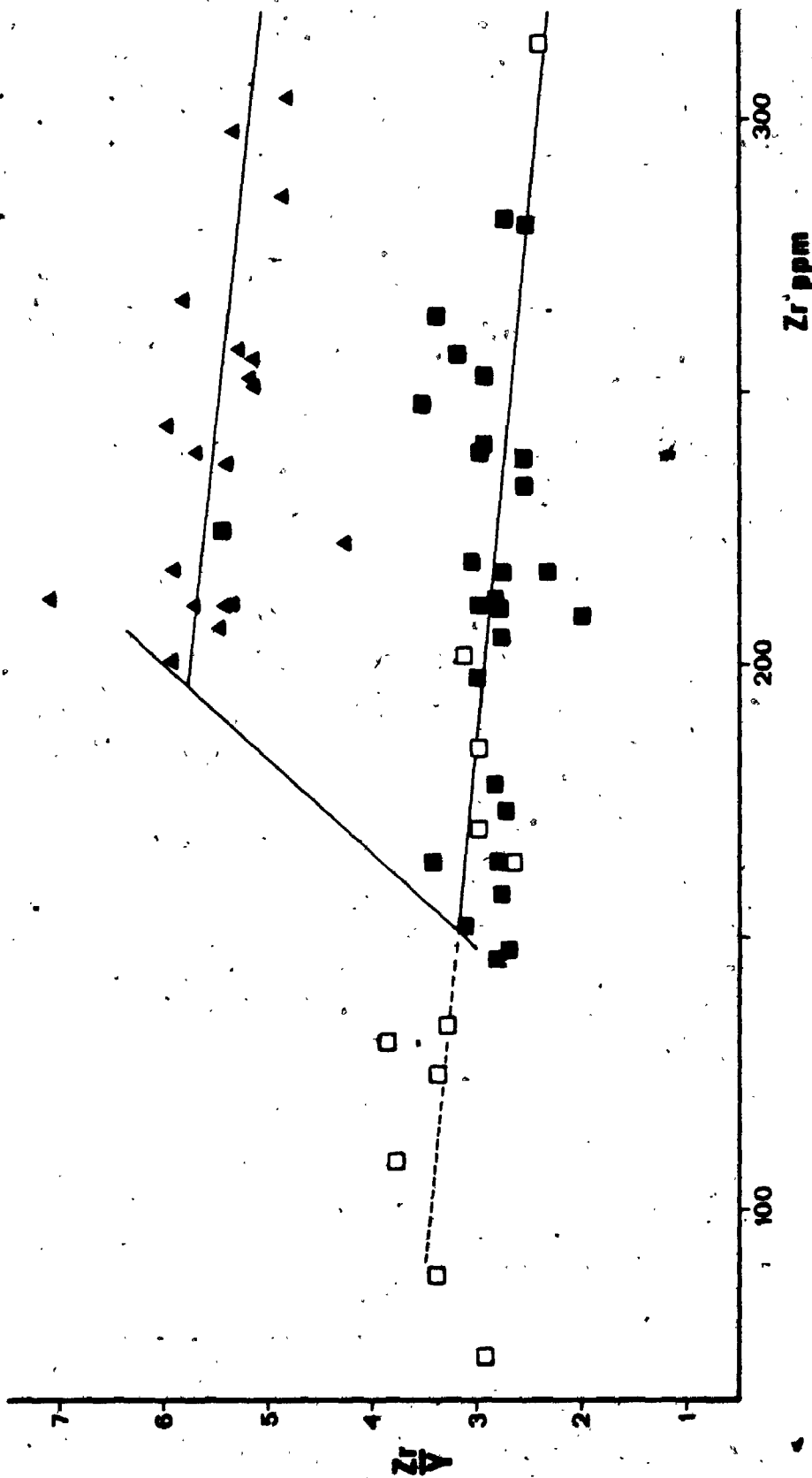


Figure 4.9. Diagram illustrating the variation of Zr/Y versus Y in the Aljustrel Volcanics. Triangles, QET; solid squares, MT; open squares are Mine tuffs depicting ore zone (stockwork) alteration. See Chapter 5.



the deeper contacts between the QET and the MT, to be expected if a significant timespan separated the eruption of the two formations. These objections, coupled with the fact that the MT is finer grained and much better bedded than the QET could mean that, alternatively to the above igneous genetic hypothesis the differences between the Quartz-eye Tuff and the Mine Tuff could simply represent physical zonation between proximal (QET) and distal (MT) facies of a zoned volcano. Within this hypothesis the geochemical differences detected would represent lateral physical separation between most igneous crystals and larger glass fragments from finer particles, deposited farther away from the central eruptive zone. But more detailed field studies are needed.

c) Rare earth elements

Rare earth elements are usually considered to be immobile during all but the most intense metasomatic processes (eg. Nance and Taylor, 1977; Jahn et al., 1978), and their coherent geochemical behaviour makes them particularly useful in petrogenetic modelling of the origin of igneous rocks. However, recent studies (Hellman and Henderson, 1977; Nesbitt, 1979; Ludden and Thompson, 1979; Martin et al., 1978; Alderton et al., 1980) clearly show that REE are significantly mobile in the course of many supracrustal processes.

Figures 4.10 and 4.11 represent chondrite normalized

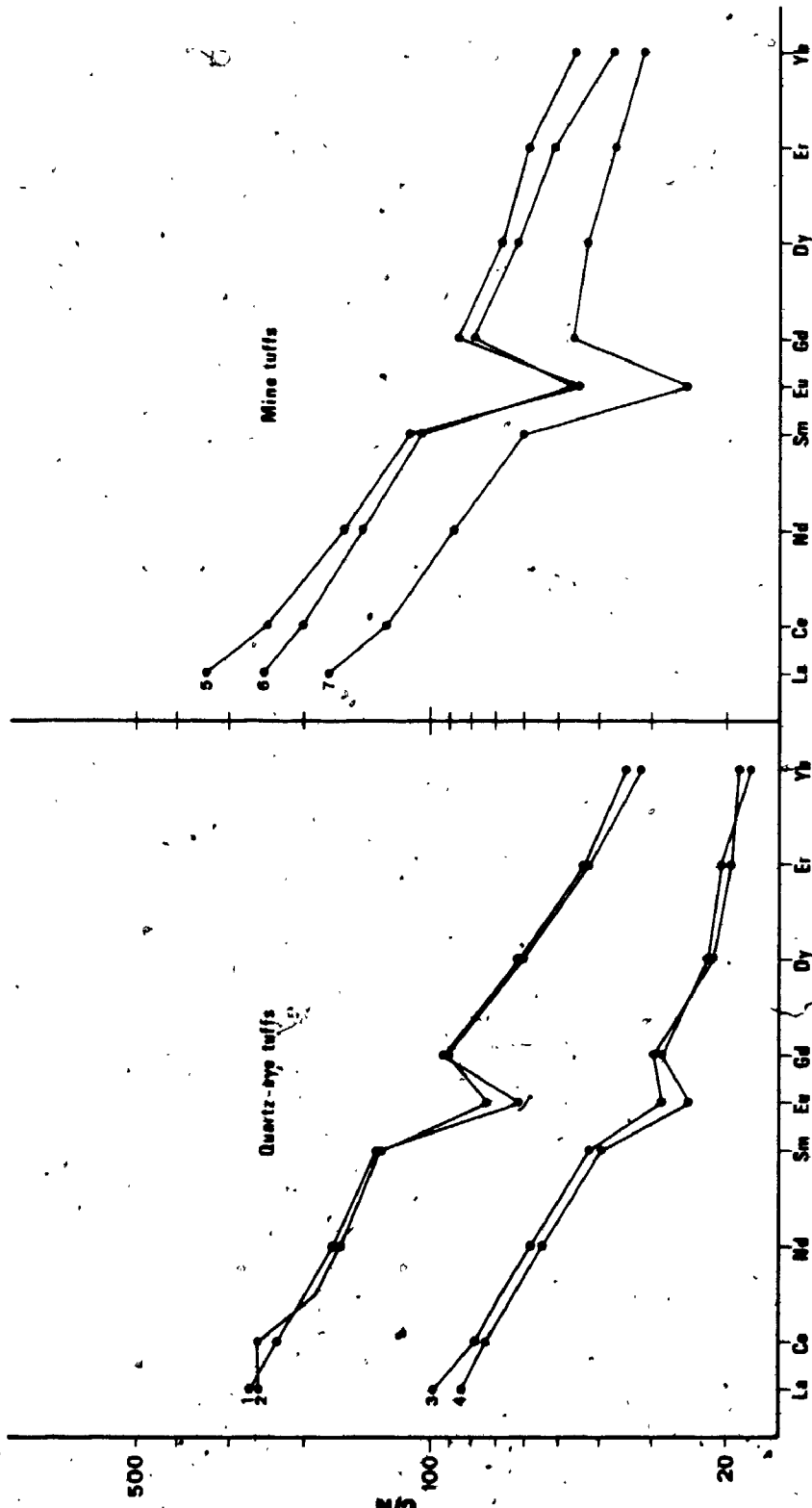


Figure 4.10. Chondrite normalized REE patterns in Aljustrel volcanic rocks.

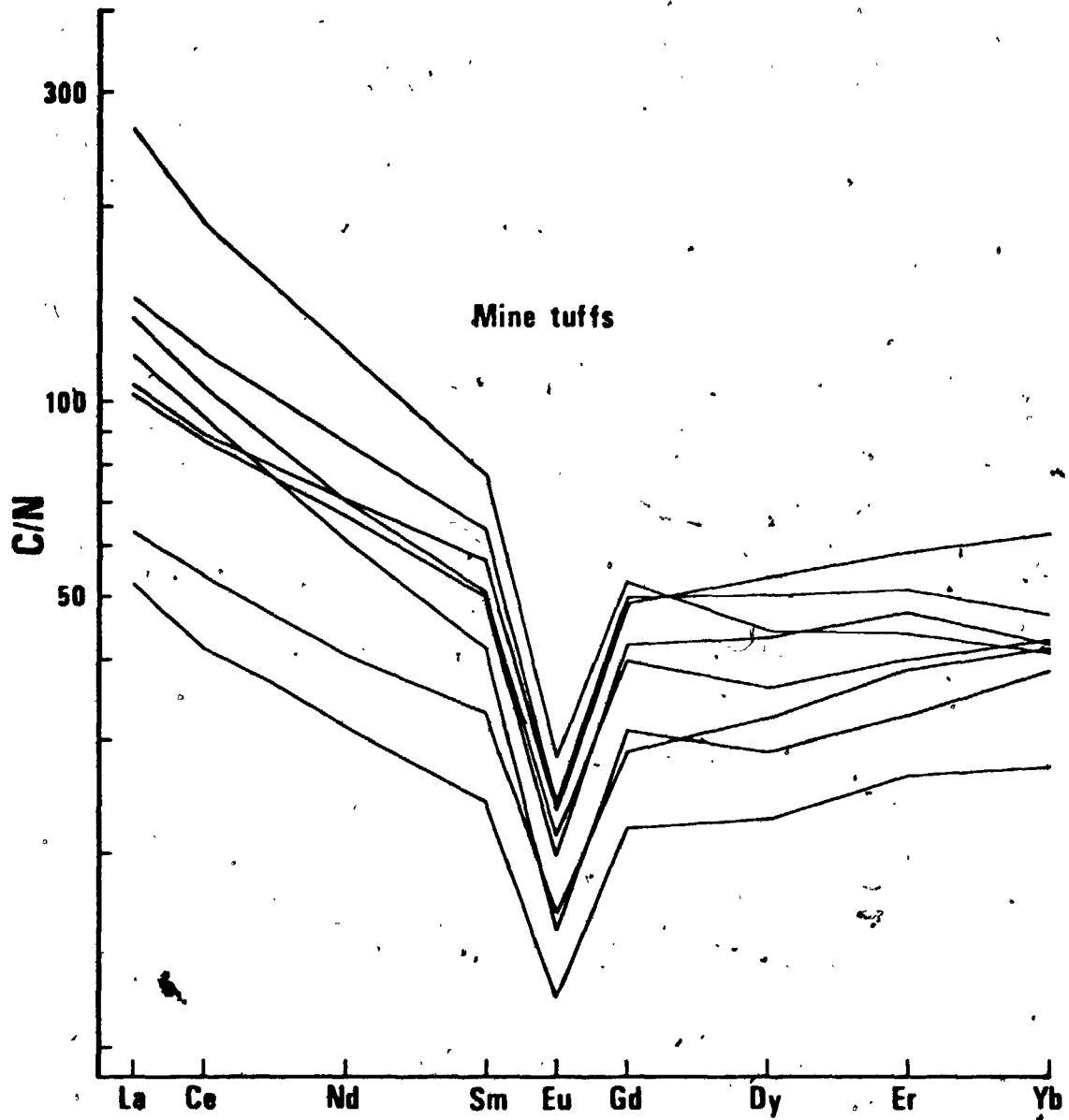


Figure 4.11. Chondrite-normalized REE patterns in chloritized Mine tuffs. Note relative enrichment in HREE.

diagrams of 15 samples from the Aljustrel Volcanics (see Appendix III for data). About half of the samples (Fig. 4.10) display patterns very similar to that of average shales (Haskin and Haskin, 1966; Haskin et al., 1968), whereas the remaining (Fig. 4.11) show similar light REE distributions and heavy REE enrichment with respect to the shale-like group. The simplest interpretation of these data is that the Aljustrel Volcanics derive from anatexis of crustal materials, and that in many cases hydrothermal alteration produced significant changes in the distribution of REE, particularly HREE.

This conclusion is in good agreement with Sr isotopic data for the Quartz-eye Tuff (Priem et al., 1978), which show extremely high Sr^{87}/Sr^{86} initial values (0.7135), and also with the studies of Munha (1981) on the felsic rocks of the Iberian Pyrite Belt, who also produced REE data and interpreted it similarly.

Regarding the metasomatic effects on the REE patterns of the Aljustrel Volcanics, there is general agreement with the conclusions of Alderton et al. (1980) concerning the effects of sericitization in REE distributions. Thus the differences in Eu anomalies in the patterns in Figure 4.10a correlate well with the degree of sericitization, whereas the HREE positive shifts depicted in Figure 4.11 can be attributed to the marked chloritization exhibited by most of these rocks.

d) Cu, Zn, Pb

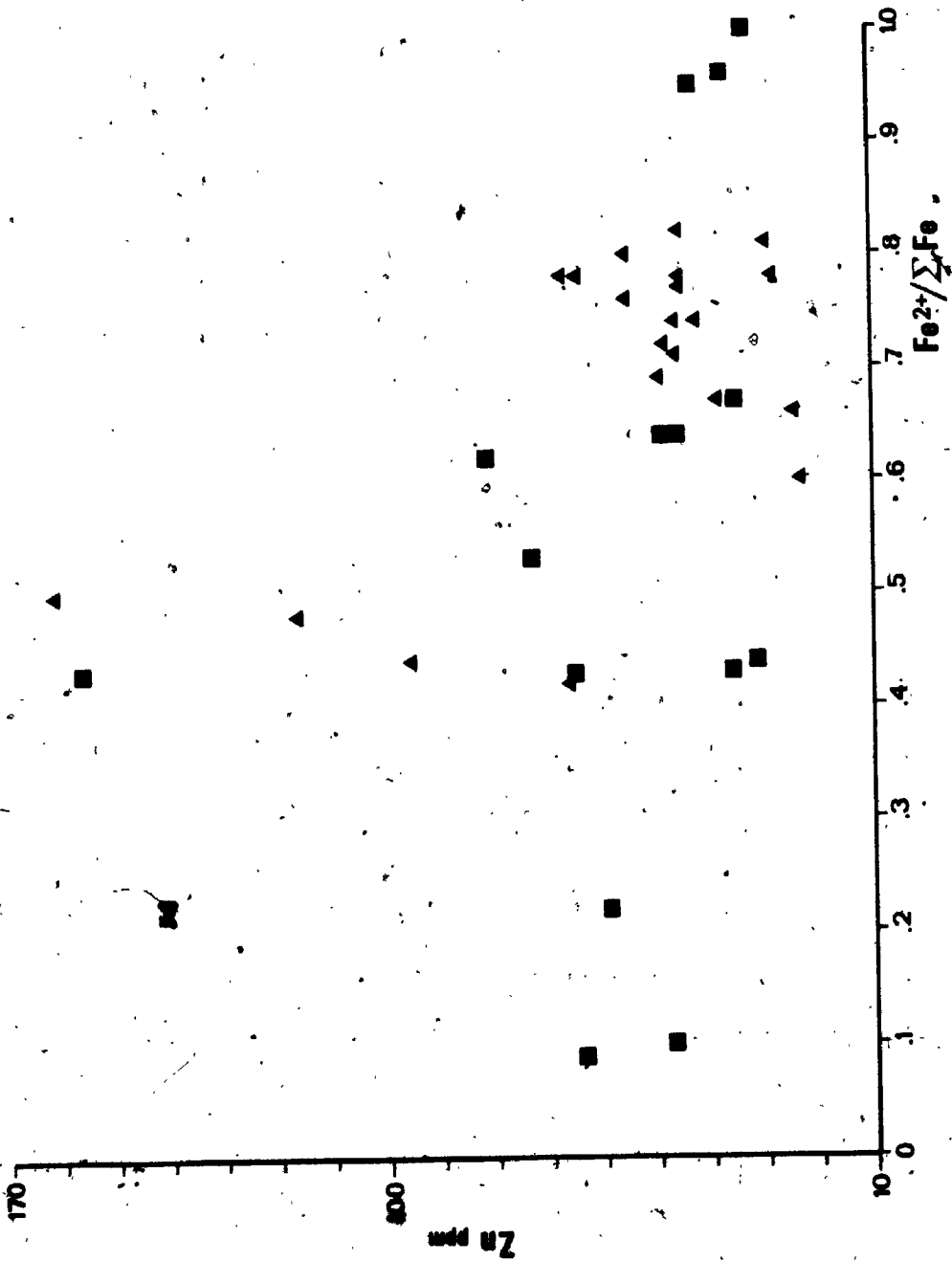
The variations in the abundances of Cu, Zn and Pb in the Aljustrel Volcanics are of particular importance to the main purpose of this thesis, given the high abundance of these transition metals in the Aljustrel massive sulphide deposits.

Cu concentrations are extremely low, below detection limit (10 ppm) for most samples. Figure 4.12, although based on insufficient data, suggests a positive correlation between intermediate degrees of whole rock Fe ratio ($0.5-0.6 \text{ Fe}^{2+}/\Sigma\text{Fe}$) and the higher Cu concentrations. The corresponding variation diagram for Zn (Fig. 4.13) reveals very similar Zn depletions in extremely oxidized or reduced rocks. Cu and Zn variations are similar, but not identical, to those detected for Fe (and perhaps Mn), as Fe was seen to vary linearly with Fe ratio whereas Cu and Zn covary with both extreme reduction and oxidation.

It is of paramount importance to the present study that the variations detected in the Cu and Zn abundances in the Aljustrel Volcanics can be explained as those found for Fe (and Mn?), as being due to leaching of metals by an initially oxidized fluid. These data therefore indicate that the Aljustrel Volcanics may have been the source material for a metal rich, potentially ore forming fluid.

Regarding Pb, data is inconclusive: Pb concentrations do not show any clear correlation, except perhaps that it

Figure 4.13. Diagram illustrating the variation of Zn versus Fe ratio in the Aljustrel Volcanics. Triangles, QET; squares, MT. Note decrease of Zn abundances with both oxidation and reduction, believed to correspond to leaching by sea water to generate a mineralized, potentially ore forming fluid.



was not detected (< 15 ppm) in the more reduced samples analysed, such as samples bis-283.5, bis-289 and bis-296.5 (Fe^{2+}/Fe 0.91, 1.00 and 0.96, respectively, see Appendix III-2).

e) Oxygen isotope compositions

With the exception of rocks affected by the Feitais-Estacao ore fluid (Chapter 5) oxygen isotope compositions of the Aljustrel Volcanic rocks are listed in Table 4.10. $\delta^{18}\text{O}$ values are very homogeneous, between 15.7 and 18.1‰, with a mean value of 16.7 ± 0.7 ‰ ($n = 13$). These values are far from normal for igneous rocks (even felsic, see Taylor, 1974, 1978), which usually vary within +6 and +10‰ $\delta^{18}\text{O}$. Given the geologic constraints outlined above the only likely explanation for the measured values is pervasive and widespread exchange with a large fluid reservoir under conditions of low temperature and high water/rock. It is of significance that several samples correspond to islands in the Feitais-Estacao stockwork unaffected by the mineralizing fluid. This fact shows that the Aljustrel Volcanics experienced an early, pre mineralization hydrothermal alteration stage which shifted the oxygen isotope composition of the rocks to unusually high values. The Aljustrel Volcanics are submarine, pyroclastic rocks, likely to have been deposited at low temperature ($\leq 200^\circ\text{C}$) and to have had extremely high initial permeability, easily similar to that of coarse sand, in the range of 10^{-8} cm^2 (see Bear, 1972). Under

Table 4.10. Oxygen isotope composition of the Aljustrel Volcanics (exclusive of samples affected by the Feltais-Estacao ore fluid).

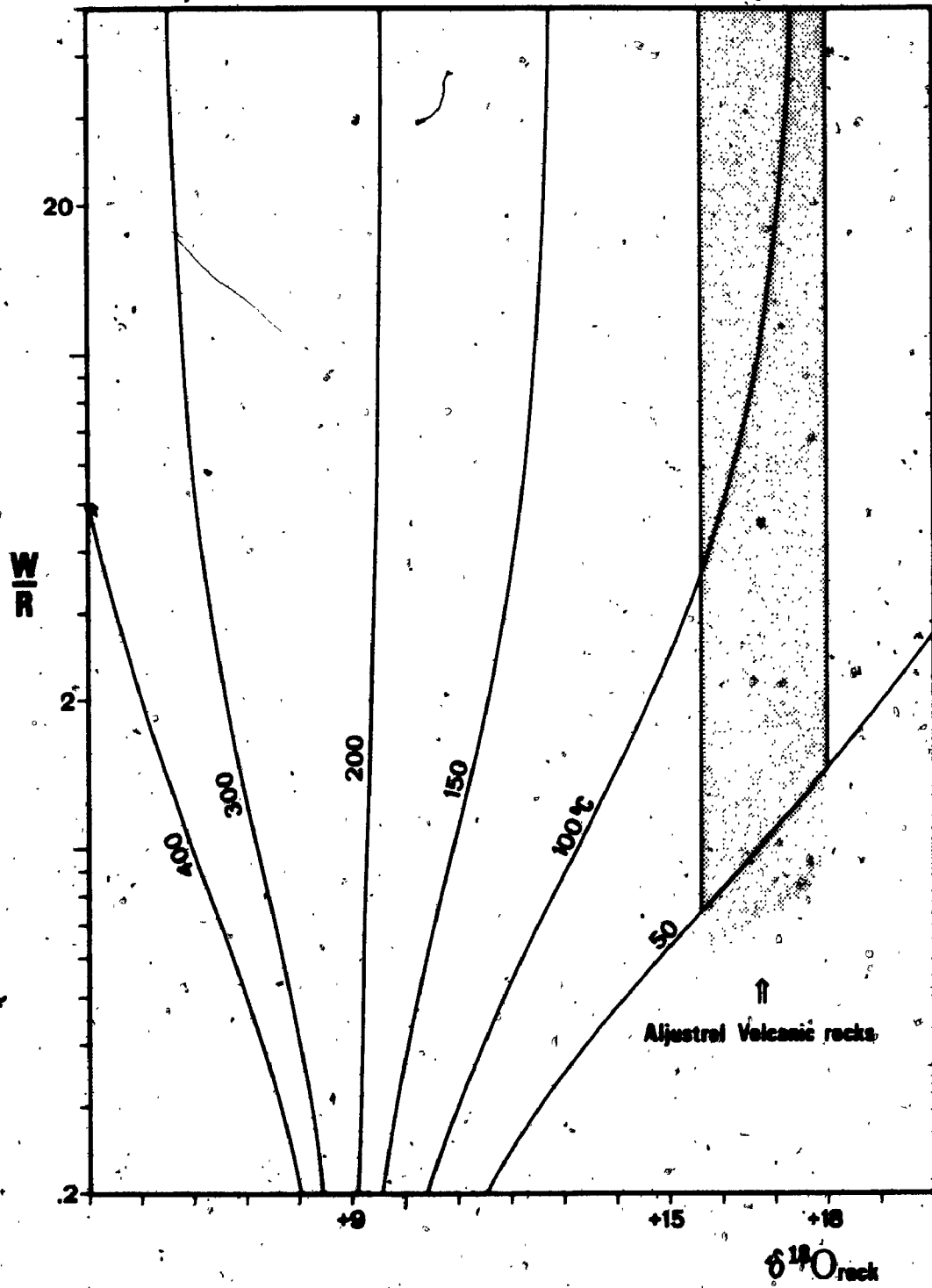
Unit and Sample	$\delta^{18}O/_{\text{oo}}$	Remarks
Quartz-eye tuffs		
		>1 km along strike from orebodies
PMTV2-CR	+16.51	Green facies (Mg-rich)
GFA	+16.18	No Feldspar megacrysts
1-GF	+15.63] Albite megacrysts
GF-84'	+16.85	
2-GF-87	+16.42] K-Feldspar megacrysts
6-GF-17	+15.7	
Felsitic tuffs		
SM-11	+16.0] Green facies] 1 km from mineralization
GF-89.5D	+16.68	
GF-93	+17.37	
GF-113	+17.6	
bis-296.5	+16.7] "Islands" in stockwork
bis-310.8	+17.1	
bis-341.2	+18.1	

these circumstances the initial cooling of the pyroclastic pile must have taken place through vigorous sea water convection driven with heat from within. The Rayleigh number must not only have exceeded the critical value necessary for convection to take place (see Lapwood, 1948) but, given the extremely high initial permeabilities inferred from geology and petrography, the second critical Rayleigh number must also have been exceeded. Above this value convection is non steady state (Straus, 1974; Combarrous and Le Fur, 1969), and drifting, irregular convection cells are thus likely to have formed. This explains the homogeneity of oxygen isotope data, as no fixed water recharge and discharge sites exist in a drifting convective system. The final isotopic result is everywhere the result of the prevailing physicochemical conditions, low temperature and high water/rock. The latter condition is required by the pronounced difference between original and final ^{18}O contents, illustrated in Fig. 4.14. This figure also shows that temperatures must have been (or decreased to) below $100^{\circ}C$ during this pre-mineralization stage.

4.4 Discussion and conclusions

As far as can be seen through major metasomatic changes, the Aljustrel Volcanics were originally constituted by two units of submarine pyroclastic rocks.

Figure 4.14. Diagram illustrating the molar water/rock and temperature ranges required to enrich the Aljustrel Volcanics in $\delta^{18}O$ from an initial value of $\delta^{18}O \approx +9\text{‰}$ (assumed) to $+15.6$ to 18.1‰ (measured) through exchange with sea water (0‰ $\delta^{18}O$). Rock (alkali feldspar)-water fractionation after O'Neil and Taylor (1967).



A high iron rhyolite (the Quartz-eye Tuff) may have erupted first, followed almost immediately thereafter by a high-silica rhyolite (the Mine Tuff). The tuff formations can be envisaged as derived from variable degrees of partial melting of a common (high-grade metamorphic?) crustal source, followed by varying degrees of shallow level crystal fractionation, or, alternatively, the QET may represent proximal volcanic facies and the MT more distal associated flow tuffs.

The main metasomatic changes experienced by the Aljustrel Volcanics seem to have been as follows:

- Major hydration, oxidation and Mg fixation in the uppermost 50 m or so of each of the QET and the MT;
- Progressive Fe (and perhaps Mn) leaching downwards in both tuff sequences;
- Progressive leaching of Cu and Zn in samples either markedly reduced or oxidized (Pb values all low);
- Significant Si leaching;
- Complex and evolving behaviour of the alkalis, with early widespread hydrolysis of igneous feldspars followed by hydrothermal growth of low temperature albite megacrysts which were subsequently partially or totally replaced by low temperature K-feldspar. Alkali feldspar megacrysts occur almost exclusively in the Quartz-eye Tuff (the central core of the Aljustrel Volcanics);

- General, homogeneous ^{18}O enrichment to extreme values around 17‰ $\delta^{18}\text{O}$.

Hercynian low grade regional metamorphism (up to lower greenschist facies and essentially isochemical, Munha, 1981; in press) may have obliterated in part the hydrothermal mineralogy, namely producing the presently observed chlorite, sericite and epidote from hydrothermal lower grade phyllosilicates such as smectite and celadonite and zeolites, respectively.

Conclusions regarding the origin of the Aljustrel Volcanics are in good agreement with previous hypothesis both for the Aljustrel Volcanics (Schermerhorn, 1976; Priem et al., 1978) and in general for the felsic volcanic rocks of the Iberian Pyrite Belt (Schermerhorn, 1970a; Soler, 1969; Hamet and Delcey, 1971; Munha, 1981).

Several aspects of the metasomatic changes detected in the Aljustrel Volcanics indicate that the fluid involved was initially oxidized, Mg bearing and very abundant. Given that these rocks were deposited in a submarine environment, the only available fluid reservoir with such characteristics is sea water.

Sea water simply trapped in the voids of the Aljustrel tuffs could not account for the high water/rock required at least during part of the metasomatic events, and the temperatures required were in the range $0\text{-}300^\circ\text{C}$ (and possibly over). The grain size of the Aljustrel Volcanics

was of the order of millimetres: initial permeabilities easily exceeded 10^{-8} cm² (Chilingar, 1963; Bear, 1972; Freeze and Cherry, 1979). Under these circumstances, and given also that metasomatism clearly predated regional metamorphism, metasomatism must have been caused by seawater convection through the initially hot (200°C) Aljustrel Volcanics, immediately after emplacement, as a result of the high heat contents of the rocks and possibly to high regional thermal gradients generated by a (presumed) magma chamber at depth. Fluid convection is the typical mechanism of heat extraction from hot permeable rocks in the presence of large amounts of fluids, as well known by students of geothermal areas (see Elder, 1965, 1967; Fyfe et al., 1978).

The complex and evolving behaviour of alkalis suggests that physicochemical conditions prevailing during the sea water hydrothermal alteration events changed markedly from the beginning to the end of hydrothermal activity. Textural relations indicate that alteration of igneous feldspars took place at an early stage, as it predates growth of hydrothermal albite. Given that experimental data shows that Mg is rapidly extracted from sea water upon interaction with rock, it is reasonable to presume that most Mg enrichment in the Green Facies rocks of both the QET and the MT also took place early in the history of the Aljustrel palaeohydrothermal system.

At least 2% Mg was in average added to Green Facies rocks, and the volume of these is of the order of 0.8×10^9 m³, corresponding to $\sim 4.5 \times 10^{10}$ kg of Mg extracted from sea water. Quantitative extraction of Mg implies that a minimum volume of sea water of the order of 45 km³ circulated through the Aljustrel Volcanics (probable total volume 5-20 km³), suggesting water/rock 100:1 - 25:1. For such values of w/r oxygen isotope data implies prevailing temperatures somewhat in excess of 100°C (Fig. 4.14).

Hydrothermal albite postdates early alteration of igneous feldspar, and the conclusions of Munha et al. (1980) indicate that temperatures for hydrothermal albite formation exceed 150°C. Thus temperature seems to have increased instead of decreasing in the course of sea water convection, suggesting the presence of a large magma chamber below.

We have also seen that hydrothermal alteration produced a reduced, Fe-Mn(?) - Cu-Zn-Pb(?) - Si bearing fluid, clearly potentially an ore forming fluid. Thus a likely candidate to generate the Aljustrel massive sulphide deposits.

CHAPTER 5

THE FEITAIS OREBODY OF ALJUSTREL, ITS ASSOCIATED METALLIFEROUS SEDIMENTS AND ORE ZONE HYDROTHERMAL ALTERATION

5.1 Introduction

From detailed study of the Aljustrel Volcanics we concluded that these have been affected by major sea water hydrothermal metamorphism which transformed rhyolites into quartz-keratophyres, and that in the course of the process sea water was modified into a Mg poor, transition-metal rich brine (given the hydration of the Aljustrel Volcanics). It was not possible to estimate the alkali metal content of this brine, in view of the complex and evolving behaviour of alkali metals in the Aljustrel Volcanics.

In this chapter we report on the study of the Feitais orebody and associated siliceous and metalliferous sediments, and on the prominent wall rock alteration that surrounds the ore zone. Much attention was dedicated to hanging wall rock alteration, particularly prominent at Feitais when compared to other orebodies, both at Aljustrel and elsewhere.

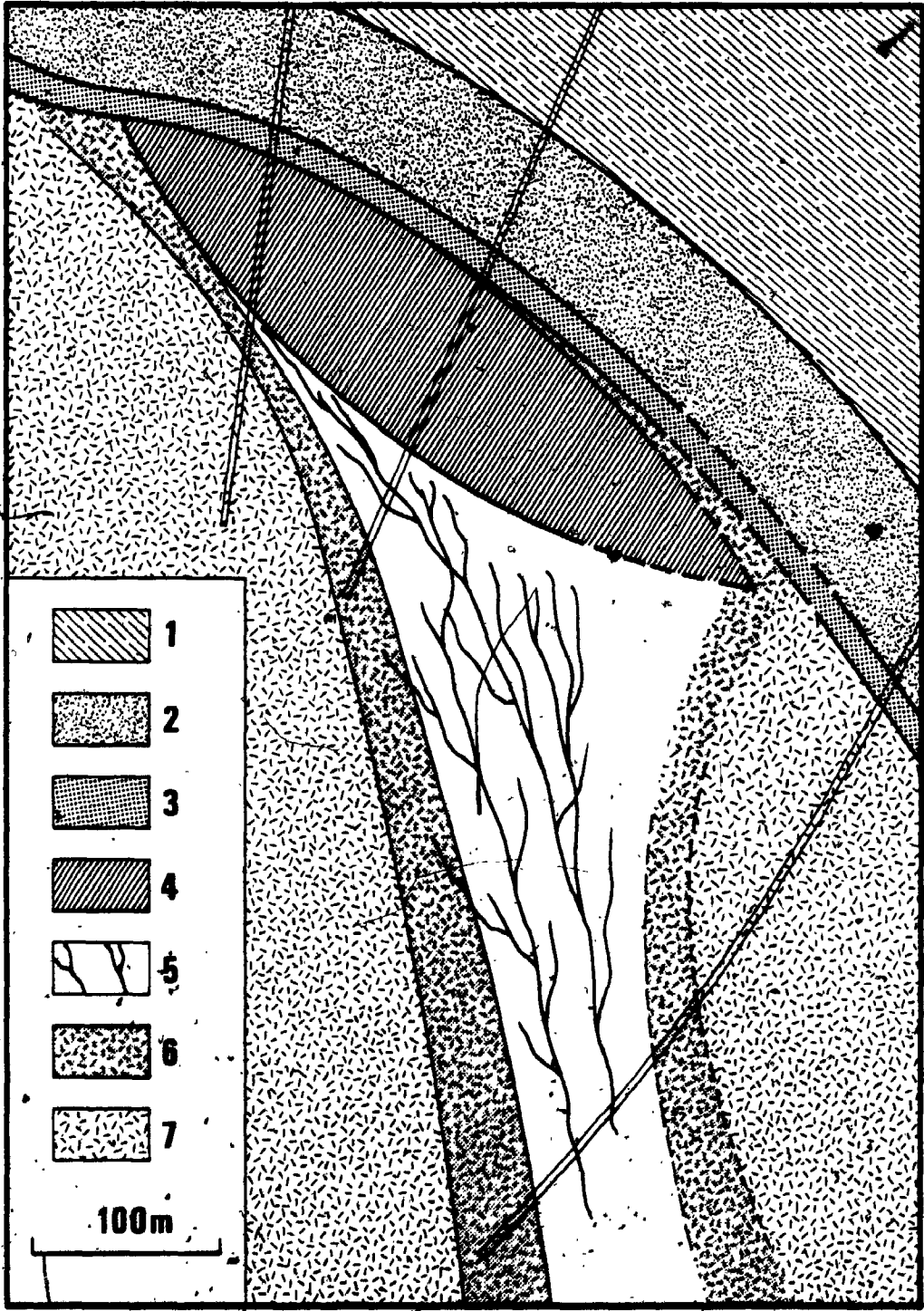
The spatial distribution of the various lithotypes constituting (and surrounding) the Feitais ore zone are schematically represented in Figure 5.1, including the approximate location of 4 drillholes from which most footwall and massive ore samples were collected. More detailed information with regard to field relationships and sample locations is presented in Appendix VI.

5.2 Petrography

5.2.1 Stockwork zone

The Feitais massive sulphide orebody is underlain by a zone of crosscutting stringer and disseminated sulphide mineralization (pyrite and/or chalcopyrite + sphalerite). This stockwork mineralization is hosted in rocks composed essentially of chlorite-quartz, sericite-quartz or sericite-chlorite-quartz. Minor amounts of carbonate are often present, and carbonates may locally become volumetrically dominant. The relative amounts of phyllosilicates (sericite, chlorite, or both) and quartz

Figure 5.1. Schematic spatial distribution of the various lithotypes constituting and surrounding the Feitais ore zone, with approximate projection of the location of several drill holes in a plane normal to the elongation of the Feitais-Estacao orebody. (Drill holes are, from left to right, LC1-bis, FS-8 and FS-21.) See also Appendix VI. 1-Culm Group; 2-Paraiso Siliceous Formation; 3-Jasper unit; 4-Feitais massive sulphide orebody; 5-Stockwork rock (quartz-chlorite-sulphides); 6-Outer stockwork rock (quartz-chlorite-sulphides); 7-Mine Tuff.



are widely variable, from sericite and/or chlorite dominated to quartz with only minor amounts of the other silicates. The absolute abundance of sulphide minerals is also widely variable, with a few metres of gradual transition to massive ore.

Chlorite + quartz + sulphides constitute an asymmetric crosscutting pipe-shaped body which occupies the core of the footwall zone of stockwork mineralization (Fig. 5:1). Barriga and Carvalho (1983) have proposed the name "stockwork rock" to this lithotype. Stockwork rock is often very rich in chalcopyrite, and grades into sericite-quartz-sulphides assemblages which in turn grade into Mine Tuff invariably depicting earlier regional hydrothermal alteration (described in Chapter 4). In other words, quartz-keratophyre grades into stockwork rock through an intermediate zone of sericite-quartz-sulphide rock which will be named "outer stockwork rock".

Plate 4C to E illustrates the textural variations mentioned above. Plate 1B is a Green Facies Mine Tuff collected away from mineralization, although perfectly equivalent textures can often be seen in intercalations of rock unaffected by mineralizing fluids but surrounded by stockwork rock. Plate 4C illustrates the effect of incipient stockwork alteration on a porphyric Mine Tuff: note the extreme degree of alteration of albite phenocrysts and the abundance of sericite, corroding the grains of

felsitic matter in the tuff matrix. Plate 4D portrays a sericite rich outer stockwork rock. Note that feldspar is now completely absent and that the sericite aggregates are texturally very similar to the matrix of the Mine Tuff. Outer (sericitic) stockwork rock grades into (chloritic) stockwork rock; illustrated in Plate 4E.

It is of significance that zircon is a frequent accessory of stockwork rocks (Plate 4F), usually enclosed in chlorite and with pleochroic haloes due to radiation damage. Zircon is generally anhedral, corroded and/or reprecipitated, although occasionally euhedral zircons indistinguishable from those of the Mine Tuff also occur. Allanite, when present, is always anhedral and also surrounded by pleochroic haloes when enclosed in chlorite.

There is weak zonation in the distribution of the various sulphides in the stockwork zone. Thus chalcopyrite occurs mainly in chloritized rocks, whereas sphalerite (with very minor galena) is particularly abundant in outer stockwork rocks (sericitized). Pyrite occurs throughout the stockwork volume, either accompanying chalcopyrite or sphalerite or as the only sulphide, and extends beyond the outer stockwork zone, into weakly ore zone altered Mine tuffs.

Mineralogical zonation in the Feitais stockwork is present at two scales: megascopically it is clear that stockwork rock (chloritic) predominates largely in the core

of the alteration pipe, and is enveloped by a relatively well defined halo of outer stockwork rocks (sericitic) before feldspar-bearing rocks are found. At the scale of individual sulphide-rich veins chlorite-quartz rock is sometimes surrounded by sericite-quartz rock (Plate 5A) which sometimes grades into Mine Tuff unaffected by ore zone alteration.

Stockwork zone mineral chemistry is best reported together with mineral chemistry of the remaining ore zone rocks (massive ore and hanging wall sediments, section 5.3.1).

5.2.2 The Feitais massive sulphide deposit

The Feitais-Estacão massive sulphide deposit is a truly gigantic orebody, with total reserves substantially in excess of 100 million metric tonnes, comparable in size to only a few other deposits in the world (see Franklin et al., 1981). A thorough study of sulphide mineralogy and textures was not attempted given the length of such a task and also in view of the fact that much relevant information could be obtained from unpublished mine reports and drillhole logs.

Pyrite is the most abundant sulphide mineral in massive ore. Sphalerite, chalcopyrite, galena and arsenopyrite are the remaining common sulphide minerals. Many other metallic minerals occur in minute quantities,

PLATE 5

(all scale bars (except A) 100 μm)

- A. Chalcopyrite + pyrite vein immediately surrounded by chlorite-quartz-chalcopyrite alteration (black) which is in turn surrounded by sericite-quartz-sulphide alteration (grey, at upper and lower edges of specimen). Note deformation. From stockwork under massive ore.
- B. Framboids in sulphide ore, composed of spherical aggregates of anhedral pyrite spotted with silicates. Reflected light, one nicol only.
- C. Framboids in Culm Group shale bed, composed of tiny pyrite cubes hosted in silicates + graphite (grey). Reflected light, one nicol only.
- D. Colloform aggregate composed of alternating bands of pyrite and chalcopyrite (cpy), hosted in massive sphalerite (sph). Reflected light, one nicol only.
- E. Colloform aggregates, including a ring composed of sphalerite (sph), chalcopyrite (cpy) and galena (G). Note euhedral pyrite in left aggregate. Reflected light (oil immersion), one nicol only.
- F. Partly recrystallized pyrite-gangue colloform aggregates. Reflected light, one nicol only.

PLATE 5

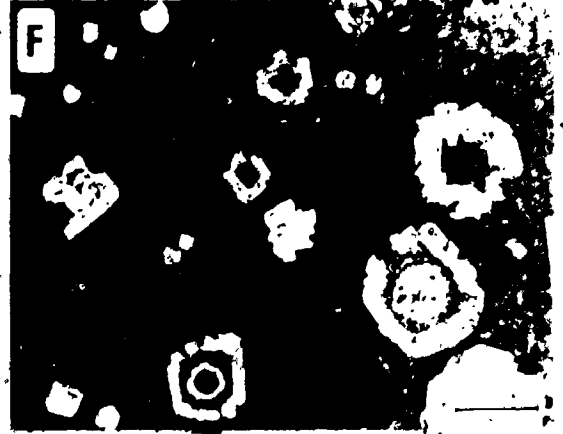
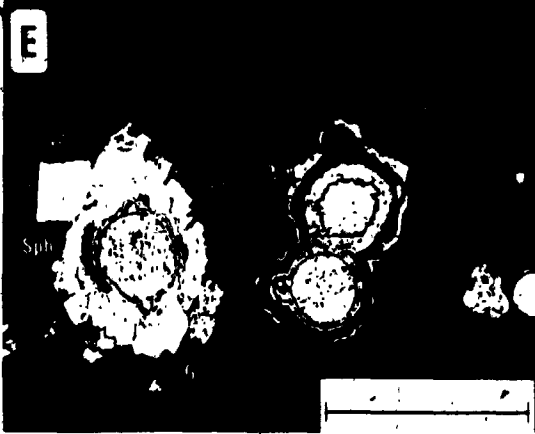
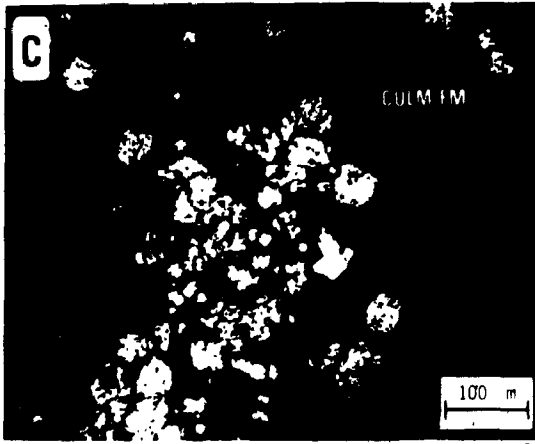
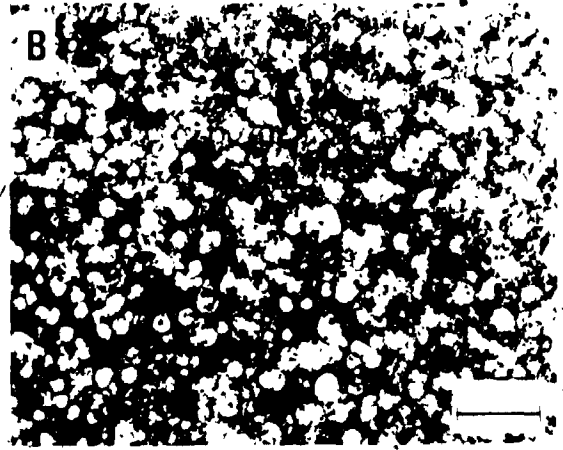
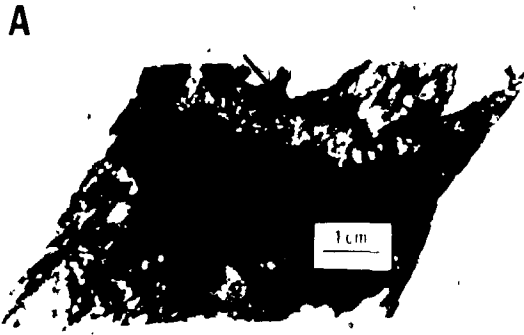
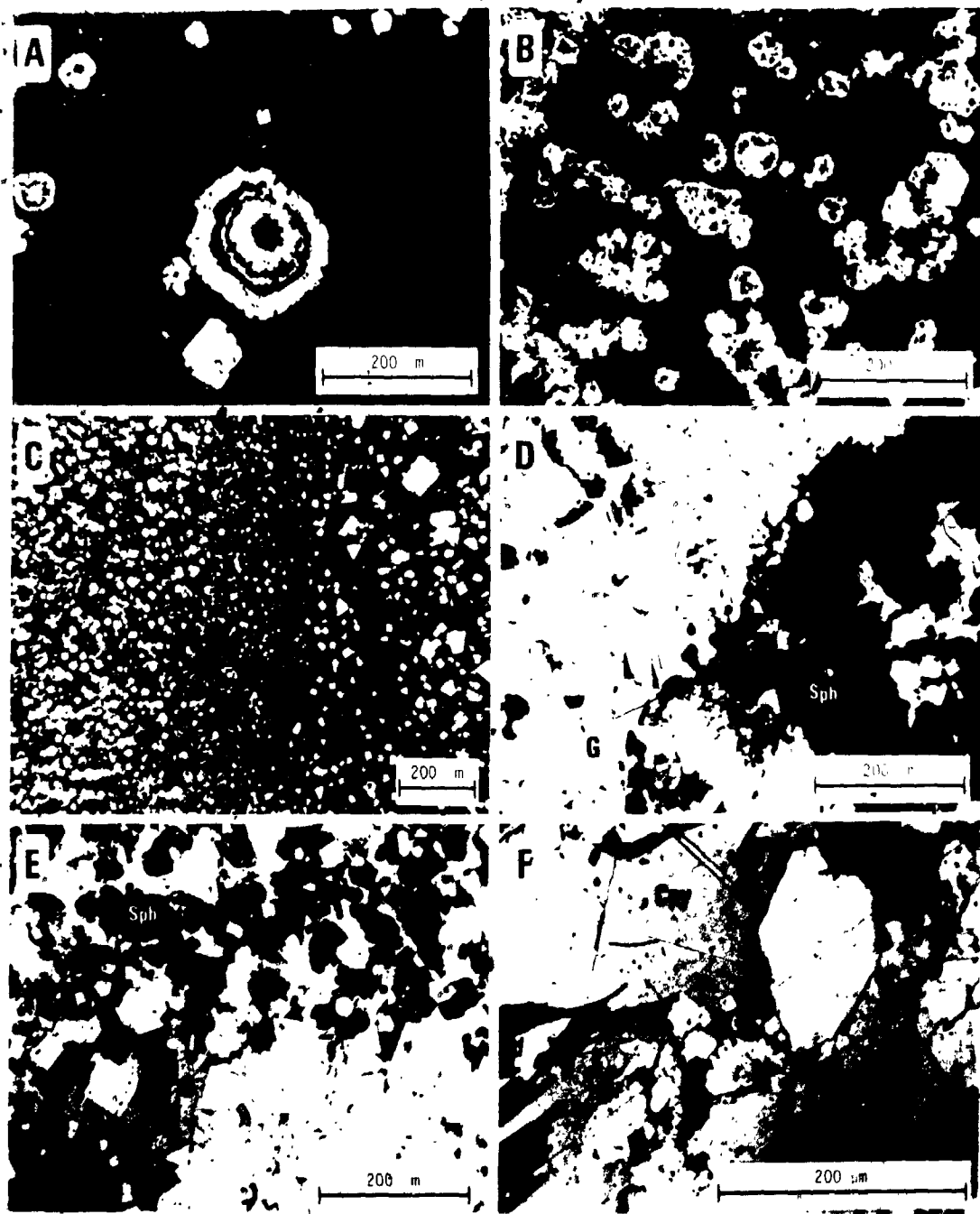


PLATE 6

(all scale bars 200 μm ; reflected light, one nicol only)

- A. Colloform pyrite. Note coalescence of pyrite rings.
- B. Pyrite aggregates exhibiting delicate cellular structures defined by radiating pyrite.
- C. Bedding (vertical, in the middle of photo) separating sharply a domain of exclusively euhedral pyrite from an adjacent bed of exclusively framboidal pyrite.
- D,E,F. Recrystallized massive sulphide ore, with idiomorphic pyrite (depicting brittle deformation) and plastically deformed sphalerite (sph), galena (G) and chalcopyrite (cpy). Pyrite is the lightest mineral in all photographs.

PLATE 6



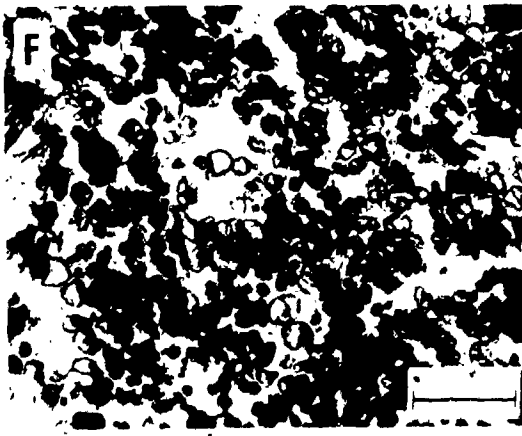
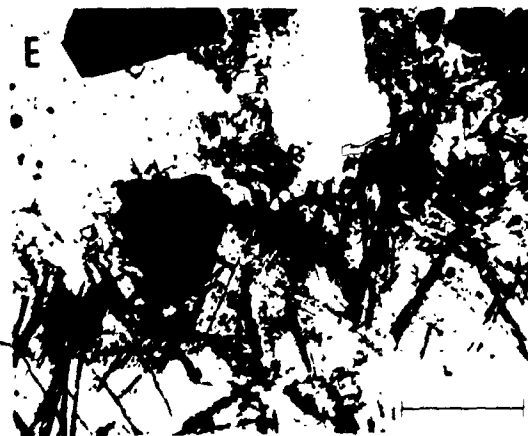
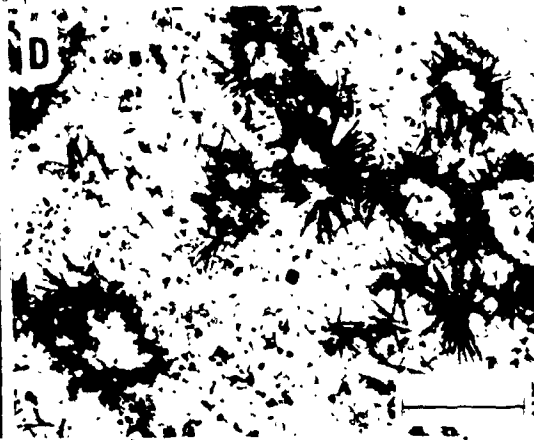
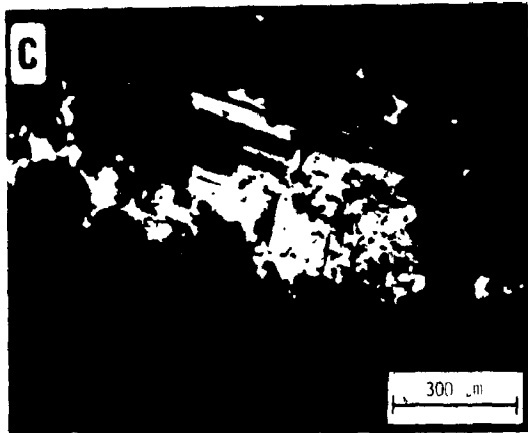
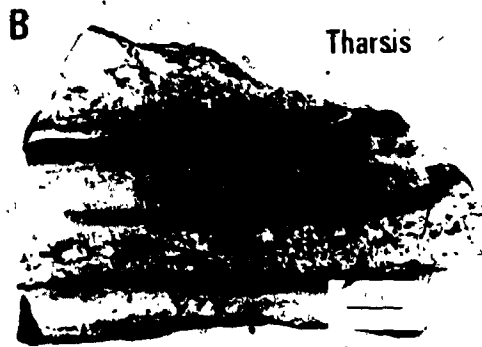
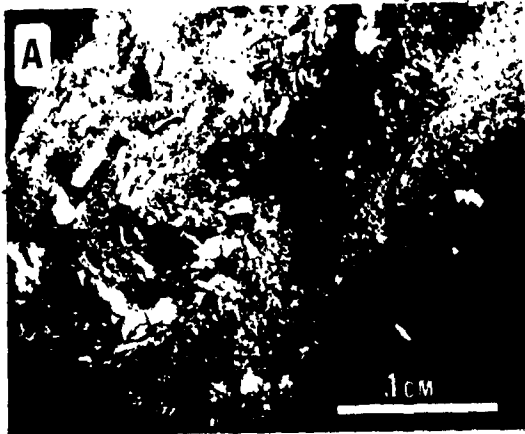
such as tetrahedrite, bournonite, tennantite, pyrrhotite, cobaltite, stannite(?) boulangerite, greenockite, and still others (Gaspar and Conde, 1978). The more abundant non-sulphide minerals are quartz, chlorite, sericite, several carbonates and barite.

Textures are extremely variable, as usual in slightly metamorphosed massive sulphide ores (Rockingham and Hutchinson, 1980). The more pyritic and massive ore varieties are often completely featureless, with only minor amounts of interstitial minerals in a continuous aggregate of pyrite. Etching (air) of this type of pyrite sometimes produces regularly spaced and sized globular figures of the same size range (15 μm) of the ubiquitous framboids (sensu lato, see Love and Amstutz, 1966) seen in less massive ore varieties (Plate 5B). It is interesting to note that framboids composed of tiny pyrite cubes (framboids sensu stricto) were not observed in the Feitais massive or stockwork ores, despite their frequent occurrence in the occasional sedimentary pyritic beds of the overlying Culm turbidites (see Chapter 2), illustrated in Plate 5C. Colloform textures are often seen, sometimes as beautiful concentric overgrowths of various sulphides and quartz, sometimes including polyminerallic single rings (Plates 5D to F and 6A). In other cases colloform aggregates include radiating pyrite (Plate 6B). Recrystallization produces fortification-type zoned aggregates as those

PLATE 7

- A. Small scale slump fold, composed of pyrite (white) and quartz. Reflected light, non polarized light. Scale bar 1 cm.
- B. "Turbidite textured" ore, typical of allochthonous massive sulphide deposits in the Iberian Pyrite Belt, with thinning upwards individual beds of clastic pyrite and black shale fragments in a fine grained matrix of pyrite + sphalerite + chalcopyrite + silicates. Tharsis mine, Spain. Scale bar 2 cm.
- C. Albite partly replaced by pyrite + sphalerite (black). Crossed nicols. Scale bar 300 μ m.
- D. Radiating aggregates of stilpnomelane in unaltered jasper. One nicol only. Scale bar 300 μ m.
- E. Stilpnomelane and magnetite (black) in slightly altered jasper. One nicol only. Scale bar 300 μ m.
- F. Spessartine garnet hosted in chert (both clear and dark). Sample 8-358.1. See Appendix IV-3. One nicol only. Scale bar 100 μ m.

PLATE 7



described by Ostwald and England (1977, 1979).

Euhedral pyrite (usually cubes, rarely pentagonal dodecahedrons) is however the more common form of occurrence of this mineral, and also that of arsenopyrite (pseudo-monoclinic prisms). Some euhedral pyrite seems to be primary/diagenetic, given that beds of pyrite cubes often occur adjacent to beds of framboidal pyrite (Plate 6C), and also because pyrite cubes often define pressure-shadows where parallel fibres of quartz developed during Hercynian deformation. Deformation also produced textures such as those depicted in Plate 6D to F, where idiomorphic (perhaps recrystallized) pyrite (and arsenopyrite) suffers brittle deformation whereas chalcopyrite, sphalerite and galena deform plastically, occupying intra and interspaces with respect to the non plastic sulphides (pyrite, arsenopyrite).

Massive ore is sometimes banded, this is particularly visible in base metal rich ore varieties. Sedimentary features such as small scale slumps (Plate 7A), convolute lamination and scour and fill occur sporadically.

Brecciated ore also occurs. All soft sediment deformation features observed can be explained by a few metres of movement (see Blatt et al., 1980). Evidence for large scale ore redeposition such as that present in allochthonous deposits elsewhere in the Pyrite Belt (Chapter 2; Plate 7B) is completely absent.



Mineralogical zonation is a prominent feature of the Feltais massive orebody. Thus chalcopyrite and chlorite are clearly concentrated towards the footwall of the massive body, in continuity with the occurrence of these minerals in the underlying stockwork zone, whereas sphalerite, galena and barite are abundant near the hanging wall and in peripheral zones. Sericite is more widespread in occurrence than chlorite, and seems to be concentrated towards the footwall and periphery of the orebody. Pyrite, arsenopyrite, quartz and carbonates are scattered throughout. Sulphide minerals are thus hosted in chlorite and/or sericite + quartz + carbonate towards the footwall and in a quartz + sericite + carbonate matrix elsewhere.

Tuff intercalations are occasionally found within the Feltais massive ore, always with gradational contacts with ore, and are particularly abundant towards the footwall, whereas near the top of the orebody highly siliceous inclusions (often quartz with minor sericite and carbonate) are dominant, in good agreement with the massive ore mineralogical zonation described above.

Ore textures indicate that the orebody was deformed and partly recrystallized during the Hercynian Orogeny (Chapter 2). Pre tectonic textures (framboids, colloform textures) are largely inconclusive: their occurrence within altered tuffs, both as inclusions in the massive orebody and in the stockwork confirms Roedder's (1968) observations

that colloform textures cannot be regarded as evidence for strictly sedimentary deposition. The origin of framboids is a matter of controversy; they are often considered evidence for biogenic processes (see Love and Amstutz, 1966), but Rickard (1970), based on physical and crystal chemical arguments concluded that framboids form through pseudomorphism of previous spherical bodies, and Berner (1969), Farrand (1970) and Sweeney and Kaplan (1973) reported on the inorganic laboratory synthesis of framboids, sometimes from earlier sulphides thus suggesting a diagenetic origin for such structures.

Mineral banding (convolute or undeformed) is believed to represent largely local bedding due to settling of sulphide particles precipitated in open space, thus contraindicating a replacement origin for a large proportion of the orebody. However, at least some replacement of previous existing rocks must have occurred, as proven by the occurrence of sulphides replacing earlier albite phenocrysts in ore zone weakly altered tuffs (Plate 7C) and as suggested by the gradational contacts of (a) the orebody as a whole (especially at the footwall) and (b) the lithic inclusions within massive ore.

Finally, it is worth noting that massive ore is conspicuously free of crosscutting veins of any kind (see frontispiece), in marked contrast with both the stockwork zone and the hanging wall Jasper unit (see next section).

5.2.3 Hanging wall siliceous and metalliferous sediments

Cherts, jaspers and Mn concentrations constitute a well defined horizon immediately above the Aljustrel Volcanics, mapped by Schermerhorn and Stanton (1969) as constituting the base of the Paraiso Siliceous Formation (see Chapter 3). For the sake of clarity we will call these siliceous and metalliferous sediments the Jasper unit.

At the scale of the Feitais Anticline the Jasper unit is a stratiform, up to 15 m thick continuous bed (except where tectonically disrupted), that outcrops extensively at the Feitais hill (Fig. 3.2) and that can be seen in most appropriate located drillholes, although sometimes as thin as 20 cm. Given that the Feitais-Estacao orebody occurs at the top of the Aljustrel Volcanics the Jasper unit is the hanging wall rock of the sulphide deposit. A few metres of ore zone altered volcanic rocks are sometimes present between massive ore and the Jasper, although this may be caused by post depositional movements, either synsedimentary or tectonic in origin, given the geological history of the area, the occurrence of hundreds of minor faults with diverse orientations, and given also the fact that the Jasper unit is often seen repeated by folding and/or small scale thrusting.

Jasper (hematitic red chert) is the predominant lithotype of the Jasper unit laterally away from the

Feitais-Estacao orebody, often accompanied by black manganiferous chert and by Mn-oxide (+ rhodonite and rhodocrosite) concentrations that have justified small open pit exploitations in the past.

A few samples of cherts and jaspers were etched with hydrofluoric acid and observed under the scanning electron microscope, but primary textures are obliterated by recrystallization. We note however that a similar SEM study of cherts and jaspers from other areas in the Iberian Pyrite Belt (F. Barriga, unpublished data), less affected by regional metamorphic recrystallization evidenced the presence of radiolarians in the cherts occurring laterally away from sulphide mineralization (> 500 m), but not in samples directly overlying massive sulphide ores, suggesting that above hydrothermal vent areas silica may have precipitated simply as a consequence of sharp temperature decrease upon contact of a Si-rich hydrothermal solution with cold sea water.

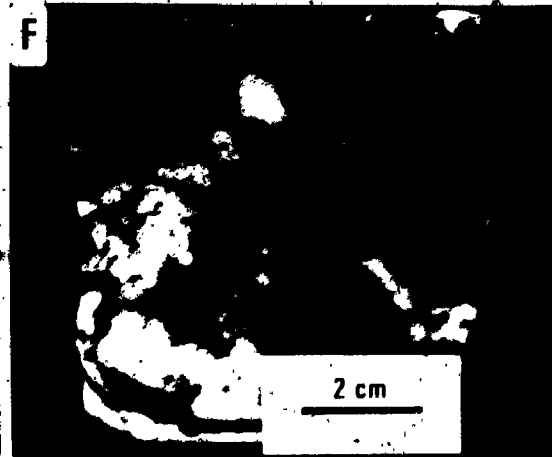
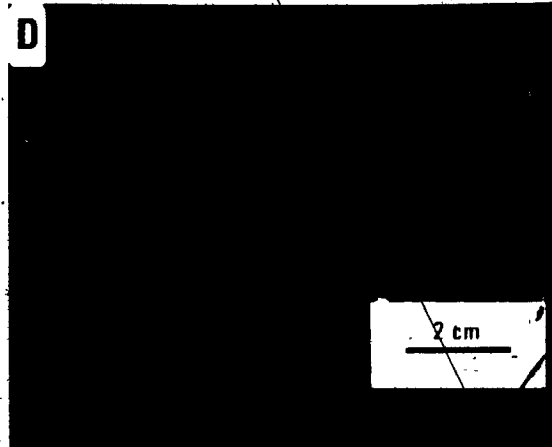
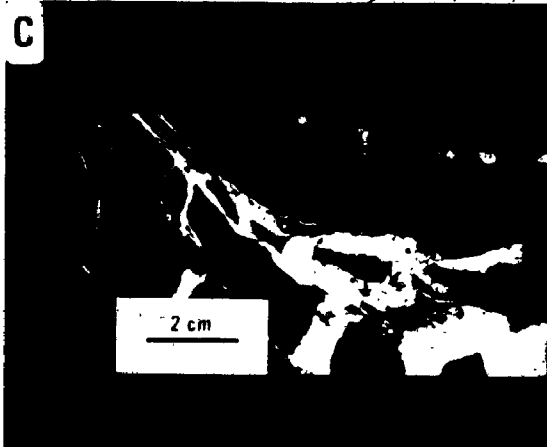
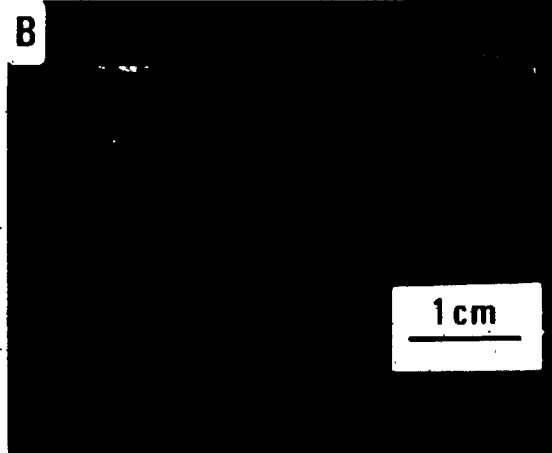
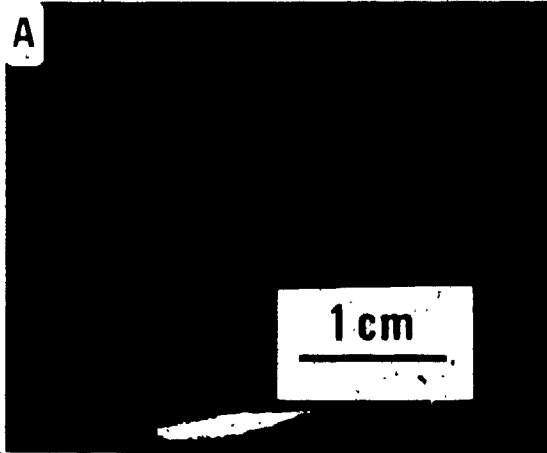
In the immediate vicinity and especially above the orebody the jasper is partially or totally altered into predominantly bluish grey pyritic chert, with reduction of hematite to magnetite and pyrite, as eloquently illustrated in Plate 8. Bright red jasper immediately above massive sulphide ore is restricted to relics of various sizes, up to a few tens of centimetres, with gradational contacts to chert of various shades of grey, containing magnetite,

PLATE 8

Illustration of reductive alteration in the Feitais
hanging wall Jasper unit

- A. Unaltered bright red jasper collected several hundred metres away from known sulphide mineralization (drill hole S-3, Esteval da Serra). Subsequent photographs collected near (<100 m) and immediately above massive sulphide ore.
- B. Incipient vein controlled reduction of hematite to magnetite. Drill hole FS-15.
- C. Breccia-pipe like quartz + carbonate + magnetite + chalcopyrite vein system in slightly altered jasper, with magnetite ribbons in a slightly iron depleted jasper matrix. Drill hole FS-11.
- D. Advanced alteration of jasper (unaltered "island" left on lower left side) with generation of magnetitic-pyritic dark grey chert. Drill hole FS-15.
- E. Complete alteration of jasper into bluish-grey pyrite-magnetite chert. Drill hole LC1-bis.
- F. Completely altered jasper (equivalent to E) depicting prominent post alteration deformation. Drill hole FS-14.

PLATE 8



pyrite and even chlorite replacing hematite. Vein controlled reducing alteration can often be seen, from the vein wall grey chert to unaltered red jasper. In other cases a network or a subparallel set of closely spaced veins leaves no unaltered relics, transforming the jasper into completely reduced pyritic and/or chloritic chert. From detailed study of the Jasper unit in 11 drillholes which also intersect sulphide mineralization (below) it is concluded that pre-tectonic veins responsible for access of the reducing fluid that altered the jasper amount to about 5% of the present volume of the Jasper unit above Feitais-Estacao. Minerals in these veins can include the following, singly or in combination: quartz, carbonates, chlorite, pyrite, magnetite, chalcopyrite, sphalerite, barite and cobaltite (cobaltite identified by X-ray diffraction). Within the chert and jasper groundmass the mineralogy does not exactly match that of crosscutting veins. Thus carbonates, magnetite and pyrite are common scattered in a recrystallized quartz matrix, whereas chlorite is less frequent, restricted to rare crystals (< 0.1 mm) associated with pyrite, magnetite or stilpnomelane, a mineral not observed in pre-tectonic veins crosscutting cherts but a frequent accessory of the cherts themselves, sometimes forming striking aggregates (Plate 7D; E). Spessartine garnet occurs sporadically as subhedral crystals up to 0.01 mm in diameter hosted in quartz,

rhodochrosite and/or chlorite, and both scattered throughout the chert or restricted in occurrence to discrete elongated domains (veins? beds?), as illustrated in Plates 7E and 9A. Hematite is ubiquitous within jaspers, of course, and is sometimes seen partly replaced by magnetite or pyrite. Some black cherts are manganeseiferous, because of the presence of Mn oxide dust, sometimes still depicting the original form of globular aggregates, despite recrystallization of the host quartz. Typical chert and jasper textures are illustrated in Plate 9B and C.

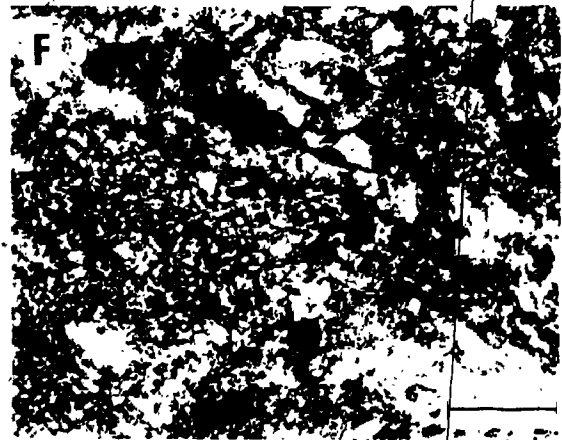
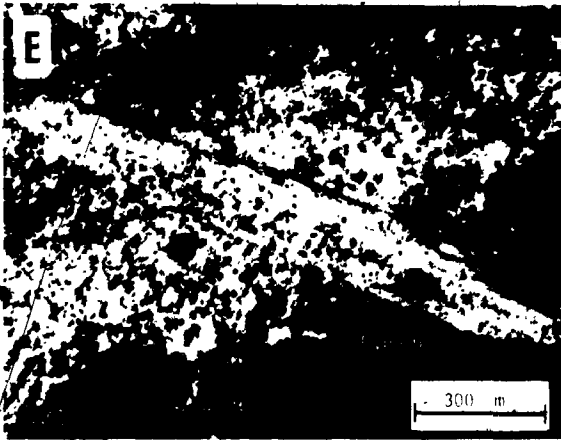
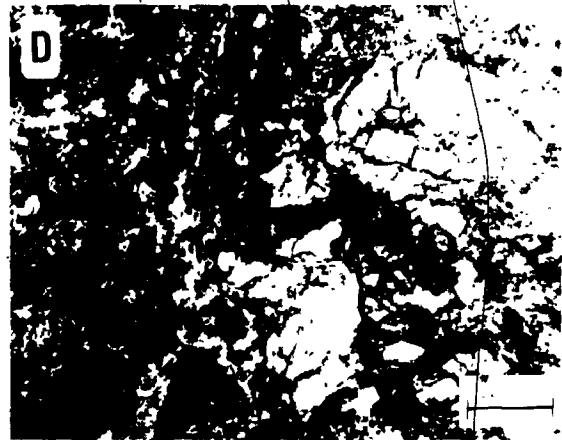
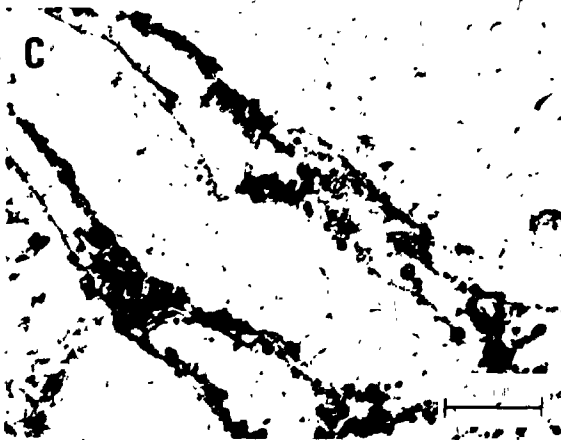
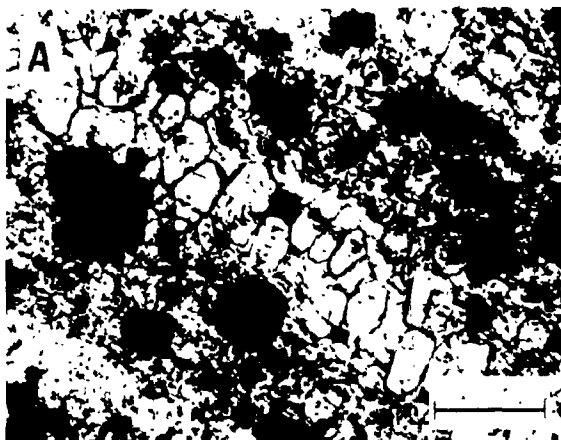
High grade Mn oxide concentrations were not observed in any subsurface samples. Instead, unweathered zones of the Jasper unit frequently include veins, pods and breccias mainly composed of various Mn rich carbonates (see section 5.3), accompanied by smaller amounts of magnetite (+ minor Mn oxides), stilpnomelane, chlorite, barite and, in one case, cymrite, a rarely reported hydrated barium Al-silicate. The textures of these Mn carbonate rocks are widely variable, but a matrix of carbonate + magnetite + stilpnomelane + chlorite is often seen hosting clear, rounded or irregular aggregates of coarse carbonate (sometimes spotted with chalcopyrite), up to several mm in diameter (Plate 9D to F).

Cymrite, clearly porphyroblastic, occurs as unoriented prisms (up to 0.8 mm) scattered in a rhodochrosite-magnetite matrix cut by frequent millimetric veins of

PLATE 9

- A. Spessartine garnet + chlorite elongated domains (veins?, beds?) in rhodochrosite-magnetite metalliferous sediment. One nicol only, scale bar 100 μm .
- B. Hematite + Mn oxide dust in jasper.
- C. Quartz + carbonate + magnetite veins in deeply altered jasper. One nicol only. Scale bar 2 mm.
- D. Typical texture of metalliferous sediment, with clear domains of calcic rhodochrosite (MnCO_3 75%) spotted with chalcopyrite in a matrix composed of manganocalcite (MnCO_3 25%) + magnetite + stilpnomelane + chlorite. One nicol only. Scale bar 500 μm .
- E. Large symrite porphyroblast, partly replaced by Mn-calcite (grey), spotted with magnetite (black) and rimmed by stilpnomelane (hardly visible, fibrous) in a rhodochrosite + magnetite + stilpnomelane. One nicol only. Scale bar 300 μm .
- F. Chert domains (finely recrystallized quartz) in metalliferous sediment suggesting either replacement or injection of metal rich fluid in soft siliceous sediment. Crossed nicols. Scale bar 100 μm .

PLATE 9



stilpnomelane, dusted with magnetite-after-hematite and partly replaced, by Mn-calcite (Plate 9E). Cymrite was previously identified at one location in the Iberian Pyrite Belt (Aye and Strauss, 1975), within the stockwork rock underlying the La Zarza orebody (Spain), associated with quartz-chlorite rock containing lesser amounts of Fe-carbonate and sericite (plus sulphides and relic igneous minerals). It is interesting to note that La Zarza is the massive sulphide deposit in the whole Pyrite Belt which most closely resembles Feitais, and that cymrite can thus occur both in footwall and hangingwall rocks. Cymrite electron microprobe analyses are presented in section 5.3.

Mn-carbonate rocks often include small, irregular areas of chert (Plate 9F) suggesting replacement of jasper (or manganiferous chert) by Mn-carbonates or, alternatively, that a Mn rich fluid "intruded" the chert prior to lithification.

Paraiso Formation phyllites and tuffites (and rare tuffs) in contact with the Jasper unit immediately above Feitais-Estacao are often (but not always) intensely veined, chloritized and carbonatized, sometimes to such extreme degrees that the rocks can become composed solely of alteration products (chlorite, carbonates, sulphides). Schermerhorn, (1978) noted the presence of these rocks and denominated them "upper chloritite". Alteration of PS aluminous rocks extends from 0 to ~10 metres above the

Jasper unit, similar to descriptions by Carvalho (1976) and Plimer and Carvalho (1982) for the hanging wall alteration above the Salgadinho deposit (see Chapter 2).

5.3 Geochemistry

5.3.1 Mineral Chemistry

a) Chlorite

Electron microprobe analyses of chlorites from the various rocks that host the Feltais-Estacao orebody are presented in Appendix IV-1, and plotted in Figure 5.2. It is apparent that ore zone chlorites do not show any well defined stratigraphic or lithologic control with respect to Fe/Mg. With one exception, stockwork and massive ore chlorites are identical to chlorites occurring in Aljustrel Volcanics not affected by ore fluids (see Fig. 4.4 and Appendix II-5); they are mostly iron rich ripidolites. Chlorites veining and scattered in Jasper unit rocks are very similar to the above, although slightly more variable, as they include the higher Si contents detected, up to 2.95 Si ions per 14 O, and also the more ferroan chlorites analysed, up to 45% FeO with only ~2.5% MgO.

The Mn content of ore zone chlorite shows marked stratigraphically controlled variations around the Feltais orebody, as illustrated in Fig. 5.3. Stockwork and Cu-rich massive ore chlorites contain the least Mn, averaging about 0.35% MnO, whereas Zn-Pb rich massive ore and the base of

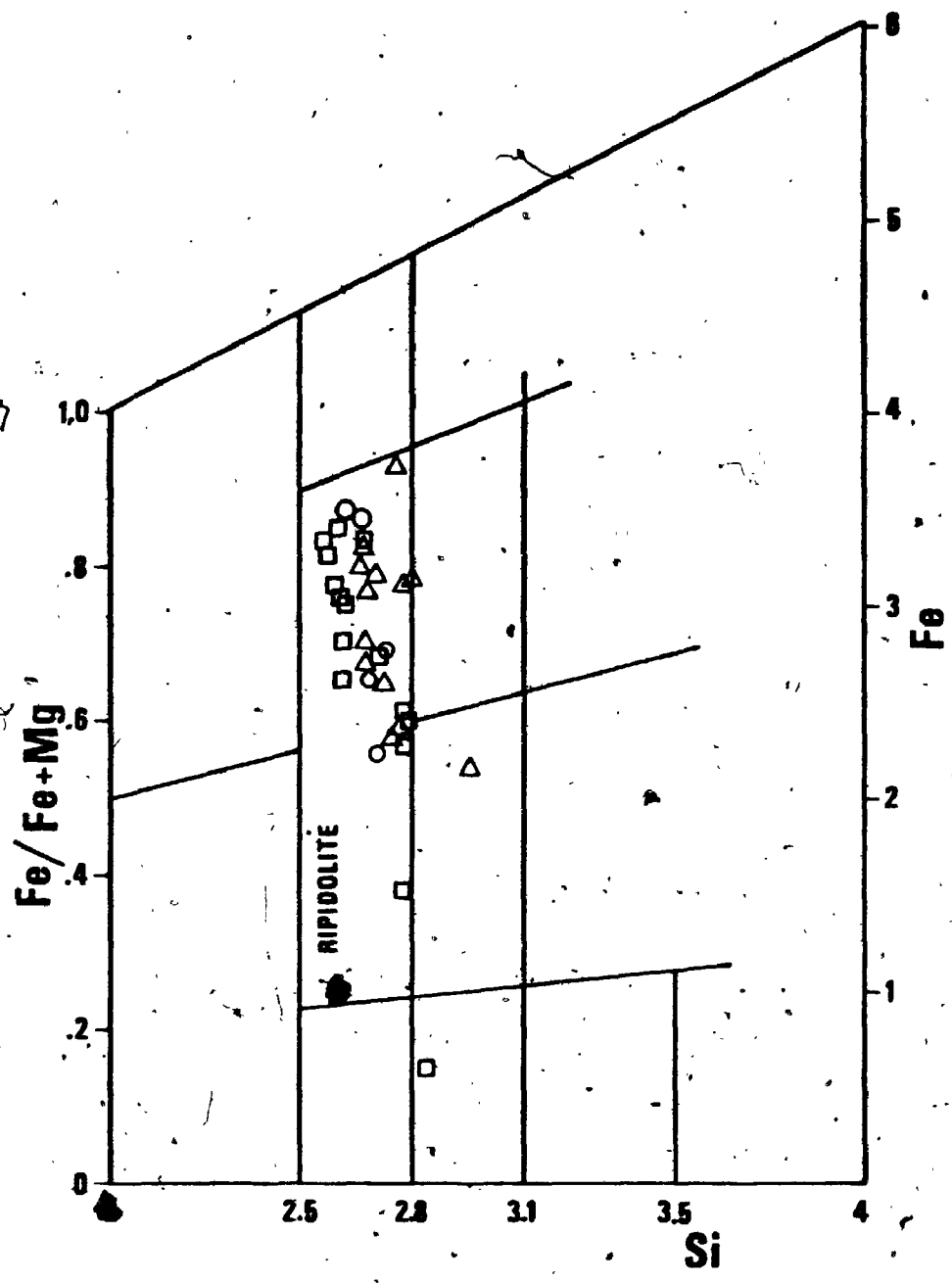
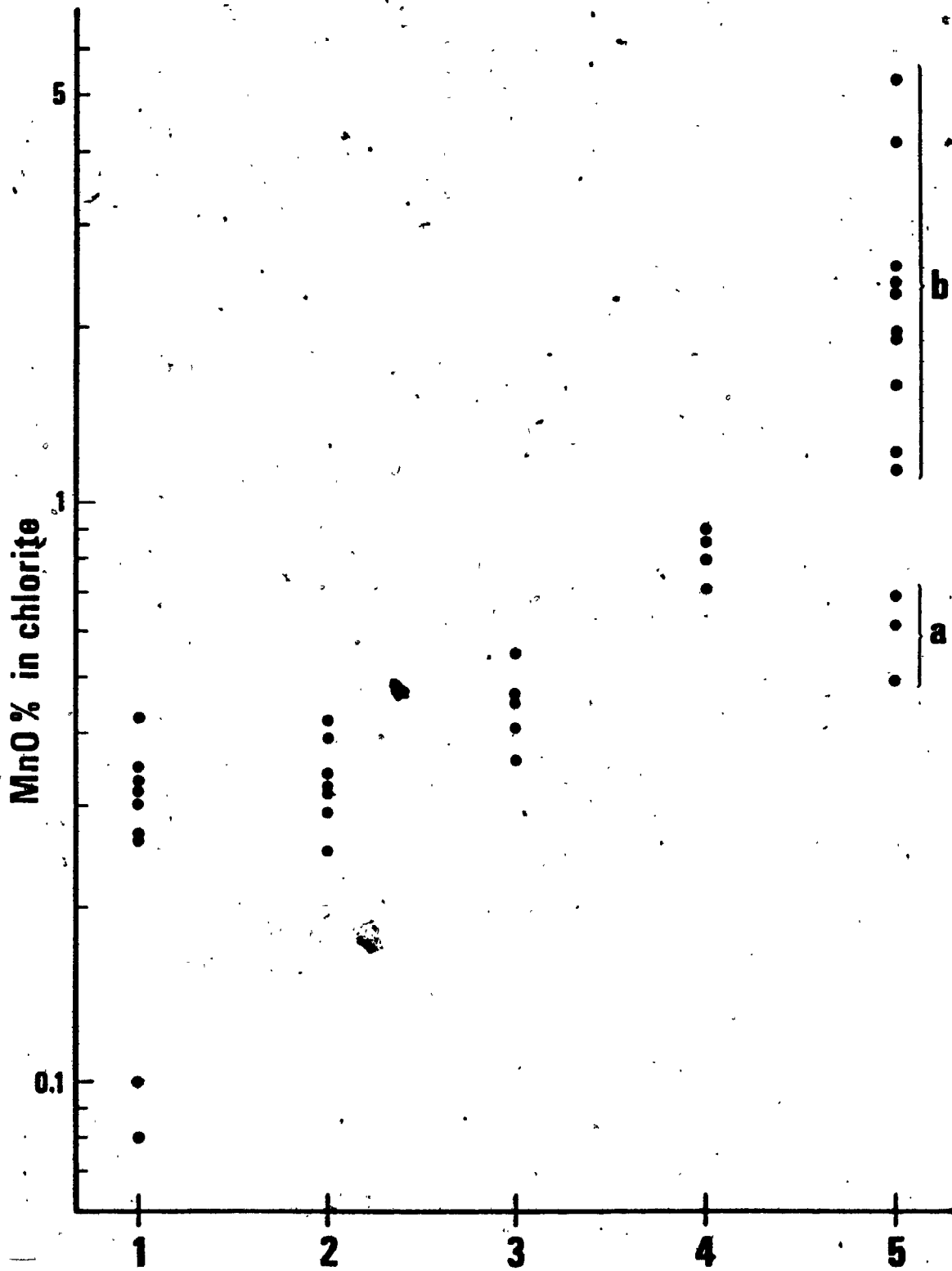


Figure 5.2. Diagram illustrating the compositional variation of chlorites from the Feitais ore zone with respect to Fe, Mg and Si. Triangles, hanging wall rocks; circles, massive ore; squares, stockwork rocks (Mine tuffs). Compare with Fig. 4.4.

Figure 5.3. Stratigraphically controlled variation of the MnO abundance in the Feltais ore zone chlorites. 1-Stockwork rocks; 2-Cu rich massive ore; 3-outer stockwork rocks; 4-Zn (Pb) rich massive ore; 5-Jasper unit (a, base; b, top).



the Jasper unit contain chlorites with $\sim 0.6\%$ MnO, and chlorites occurring near the stratigraphic top of the Jasper unit or laterally away from sulphide mineralization contain 1.1 to 5.3% MnO. These variations are strongly suggestive of a redox gradient, with low P_{O_2} in the core of the ore system, and progressively less reducing conditions away from it, as expected in such an environment (see Whitehead, 1973).

b) Sericite

Ore zone sericite is often so fine grained and intimately mixed with quartz that it could not be successfully analysed in most peripheral stockwork rocks. Electron microprobe analyses (Appendix IV-2) show striking BaO contents in ore zone sericites, up to $>9\%$ BaO, especially in samples and zones where barite was not seen under the optical microscope. Figure 5.4 shows that Ba is indeed in the phyllosilicate structure, as it illustrates the Ba distribution detected by high definition electron microprobe analysis (electron beam diameter $\sim 0.5 \mu\text{m}$) in more than 1300 closely spaced spots (rectangular grid of $5 \times 3 \mu\text{m}$).

c) Spessartine garnet

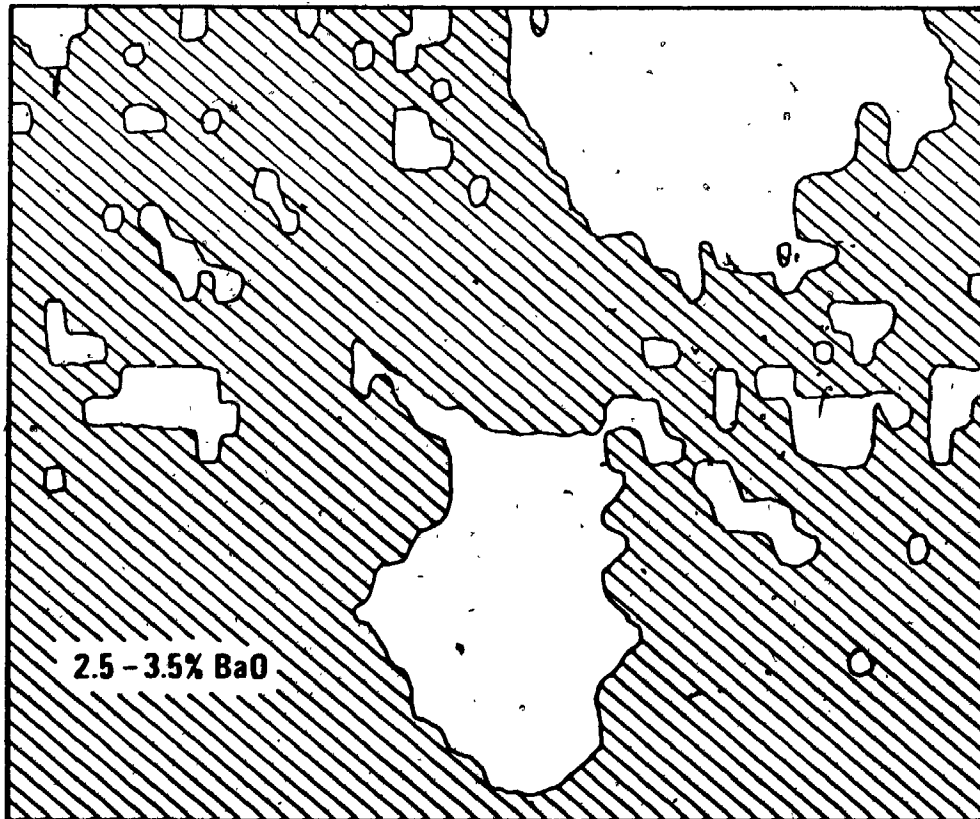
Electron microprobe analyses (Appendix IV-3) show that the spessartine garnet that occurs in the Jasper unit is composed of nearly 84% spessartine end member, with ~ 10 to 13% grossular end member molecule and small amounts of

Figure 5.4. SEM photograph of outer stockwork rock, composed of Ba-sericite (note ultra fine grain size of individual crystals), quartz and pyrite. More than 1300 closely spaced spot analyses for Ba were performed within the area indicated (rectangular grid of $3 \times 5 \mu\text{m}$), using a cymrite mineral standard (electron beam diameter $0.5 \mu\text{m}$), revealing the distribution represented below (white areas $< 0.01\%$ BaO). Sample 8-365.4, compare with Table IV-2. Scale bar in photograph (lower right) $10 \mu\text{m}$, in map $15 \mu\text{m}$.

Data obtained with the newly installed Jeol JX-733 Super Probe of the Department of Geology, University of Lisbon.



15 μm



2.5 - 3.5% BaO

either andradite or almandine. It is not known whether this mineral was generated in the course of hydrothermal activity or is a product of subsequent regional metamorphism (see Deer et al., 1962).

d) Cymrite

Cymrite electron microprobe analyses are presented in Table 5.1, recalculated on the basis of 8 oxygens, according to the formula proposed by Carron et al. (1964) and Essene (1967). Structural formulae depict a slight excess of Si and the presence of significant amounts of Ca and K substituting Ba. Again it is not known whether cymrite is hydrothermal or regional metamorphic in origin. Cymrite is now known to occur in various environments and host rocks and it is interesting to note that no other Ba minerals have been reported to coexist with cymrite in the same mineral assemblage (see Smith et al., 1949; Runnels, 1964; Essene, 1967; Froelich and Sandrea, 1973; Aye and Strauss, 1975; Soong and Olivecrona, 1975).

e) Carbonates

Electron microprobe analysis of (97) carbonates occurring in ore zone rocks are tabulated in Appendix IV-4. Calcites are the only carbonates found within stockwork and massive ore samples, usually with only minor proportions of Mn or Fe, and sometimes significant zinc (up to ~4% ZnO or ~6% ZnCO₃ equivalent), when in contact with sphalerite. Carbonates scattered in chert and jasper

Table 5.1. Electron microprobe analyses of cymrite.

Anal. no.	40	42	29	30	60	Average of 5	Stoich-cymrite
SiO ₂	31.63	32.76	29.48	29.53	30.39	30.76	30.51
Al ₂ O ₃	25.26	26.01	24.50	24.12	24.44	24.87	25.90
FeO _t	0.57	0.86	0.95	0.64	0.92	0.79	
MnO	0.22	0.16	0.29	0.24	0.31	0.24	
MgO	0.06	0.12	0.11	0.07	0.05	0.08	
CaO	0.32	0.24	0.37	0.39	0.28	0.32	
BaO	34.73	36.20	35.00	36.30	37.60	35.97	39.00
Na ₂ O	0.23	0.28	0.17	0.09	0.30	0.21	
K ₂ O	0.55	0.64	0.18	0.13	0.27	0.35	
TOTAL	93.57	97.27	91.05	91.51	94.56	93.59	95.41
Number of ions on the basis of 8 O							
Si	2.054	2.053	2.001	2.013	2.016	2.028	2.000
Al	1.933	1.921	1.960	1.938	1.911	1.933	2.000
Fe	0.031	0.045	0.054	0.036	0.051	0.044	
Mn	0.012	0.008	0.017	0.014	0.017	0.013	
Mg	0.006	0.011	0.011	0.007	0.005	0.008	
Ca	0.022	0.016	0.027	0.028	0.020	0.023	
Ba	0.884	0.889	0.931	0.970	0.977	0.929	1.000
Na	0.029	0.034	0.022	0.012	0.038	0.027	
K	0.046	0.051	0.016	0.011	0.023	0.029	
Σ ions	5.017	5.029	5.038	5.030	5.059	5.034	5.000

include not only calcite but dominantly siderite (sometimes slightly magnesian - sideroplesite), whereas a wide variety of Mn-Ca-Fe carbonates characterizes the carbonate rich veins, pods and breccias found within the siliceous sediments, where up to 5 different carbonate minerals were analysed within areas of a few square millimetres. The more abundant carbonate species in these rocks are highly manganoan calcite, Mg-poor ankerites and rhodochrosite. The distribution and nature of the various carbonates within Mn-rich carbonate rocks of the Jasper unit suggests that the variability detected is due to immiscibility gaps in the solid solutions within the system $FeO-MnO-CaO-CO_2$ (see Deer et al., 1962) and thus to variations in the local proportions of Fe, Mn and Ca at the time of carbonate formation.

Carbonates are also locally abundant within the altered PS Formation phyllites and tuffites, chemically different from all other ore zone carbonates essentially because Mg is here a frequently abundant component of ankerites (up to 15% MgO) and even of siderite. No dolomite or magnesite were found, however.

The spatial distribution of the dominant cations in ore zone carbonates is schematically represented in Figure 5.5.

f) Sphalerite

Electron microprobe analyses of sphalerites from

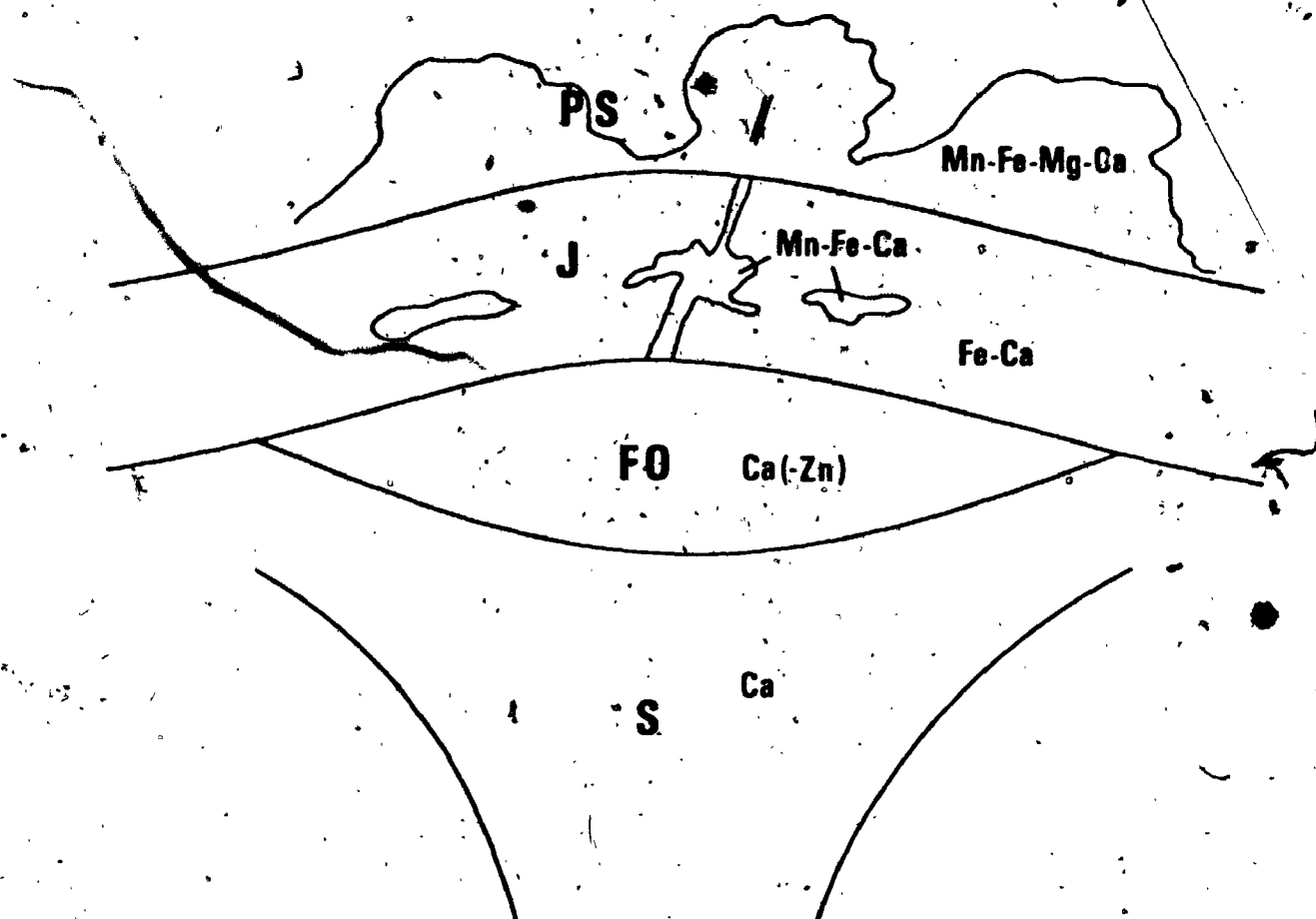


Figure 5.5. Schematic distribution of the dominant cations in ore zone carbonates. MT-Mine Tuff; S-Stockwork; FO-Feitais massive sulphide orebody; J-Jasper unit; PS-Paraiso Siliceous Formation.

stockwork, massive ore and Jasper unit samples are tabulated in Appendix IV-4, and show undetected or very low Mn abundances (generally $<0.04\%$ Mn), and also low Cd contents (up to 0.23%) in good agreement with the occurrence of greenockite within massive sulphide ore (Gaspar and Conde, 1978). The FeS mole % content of sphalerites varies from 1 to 11. Low Fe sphalerites are the lighter brown coloured, and no correlation was found between Fe content and stratigraphic position, lithologic type, ore type or degree of recrystallization.

5.3.2 Whole rock geochemistry

Extensive whole rock geochemical determinations were performed in samples from stockwork rocks, the hanging wall Jasper unit and also in altered and unaltered PS phyllites, tuffites and tuffs (Appendix V) in order to

- document as many as possible zonations around the sulphide orebody, especially those of genetic significance and/or potentially useful in mineral exploration;
- gain insight into the pre mineralization nature of altered lithologies, namely stockwork rocks;
- elucidate the composition and origin of the ore forming fluid(s)
- reconstruct as far as possible the history of the Aljustrel paleo hydrothermal system.

a) Stockwork rocks and massive sulphide ore

a1) Major elements

Major element abundances in stockwork rocks from the footwall of the Feltais orebody closely reflect the mineralogical composition and zonation described in previous sections. Thus rocks showing the least ore zone alteration are closely similar to other Mine tuffs (Chapter 4), but variably enriched in S, Fe and Ba, and sometimes depleted in Na, reflecting the presence of pyrite and Ba-sericite and partial corrosion of albite.

Outer stockwork rocks, apart from containing widely variable proportions of Fe and S reflecting the heterogeneous distribution of pyrite described before show relatively constant ratios of $(K_2O + BaO)/Al_2O_3$ around 0.2 to 0.3, expressing clearly the predominance of sericite and Ba-sericite over the other aluminosilicates, namely feldspar or chlorite. High BaO concentrations occur at the stratigraphic top of outer stockwork rocks, and reflect the spatial distribution of Ba-sericite; the only Ba mineral found in stockwork rocks. Thus Ba-sericite occurs mainly near (and within) peripheral massive sulphide ore, as schematically illustrated in Figure 5.6. Additional characteristics of outer stockwork rocks are extremely low Na (given the absence of feldspars), and widely variable Al/Si, a consequence of the equally variable relative modal proportions of sericite and quartz. The average SiO₂ abundance of outer stockwork rocks is ~62% (70% on a

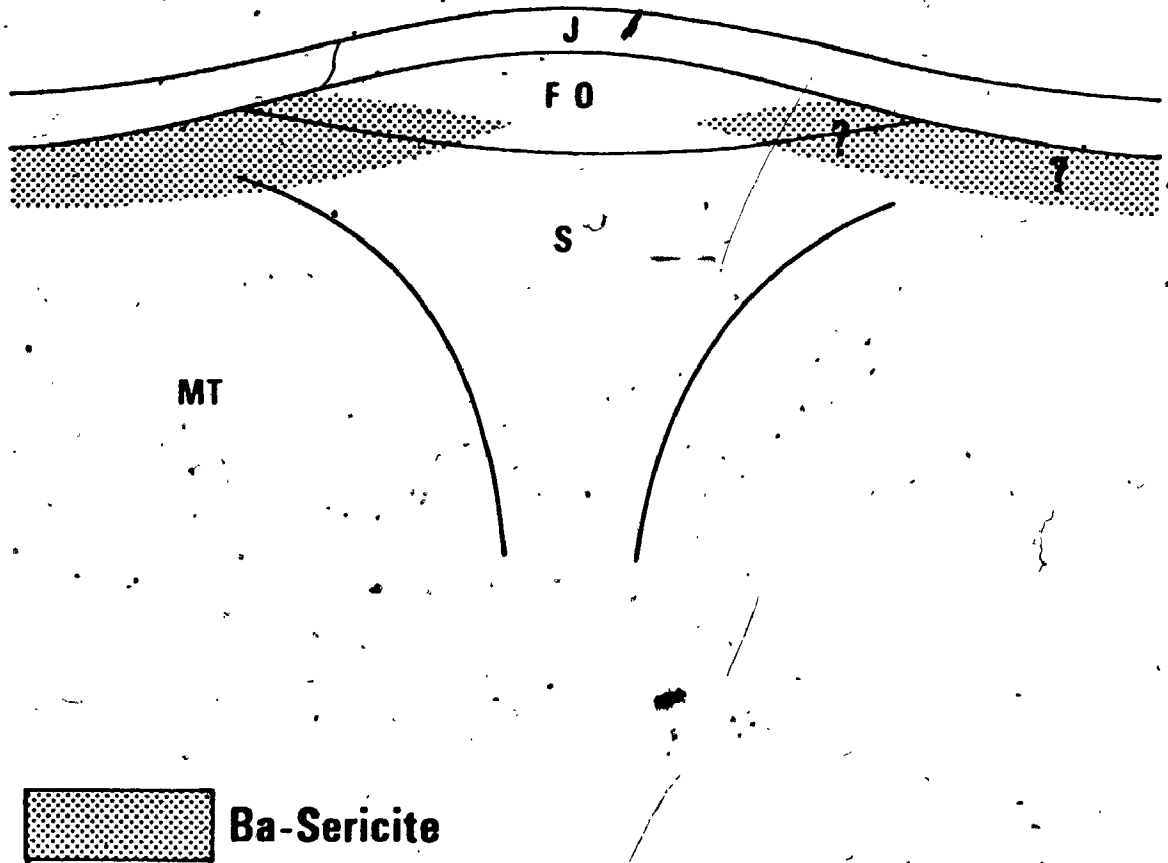


Figure 5.6. Schematic illustration of the spatial distribution of Ba-sericite around the Feitais orebody. Symbols as in Fig. 5.5.

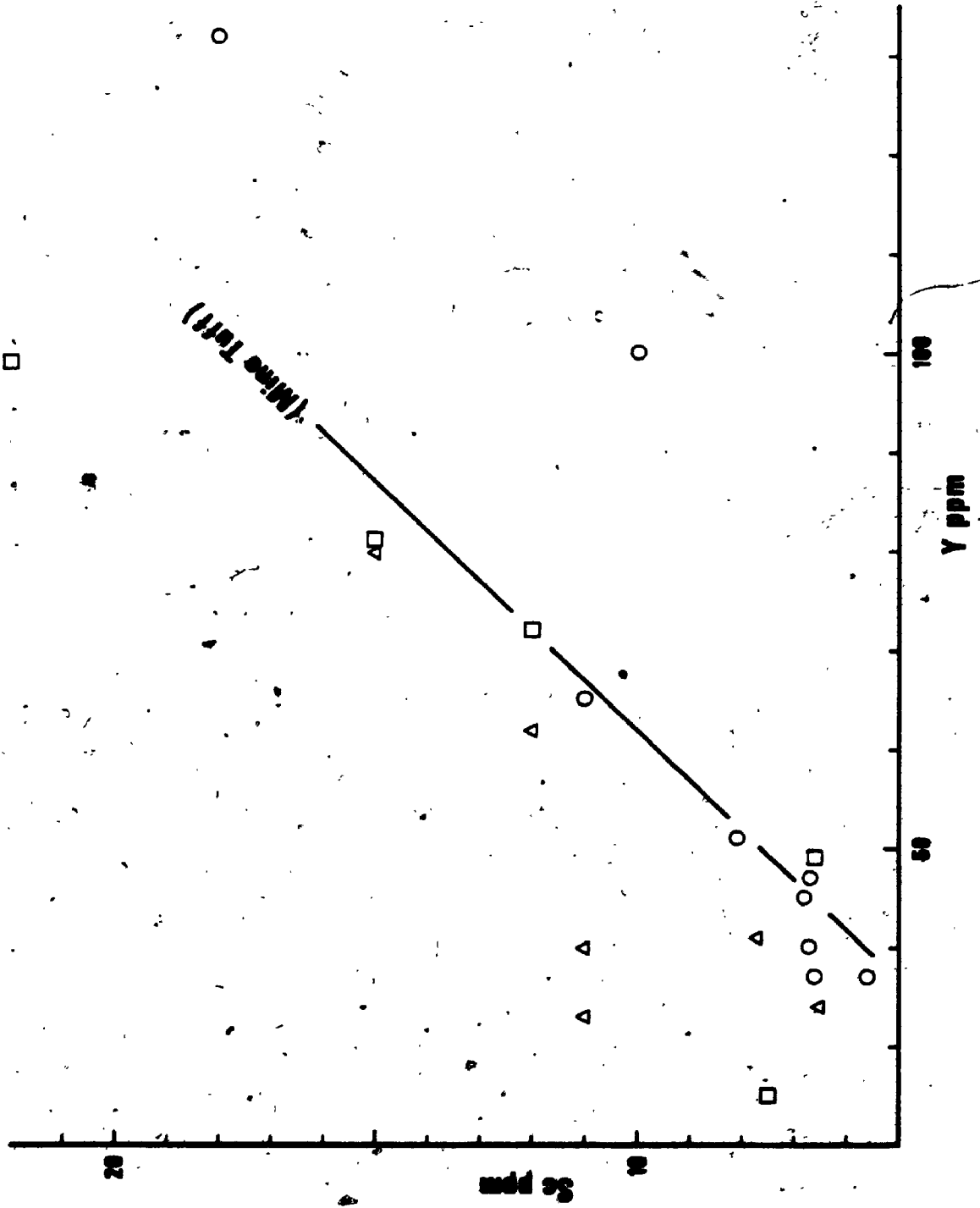
sulphide free basis).

Regarding stockwork rock (*sensu stricto*, quartz-chlorite-sulphides) the major element analyses are remarkable especially with respect to MgO contents generally comparable to those of Green facies Mine tuffs. The approximate weighted average of the MgO abundance in the Feitais stockwork rock is $\sim 4.5\%$, given that the higher MgO values in Appendix V-1c, up to $>27\%$, correspond to volumetrically insignificant samples. Average SiO₂ in stockwork rock is $\sim 59\%$, equivalent to 62.8% on a sulphide free basis. Undetected (or very low) Na, K and Ba reflect perfectly the absence of feldspar and sericite.

a2) Immobile trace elements

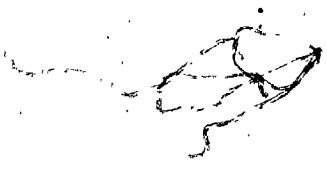
Abundances and ratios of high field strength elements in stockwork rocks (*sensu lato*) depict a considerably higher scatter than detected in Mine tuffs not affected by ore zone alteration but, nevertheless, the majority of stockwork samples analysed are indistinguishable from Mine tuffs with respect to ratios of high field strength elements; illustrated in Figure 5.7 a and b for the case of Sc versus Y and Zr/Y versus Zr (see Appendix V for the analyses). These data show that the Feitais stockwork rocks are indeed ore zone altered Mine tuffs, and suggest that this type of alteration was accompanied by extreme variations in major element relative abundances (given the marked differences in the ranges of absolute concentrations

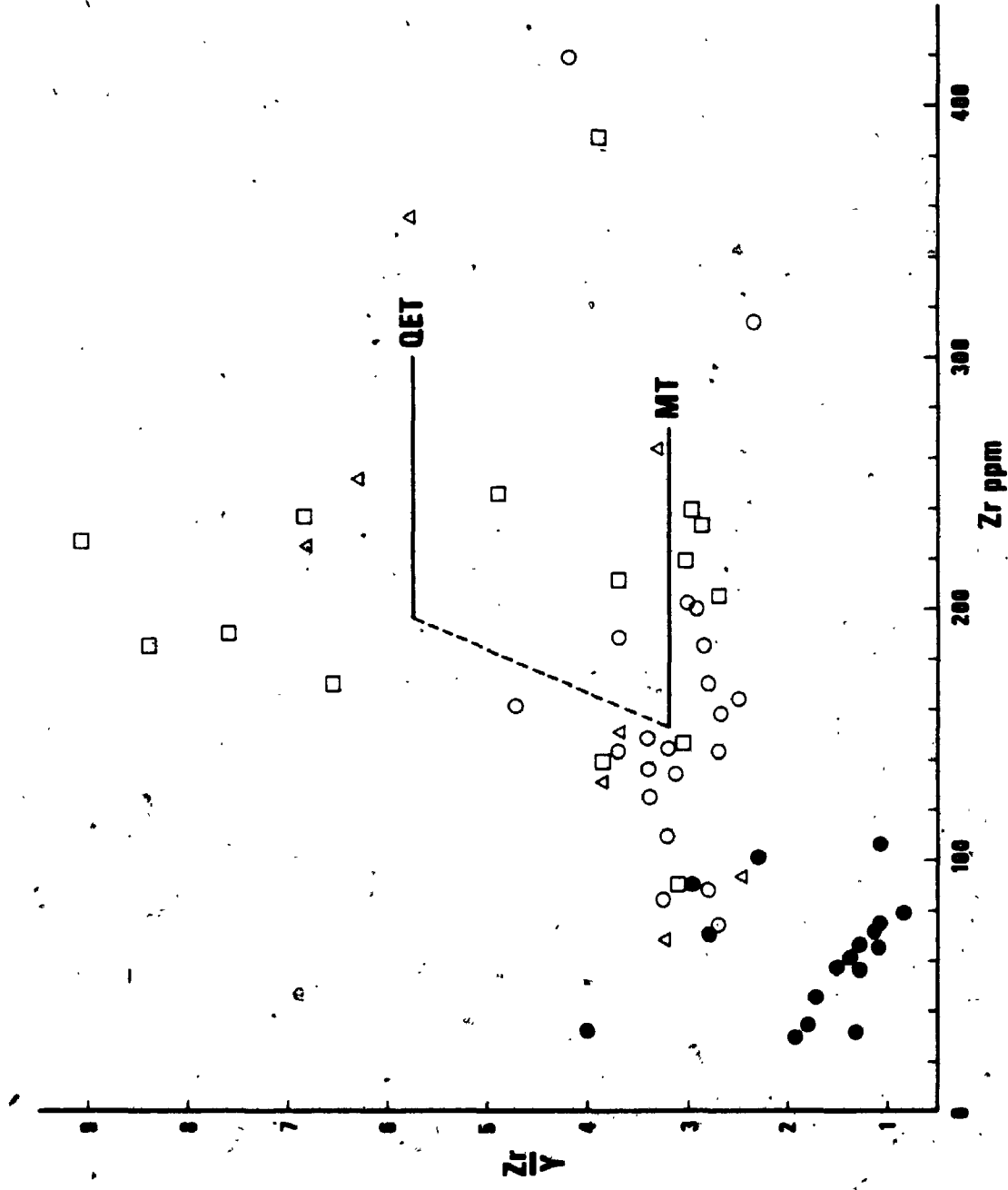
Figure 5.7a. Diagram illustrating the variation of Sc versus Y in the Feitais stockwork. Mine Tuff line shown for comparison (see Fig. 4.8). Circles, stockwork rock (chlorite-quartz); squares, outer stockwork rock (sericite-quartz); triangles, weakly ore zone altered Mine tuffs.



213

Figure 5.7b. Zr/Y versus Zr diagram for stockwork and massive ore (solid circles) samples. Other symbols as in Fig. 5.7a. Note the degree of scatter of data, much more pronounced than that found in Mine tuffs proper (see Fig. 4.9).





of Zr and Y). Larger scatter in the ratios between these elements also suggest that Zr, Y, Sc (and others) were at least locally mobile in the course of ore zone rock alteration, in agreement with textural evidence for corrosion and/or reprecipitation of minerals such as zircon (see section 5.2). However, some of the scatter in "immobile" element data from stockwork rocks may partly reflect the presence of wider primary compositional variations than those detected in Mine tuffs proper, given that some of the samples depicting marked deviations from typical Mine tuffs with respect to Sc/Y and Zr/Y are only incipiently affected by ore zone rock alteration:

Zr/Y versus Zr plots of massive sulphide ore samples are also included in Figure 5.7, for comparison (analyses in Appendix V). Data are insufficient, but show that most ore samples are markedly different from Mine tuffs with respect to Zr and Y abundances and ratios. However, some samples plot clearly within the range of stockwork rocks, confirming the hypothesis raised by textural evidence (see section 5.2) that part of the Feitais massive ore may have formed through almost complete replacement of previous Mine tuffs.

a3) Lanthanide element (REE) abundances in stockwork rocks (Appendix V; Figure 5.8) further confirm that these rocks are altered Mine tuffs, given the similarity in absolute and relative abundances of LREE (compare with Figures 4.10

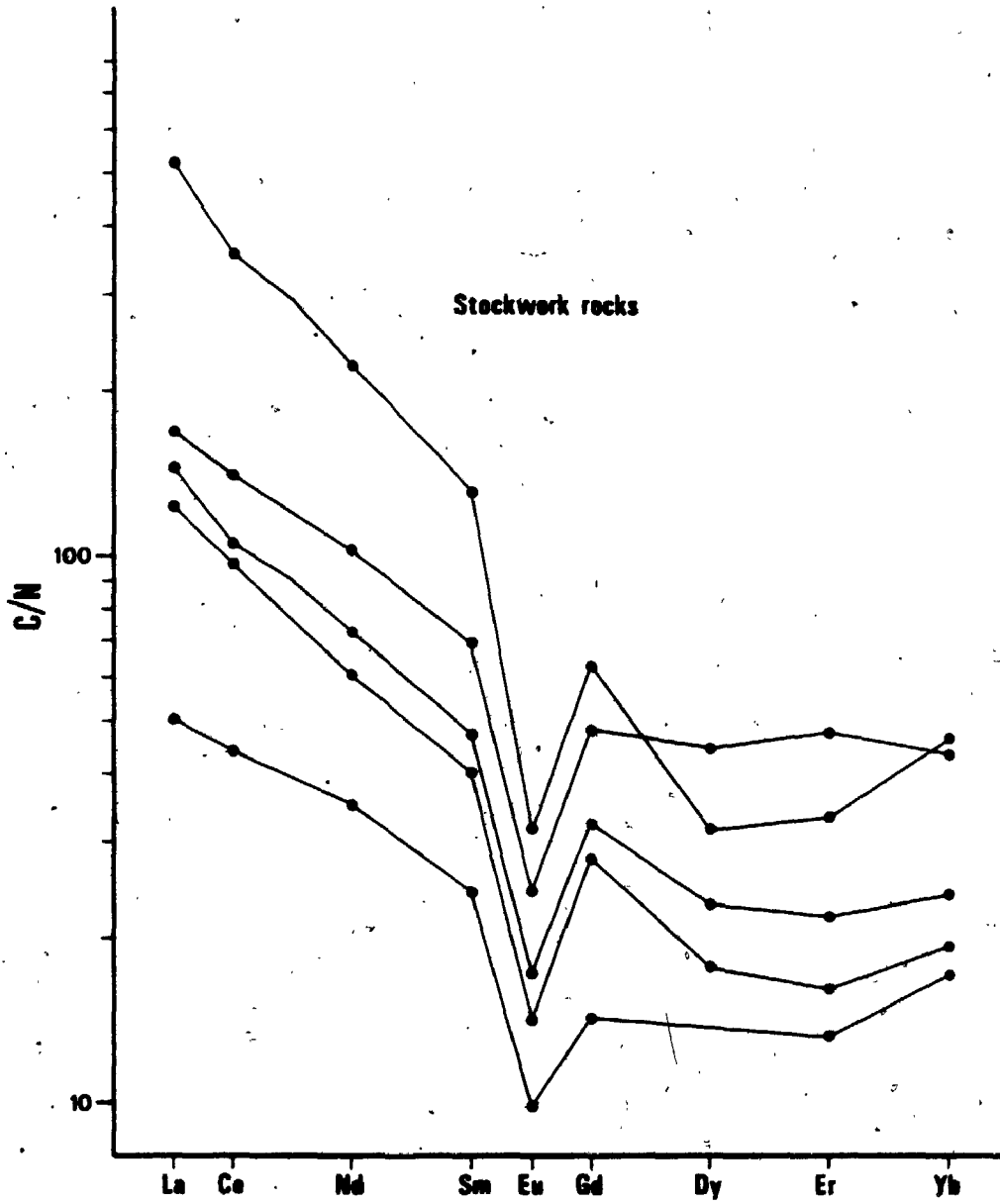


Figure 5.8. Chondrite normalized patterns in Feitais stockwork rocks. Compare with figs. 4.10 and 4.11.

and 4.11). HREE are variably enriched (especially Yb and Er), as expected given the relative mobility of HREE in alteration processes (Alberton et al., 1980), similarly as found for many regionally altered (but not ore zone altered) Aljustrel volcanic rocks (Figure 4.11).

REE abundances in one Pb-rich and one Cu-rich massive sulphide ore samples are plotted (chondrite normalized) in Figure 5.9. The Pb-rich sample is similar to those analysed by Munha (1981), with a sea water like pattern except for the lack of a Ce anomaly and for a positive instead of negative Eu anomaly. Munha suggested that the REE distributions in Pb-rich ore (containing barite) can be explained as largely reflecting the REE content of barite (see Guichard et al., 1979), precipitated from a sea water derived fluid possibly enriched in Eu^{2+} through interaction with felsic footwall volcanic rocks rich in feldspars. Alteration of these feldspars would have released Eu^{2+} preferentially to other REE, given the high relative concentration of Eu^{2+} in feldspar minerals. The Cu-rich sample (Fig. 5.9) is very similar to recent sea floor hydrothermal sulphide material with respect to LREE (including Ce, Bonatti et al., 1976).

b) Hanging wall siliceous and metalliferous sediments

(Jasper unit)

b1) Si/Mn/Fe ratios (Figure 5.10) illustrate well the more significant variations found in the Feitais hanging wall

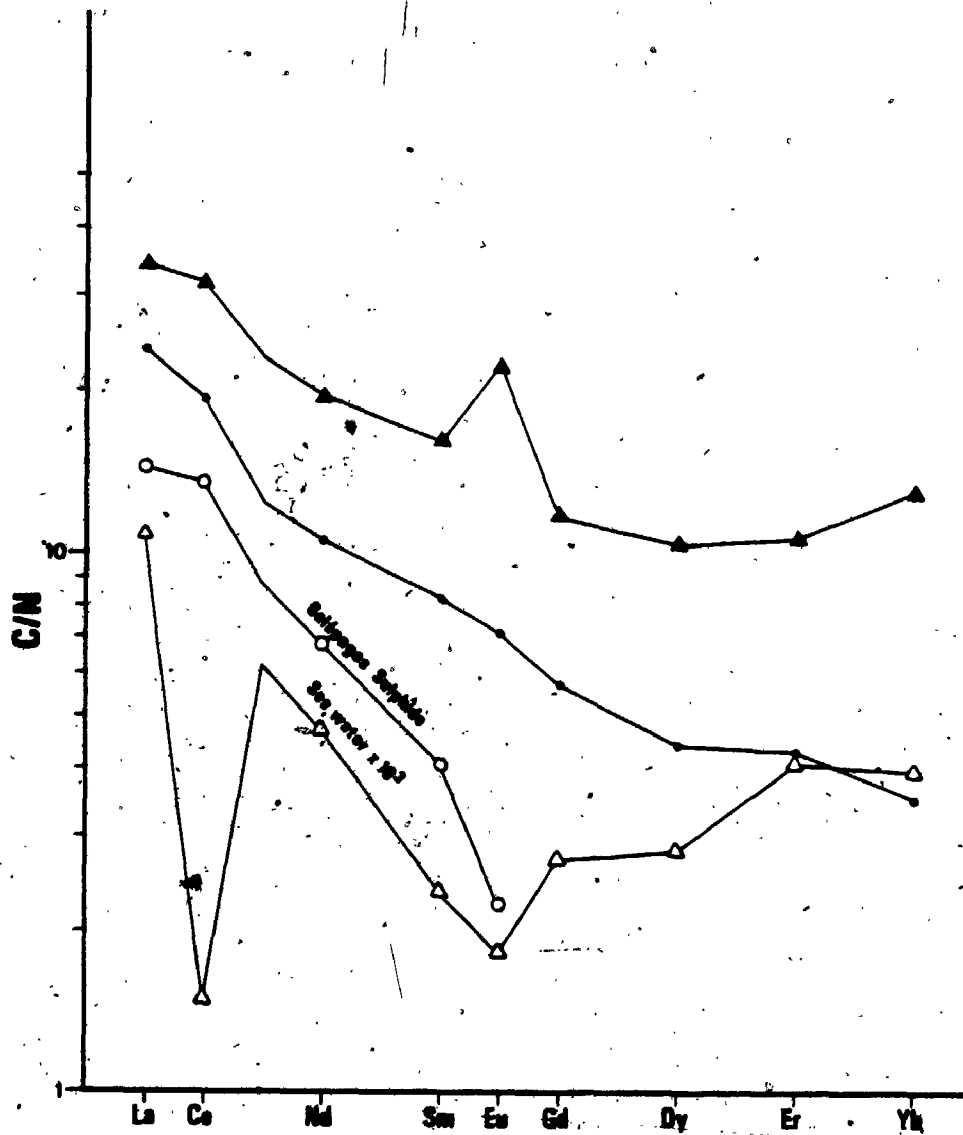


Figure 5.9. Chondrite normalized REE patterns in Feitais massive sulphide ore samples: Galapagos sulphide after Bonatti (1981) and sea water after Hogdahl et al. (1968). Solid circles, Cu-rich ore; solid triangles, Pb-Zn rich ore.

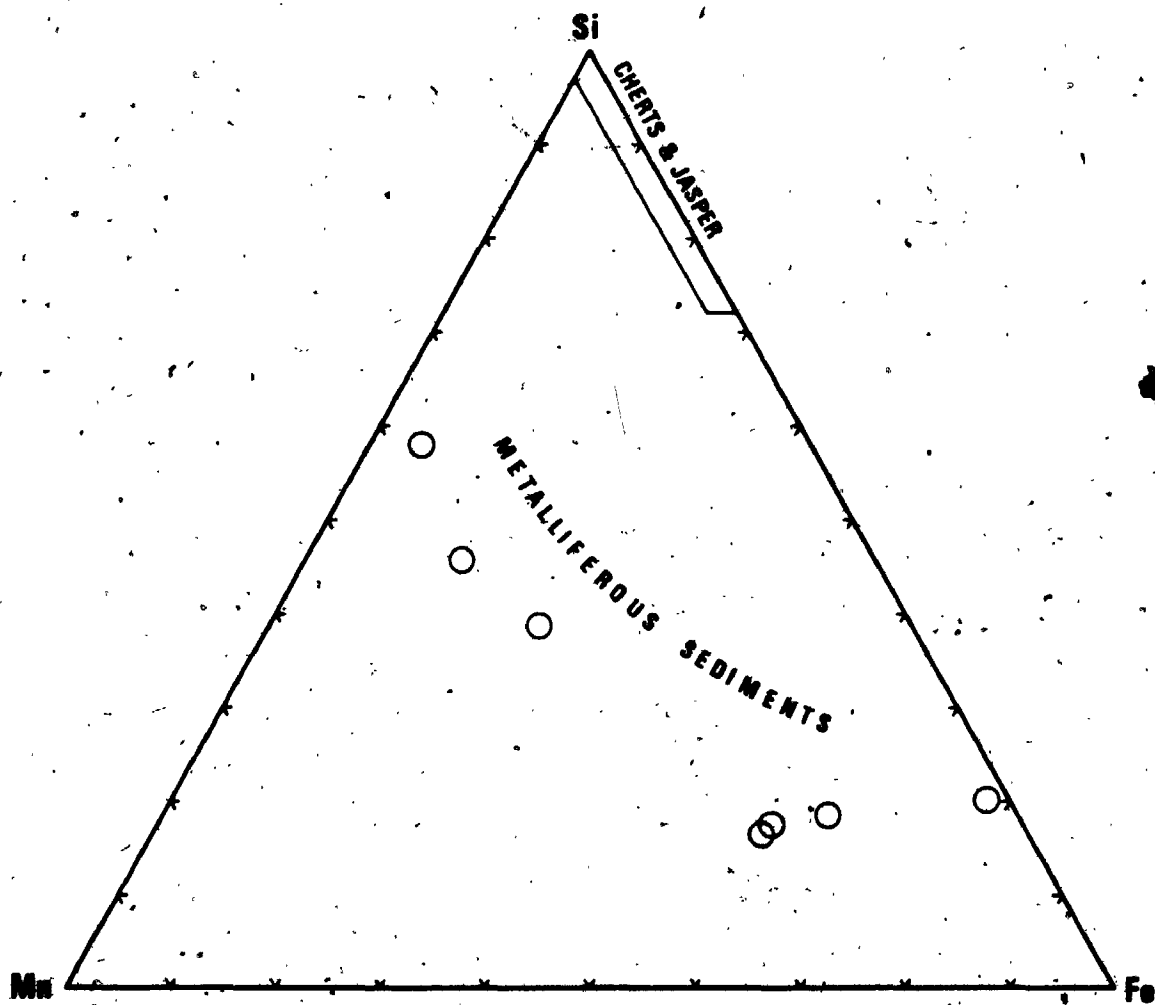


Figure 5.10. Ratio Si/Mn/Fe in the Feitais siliceous and metalliferous sediments.

siliceous and metalliferous sediments (analyses in Appendix V-2). It is apparent from this figure that great variations exist in Fe/Mn ratio and also that there seems to exist a clear compositional gap between these and the high silica samples, confirming the petrographic observations previously reported. Also, chemical analyses of cherts and jaspers often depict relatively high iron contents (up to ~12% Fe), but the higher metal abundances correspond mostly to the presence of Fe rich pre tectonic veins crosscutting the material analysed (that is, to alteration of the Jasper).

b2) Jasper reduction above sulphide ore is a prominent characteristic of the Feitais ore zone. Thus Fe-rich siliceous sediments occurring laterally away from the Feitais orebody are exclusively red hematitic jasper, with whole rock Fe ratios ($Fe^{2+}/\Sigma Fe$) < 0.1 (Plate 8 and Appendix V-2), whereas in the vicinity and directly above the sulphide orebody jaspers are partly or totally altered into Fe^{2+} rich minerals, as described in section 5.2.3. These changes are eloquently reflected in ore zone jasper and chert Fe ratios up to > 0.9 , schematically illustrated in Figure 5.11.

b3) Jasper unit sediments compare well with present day sub sea floor hydrothermal metalliferous sediments, that is, those formed through precipitation of metals extracted from the oceanic igneous rocks in the course of sub sea floor

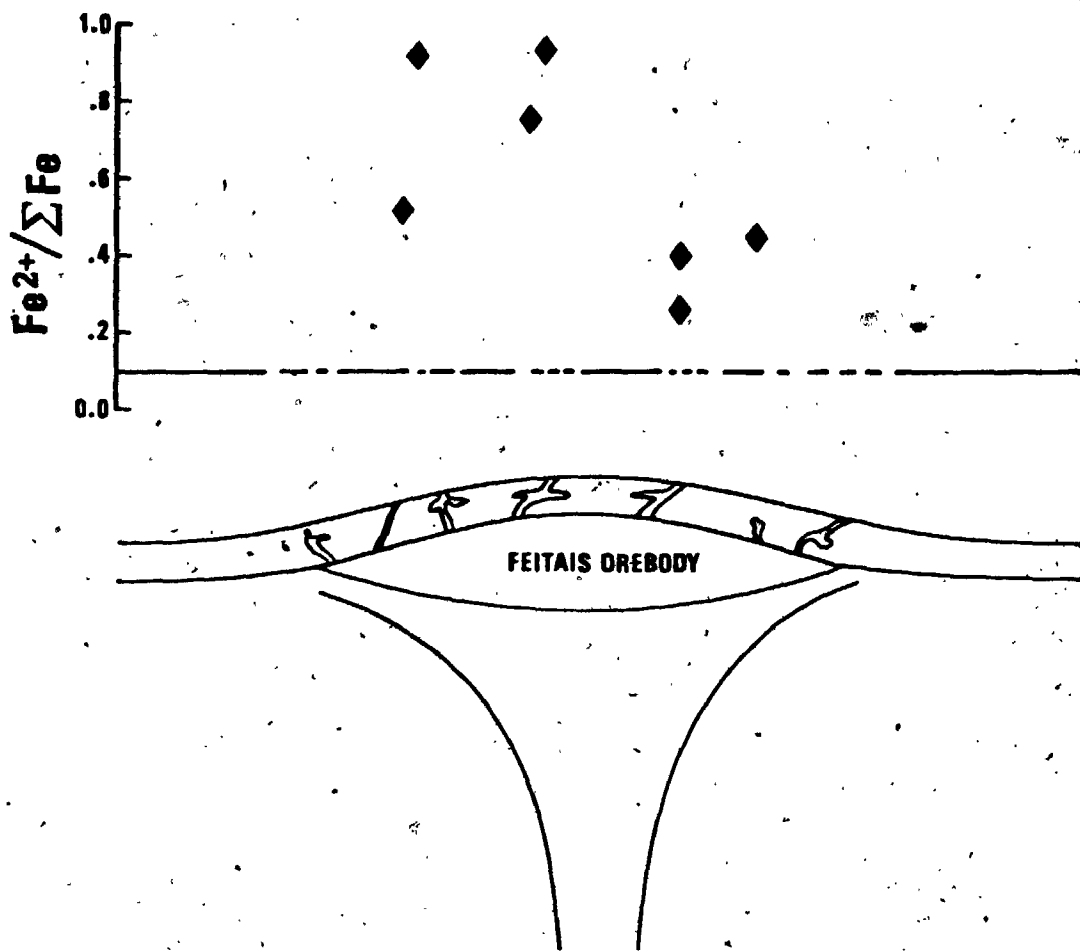


Figure 5.11. Schematic representation of the spatial distribution of Fe ratios along the Feitais Jasper unit. Diamonds are cherts (reduced jasper). Horizontal line represents Fe ratio of unaltered jaspers. See also Appendix V-2 for data.

sea water convection through the permeable, hot oceanic crust, especially near mid ocean ridges (Arrhenius and Bonatti, 1965; Bostrom and Peterson, 1966; Bonatti and Joensu, 1966; Bonatti et al., 1972; Fyfe and Lonsdale, 1981). Thus the Aljustrel Jasper unit rocks plot clearly within the hydrothermal field in the $Fe/Mn/(Co+Ni+Cu) \times 10$ diagram (Figure 5.12) proposed by Bonatti et al. (1972; see also Bonatti, 1981) as a simple means of distinguishing hydrothermal from hydrogenous recent sub sea floor metalliferous deposits.

b4) The Thorium abundances of Jasper unit rocks are also in the same range of the Th abundances in recent hydrothermal metalliferous sediments, as illustrated in Fig. 5.13 (compare Bonatti et al., 1972).

b5) Chondrite-normalized REE abundances of Jaspers showing little or no alteration are plotted in Figure 5.14. It is apparent that they follow a concave upwards v-shaped pattern, and that Ce is markedly depleted generating a negative Ce anomaly in all the patterns. These characteristics are very similar to the REE pattern of sea water (Hogdahl et al., 1968), strongly suggesting that the jaspers formed in equilibrium with a fluid indistinguishable from sea water with respect to REE abundances.

REE patterns for Mn ores (carbonate and oxide) are presented in Figure 5.15. They are clearly distinct from

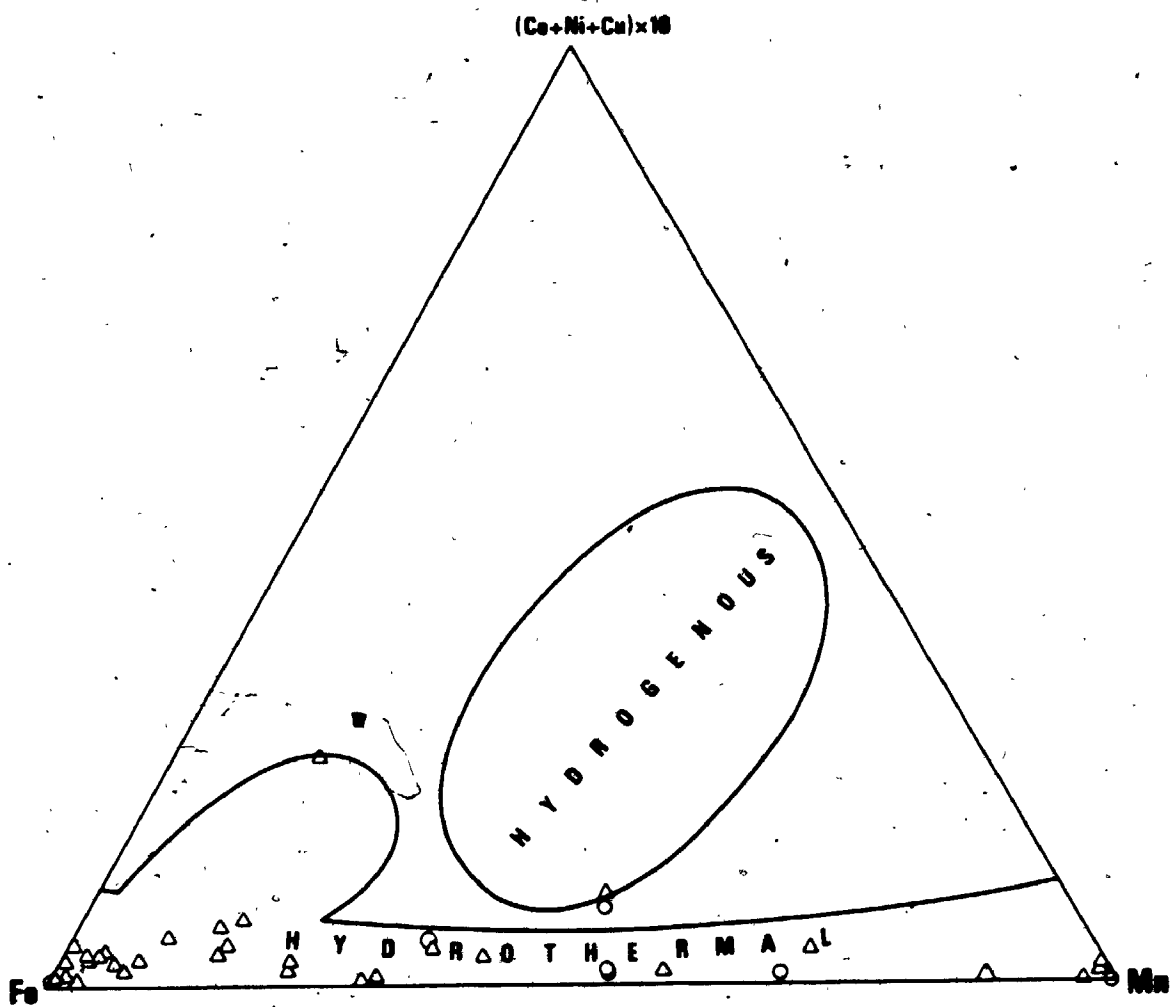


Figure 5.12. Ratio $Fe/Mn/(Ni+Co+Cu) \times 10$ in the Aljustrel metalliferous sediments. Triangles, Feitais; circles, Moinho.

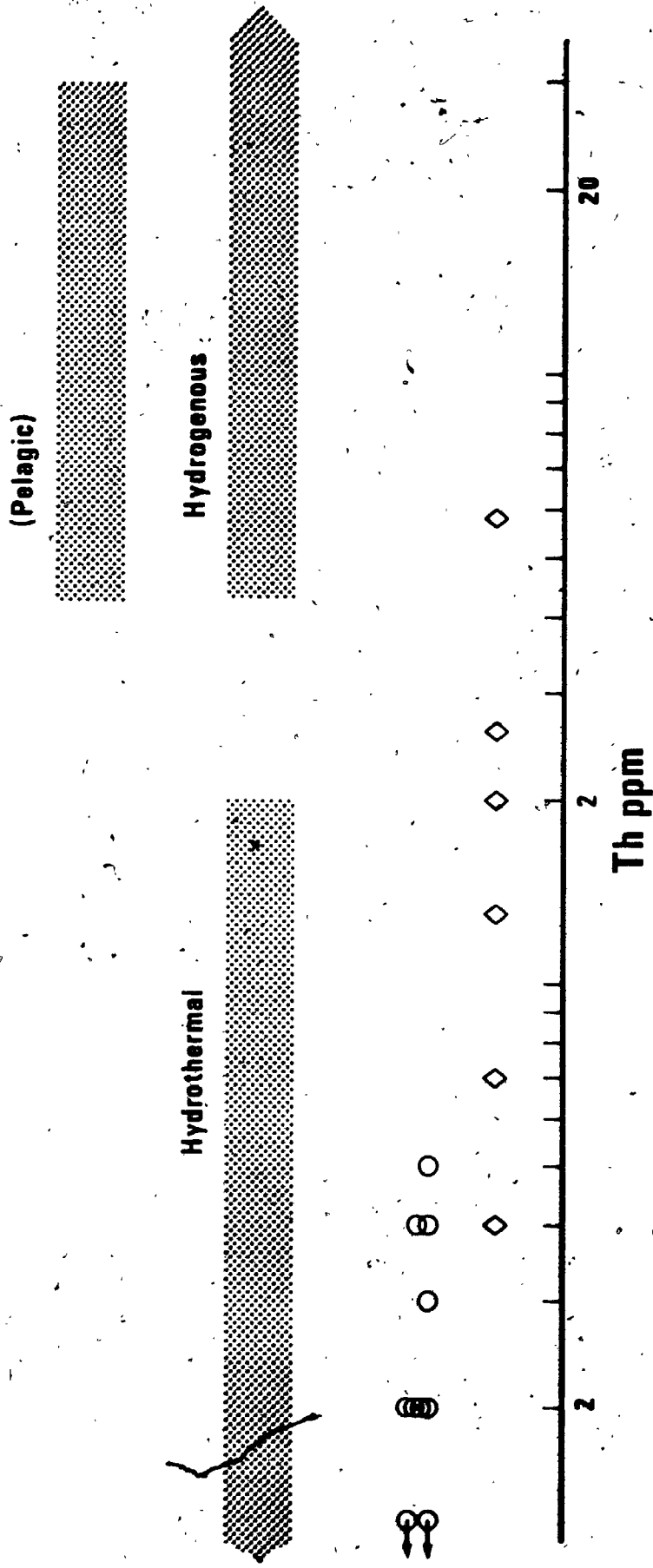
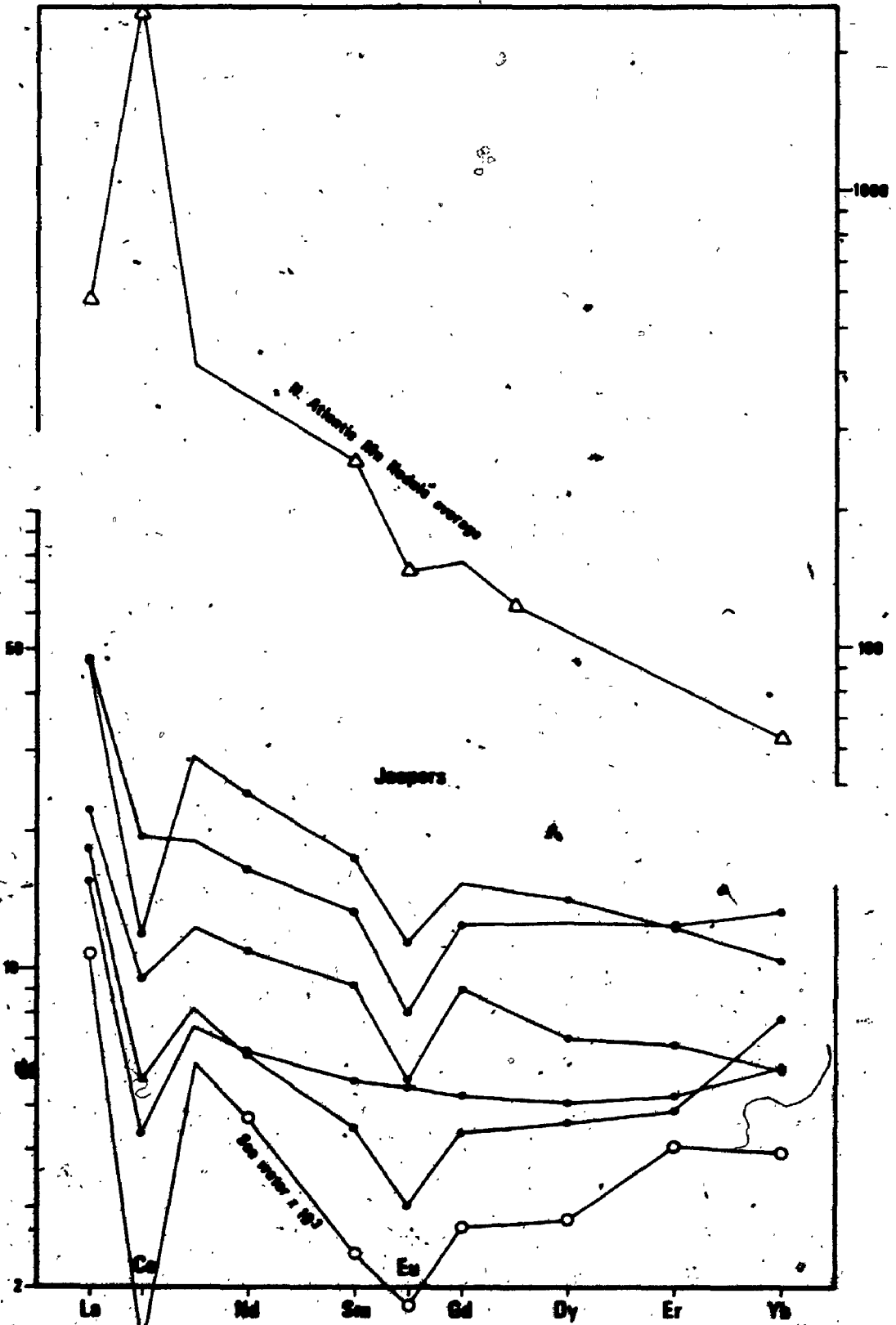


Figure 5.13. Thorium abundances in Jasper unit rocks (Feitais). Fields after Bonatti et al. (1972). Circles, cherts and jaspers; diamonds, metalliferous sediments.



Figure 5.14. Chondrite normalized REE abundances in Jaspers showing little or no alteration. Sea water after Hogdahl et al. (1968) and N. Atlantic nodule average after Addy (1979).



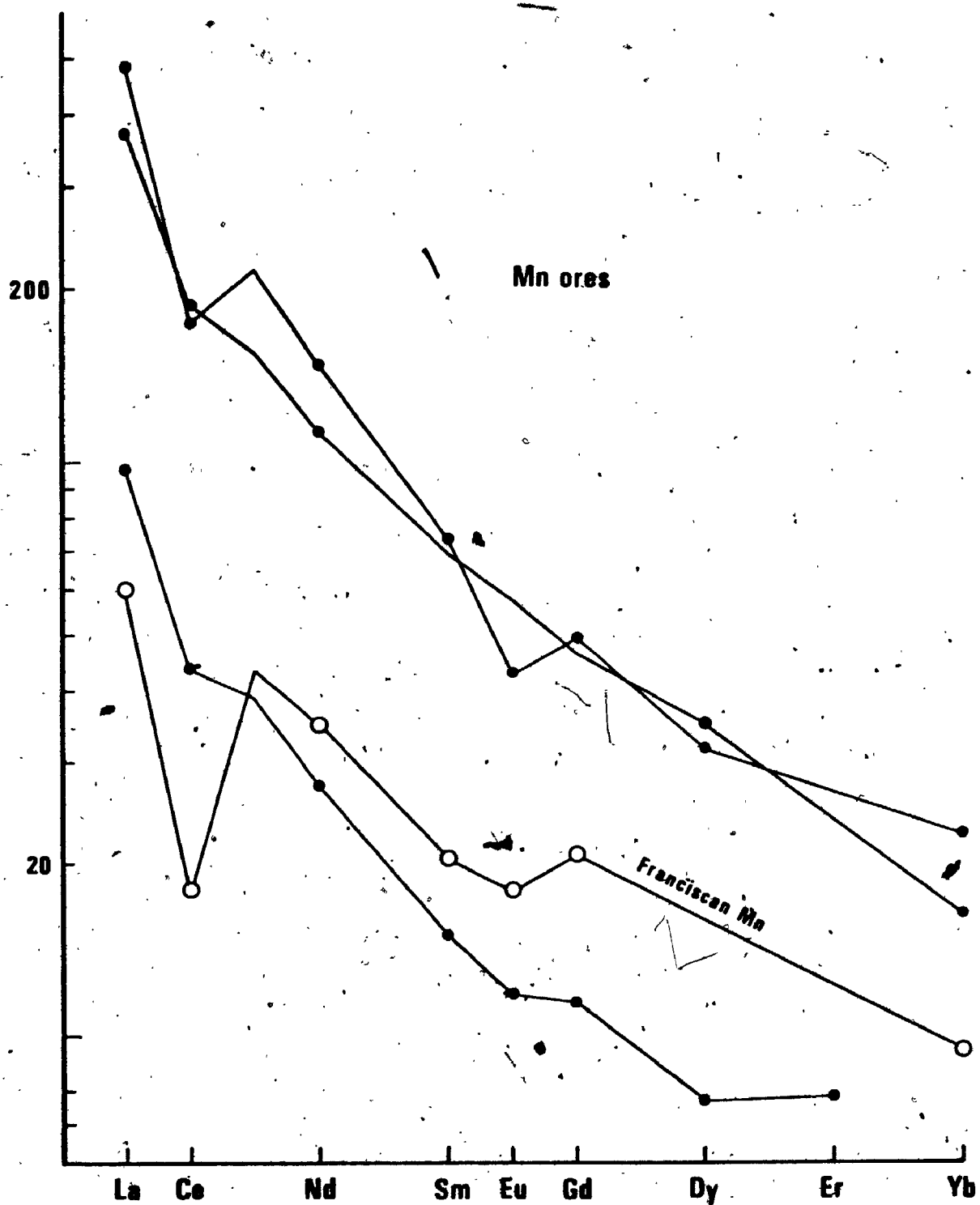


Figure 5.15. Chondrite normalized REE abundances in Feitais metalliferous sediments. Franciscan (California) hydrothermal Mn ore after Crerar et al. (1982).

those of jaspers (Fig. 5.14), closely resembling those of the Mn ores of the Franciscan assemblage (Crerar et al., 1982), attributed to a sea floor hydrothermal origin.

Recent hydrothermal Mn deposits on the sea floor usually contain lower concentrations of LREE (Toth, 1980), expressed in chondrite-normalized patterns that are less steep than those of the Aljustrel or Franciscan Mn ores. Recent hydrogenous Mn deposits (Mn nodules) are clearly distinct from the Aljustrel Mn ores with respect to REE (see Fig. 5.13) not only on the markedly higher absolute REE abundances but also on their characteristic positive Ce anomaly (Piper, 1974; Addy, 1979).

b6) Gold abundances in the Jasper unit

Gold abundances in rocks from the Feitais Jasper unit are presented in Table 5.2, together with some determinations of Au in other ore zone rocks. It is apparent that the Feitais massive sulphide orebody is surrounded by a halo of anomalous Au concentrations (see Wedepohl, 1978; the massive sulphide ore itself contains in average ~800 ppb Au, Carvalho et al., 1976). Particularly anomalous Au concentrations (>50 ppb) are present in stockwork rocks and especially in the Jasper unit, where Mn rich metalliferous sediments containing up to 350 ppb Au exist, at considerable distances from sulphide mineralization (>500 m along strike). These data suggest that Au abundances in other metalliferous sediments in

Table 5.2. Au abundances (ppb) in selected Aljustrel ore zone rocks.

	Au ppb	Remarks
JASPER UNIT		
Cherts and Jaspers		
15-315	20	↑
15-319.3*	29	
11-351.9	51	
bis-160.2	11	on or near massive sulphide ore
bis-161	14	
bis-166	15	
14-133.4	110	↓
SF-41 (*)	1	>500 m along strike from massive sulphide ore
SM-13-D' (*)	8	
Metalliferous sediments		
9-285	21	on or near massive sulphide ore
6-103.4	15	
6-106.9	51	
SF-22 (*)	350	>500 m along strike away from massive sulphide ore
SM-13-B' (*)	240	
STOCKWORK ROCKS		
8-358.1	82	Qz-ser outer stockwork rocks
8-370	140	
8-479.5	100	Qz-chl stockwork rocks
8-504.4	32	
WEAKLY ALTERED PS TUFFITES		
bis-143.1	19	Above massive sulphide ore
8-346	30	

(*) Weathered jaspers and Mn oxide metalliferous sediments

the Pyrite Belt and elsewhere are at least potentially of importance in exploration for massive sulphide deposits.

c) Anomalous PS Formation rocks above Feitais

The Jasper unit of Aljustrel is conformably overlain by a 50 m thick sequence of phyllites, tuffites and rare tuffs (PS Formation) that represent the sedimentary and volcanoclastic infilling of the Iberian Pyrite Belt basin in the Aljustrel area, concomitantly with the last pulses of local volcanism (see Chapter 3). Above the Feitais orebody the base of the PS Formation (in contact with the Jasper unit) is characterized by the occurrence of irregular and discontinuous bodies of very unusual rocks which include pyritized and carbonatized phyllites and deeply chloritized tuffs and tuffites, generally pervasively, pre tectonically veined by quartz-pyrite-carbonates (see sections 5.2 and 5.3). On the basis of field relations and textural studies it was concluded that these anomalous PS rocks result from alteration of formerly normal PS phyllites, tuffites and tuffs.

Whole rock analyses of PS rocks are presented in Appendix V-3. It is apparent that anomalous rocks (App. V-3a) are highly enriched in Fe and/or Mn, and that their abundances in alkaline and alkaline earth elements are widely variable, particularly so for Mg and Ca. The anomalous group contrasts markedly with the "normal" PS rocks (App. V-3b), in which the only striking anomaly is

the sporadic presence of very high Ba concentrations up to ~2% BaO. Figure 5.16 illustrates the variations of Fe/Ti versus Al/(Al+Fe+Mn) in PS formation rocks. It is apparent that unaltered PS rocks are very similar to normal recent pelagic sediments and that the altered rocks resemble Bonatti's (1981) "diluted" metalliferous sediments (see also Bostrom, 1970). Co+Ni+Cu abundances in PS rocks are consistently low, precluding any significant hydrogenous contribution to the genesis of the anomalous group.

Thorium abundances in PS rocks are all remarkably similar to those of normal pelagic sediments (Bonatti et al., 1972; Figure 5.17), irrespective of the degree of Fe-Mn enrichment, again in good agreement with a hydrothermal alteration origin for the anomalous rocks, given the exceedingly low Th abundances that characterize hydrothermal metalliferous deposits.

d) Geochemical data on Culm rocks

The PS Formation is conformably overlain by the Culm Formation, a thick (<3 km) sequence of turbidites (see Chapters 2 and 3), including frequent pyritic black shale beds. Appendix V-4 lists the results of major element and selected trace element analyses of Culm greywackes and shales, and shows that Culm rocks are normal terrigenous sediments without any noticeable hydrothermal or hydrogenous metalliferous concentration.

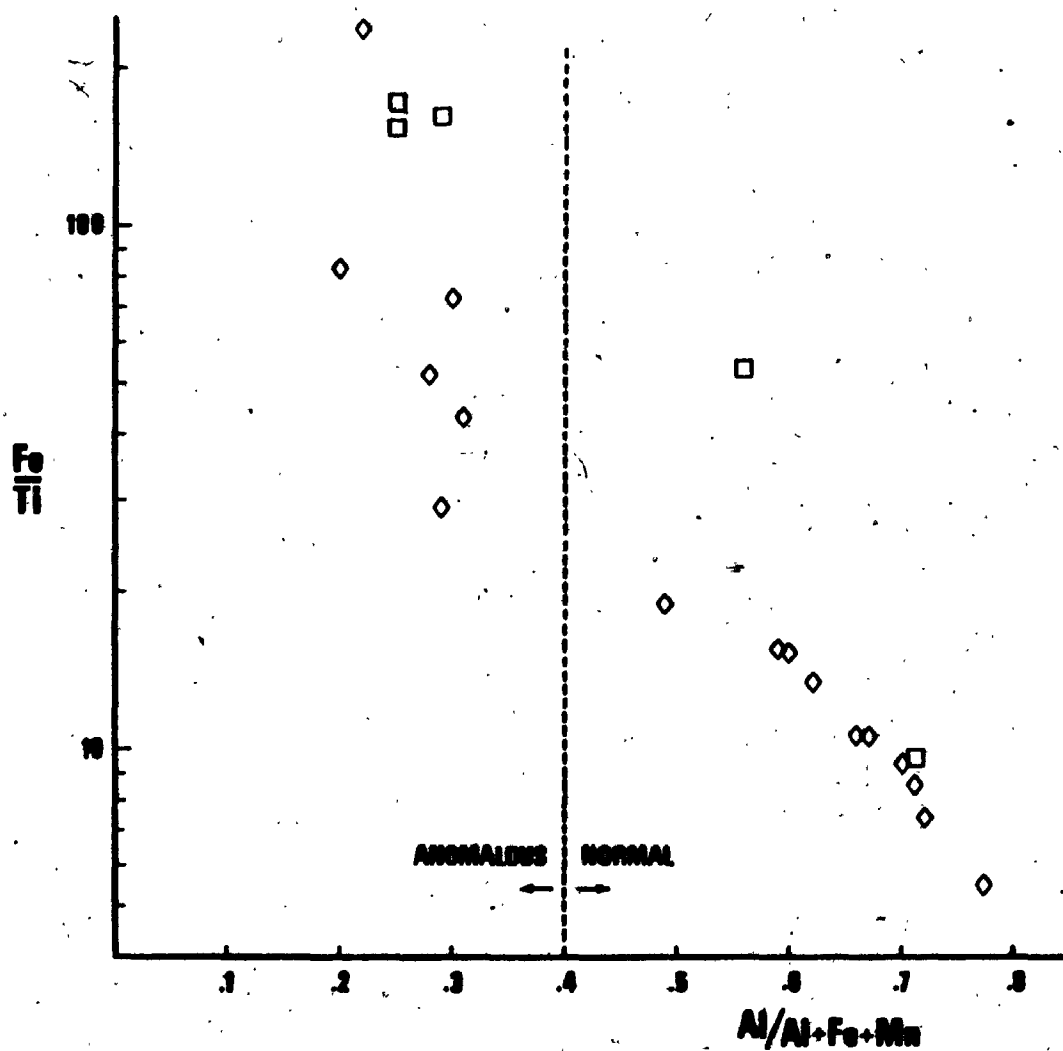


Figure 5.16. Diagram illustrating the variation of Fe/Ti versus Al/(Al+Fe+Mn) in PS Formation rocks (above Jasper unit). Squares, tuffs; diamonds, phyllites and tuffites.

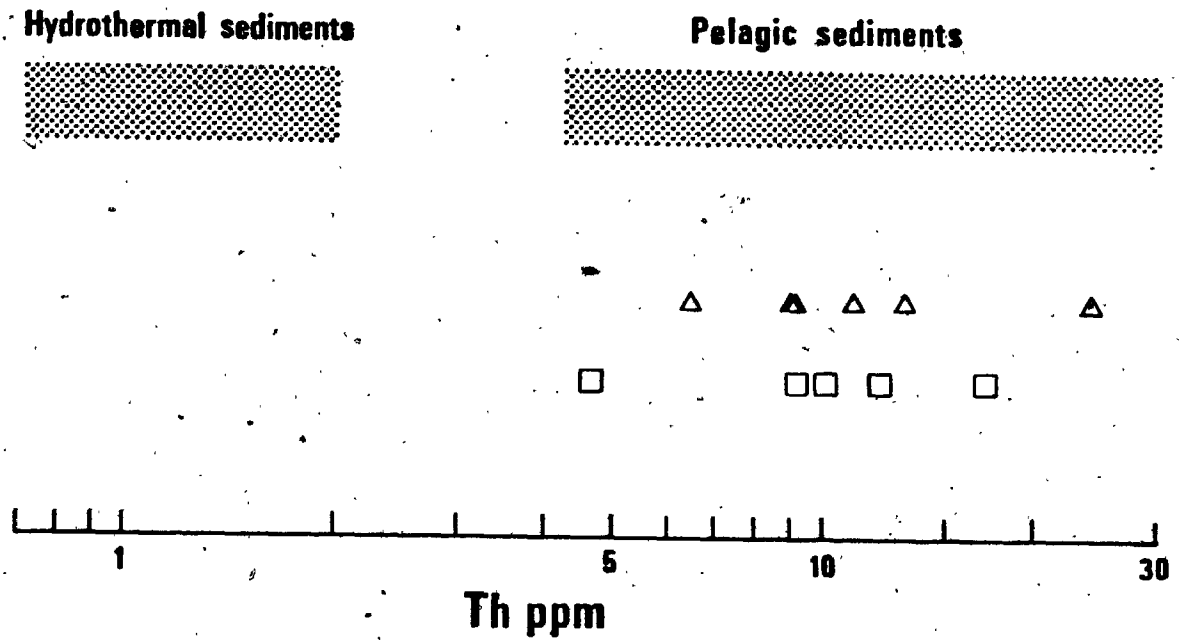


Figure 5.17. Thorium abundances in highly altered (triangles) and unaltered (squares) PS formation sediments (above Jasper). Fields after Bonatti et al. (1972).

5.3.3 Oxygen isotope geochemistry

Oxygen isotope data for whole rocks and some mineral separates from the various levels of the Feitais-Estacao ore environment are listed in Table 5.3. Stockwork whole rock $\delta^{18}\text{O}$ values are relatively uniform at 11.6 to 12.5‰. Tuffs partly transformed into stockwork rocks (less intensely affected by mineralizing solutions) have $\delta^{18}\text{O}$ 13.9 and 14.4‰, intermediate between those of stockwork rocks proper and the even higher values of the Aljustrel Volcanics, islands of which occur as remnants within the stockwork itself. These relations signify that ore formation postdates the early hydrothermal event that enriched the Aljustrel Volcanics in ^{18}O as described before (Chapter 4). The present $\delta^{18}\text{O}$ values of $\sim 12\text{‰}$ of the stockwork rocks are therefore believed to have been reached through two successive stages of hydrothermal alteration: early ^{18}O enrichment to values near 17‰ followed by ^{18}O loss to around 12‰.

Quartz-chlorite fractionations from stockwork rocks indicate that the hydrothermal ore fluid was at ambient temperatures of 220 to 270°C, and had $\delta^{18}\text{O}$ spanning +1.4 to 5.7‰. Within massive ore quartz-chlorite fractionations correspond to temperatures of 200 to 220°C and $\delta^{18}\text{O}$ +5‰ (Table 5.3). In the absence of triply concordant oxygen isotope fractionation between three cogenetic minerals, it is not possible with the present data to confer total

Table 5.3. Oxygen isotope composition of rocks and minerals from the Feitais-Estacao ore environment.

Unit and sample	Whole rock	Quartz	Chlorite	$\delta^{18}\text{O}_{\text{fluid}}$	tOC
Jaspers					
bis-160.2		+18.66			130
bis-161		+19.6			120
bis-166		+17.9			130
15-315		+19.0			120
15-329		+20.1			110
Massive Sulphide Ores					
8-446.85		+17.1	+6.8	5.0	220
10-350		+18.3	+7.3	4.9	200
Stockwork rocks					
S.1-3A (a)		+13.55	+3.19	+1.4	216
S.1-1 (a)		+13.72	+3.44	+1.7	218
S.1-5 (a)		+13.87	+5.00	+4.3	266
F.1 (a)		+15.40	+6.06	+5.0	249
21-735.9	+12.4	+14.90	+5.80	+5.0	258
21-800.5	+11.6	+15.10	+6.30	+5.7	269
S.1-3B (a)		+13.33			
bis-246.5	+12.5				
8-511.1	+11.9				
21-738	+11.7				
Peripheral Stockwork					
8-365.4	+13.9				
8-533.8	+14.4				

(a) after Munha and Kerrich (1981). Jaspers temperatures calculated assuming precipitation from 1.50/00 $\delta^{18}\text{O}$ fluids. Oxygen isotope fractionations after Wenner and Taylor (1971), chlorite-water, Clayton et al. (1972), quartz-water.

reliability on the estimated temperatures and $\delta^{18}\text{O}$ fluid. However, the positive covariance of $\delta^{18}\text{O}$ quartz with $\delta^{18}\text{O}$ fluid, plus preservation of a systematic disparity between the $\delta^{18}\text{O}$ of quartz in stockwork and ore, collectively suggest an absence of complete isotopic homogenisation, and that the observed variations in mineral $\delta^{18}\text{O}$ may reflect real variations in the hydrothermal system. Furthermore, the minerals analysed are believed to have crystallized during the hydrothermal episode, as opposed to being earlier phases isotopically modified by hydrothermal activity, in which case mineral pairs would be clearly insufficient for reliable temperature and δ -fluid estimates.

Quartz separates from the overlying jaspers range from 17.9 to 20.1‰. Such δ -values could correspond to deposition temperatures of $140 \pm 20^\circ\text{C}$ assuming precipitation in equilibrium with a mixture of 50% sea water (0‰, 0°C) plus 50% ore fluids (3‰, 250°C). It is noteworthy that the oxygen isotope composition of the Feltais-Estacao cherts and jaspers is low compared to Phanerozoic marine cherts (cf. Knauth and Lowe, 1978). The relatively high temperatures inferred from such values are good evidence that they are hydrothermal sediments, as postulated by Carvalho (1979), formed where geothermal discharge perturbed ambient ocean bottom water temperatures.

Overall, the calculated temperatures are rather normal

for massive sulphide environments (see Franklin et al., 1981; Costa et al., 1983), with a steep thermal gradient from stockwork (220-270°C) through massive ore (200-220°C) to the overlying cherts (140 ± 20°C); the result of heat loss from an uprising hot buoyant fluid undergoing conductive heat loss and/or progressive mixing with marine water beneath and at the sea floor.

5.4 Discussion and conclusions

The Feitais-Estacao orebody of Aljustrel is composed of a massive sulphide lens shaped body underlain by a crosscutting zone of stringer and disseminated mineralization hosted in chlorite-quartz and sericite-quartz rock that are the product of alteration of the surrounding Mine Tuff formation rocks. The orebody is capped by a laterally extensive bed of jaspers and Fe-Mn sediments with prominent alteration immediately above the orebody. Hanging wall rock alteration is also present in the lowermost metres of the Paraiso Siliceous formation aluminous sediments and (rare) pyroclastic rocks that overlie the jasper unit.

Petrography, mineral chemistry, whole rock geochemistry and oxygen isotope compositions leave little room for doubt that the Feitais sulphide ores and associated lithologies and ore zone alteration are the product of interaction of a hot, reduced, metalliferous

brine with sea water, at or near the sea floor, as almost unanimously proposed for other massive sulphide deposits throughout the world (see Franklin et al., 1981).

Stockwork

Riverin and Hodgson (1980) recently reported on the nature, zonation and origin of stockwork wall rock alteration at the Millenbach massive sulphide deposit (Noranda), concluding that alteration pipes initially had a quartz-chlorite core which graded laterally and vertically into a sericite rich outer zone and finally to unaltered rocks; similar zoning was found to be present on the selvages of individual sulphide veins within the alteration pipes. Stockwork alteration at Feitais and in the Noranda camp are thus strictly comparable, and differ significantly from the alteration that accompanies stockwork pipes in the Kuroko deposits, where quartz-sericite are the principal non sulphide minerals in the pipes (alteration zone IV; see Ijima, 1974; Shirozu, 1974; Lambert and Sato, 1974), and chlorite predominates immediately around massive ore only, although present also in a more peripheral alteration aureole (zones III and II, respectively, see Shirozu, 1974). Kuroko deposits are surrounded by a further broad external halo of weak alteration characterized by the presence of minor amounts of montmorillonite, zeolites and cristobalite, without

equivalent in older massive sulphide deposits, possibly because these minerals will react promptly under conditions of even very low grade (prehnite-pumpellyite facies) later regional metamorphism to minerals such as sericite, quartz and epidote, which are common accessories of "unaltered" rocks around older massive sulphide deposits.

Regarding geochemical losses and gains it is generally accepted that stockwork alteration is characterized by a major loss in sodium and by equally important gains in sulphur, iron and magnesium (e.g. Roberts and Reardon, 1978; Costa, 1980; Riverin and Hodgson, 1980). Stockwork rocks are usually rich in quartz, which has been variably interpreted as silicification or as quartz formation and/or reprecipitation at the expense of local precursors. At Feltais, ore formation was indeed accompanied by Na loss and Fe and S gains, but the geochemical evidence presented in this study does not require bulk Mg enrichment in stockwork rocks at the time of ore formation, given that the uppermost 50 metres or so of the Mine Tuff were markedly enriched in Mg prior to mineralization, as shown in Chapter 4, as the result of downflowing of sea water through the pyroclastic rocks in the course of early cooling of the volcanic piles. Significant redistributions seem to have taken place, however, expressed firstly on the stockwork zonation in chlorite rich and chlorite poor (sericitic) assemblages and secondly on the chlorite-quartz

ratio in chloritic rocks, variable from quartz with less than 5% chlorite to almost monomineralic chlorite aggregates (chloritite, Schermerhorn, 1978); chlorite compositions (with one exception) match closely the compositions of chlorites in Aljustrel volcanic rocks unrelated with mineralization.

Ore zone

The Feltais-Estacao orebody is markedly zoned, with sphalerite, galena, several sulphosalts and barite concentrated towards the top, whereas chalcopyrite, sericite and chlorite predominate towards the footwall. Pyrite, quartz, carbonates and arsenopyrite are scattered throughout. Microprobe data revealed that the MnO content of ore zone chlorites varies significantly with stratigraphic position, increasing from stockwork and Cu rich massive ore to the overlying jaspers and metalliferous sediments. Oxygen isotope compositions indicate that the ore fluid was at 250°C in the stockwork and cooled to 200°C within massive ore, and finally to ~130°C at the ocean floor. These together with the extreme Fe/Mn fractionation on passing from sulphide ores to the overlying Mn sediments suggest that the hydrothermal mineralizing solutions moved upwards through the footwall pyroclastic rocks along a thermal gradient acquiring progressively higher oxidation potential, as the result of mixing with

unmodified sea water (Krauskopf, 1957; Lovering, 1961; Helgeson, 1970; Large, 1977).

Hanging wall rocks and alteration

The Feitais-Estacao orebody is capped by a laterally continuous bed of jasper which immediately above sulphide ore is markedly altered by reducing fluids which were injected in the jasper shortly before lithification, producing marked vein-controlled reduction of the jasper into predominantly bluish grey magnetitic and pyritic chert. Frequent veins, pods and breccias dominantly composed of a host of Mn bearing carbonates are possibly part of the hanging wall alteration episode, as they seem to have formed from fluids injected through the unconsolidated jasper in the same manner as the remaining pre tectonic veins. Hanging wall alteration persists in the lowermost ten metres or so of the detrital sediments (phyllites, tuffites) and rare tuffs that occur above the jasper as discontinuous, irregularly shaped areas of intense pyritization, chloritization and carbonatization.

The Feitais jaspers are largely hydrothermal chemical precipitates, and not radiolarian cherts with a hydrogenous component, as evidenced by REE patterns, low Ni+Co+Cu abundances, low Th abundances and oxygen isotopic compositions indicating formation temperatures $\sim 130^{\circ}\text{C}$ (microtextures are inconclusive because of later

recrystallization).

Crerar et al. (1982) have recently reported on the manganiferous cherts of the Franciscan assemblage, concluding that Mn mineralization was formed through injection of pre tectonic veins into unconsolidated siliceous sediment producing a characteristic bleached and pseudobrecciated texture, and proposed that the sediment/Mn chert sequences developed as a result of sea floor spreading over a series of deep hydrothermal sea water convection cells paralleling a spreading centre and spaced 5-10 km apart. Crerar et al. have also shown that the Franciscan Mn ores are strictly comparable to the Galapagos hydrothermal mounds (Lonsdale, 1977; Corliss et al., 1978, 1979). Mn occurs mainly as oxides in both situations. The absence of calcite has been interpreted as the result of water depths below the carbonate compensation level (Crerar et al., 1982).

At Aljustrel the sediments which were brecciated by the Mn bearing fluid were the unconsolidated precursor of hydrothermal jaspers, most probably still in the form of silica gel, given the lack of evidence or even indications of a biogenic origin. Recent authigenic sea floor silica (cherts and porcellanites) has been generally attributed to replacement or alteration of original, primary biogenic amorphous silica (Kastner, 1981). However, inorganic opal occurs in hydrothermal sea floor siliceous precipitates; it

has been found by Bertine and Keene (1975) together with barite in the Lau Basin (NE of Australia), and also in the East Pacific Rise 21°N hydrothermal site, where silica gel itself seems to occur (Haymon and Kastner, 1981). Bertine and Keene (1975) point out that inorganic opal-A is difficult to distinguish from organic opal-A (see Jones and Segnit, 1971), which may in part explain the apparent scarcity of its reported occurrence.

Robertson (1977) described a siliceous matrix in the Troodos (Cyprus) radiolarian cherts that cannot be attributed to diagenesis of the radiolaria, given their excellent state of preservation, and admitted that direct chemical precipitation of the matrix silica is indeed a likely possibility. Matrix silica is also present in the Ligurian cherts (Italy), where the degree of preservation of the radiolaria is poor (Thurston, 1973). The conclusions of Robertson suggest that at least part of the Ligurian siliceous chert matrix may also be due to direct chemical precipitation. These considerations suggest that the chert intersected by DSDP hole 504B (Costa Rica rift) may have lithified through inorganic direct chemical precipitation of hydrothermal silica (see Anderson et al., 1982).

The hydrothermal contribution to the silica budget in the oceans may result from leaching of fractured basaltic rocks, whereas at Aljustrel hydrothermal silica derives

from highly permeable rhyolitic and even high silica rhyolitic pyroclastic rocks (the Mine Tuff, see Chapter 4), clearly capable of supplying large quantities of silica to sea water convectively circulated through them.

Timing of hydrothermal events

We have shown that the Feitais jaspers were originally highly oxidized, even immediately above the Feitais massive sulphide deposit. Given that the sulphide ore forming fluid was strongly reduced, jasper precipitation could have taken place either before or after the sulphide ores. The fact that the jasper was altered by reduced fluids shortly after its formation indicates that the fluid responsible for the alteration was the sulphide ore forming fluid, or a mixture of this fluid with unmodified sea water, as these are the only fluids known to have ever vented in the area. This thus raises the interesting hypothesis that jasper formation may predate sulphide mineralization. The sulphide orebody may consequently have formed under a blanket of unconsolidated siliceous sediment, probably a silica gel. Silica gel is a lightweight ($d \approx 1.3$) material comparable to a sheet of rubber - rubber itself is a gel. (Note, freshly precipitated SiO_2 gels can float in water but as they polymerize the density change is considerable, as the OH^- groups are expelled and the structure approaches silica glass). Space for sulphide precipitation may have

been created principally through floating of the jasper, given that sulphide ore geochemistry and textures indicate that most sulphide precipitation took place in a fluid medium, with only minor replacement phenomena. It is interesting to note that "silica is unique among the inorganic jellies in possessing, when freshly formed, an elasticity of the same order of magnitude as gelatin jelly. Moreover, silica jellies vibrate like a rigid body under certain conditions" (Weiser, 1949, pg. 317).

The average thickness of the jasper is of the order of ten metres, corresponding to a load of the order of 3×10^3 g cm⁻². The mineralizing fluid had to be less dense than sea water, or it would not have risen through the sea water immersed highly porous Aljustrel volcanic rocks (see Sato, 1972; Turner and Gustafsson, 1978; Solomon and Walshe, 1979). Within the Feitais stockwork zone the ore fluid was at >250°C. Assuming that its salinity was ~2 m NaCl (see Sato, 1972) implies that it was ~10% less dense than sea water, or that its buoyancy (negative apparent weight) was ~0.1 g cm⁻². Under these circumstances a >300 m long column of ore fluid would readily lift the silica gel blanket immediately above the ore fluid column, with generation of a sill shaped pond of mineralizing fluid at the interface between the volcanic rocks and the jasper. Hanging wall alteration in the jasper would then represent minor leakage of ore fluid through the otherwise impervious

blanket.

We wish to note here that subsurface sulphide precipitation has just been observed in the Guayamas Basin, Gulf of California, believed to be caused by interaction of an uprising mineralized fluid with sediment "groundwater" (Edmond and Von Damm, 1983). According to these authors "the overwhelming proportion of the ore-forming elements are precipitated in the sediment pile to form a sediment hosted massive sulphide. At Guayamas and in the geologic record these are very much larger than the ophiolite deposits since little is lost as "black smoke".

Sulphide precipitation

Theory (Barnes and Czamanske, 1967; Krauskopf, 1967; Helgeson, 1970), and experiments (Hajash, 1975; Bischoff and Dickson, 1975; Bischoff and Seyfried, 1978; Mottl and Holland, 1978) and observation of natural hydrothermal solutions (Salton Sea brine, White et al., 1973; Red Sea brine, Craig, 1966; Galapagos springs, Corliss et al., 1979; East Pacific Rise "black smokers", RISE Project Group, 1980) strongly suggest that metal transport in massive sulphide forming systems is as chloride or mixed halide complexes (see also Andrews and Fyfe, 1976; Hutchinson et al., 1980; Plimer and Carvalho, 1982), which seems to preclude significant amounts of reduced sulphur in the mineralizing solution (Barnes and Czamanske, 1967, pg.

355). Given that the latter is known to be reduced (from ore zone alteration assemblages) it cannot transport SO_4^{2-} either. A separate sulphur source is therefore indicated. This hypothesis was first postulated by Lovering (1961), and study of the Red Sea and East Pacific Rise ore systems shows that in the case of massive sulphide deposits the sulphur source is unmodified sea water. Reduction of sea water sulphate can be accomplished by inorganic high (>200°C) temperature mechanisms or by biogenic activity (indicated in some important deposits, such as Kidd Creek, Ontario, where abundant graphite is found in the ore zone, Walker et al., 1975). For details on this aspect see Hutchinson et al. (1980) and Fyfe and Lonsdale (1981).

The above requires that unmodified sea water must be available at the site of sulphide ore deposition (see also Munha and Kerrich, 1980; Munha, 1981). At Feitais pristine sea water may have reached the ore zone through flow subparallel to bedding immediately below the jasper layer, driven by dominantly lateral escape of the mineralized fluid upslope (the Feitais orebody formed on the flank of a submarine volcano), as schematically illustrated in Figure 5.18.

A further aspect of importance is the degree of purity of a large ore mass such as the Feitais-Estacao orebody, which requires open system, free volume, essentially isothermal precipitation. This suggests that the key ore

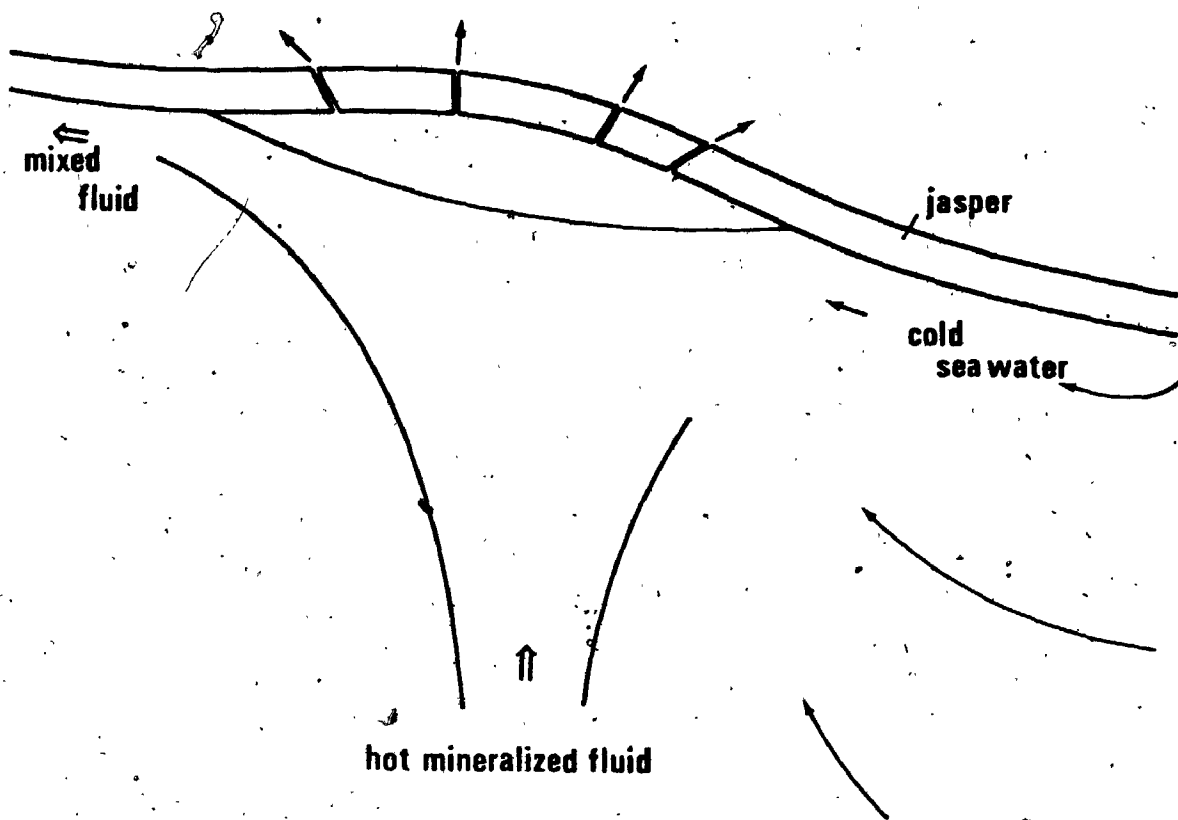


Figure 5.18. Schematic representation of the possible mode of access of unmodified sea water to a pond of ore fluid under an essentially impervious blanket.

forming process is mixing S^{2-} with M^{++} .

Origin of mineralizing fluid: evolving convective regimes

The origin of ore forming fluids specifically in volcanic associated massive sulphide deposits has been a matter of great controversy (see Franklin et al., 1981). However, most authors currently favour a hydrothermal metamorphic model whereby convective circulation of sea water through footwall rocks, driven by heat released from within the rocks themselves and from below (magma chambers, intrusions) eventually modifies sea water into a hot (250-450°C), reduced, acidic, mineralized brine which upon focussed return flow to the ocean and given appropriate conditions at the site of discharge may lead to the fast and concentrated precipitation of metal sulphides (Spooner and Fyfe, 1973; Ohmoto and Rye, 1974; Solomon, 1976; Heaton and Sheppard, 1977; Andrews and Fyfe, 1976; Hutchinson et al., 1980; Franklin et al., 1981).

This general model was recently shown to be applicable to the genesis of the Iberian Pyrite Belt sulphide ores in general (Munha and Kerrich, 1980; Munha et al., 1980; Munha, 1981), and the data presented in the present study also supports well that the Feitais-Estacao orebody specifically may have formed through sea water hydrothermal metamorphism of the Aljustrel Volcanics. Thus we have shown in Chapter 4 that the Aljustrel Volcanics interacted

with convectively circulated sea water which extracted Fe - Mn(?) - Cu - Zn - Pb(?) and Si from them. These elements are most of those defining the gigantic geochemical anomaly represented by the Feitais-Estacao ore environment (including the various alteration products that surround the ore zone).

Barium and gold deserve special mention, as they are two further elements found to be markedly concentrated in the ore zone. There is some evidence that Ba could also have been leached from the Aljustrel Volcanics, as away from sulphide mineralization (see Chapter 4) Ba occurs, sporadically concentrated in hydrothermal minerals (K-feldspar and sericite): this suggests that Ba was present in the modified sea water from which the Ba bearing minerals formed, causing local reprecipitation within the source rocks themselves. Regarding Au, the Aljustrel massive sulphide deposits contain $\sim 2 \times 10^8$ g Au. If this amount was leached from the Aljustrel Volcanics with background concentrations of the order of parts per billion it follows that the total mass of protolith involved was of the order of 10^{16} - 10^{17} g (6 to 60 km³); this estimate is compatible with local geological constraints (see Chapter 3).

We have seen that the composition and size of the Aljustrel sulphide deposits are compatible with a sea water, hydrothermal metamorphic origin for the ore fluid. The

oxygen isotopic composition, calculated for the Feitais-Estacao ore forming fluid varies from ~ 1.5 to $60/100 \delta^{18}O$, thus including compositions significantly heavier than those of fluids involved in most volcanogenic massive sulphide deposits, in which $\delta^{18}O$ is $0 \pm 20/100$ and sea water implicated as the dominant fluid reservoir (Ohmoto and Rye, 1974; Sakai and Matsubaya, 1974; Heaton and Sheppard, 1977; Hattori and Sakai, 1979; Hattori and Muelenbachs, 1980; Pisutha-Arnond and Ohmoto, 1980; Costa et al., 1980; Beatty and Taylor, 1972). But Feitais is not the only exception to this apparent rule. Isotopic studies on the Raul (Ripley and Ohmoto, 1979) and Kidd Creek (Beatty et al., 1980) mines have also indicated ^{18}O enriched ore forming fluids. Within the Iberian Pyrite Belt itself preliminary data from the Rio Tinto and Chanca deposits indicate near $0/100$ fluids whereas Salgadinho (Cercal) seems to be related with ^{18}O -rich fluids (Munha and Kerrich, 1981). In all cases it was suggested that the ore fluid might have been sea water which was modified in some way.

Given the complex and evolving hydrothermal history of the Aljustrel Volcanics described in Chapter 4, which includes early sea water Mg fixation and hydrolysis of igneous feldspars with extreme, homogeneous ^{18}O enrichment of the volcanic rocks, followed by stabilization of albite in turn followed by formation of K-feldspar, suggesting early convective cooling of the volcanic rocks followed by

reheating (see Chapter 4), and given also the relations between hydrothermal jasper, massive sulphide formation and hanging wall rock alteration described in this chapter, we propose that the Feitais-Estacao mineralizing fluid may also have been evolved sea water, enriched in ^{18}O by convective circulation through the Aljustrel Volcanics when these were already enriched in ^{18}O (as measured, $\delta^{18}\text{O} = 17\text{‰}$), that is, through a second stage of convective circulation. Figure 5.19 shows that fluids enriched in ^{18}O could readily evolve through interaction of sea water ($\delta^{18}\text{O} = 0\text{‰}$) with $+17\text{‰}$ rocks, if temperatures are above 100°C and low water/rock prevails (this condition required to preserve high ^{18}O in the rocks, as measured). Thus sea water convection would have been initially water dominated (to enrich the rocks in ^{18}O), evolving to rock dominated conditions towards later stages. This change in water/rock could be explained by progressive permeability reduction from hydration accompanied by rock expansion (Fyfe and Loonsdale, 1981). However, the presence of the jasper bed above the Aljustrel Volcanics suggests that jasper formation, which took place during the hydrothermal events, may have switched fluid convection in the volcanic rocks from an early free discharge regime (high w/r) to a subsequent stage of more or less perfect closed system recirculated flow, effectively reducing the bulk water/rock to the proportions of porosity/volume of rock. An average

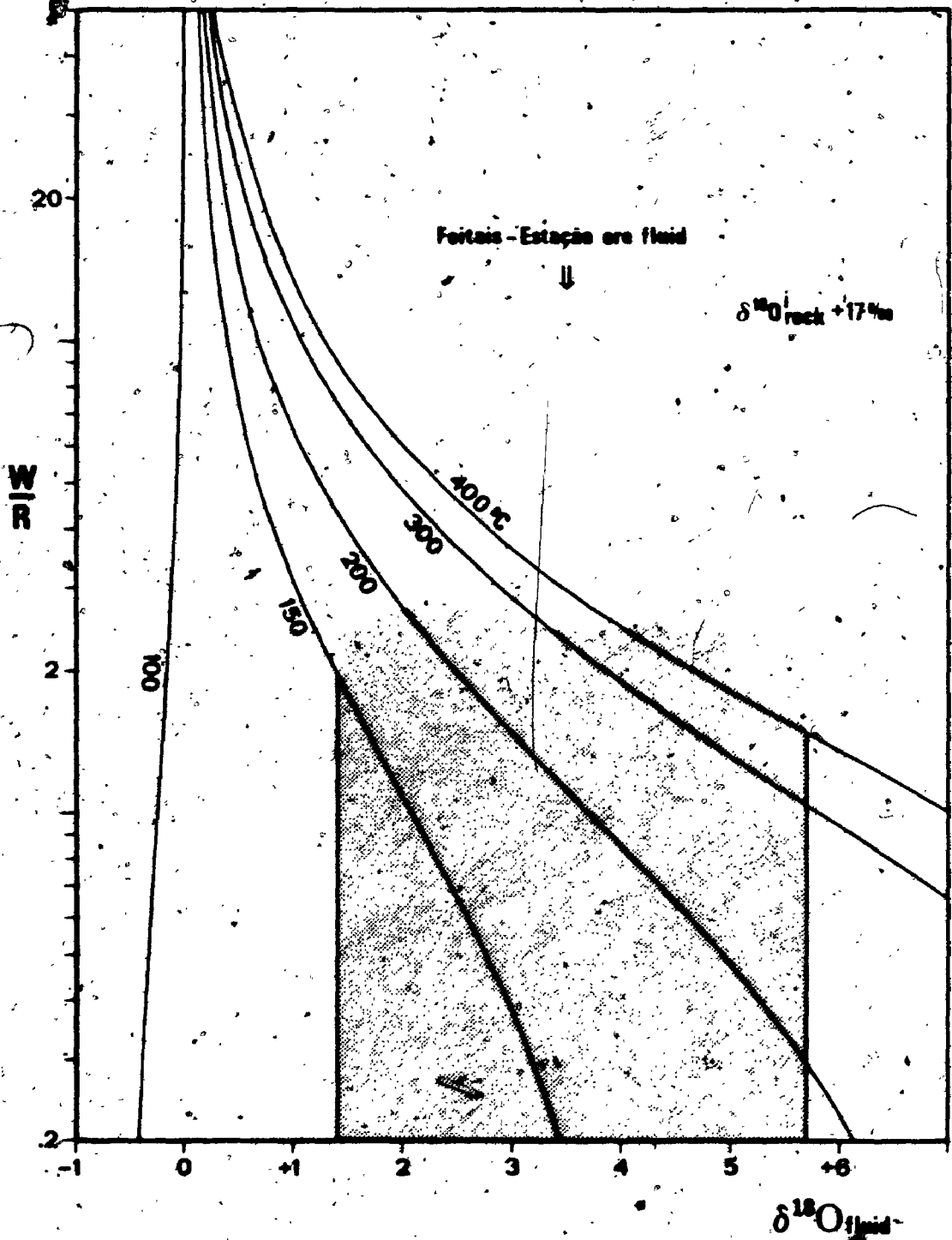


Figure 5.19. Diagram illustrating the water/rock and temperature ranges required to produce high ^{18}O fluids from sea water, through exchange with rocks at $+17\text{‰}$ $\delta^{18}\text{O}$.

porosity of 10% corresponds to the permeability and grain size estimated before (Chapter 4) and to a molar water/rock of ~ 0.075 . The impervious barrier constituted by the jasper would also greatly reduce heat loss from the system, as this would then be largely limited to heat conduction through the impermeable cover, thereby explaining the reheating indicated by oxygen isotope and mineral chemical data: the heat dissipated from an underlying magma chamber would in fact have a larger residence time within the volcanic rocks in the presence of a cover restricting fluid flow between the Aljustrel Volcanics and the basin waters.

Fluid convection is possible under thermal gradients in excess of the adiabatic gradient, and the vigour of fluid convection is appropriately described by a dimensionless parameter that relates the various factors influencing thermally driven fluid motion (the Rayleigh number, see Lapwood, 1948; Spooner, 1977; Fyfe et al., 1978; Fyfe and Lonsdale, 1981). The critical Ra for free discharge porous medium convection is ~ 27 (Lapwood, 1948), and for the same situation the second critical Ra (Straus, 1974) above which convection is non steady is around 240-280 (about ten times Ra_{crit} , Combarrous and Le Fur, 1969; Caltagirone et al., 1971). The early sea water convective regime (free discharge) invoked in Chapter 4 to explain the ^{18}O , Mg and H_2O enrichment of the Aljustrel Volcanics must have had $Ra \gg Ra_c \times 10$, given the extreme

permeabilities inferred from geology and petrography. Under these conditions, drifting, irregular convection cells will be generated (Figure 5.20a), thus explaining the homogeneity of the $\delta^{18}O$ data on the Aljustrel Volcanics, as no fixed recharge or discharge sites exist in a drifting convective system. Given the discussion above we propose that the jasper bed may have formed concomitantly with this early non steady state convective regime. Most of the silica and part of the iron and manganese extracted from the Aljustrel Volcanics are thus thought to have reprecipitated just above the volcanic pile, as a consequence of cooling (Si) and oxidation (Fe, Mn).

Within the framework of the above model the second sea water convective stage (closed system recirculated flow under the jasper) must have proceeded at $Ra < Ra_c \times 10$, to account for the stable geometry required by the presence of the well defined hydrothermal discharge sites (Fig. 5.20b) fossilized by the stockworks. It is indeed likely that Ra became less than $Ra_c \times 10$ during the second convective stage, firstly because of Ra decrease caused by permeability reduction (precipitation of hydrothermal minerals in the voids of the volcanic rocks, Fyfe and Lonsdale, 1981) and secondly because Ra_c for closed system convection is ~ 40 (Lapwood, 1948) and therefore stable convection will take place up to $Ra \sim 400$, instead of ~ 270 in the free discharge situation. In other words, the

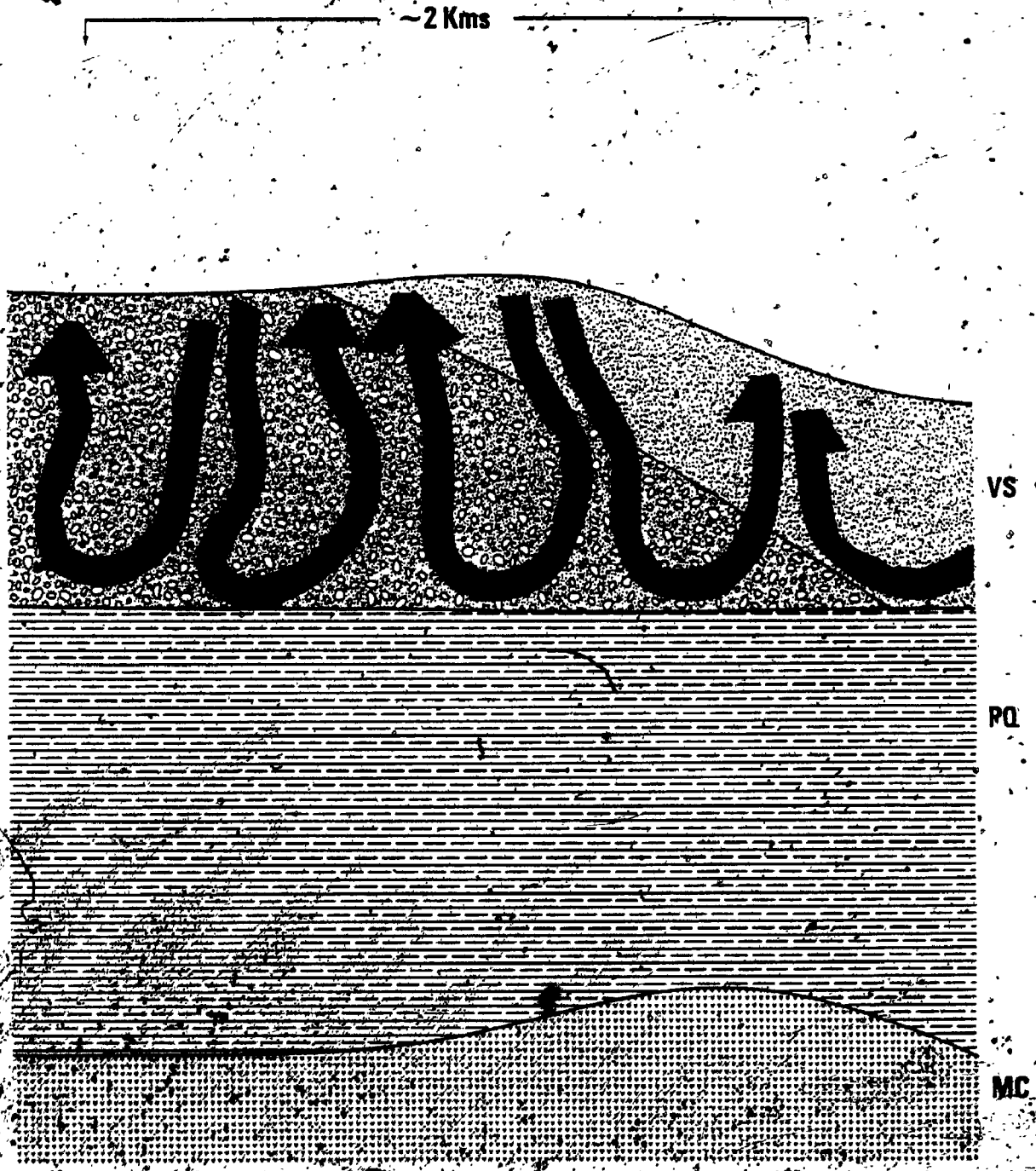


Figure 5.20a. First stage of sea water hydrothermal metamorphism at Aljustrel. VS, Volcanic Sedimentary Complex (Aljustrel Volcanics); PQ - underlying Phyllite-Quartzite Group; MC - magma chamber. See text.



Figure 5.20b. Second stage of sea water hydrothermal metamorphism at Aljustrel. Units as in: Fig 5.20a. Black is jasper. White areas above sulphide mineralization represent hanging wall alteration. See text.

formation of an impervious cover will contribute to stabilize the geometry of the convective regime. This second convective stage would thus be responsible for the generation of the Feitais-Estacao massive sulphide deposit (and possibly the remaining Aljustrel sulphide orebodies) and also for the ore zone wall rock alteration, both above and below sulphide mineralization.

Origin of mineralizing fluid: other hypotheses

Our preferred model of evolving regimes of sea water convection through the Aljustrel Volcanics has perhaps the merit of explaining both the genesis and nature of the mineralizing fluid and all the metasomatic changes described in the Aljustrel Volcanics and ore zone rocks. However, the origin of the Feitais-Estacao mineralizing fluid can be explained by other mechanisms, as follows:

(1) Magmatic fluid contribution. Although minor amounts of magmatic fluid are perfectly compatible with the data and the model proposed above, it is considered unlikely that magmatic solutions were the dominant metal transporting medium, as the sulphide deposit is associated with the waning stages of volcanic activity, which must have postdated any significant magma degassing (cf. Ohmoto and Rye, 1974; see also Williams and McBirney, 1979).

Also, sulphide orebodies at Aljustrel contain more than 100 million tonnes of transition metals, and there are neither

firm data nor indications that such metals could be concentrated in a volatile phase of appropriate mass by purely igneous processes from a reasonably sized plutonic body (see for example Krauskopf, 1967, pg. 484).

(2) Sea water convection through Phyllite-Quartzite Group rocks. It was mentioned above that the late stages of sea water convection in the Aljustrel area were driven by heat from below, probably from a shallow magma chamber (see also Campbell et al., 1981). Large local thermal gradients were therefore produced, and convective sea water circulation must have taken place through whatever permeable rocks were present above the heat source. At Aljustrel the two orebody lineaments mentioned in Chapter 3 had a pre deformation spacing of 3 to 5 km (L. Conde; J. T. Oliveira; V. Oliveira; A. Ribeiro, personal communications, 1981), corresponding to a convection half-cell width of 2 km. Even if a third, interposed ore zone exists, as suspected by mine geologists (L. Conde; J. C. Leitao, personal communications, 1981), convection half-cell widths would still be near 1.5 km. If a normal aspect ratio of these convection cells prevailed the depth of sea water circulation must have been 1 to 2 km (see Lapwood, 1948; Ribando et al., 1976). The known thickness of the Aljustrel Volcanics is only 250 m (base not seen), and from the thickness of the VS Group elsewhere it is unlikely that it exceeds 500 m. It is therefore quite possible that the

lowermost (and hotter) portions of the convection cells were through PQ sediments, which include frequent quartzite beds (see Chapter 2). Detrital quartz is a high permeability, often high ^{18}O material (Hoefs, 1980), and interaction at moderate water/rock and elevated temperatures will increase the $\delta^{18}\text{O}_{\text{fluid}}$. Oxygen isotope data for PQ rocks is needed.

(3) Connate water from underlying formations. Pore water can be trapped, heated, modified, and later expelled by burial, compaction and seismic pumping in such a manner as to conform with most of the available data on massive sulphide deposits (see Hutchinson et al., 1980; Lydon, 1981; Franklin et al., 1981). The main objection against such a model for Aljustrel specifically and the Iberian Pyrite Belt in general is the fact that in these examples sulphide mineralization is invariably related with felsic volcanism, despite the fact that solely sedimentary stratigraphic sections are ubiquitous between the various volcanic centres (Schermerhorn, 1971; Carvalho et al., 1976).

(4) Metamorphic water. We have repeatedly invoked the presence of a large, shallow level magma chamber under the Aljustrel Volcanics (presumably within the pre volcanic Rhyllite-Quartzite Group) to account for the large volume of volcanic rocks present in the area and also to act as a major heat source required to drive sea water convection

beyond the early stage of dissipation of heat from the volcanic rocks themselves.

Campbell et al. (1981) have recently documented the presence of sill-shaped magma chambers stratigraphically under massive sulphide deposits in the Sturgeon Lake and Kam-Kotia areas of the Canadian Precambrian Shield, and cited many other examples of the same association in such important massive sulphide camps as Matagami, Flin Flon and Noranda. They (ibid.) state that "Precambrian massive sulphide deposits.....are commonly turned on their side by postore tectonic processes exposing the underlying rock sequence for inspection". At Aljustrel not even the base of the volcanic rocks is exposed, but given the above considerations it is not unreasonable to admit that the Aljustrel magma chamber may also be sill-shaped, in good agreement also with magma density considerations (see Herzberg et al., in press). If so, magma uprise to shallow levels and lateral spreading will create a large volume where the rocks surrounding the magma conduit(s), possibly wet PQ sediments, will be subjected to very high thermal gradients, with consequent dehydration metamorphic fluids, which would likely have $\delta^{18}O$ 60/00 (Taylor, 1974) and, if metamorphic degassing temperatures exceeded 500°C, also likely to contain significant amounts of gold (Henley, 1973; Fyfe, 1974). If, there is a contribution from deeply derived metamorphic water, it could explain gold enrichment

and CO_2 contribution and could generate transient conditions of $P_{\text{fluid}} > P_{\text{load}}$.

Sea floor metamorphism

Despite the possible applicability of some of the mechanisms of ore fluid generation briefly discussed above, our preferred model of evolving sea water convective regimes through the Aljustrel Volcanics does not require fluid contributions from other sources, and furthermore, is comparable to present day sea floor metamorphism.

Evidence accumulated during the last decade or so leaves little room for doubt that present day oceanic lithosphere cools principally through sea water convective circulation (Elder, 1965; Lister, 1972, 1977; Williams et al., 1974), and that oceanic hydrothermal metamorphism is the net result of sea water - rock interaction, with formation of the spilitic rocks and serpentinites that occur in the sea floor and in ophiolites, as well as the massive sulphide deposits present within the volcanic portions of both rock suites. (Spooner and Fyfe, 1973; Andrews and Fyfe, 1976; Spooner et al., 1974, 1977a,b; Spooner, 1977; Francheteau et al., 1979; Moody, 1979; McCulloch et al., 1980; Hutchinson et al., 1980; Fyfe and Lonsdale, 1981).

Sub sea floor marine water convection persists in time and space to tens of millions of years and hundreds of

kilometres from the origin of these rocks at mid ocean ridges (Anderson et al., 1977, 1979, 1981; Lawrence and Gieskes, 1981), and takes place through different cellular regimes that evolve as the sea floor thermal conditions change. At mid ocean ridges the young hot crust lacking sediments, cools through free discharge convection driven initially with heat from within the permeated lithologies. As the crust cools, ages and is transported away from ridges, convection switches to that driven by heat from below, and formation of a low permeability sediment cover generates more or less perfect closed system recirculated flow; heat loss becoming dominated by conduction through the sediment cap (Lister, 1972, 1974; Ribando et al., 1976; Davis and Lister, 1977; Anderson et al., 1981; Fyfe and Lonsdale, 1981; Barriga et al., 1983). Thermal gradients through the impermeable cap can be very steep as demonstrated for the Juan de Fuca ridge system by Davis and Lister (1977), who have reported temperatures up to 200°C at the sediment-basalt interface. This suggests that the sediment-basalt interface may also be a good site of ore deposition, in agreement with recent observations of metal rich muds in the Juan de Fuca region (Geotimes, Dec. 1981, 25-26). Closed cell convective ore generation under sediments in the sea floor environment has been advocated by Fyfe and Kerrich (1976), Fyfe et al. (1978), Hutchinson et al. (1980) and Barriga et al. (1983).

The similarities between the evolution of the sea floor metamorphic regime, briefly outlined above, and the hydrothermal history proposed in this study for the 350 Ma old Aljustrel sea floor area are obvious.

CHAPTER 6

SUMMARY AND CONCLUSIONS

The purpose of the present study was to contribute to the understanding of the genesis of massive sulphide deposits associated with volcanism. The Feitais-Estacao massive sulphide deposit of Aljustrel, South Portugal was chosen as a suitable object of study.

Aljustrel is one of the most important mining centres of the Iberian Pyrite Belt, with massive polymetallic sulphide ore reserves beyond 200 million metric tonnes. The Iberian Pyrite Belt is located in South Portugal and Southwest Spain and constitutes western Europe's most prominent stock of base metals. Extremely large massive sulphide deposits occur associated with the waning stages

of felsic explosive volcanism which took place in early Carboniferous times, on a phyllite-quartzite (PQ), shelf facies, conformable basement. Subordinate mafic volcanism accompanied the felsic volcanic activity, producing a bimodal association in which the two types of igneous rocks are not related by magmatic differentiation; basaltic rocks seem to derive from heterogeneous mantle peridotite and felsic rocks resulted from partial melting of crustal material. Volcanic rocks were affected by widespread sea water hydrothermal metamorphism responsible for the present spilitic and quartz-keratophytic (felsic spilitic) compositions of the rocks, for the massive sulphide deposits and also for abundant volcanogenic sediments such as manganese accumulations, Fe-Mn cherts, purple and red slates genetically equivalent to present day sea floor Fe-Mn hydrothermal and perhaps hydrogenous metalliferous concentrations.

Volcanism took place along lineaments of discrete volcanic centres in a framework of detrital, biogenic and chemical sediments, generating a widely variable (ore hosting) Volcanic-Sedimentary Complex. After volcanism the area experienced pronounced subsidence, with deposition of a conformable, several km thick Flysch Group (base Viséan to Westphalian). During the time of Flysch deposition, large scale synsedimentary deformation took place, enhanced by probably continuous, subsequent tectonic compression,

generating a complex imbricate structure of tight folds and folded overthrusts where VS anticlines are exposed between, and often thrust on, Flysch synclines. Deformation was accompanied (and followed) by low grade (zeolite - lower greenschist) and low pressure regional metamorphism of essentially isochemical nature. The plate tectonic setting of the Iberian Pyrite Belt thus probably corresponds to an early continental rifting situation, or to a back arc associated with subduction (further North), in which case the Flysch phase of the basin and the tectonic activity would be related to closure of an adjacent ocean and continental collision.

At Aljustrel exclusively felsic, submarine, explosive volcanism took place ~330 Ma before present (Visean) and produced >5 km³ of pyroclastic rocks. These can be grouped into a central unit of coarse quartz and feldspar phyrlic tuffs, the Quartz-eye Tuff (Megacryst Tuff and Green Tuff), flanked on either side by finer grained felsic tuffs devoid of quartz phenocrysts (felsitic and feldspar phyrlic tuffs, the Mine Tuff). At the waning stages of volcanic activity nearly 250 Mt of massive sulphides were deposited on the two symmetrical units of the Mine Tuff. Prominent siliceous and metaliferous sediments cap and surround the sulphide deposits. Footwall rocks contain stockwork ores in variably altered lithologies, attesting that mineralized ore forming fluids penetrated to near the coeval sea floor.

and that the sulphide deposits are thus exhalative. After deposition of a few tens of metres of fine grained epiclastic and tuffitic sediments on top of the ores and associated metalliferous sediments the area underwent major subsidence, with concomitant deposition of the several kilometre thick Culm Group turbidites. Hercynian deformation took place in subsequent phases, from early synsedimentary deformation producing major overthrusts and gentle folding, through a main (nearly coaxial) compressive phase responsible for tightening and overturning of folds with cleavage generation and thrusting of the inverse flanks of the anticlines. Late stage compression generated a set of dextral wrench faults and provoked large scale movement along the major Messejana wrench fault.

6.1 Conclusions

The main conclusions of this study, based on field relations, petrography, mineral chemistry, rock geochemistry and oxygen isotope geochemistry are as follows:

1. As far as can be seen through major metasomatic changes, the Aljustrel Volcanics originally consisted of two units of submarine pyroclastic rocks. A high iron rhyolite (the Quartz-eye Tuff) may have erupted first, followed almost immediately thereafter by a high silica rhyolite (the Mine Tuff). The two tuff formations derive

from partial melting of a common crustal source, possibly high grade metamorphic. Their differences can be explained either by different degrees of partial melting of their source followed by variable degrees of shallow level crystal fractionation or, alternatively, the QET may represent proximal volcanic facies and the MT more distal associated flow tuffs.

2. The main metasomatic changes experienced by the Aljustrel Volcanics seem to have been as follows:

- major hydration, oxidation, and Mg fixation in the uppermost 50 m or so of each of the QET and the MT;

- progressive Fe (and perhaps Mn) leaching downwards in both tuff sequences;

- progressive leaching of Cu and Zn in samples either markedly reduced or oxidized (Pb values all low);

- significant Si leaching;

- complex and evolving behaviour of the alkalis, with early widespread hydrolysis of igneous feldspars followed by hydrothermal growth of low temperature albite megacrysts which were subsequently partially or totally replaced by low temperature K-feldspar. Alkali feldspar megacrysts occur almost exclusively in the Quartz-eye Tuff (the core of the Aljustrel Volcanics);

- General, homogeneous $\delta^{18}O$ enrichment to extreme values around 17‰ to 18‰ .

3. Hercynian low grade regional metamorphism (up to

lower greenschist facies and essentially isochemical) has overprinted the rocks and may have obliterated in part the hydrothermal mineralogy, namely producing the presently observed chlorite, sericite and epidote from hydrothermal lower grade phyllosilicates such as smectite and celadonite and zeolites, respectively.

4. The Feltais-Estacao orebody of Aljustrel (100 Mt) is composed of a massive sulphide lens shaped body underlain by a crosscutting zone of stringer and disseminated mineralization hosted in chlorite-quartz and sericite-quartz rocks that are the product of alteration of the surrounding Mine Tuff Formation rocks. The orebody is capped by a laterally extensive bed of jaspers and Fe-Mn sediments showing prominent alteration immediately above the orebody. Hanging wall rock alteration is also present in the lowermost metres of the Paraiso Siliceous Formation aluminous sediments and (rare) pyroclastic rocks that overlie the jasper unit. The Feltais sulphide ores and associated lithologies and ore zone alteration are the product of interaction of a hot, reduced, metalliferous brine with sea water at or near the sea floor.

5. Stockwork alteration at Feltais is characterized by the formation of a crosscutting pipe of mainly quartz-chlorite-sulphide rock surrounded both megascopically and at the scale of individual vein aureoles by quartz-sericite-sulphide (+ carbonate) rock, strictly comparable

to stockwork alteration in the Archean Noranda massive sulphide deposits. Stockwork alteration clearly postdates the early hydrothermal metasomatic episode responsible for the conformable regional alteration mentioned in 2.

6. The main ore zone metasomatic changes produced in Mine Tuff rocks by the mineralizing process were large scale Fe and S and lesser Ba enrichment and almost quantitative extraction of Na. Mg enrichment at the time of ore formation is not required, given that the top layers of the Mine Tuff were markedly enriched in Mg prior to mineralization.

7. The Feitais-Estacao orebody is markedly zoned, with sphalerite, galena, several sulphosalts and barite concentrated towards the top, whereas chalcopyrite, sericite and chlorite predominate towards the footwall. Pyrite, quartz, carbonates and arsenopyrite are scattered throughout. Microprobe data revealed that the MnO content of ore zone chlorites varies significantly with stratigraphic position, increasing from stockwork and Cu rich massive ore to the overlying jaspers and metalliferous sediments. Oxygen isotope compositions indicate that the ore fluid was at $\sim 250^{\circ}\text{C}$ in the stockwork and cooled to 200°C within massive ore, and finally to $\sim 130^{\circ}\text{C}$ at the ocean floor. These together with the extreme Fe/Mn fractionation on passing from sulphide ores to the overlying Mn sediments suggest that the hydrothermal

mineralizing solutions moved upwards through the footwall pyroclastic rocks along a thermal gradient acquiring progressively higher oxidation potential, as the result of mixing with unmodified sea water.

8. The oxygen isotope composition calculated for the Feltais-Estacão ore forming fluid varies from +1.5 to +60/00 $\delta^{18}O$.

9. The Feltais-Estacão orebody is capped by a laterally continuous bed of jasper (hematitic chert) which immediately above sulphide ore is markedly altered by reducing fluids which were injected in the jasper shortly before lithification, producing marked vein controlled reduction of the jasper into predominantly bluish grey magnetitic and pyritic chert, as well as frequent veins, pods and breccias dominantly composed of a host of Mn bearing carbonates. Hanging wall alteration persists in the lowermost ~10 metres of the detrital and volcanogenic sediments (phyllites, tuffites) and rare tuffs that occur above the jasper, as discontinuous, irregularly shaped areas of intense pyritization, chloritization and carbonatization.

10. The Aljustrel jaspers are largely hydrothermal chemical precipitates, as evidenced by REE patterns, low Ni+Co+Cu abundances, low thorium abundances, oxygen isotopic compositions indicating formation temperatures ~130°C and lack of fossil radiolarians.

11. The clear evidence for deformation of mineralized structures in the hanging wall sediments clearly shows that this mineralization occurred pre-deformation and was not simply a result of dispersion during later regional metamorphism (see Plate 8).

6.2 Genetic model

The Aljustrel Volcanics are submarine pyroclastic rocks, likely to have been deposited at low temperature (>200°C) and to have had extremely high initial permeability, similar to that of coarse sand, in the range of 10^{-8} cm². Under these circumstances and given also that the fluid responsible for early metasomatism was initially oxidized, Mg rich and very abundant, initial cooling of the pyroclastic pile must have taken place through vigorous sea water convection driven by heat from within. The Rayleigh number must not only have exceeded the critical value necessary for convection to take place but, given the extremely high initial permeabilities inferred from geology and petrography, the second critical Rayleigh number may also have been exceeded. Above this value convection in non steady state and drifting, irregular convection cells are thus likely to have formed. This would explain the relative homogeneity of oxygen isotope data for the volcanic rocks, as no fixed water recharge and discharge sites exist in a drifting convective system. The final

Isotopic result is everywhere the result of the prevailing physicochemical conditions, low temperature and high water/rock.

We propose that the Aljustrel jasper may have formed concomitantly with this early non steady state convective regime. Most of the silica and part of the Fe and Mn leached by sea water from the Aljustrel Volcanics are thus thought to have reprecipitated just above the volcanic pile, as a consequence of cooling (Si) and oxidation (Fe, Mn).

Given the complex and evolving hydrothermal history of the Aljustrel Volcanics, suggestive of early cooling followed by reheating and concomitant metal extraction from the rocks, and given also the relations between hydrothermal jasper, massive sulphide formation and hanging wall rock alteration at Feitais, we propose that the Feitais-Estacao mineralizing fluid may also have been evolved sea water, enriched in base metals and ^{18}O by convective circulation through the Aljustrel Volcanics when these were already enriched in ^{18}O , that is, through a second stage of closed system recirculated flow under the impermeable blanket represented by the jasper and perhaps also by some of the fine grained, low permeability sediments (now phyllites) of the Paraiso Siliceous Formation. Both permeability decrease in the course of hydrothermal activity because of precipitation of

hydrothermal minerals in rock voids and closed system convection will favour stable convective cell geometries during this second stage of sea water circulation and under an impermeable cap heat dissipation will be markedly reduced, thus explaining the reheating indicated by the data. The second convective stage will be characterized by low bulk water/rock, limited to the proportions of porosity/volume of rock, appropriate to enrich the fluid in ^{18}O , as measured.

Within the framework of the above model massive sulphide precipitation may have taken place under a blanket of unconsolidated siliceous sediment, probably a silica gel, a substance comparable to a sheet of rubber. Space for sulphide precipitation may have been created principally through floating the jasper, given that sulphide ore geochemistry, textures and gangue mineralogy indicate that most sulphide precipitation took place in an essentially isothermal fluid medium, with only minor replacement phenomena. A simple calculation indicates that the buoyancy of a 300 m long column of hot mineralizing fluid 10% less dense than sea water would be sufficient to lift the jasper (~10 m thick) above the hot plume of fluid. Hanging wall alteration would then represent minor leakage of ore fluid through the otherwise impervious blanket.

Our preferred model of evolving regimes of sea water

convection through the Aljustrel Volcanics has perhaps the merit of explaining both the genesis and nature of the mineralizing fluid and all the metasomatic changes described in the Aljustrel Volcanics and ore zone rocks. However, the ore fluid could possibly derive from other mechanisms, namely sea water convection through "basement" (PQ Formation) rocks, or through discharge of connate waters from underlying formations through burial, compaction and seismic pumping and, above all, through discharge of metamorphic water produced by emplacement of a large shallow level magma chamber under the Aljustrel area, not observed at the present level of erosion but indicated by the large volume of volcanic rocks present and by theoretical considerations. A metamorphic fluid contribution is attractive also in view of the large total amount of gold present in the Aljustrel orebodies (and around them), of the order of 2×10^8 g: Au geochemistry suggests that its transport is facilitated at higher temperatures than those implicated in the purely sea water convective model.

6.3 Exploration implications

Some of the geochemical features that characterize the ore forming hydrothermal activity at Aljustrel suggest that lithochemical exploration may provide insight into the nature of potential ore targets in the Iberian Pyrite Belt,

once good geologic control exists and in addition to the exploration methodologies currently in use.

Firstly, the degree of regional hydrothermal alteration, as expressed by petrography, transition element geochemistry (in rocks, not soils) and oxygen isotope geochemistry may contribute to define the more attractive volcanic centres (those more intensely affected by hydrothermal metamorphism). Secondly, reduced volcanic rocks depicting Ba and/or Au anomalies may indicate proximity to ore. Thirdly, and perhaps above all, the detailed study of cherts and jaspers, with emphasis on transition and RE element distributions and oxydation states (and microtextures where possible) may prove capable of distinguishing various origins in such sediments, and distance to ore in the case of hydrothermal sediments.

APPENDIX I

SUMMARY OF ANALYTICAL TECHNIQUES

I - 1 Structural state of alkali feldspars

Alkali feldspar megacrysts were extracted from the rocks by diamond sawing, subsequent light crushing and hand picking of millimetric fragments free from other minerals. These were subsequently manually comminuted to <200 mesh in an agate mortar, and the resulting powder was used to diffract Fe K α_1 radiation, in a Guinier-Jagodzinski double cylinder camera with precision monocromator produced by Rich. Seifert & Co., Röntgenwerk (2070 Ahrensburg B., Hamburg, F.R.G.), which "consists of a double cylinder of high resolving power designed on the principles of the Seemann-Bohlin focusing method (for transmission and back-reflection exposures) in combination with a precision quartz crystal monocromator based on the Johansson principle" (from the camera manual). Film intensities were read in an automated densitometer, and subsequently interpreted and plotted using a set of appropriate computer programs developed by Prof. J. Starkey (U.W.O). The precision and accuracy of the Bragg angle obtained by this method are within ± 0.002 $^{\circ}2\theta$.

I - 2 Electron microprobe mineral analyses

With the exception of data presented in Figure 5.4 (see figure caption), mineral chemical analyses were obtained on 25 mm diameter polished thin sections coated with carbon, using a Materials Analysis Company model 400 electron microprobe equipped with three diffractometers and KRISSEL automation. Working conditions were 15 to 20 kV excitation voltage and 0.25 to 0.5 μ A beam current (depending on the mineral being analysed), at counting conditions of 30 seconds or 20000 counts. The standards used were well analysed natural minerals and

synthetic glasses, selected to minimize necessary corrections (MAGIC corrections were used throughout). Replicate determinations indicate a precision generally better than 2% of the amount present, for major elements.

I - 3 Whole rock geochemistry

Whole rock samples were diamond cut into several slabs ~0.5 cm thick, subsequently grinded with Al_2O_3 abrasives to eliminate brass contamination, and thoroughly washed and dried, and lightly hammered between cloths to avoid any contact with metal, and the resulting fragments subsequently split to about 50 g. This amount was in turn powdered for ~30 seconds in a Bleuler mill.

Major elements (with the exception of Na) were determined by X-ray fluorescence spectrometry, in a Philips PW 1450 spectrometer fitted with a Cr tube, using the heavy absorber fusion technique of Norrish and Hutton (1969), where a glass disk is made, composed of 2.0000 g of flux (lithium tetraborate, lithium carbonate and lanthanum oxide), 0.0267 g of sodium nitrate and 0.3733 g of sample. Samples with high concentrations of Fe (>20%) and/or S (>2%) were diluted with 50.0000% specpure SiO_2 . Calibration monitor samples FS-94 and FS-84 (supplied by Dr. K. Norrish, CSIRO, Australia) were used for calculation of the concentrations in the samples. Na and S were determined in pressed pellets of rock powder, with reference to calibration lines defined by international (Na) and departmental (S) standards.

Most trace elements were determined on pressed pellets, by X-RF spectrometry (W tube) with reference to selected international standards. Data were reduced using interference and matrix calculations

through program TRACE developed by G. Barker, H. Hunter and T. LaTour (unpublished, U.W.O.).

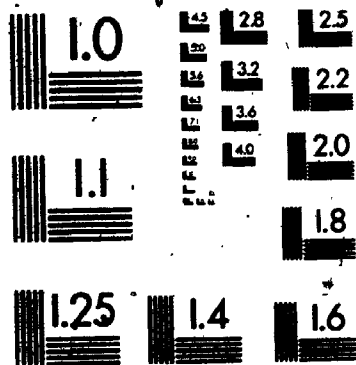
International standards and duplicate unknown samples were run for accuracy check, and results indicate that major element determinations are generally accurate within 1-2% of the amount present, and trace elements accurate within 10% (20% for Nb and Cu).

Sc, Hf, Ta, Au and Th were determined by instrumental neutron activation analysis at Neutron Activation Services, Hamilton, Ontario. Results of duplicate analyses indicate precisions better than 5%.

Rare earth elements were determined by a modified version (Fryer, 1977) of the thin-film X-ray fluorescence (W tube) procedure of Eby (1972). The REE were separated as a group by ion-exchange chromatography and transferred onto Reeve Angel SA-2 ion-exchange paper circles ($\phi=25$ mm). Prior to separation, 50 μ g of Tm were added as an internal yield standard. Precision is generally better than 10%.

Ferrous iron was determined after the method of Wilson (1955). International standard SY-3 was analysed as an unknown with each batch, and results indicate that accuracy and precision are better than 5% of the amount present. Volatiles were determined by weight loss on rock powder following heating at 1100°C.

4



APPENDIX II

REPRESENTATIVE MICROPROBE ANALYSES
OF MINERALS FROM THE ALJUSTREL VOLCANIC ROCKS

- II-1. Igneous feldspars
- II-2. Hydrothermal feldspars
- II-3. Fe-Ti oxides and sphene
- II-4. Almandine garnet
- II-5. Chlorites (averages)
- II-6. Sericites
- II-7. Epidotes
- II-8. Calcites

Table II-1. Igneous feldspar analyses from the Ajustré volcanic rocks.

Sample Anal. no.	(a) GF-A 31		(a) GF-A 33		(a) GF-A 32		(b) GF-A 38		(b) GF-A 39		(b) GF-A 40		(a) GF-A 9		(a) GF-A 13		(a) GF-A 17		(a) GF-A 45		(a) GF-A 49		
	SiO ₂	65.43	67.39	67.42	67.53	67.62	67.07	67.81	66.92	67.98	67.95	67.87	68.03	22.04	20.82	21.08	20.86	19.95	20.83	21.64	20.62	20.13	20.73
Al ₂ O ₃	0.48	0.04	0.05	0.14	0.07	0.24	0.35	0.17	0.09	0.13	0.27	0.00	1.25	1.06	1.47	1.42	0.42	1.34	1.02	0.77	0.61	0.67	0.73
CaO	0.14	0.00	0.11	0.09	0.11	0.07	0.04	0.03	0.09	0.09	0.02	0.04	10.07	10.52	10.42	10.23	9.84	10.50	10.56	11.14	10.97	10.41	11.39
Na ₂ O	0.95	0.08	0.08	0.08	1.20	0.08	0.54	0.20	0.11	0.20	0.09	0.09	100.36	100.63	100.63	100.36	99.21	100.14	101.96	99.83	99.99	100.16	100.62
TOTAL	11.504	11.783	11.730	11.771	11.931	11.737	11.676	11.753	11.886	11.841	11.815	11.836	4.566	4.291	4.322	4.285	4.149	4.296	4.391	4.268	4.148	4.258	4.172
Si	0.070	0.006	0.007	0.020	0.010	0.035	0.051	0.025	0.013	0.019	0.039	0.000	0.234	0.199	0.274	0.265	0.079	0.251	0.188	0.145	0.114	0.125	0.137
Al	0.008	0.001	0.007	0.006	0.008	0.005	0.004	0.002	0.006	0.006	0.001	0.004	3.434	3.566	3.515	3.457	3.366	3.562	3.523	3.793	3.719	3.517	3.844
Fe	0.215	0.018	0.018	0.018	0.270	0.018*	0.121	0.045	0.025	0.044	0.020	0.020	0.070	0.018	0.018	0.018	0.270	0.018*	0.121	0.045	0.025	0.044	0.020

Number of ions on the basis of 32 O

(a) Albite phenocrysts

(b) Albite in tuff matrix

Table II-1. Continued (Igneous feldspars)

Sample Anal. no.	(a) GF-15.8		(a) GF-15.8		(c) GF-15.8		(a) GF-62		(a) 2-GF-87		(a) 2-GF-87		(a) 2-GF-87	
	4	6	17	12	19	20	32	22	21	20	19	19	20	17
SiO ₂	67.61	67.59	68.03	68.39	65.59	65.18	68.28	67.32	67.71	66.90	67.70	67.70	66.90	67.68
Al ₂ O ₃	20.86	20.16	20.43	20.05	17.71	18.47	20.37	20.50	20.21	20.25	20.69	20.47	20.25	20.47
FeO	0.00	0.00	0.00	0.00	0.23	0.00	0.00	0.14	0.31	0.00	0.26	0.00	0.00	0.00
CaO	1.07	1.10	1.23	0.79	0.00	0.00	1.00	1.33	1.24	1.74	1.16	1.27	1.74	1.27
BaO	0.00	0.00	0.00	0.00	0.21	0.04	0.00	0.05	0.02	0.05	0.04	0.05	0.05	0.05
Na ₂ O	10.38	11.34	10.90	10.92	0.16	0.20	10.11	10.83	10.19	10.91	10.27	10.45	10.91	10.45
K ₂ O	0.11	0.05	0.05	0.07	16.13	16.52	0.07	0.07	0.24	0.07	0.08	0.05	0.07	0.05
TOTAL	100.03	100.24	100.64	100.42	100.04	100.41	99.82	100.25	99.92	99.92	100.19	99.97	99.92	99.97
Number of ions on the basis of 32 O														
Si	11.798	11.817	11.824	11.898	12.117	12.004	11.907	11.772	11.854	11.755	11.809	11.828	11.755	11.809
Al	4.290	4.154	4.184	4.113	3.859	3.879	4.187	4.225	4.170	4.194	4.254	4.216	4.194	4.254
Fe	0.000	0.000	0.000	0.000	0.035	0.000	0.000	0.020	0.045	0.000	0.039	0.000	0.000	0.000
Ca	0.200	0.206	0.230	0.184	0.000	0.000	0.187	0.249	0.233	0.328	0.219	0.238	0.328	0.219
Ba	0.000	0.001	0.000	0.000	0.016	0.004	0.001	0.003	0.001	0.003	0.004	0.003	0.003	0.003
Na	3.512	3.844	3.672	3.684	0.055	0.070	3.418	3.672	3.459	3.717	3.473	3.541	3.717	3.473
K	0.024	0.011	0.012	0.016	3.801	3.879	0.016	0.016	0.054	0.016	0.020	0.011	0.016	0.020

(a). Albite phenocrysts

(c) K-feldspar phenocrysts

Table II-1. Continued (Igneous feldspars)

Sample Anal. no.	(a)	(a)	(a)	(a)	(a)	(a)	(a)	(a)	(a)	(a)	(a)	(a)	(a)
	MD4F 15	MD4F 16	MD4F 18	MD4F 19	MD4F 25	MD4F 47	bis-330.25 1	bis-330.25 4	bis-330.25 8	bis-330.25 9	bis-330.25 11	bis-330.25 13	bis-330.25 13
SiO ₂	68.80	67.63	67.82	68.39	68.21	68.08	67.54	67.94	67.29	67.24	68.02	67.28	67.28
Al ₂ O ₃	19.59	20.48	20.16	19.56	19.98	20.17	19.61	19.92	20.09	19.97	19.59	20.25	20.25
FeO	0.08	0.15	0.07	0.04	0.09	0.20	-	-	-	-	-	-	-
CaO	0.68	1.33	1.27	0.70	0.94	0.89	0.51	0.10	0.68	0.47	0.35	0.81	0.81
BaO	0.06	0.11	0.04	0.04	0.06	0.13	-	-	-	-	-	-	-
Na ₂ O	11.37	10.11	11.08	11.25	10.84	10.69	11.29	11.62	11.34	11.42	11.27	11.36	11.36
K ₂ O	0.04	0.78	0.04	0.12	0.03	0.07	0.05	0.02	0.06	0.19	0.35	0.06	0.06
TOTAL	100.62	100.59	100.48	100.10	100.14	100.23	99.00	99.60	99.46	99.29	99.30	99.75	99.75
Number of ions on the basis of 32 O													
Si	11.957	11.802	11.828	11.949	11.902	11.879	11.922	11.914	11.840	11.855	11.957	11.813	11.813
Al	4.016	4.212	4.145	4.027	4.109	4.148	4.078	4.117	4.166	4.152	4.059	4.188	4.188
Fe	0.012	0.022	0.012	0.008	0.012	0.021	-	-	-	-	-	-	-
Ca	0.125	0.249	0.238	0.129	0.176	0.168	0.098	0.020	0.128	0.090	0.066	0.152	0.152
Ba	0.004	0.008	0.004	0.004	0.004	0.008	-	-	-	-	-	-	-
Na	3.832	3.421	3.746	3.813	3.668	3.617	3.863	3.949	3.869	3.906	3.844	3.867	3.867
K	0.008	0.174	0.008	0.027	0.008	0.016	0.012	0.004	0.013	0.043	0.020	0.016	0.016

(a) Albite phenocrysts

(c) K-feldspar phenocrysts

(b) Albite in tuff matrix

(d) Albite in tectonic dilatancy vein

Table II-2a) Hydrothermal albite analyses from the Aljustrel Volcanic rocks.

Sample Anal. no.	(a) GF-158 8		(b) 4-GFM 10		(b) 4-GFM 14		(b) 4-GFM 15		(b) GF-62 23		(b) GF-62 26		(b) GF-62 27		(b) GF-62 41		(b) 2-GF-87 8		(b) 2-GF-87 9	
	SiO ₂	68.95	67.47	68.58	68.68	68.41	68.13	67.59	68.75	67.98	67.56	67.98	67.98	67.98	67.98	67.98	67.98	67.98	67.98	67.98
Al ₂ O ₃	19.39	19.95	19.59	19.64	19.45	19.70	19.13	19.16	19.39	20.16	19.39	19.39	19.39	19.39	19.39	19.39	19.39	19.39	19.39	19.39
FeO	0.00	0.00	0.00	0.00	0.00	0.00	0.00	0.00	0.00	0.00	0.00	0.00	0.00	0.00	0.00	0.00	0.00	0.00	0.00	0.00
CaO	0.12	0.05	0.17	0.09	0.23	0.26	0.31	0.25	0.02	0.05	0.02	0.02	0.02	0.02	0.02	0.02	0.02	0.02	0.02	0.02
BaO	0.00	0.05	0.02	0.14	0.05	0.00	0.00	0.00	0.00	0.00	0.00	0.00	0.00	0.00	0.00	0.00	0.00	0.00	0.00	0.00
Na ₂ O	11.89	11.61	11.78	11.24	11.43	10.65	11.46	11.30	11.93	11.68	11.93	11.93	11.93	11.93	11.93	11.93	11.93	11.93	11.93	11.68
K ₂ O	0.08	0.05	0.10	0.14	0.09	0.05	0.04	0.05	0.09	0.07	0.09	0.09	0.09	0.09	0.09	0.09	0.09	0.09	0.09	0.07
TOTAL	100.43	99.17	100.25	99.86	99.64	98.79	98.53	99.50	99.43	99.53	99.53	99.53	99.53	99.53	99.53	99.53	99.53	99.53	99.53	99.53

Number-of ions on the basis of 32 0

(a) Early hydrothermal albite fetic in late hydrothermal K-feldspar megacryst
 (b) Mostly chessboard textured megacrysts

Table II-2a) Continued (Hydrothermal albites)

Sample Anal. no.	(b) MD4F 29	(b) MD4F 35	(b) MD4F 36	(b) MD4F 39	(b) MD4F 40	(b) MD4F 41	(b) MD4F 42	(b) MD4F 43	(b) MD4F 52
SiO ₂	68.75	68.31	68.04	68.52	68.03	68.32	68.54	69.13	67.66
Al ₂ O ₃	19.50	19.16	19.33	19.37	19.47	19.68	19.64	19.44	19.43
FeO	0.10	0.00	0.09	0.08	0.14	0.04	0.04	0.06	0.00
CaO	0.57	0.19	0.23	0.40	0.37	0.38	0.41	0.21	0.36
BaO	0.09	0.09	0.07	0.04	0.03	0.10	0.12	0.07	0.09
Na ₂ O	11.25	11.41	11.43	11.48	10.99	11.32	11.11	11.61	11.57
K ₂ O	0.07	0.04	0.05	0.03	0.04	0.03	0.03	0.04	0.08
TOTAL	100.30	99.20	99.25	99.92	99.06	99.86	99.88	100.54	99.20

	Number of ions on the basis of 32 O									
Si	11.980	12.023	11.980	11.984	11.980	11.896	11.977	12.008	11.938	
Al	4.004	3.973	4.012	3.992	4.043	4.114	4.047	3.980	4.043	
Fe	0.016	0.000	0.012	0.012	0.020	0.006	0.008	0.008	0.000	
Ca	0.109	0.035	0.047	0.074	0.070	0.072	0.078	0.039	0.066	
Ba	0.004	0.008	0.004	0.004	0.004	0.007	0.008	0.004	0.008	
Na	3.801	3.895	3.902	3.895	3.754	3.893	3.762	3.910	3.961	
K	0.016	0.008	0.012	0.008	0.008	0.007	0.008	0.008	0.020	

Table II-2b) Continued (Hydrothermal K-feldspar)

Sample Anal. No.	(c)	(c)	(a)	(a)	(a)	(a)	(a)	(b)	(d)	(d)	(e)
	4-GFW 32	4-GFW 34	4-GFW 37	4-GFW 40	4-GFW 41	4-GFW 42	GF-15.8 7	GF-15.8 9	GF-15.8 11	GF-15.8 58	G-GF-17 59
SiO ₂	64.82	64.60	63.56	63.37	63.29	63.03	64.35	64.52	64.13	64.11	63.83
Al ₂ O ₃	19.26	18.98	18.76	18.45	19.09	19.02	18.10	17.91	18.56	18.36	18.00
FeO	0.06	0.04	0.09	0.01	0.01	0.13	0.10	0.00	0.00	0.00	0.06
CaO	0.00	0.05	0.02	0.03	0.02	0.03	0.00	0.02	0.04	0.00	0.00
BaO	2.14	2.77	2.84	2.79	3.13	3.08	0.46	0.35	0.48	0.37	0.23
Na ₂ O	0.18	0.30	0.37	0.32	0.30	0.26	0.22	0.29	0.25	0.25	0.11
K ₂ O	14.71	14.93	14.36	14.99	14.69	14.78	16.32	16.15	16.49	16.13	16.06
TOTAL	101.18	101.67	99.83	100.00	100.52	100.36	99.55	99.23	99.94	99.22	98.29
Number of ions on the basis of 32 O											
Si	11.912	11.898	11.844	11.891	11.827	11.813	12.000	12.043	11.926	11.973	12.016
Al	4.171	4.121	4.199	4.137	4.204	4.203	3.977	3.941	4.066	4.043	3.992
Fe	0.009	0.004	0.012	0.016	0.002	0.020	0.016	0.000	0.000	0.000	0.008
Ca	0.000	0.012	0.004	0.004	0.004	0.008	0.000	0.004	0.008	0.000	0.000
Ba	0.154	0.199	0.191	0.207	0.229	0.227	0.035	0.027	0.035	0.027	0.016
Na	0.064	0.109	0.129	0.133	0.109	0.102	0.082	0.105	0.090	0.090	0.043
K	3.448	3.508	3.477	3.426	3.502	3.531	3.883	3.844	3.914	3.844	3.859

- (a) Replacing hydrothermal albite megacrysts
- (b) Replacing igneous albite phenocrysts
- (c) Adularia (in veins, often with rhombic sections)
- (d) Hydrothermal megacrysts
- (e) In tuff matrix

Table II-2b). Continued (Hydrothermal K-feldspar)

Sample Anal. No.	(d) 6-GF-17 55	(d) 6-GF-17 56	(c) GF-62 46	(a) GF-62 36	(a) GF-62 34	(a) GF-62 40	(a) GF-62 42	(a) GF-62 39	(d) 2-GF-87 4	(d) 2-GF-87 6	(d) 2-GF-87 7	(c) 2-GF-87 47
SiO ₂	64.17	63.86	63.65	64.20	65.30	64.05	65.51	65.37	65.56	65.68	65.18	64.57
Al ₂ O ₃	18.35	18.28	18.21	18.79	17.58	17.90	17.89	18.30	18.13	18.11	18.22	17.62
FeO	0.00	0.00	0.04	0.00	0.00	0.00	0.00	0.00	0.00	0.00	0.00	0.04
CaO	0.03	0.04	0.00	0.02	0.04	0.03	0.02	0.00	0.00	0.00	0.00	0.00
BaO	0.34	0.28	1.13	1.71	1.52	1.22	1.20	1.39	0.24	0.16	0.31	0.21
Na ₂ O	0.16	0.12	0.18	0.25	0.26	0.18	0.45	0.30	0.14	0.13	0.18	0.20
K ₂ O	16.65	16.39	15.89	15.36	15.58	15.46	14.74	15.63	16.88	16.91	16.72	16.93
TOTAL	99.71	98.96	99.11	100.32	100.29	98.84	99.80	100.99	100.95	101.00	100.61	99.57
Number of ions on the basis of 32 O												
Si	11.958	11.969	11.961	11.920	12.113	12.035	12.121	12.029	12.047	12.055	12.020	12.065
Al	4.030	4.035	4.031	4.112	3.844	3.965	3.898	3.969	3.926	3.918	3.961	3.877
Fe	0.000	0.000	0.008	0.000	0.000	0.000	0.000	0.000	0.000	0.000	0.000	0.006
Ca	0.006	0.008	0.000	0.004	0.008	0.008	0.004	0.000	0.000	0.000	0.000	0.000
Ba	0.025	0.020	0.082	0.124	0.109	0.090	0.086	0.100	0.020	0.012	0.023	0.015
Na	0.058	0.043	0.066	0.090	0.94	0.006	0.160	0.107	0.051	0.047	0.063	0.072
K	3.958	3.918	3.809	3.638	3.688	3.707	3.480	3.669	3.957	3.961	3.934	4.032

(a) Replacing hydrothermal albite megacrysts.

(b) Replacing igneous albite phenocrysts.

(c) Adularia (in veins, often with rhombic sections)

(d) Hydrothermal megacrysts

(e) In buff matrix

Table II-3a) Analyses of coexisting Fe-Ti oxides in Green facies rocks.

Anal. no.	(a)	(a)	(a)	(b)	(b)
	6	8	15	13	14
SiO ₂	1.30	1.50	1.05	1.32	1.62
TiO ₂	5.96	4.81	7.24	0.59	0.99
Al ₂ O ₃	0.54	0.52	0.56	0.50	0.96
Cr ₂ O ₃	0.00	0.01	0.04	0.06	0.00
Fe ₂ O ₃	90.48	90.98	89.33	95.11	93.03
MnO	0.00	0.00	0.02	0.00	0.02
MgO	0.07	0.08	0.05	0.10	0.38
CaO	0.00	0.00	0.03	0.53	0.10
TOTAL	98.35	97.90	98.32	98.21	97.10
Number of ions on the basis of 3 O					
Si	0.034	0.039	0.027	0.035	0.043
Ti	0.117	0.095	0.142	0.012	0.020
Al	0.017	0.016	0.017	0.016	0.030
Cr	0.000	-	-	-	-
Fe ³⁺	1.780	1.802	1.755	1.909	1.873
Mu	0.000	0.000	0.000	0.000	0.000
Mg	0.000	0.003	0.002	0.004	0.015
Ca	0.000	0.000	0.001	0.015	0.003

(a) Ti-hematite rimming opaque microphenocrysts and scattered in rock matrix

(b) Hematite in lithic fragments

Table II-3a). Continued (Fe-Ti oxides, Green facies)

Anal. no.	(c) 4	(c) 5	(c) 9	(c) 11	(c) 12	(c) 17	(c) 19	(c) 21	(c) 30	(c) 31
SiO ₂	0.50	0.58	0.53	0.71	0.57	0.63	0.73	0.57	0.76	0.71
TiO ₂	44.84	50.34	58.82	48.25	58.00	52.23	56.80	60.02	51.29	54.27
Al ₂ O ₃	0.17	0.24	0.17	0.21	0.29	0.29	0.41	0.08	0.32	0.24
Cr ₂ O ₃	0.08	0.06	0.02	0.00	0.04	0.04	0.02	0.05	0.24	0.33
Fe ₂ O ₃	53.42	46.26	37.63	50.40	39.50	44.04	39.51	37.62	45.32	41.36
MnO	0.00	0.00	0.00	0.00	0.00	0.00	0.00	0.00	0.15	0.14
MgO	0.02	0.05	0.05	0.08	0.11	0.04	0.06	0.04	0.01	0.00
CaO	0.00	0.00	0.01	0.05	0.00	0.01	0.02	0.00	0.06	0.04
TOTAL	99.03	97.53	97.23	99.70	98.51	97.28	97.55	98.38	98.15	97.09

- (a) Ti-hematite rimming opaque microphenocrysts and scattered in rock matrix.
- (b) Hematite in lithic fragments
- (c) Ultra fine grained leucoxene + hematite ± pseudobrookite microphenocrysts.

Table II-3b). Analyses of coexisting Ti-Fe oxides and sphene
(sample 3-6F).

Anal. no.	one crystal			one crystal	
	(a) 50	(a) 51	(a) 52	Ilm 53	(b) 54
SiO ₂	16.90	10.67	14.76	0.39	2.22
TiO ₂	46.44	49.21	50.54	52.31	93.75
Al ₂ O ₃	4.06	0.60	3.93	0.14	0.29
Cr ₂ O ₃	0.13	0.04	0.10	0.32	0.00
FeO	15.80	27.38	7.43	44.06	0.00
MnO	0.89	2.17	0.54	3.83	0.00
MgO	0.04	0.07	0.03	0.07	0.03
CaO	17.94	10.77	21.81	0.08	0.76
TOTAL	102.24	100.92	99.14	101.20	97.04
Si				0.010	
Ti				0.980	
Al				0.004	
Cr				0.006	
Fe ²⁺				0.918	
Mn				0.081	
Mg				0.003	
Ca				0.002	

(a) Ultra fine grained Ilmenite + sphene composite materials

(b) Leucoxene + sphene

(c) In vein

Ilm, ilmenite; Lcx, leucoxene; Sp, sphene

Number of ions on the basis of 4 Si (sphene) and 3 O (ilmenite)

Table II-3b). Continued (Fe-Ti oxides and sphene)

Anal. no.	— one crystal —			— one crystal —	
	Ilm 57	Lcx 58	Sp 59	Ilm 60	Lcx 61
SiO ₂	4.84	3.40	29.78	6.68	1.07
TiO ₂	51.57	94.04	28.82	51.45	98.10
Al ₂ O ₃	0.29	0.55	6.53	0.15	0.30
Cr ₂ O ₃	0.29	0.17	0.14	0.69	0.00
FeO	39.03	0.00	2.53	35.68	0.02
MnO	4.07	0.00	0.00	3.52	0.00
MgO	0.03	0.15	0.83	0.09	0.04
CaO	0.57	2.41	25.68	0.67	0.51
TOTAL	100.69	100.72	94.32	98.92	100.04
Si	0.116		(4)	0.160	
Ti	0.932		2.911	0.925	
Al	0.008		1.034	0.004	
Cr	0.006		0.015	0.013	
Fe ²⁺	0.784		0.284	0.713	
Mn	0.008		0.000	0.071	
Mg	0.001		0.166	0.003	
Ca	0.015		3.696	0.017	

Table II-3b). Continued (Fe-Ti oxides and sphene)

Anal. no.	one crystal			one crystal	
	Sp 62	Ilm 63	Lcx 64	Lcx 65	Sp(c) 69
SiO ₂	29.12	0.64	0.50	0.70	38.27
TiO ₂	33.60	52.60	99.13	96.74	19.75
Al ₂ O ₃	3.41	0.01	0.20	0.22	8.14
Cr ₂ O ₃	0.00	0.11	0.07	0.31	0.00
FeO	1.97	43.36	0.00	0.00	0.11
MnO	0.00	3.59	0.00	0.00	0.00
MgO	0.07	0.09	0.04	0.04	0.27
CaO	28.27	0.57	0.19	0.13	21.69
TOTAL	96.45	100.97	100.14	98.13	88.23
Si	(4)	0.016			
Ti	3.471	0.984			
Al	0.552	0.000			
Cr	0.000	0.002			
Fe ²⁺	0.226	0.902			
Mn	0.000	0.076			
Mg	0.014	0.003			
Ca	4.161	0.015			

(c) In vein

Table II-3c). Analyses of leucoxene, titanite and sphene in Aljustrel Volcanic rocks.

Sample Anal. no.	Lcx 6-GF-17		Lcx 6-GF-17		Lcx 6-GF-17		Lcx 6-GF-17		Lcx 4-GFW		(a) MDAF		(a) MDAF	
	34	35	36	37	38	39	40	24	26	27	74	75	78	78
SiO ₂	0.09	0.24	0.00	0.30	0.32	0.40	0.64	0.68	0.48	0.68	27.03	6.26	2.68	2.68
TiO ₂	95.16	96.93	98.45	96.68	96.88	96.75	97.72	77.90	89.08	77.90	54.96	91.87	94.97	94.97
Al ₂ O ₃	0.17	0.13	0.13	0.16	0.28	0.14	0.23	0.14	0.15	0.14	2.25	2.43	0.40	0.40
Cr ₂ O ₃	0.21	0.10	0.05	0.05	0.13	0.14	0.00	0.00	0.00	0.00	0.00	0.00	0.00	0.00
FeO	0.11	0.26	0.07	0.06	0.20	0.14	0.00	17.26	7.80	17.26	0.00	0.23	0.00	0.00
MnO	0.03	0.00	0.02	0.04	0.05	0.00	0.00	1.80	0.59	1.80	0.00	0.00	0.00	0.00
MgO	0.05	0.04	0.03	0.09	0.08	0.04	0.05	0.05	0.06	0.05	0.00	0.19	0.05	0.05
CaO	0.08	0.13	0.03	0.31	0.50	0.06	0.23	0.00	0.00	0.00	17.06	0.27	2.89	2.89
TOTAL	95.89	97.83	98.78	97.69	98.44	97.68	98.88	97.83	98.16	97.83	101.30	101.24	101.00	101.00

(a) Ultra fine grained sphene + leucoxene microphenocrysts.

Lcx, leucoxene

Table II-3c). Continued (Leucoxene, ilmenite and sphene)

Sample Anal. no.	Mn-Ilm MDAF 80	Mn-Ilm MDAF 81	Sp MDAF 79	Sp 2-GF-87 26	Sp 2-GF-87 27	Sp 2-GF-87 28	Sp 2-GF-87 29	Sp 2-GF-87 30
SiO ₂	0.68	0.34	29.38	31.26	31.24	31.27	30.94	30.88
TiO ₂	56.01	52.92	37.67	29.06	33.98	29.18	34.44	34.00
Al ₂ O ₃	0.65	0.07	1.69	8.48	4.45	7.77	4.24	4.30
Cr ₂ O ₃	0.00	0.03	0.00	0.01	0.09	0.01	0.04	0.03
FeO	29.59	41.12	1.00	0.34	0.38	0.48	0.40	0.09
MnO	13.46	5.92	0.00	0.01	0.00	0.05	0.02	0.02
MgO	0.10	0.03	0.05	0.05	0.06	0.11	0.03	0.03
CaO	0.62	0.10	28.78	28.93	29.36	27.82	28.36	29.16
Na ₂ O	-	-	-	0.07	0.09	0.09	0.09	0.10
K ₂ O	-	-	-	0.29	0.24	0.68	0.08	0.00
TOTAL	101.11	100.55	98.52	98.50	99.87	97.46	98.64	98.61
Number of ions on the basis of 3 O (Ilm) and 4 Si (sp)								
Si	0.016	0.009	(4)	(4)	(4)	(4)	(4)	(4)
Ti	1.021	0.995	3.857	2.796	3.270	2.807	3.348	3.312
Al	0.019	0.002	0.271	1.279	0.672	1.171	0.646	0.656
Cr	0.000	0.000	0.000	0.001	0.009	0.001	0.004	0.003
Fe ²⁺	0.600	0.860	0.144	0.036	0.041	0.051	0.043	0.010
Mn	0.276	0.125	0.000	0.001	0.000	0.005	0.002	0.002
Mg	0.004	0.001	0.010	0.010	0.011	0.021	0.006	0.006
Ca	0.016	0.003	4.191	3.966	4.028	3.813	3.928	4.047
Na	-	-	-	0.017	0.022	0.022	0.023	0.025
K	-	-	-	0.047	0.039	0.111	0.013	0.000

Ilm, ilmenite; Sp, sphene

Table II-4. Analyses of almandine garnet from QET rocks (this page sample GF-15.8).

Anal. No.	7	8	9	10	11	12	13
SiO ₂	37.29	37.12	37.04	37.62	36.16	36.35	37.05
Al ₂ O ₃	21.02	20.89	20.90	20.85	21.03	20.92	21.35
FeO	36.41	36.35	36.87	36.89	37.00	36.70	36.44
MnO	1.67	1.67	1.66	1.71	1.79	1.76	1.80
MgO	2.27	2.31	2.23	2.21	2.28	2.21	2.40
CaO	1.02	-0.94	0.98	1.00	1.00	1.00	1.02
TOTAL	99.67	99.28	99.67	100.28	99.25	98.94	100.07
Number of ions on the basis of 24 O							
Si	6.044	6.042	6.021	6.069	5.855	5.932	5.975
H ₄ Calc	0.000	0.000	0.000	0.000	0.145	0.068	0.025
Al	4.015	4.009	4.004	3.964	4.013	4.024	4.058
Fe ³⁺	0.000	0.000	0.000	0.000	0.000	0.000	0.000
Fe ²⁺	4.935	4.949	5.012	4.977	5.011	5.008	4.915
Mn	0.229	0.230	0.229	0.234	0.246	0.243	0.246
Mg	0.548	0.560	0.540	0.531	0.550	0.538	0.577
Ca	0.177	0.164	0.171	0.173	0.173	0.175	0.176

Table II-4. Continued (alm. garnet, sample 3-GF).

Anal. no.	14	15	16	17	25	26	27	28	29
SiO ₂	36.65	37.37	36.07	37.01	37.44	36.93	36.73	37.07	37.10
Al ₂ O ₃	20.98	20.63	21.09	21.18	21.73	21.38	21.68	21.48	21.15
FeO	34.92	35.03	35.17	35.01	35.62	35.65	35.90	35.37	35.30
MnO	1.04	1.17	1.02	1.11	1.19	1.08	1.07	1.16	1.24
MgO	3.82	3.74	3.64	3.63	3.77	3.68	3.71	3.56	3.64
CaO	1.09	1.10	1.02	1.06	1.07	1.07	1.10	1.00	
TOTAL	98.51	99.04	98.81	98.99	100.82	99.78	100.17	99.73	99.52
Number of ions on the basis of 240									
Si	5.940	6.050	5.843	5.985	5.914	5.896	5.804	5.929	5.979
H ₄ Calc	0.060	0.000	0.157	0.015	0.086	0.104	0.196	0.071	0.021
Al	4.008	3.936	4.027	4.036	4.046	4.023	4.038	4.049	4.017
Fe ³⁺	0.000	0.000	0.000	0.000	0.000	0.000	0.000	0.000	0.000
Fe ²⁺	4.734	4.743	4.746	4.735	4.795	4.760	4.745	4.732	4.758
Mn	0.143	0.160	0.140	0.152	0.159	0.146	0.143	0.157	0.169
Mg	0.923	0.902	0.879	0.875	0.888	0.876	0.874	0.849	0.874
Ca	0.189	0.191	0.177	0.184	0.179	0.183	0.181	0.189	0.173

Table II-4. Continued (alm. garnet, sample 4-GFW)

Anal. no.	18	20	21	22	23	24	62	61
SiO ₂	36.89	36.88	36.78	36.63	36.92	36.51	37.25	37.16
Al ₂ O ₃	20.77	21.40	20.97	21.81	21.64	21.48	20.14	20.55
Cr ₂ O ₃	-	-	-	-	-	-	0.08	0.05
FeO	35.91	36.90	35.85	36.66	36.45	36.26	36.14	36.98
MnO	1.57	1.71	1.73	1.63	1.73	1.71	1.52	1.65
MgO	2.34	2.33	2.11	2.35	2.47	2.34	2.52	2.54
CaO	1.04	1.03	1.04	1.02	0.98	1.02	1.06	1.07
TOTAL	98.51	100.25	98.48	100.09	100.20	99.31	98.77	100.83
Number of ions on the basis of 24 O								
Si	6.045	5.923	6.032	5.846	5.912	5.894	6.098	6.027
H ₄ Calc	0.000	0.077	0.000	0.154	0.088	0.106	0.000	0.000
Al	4.011	4.051	4.053	4.102	4.084	4.087	3.886	3.929
Cr	-	-	-	-	-	-	0.010	0.006
Fe ³⁺	0.000	0.000	0.000	0.000	0.000	0.000	0.000	0.000
Fe ²⁺	4.921	4.956	4.917	4.893	4.882	4.896	4.948	5.016
Mn	0.218	0.233	0.240	0.220	0.235	0.234	0.211	0.227
Mg	0.572	0.558	0.516	0.559	0.590	0.563	0.615	0.614
Ca	0.183	0.177	0.183	0.174	0.168	0.176	0.186	0.186

Table II-5. Averages of closely similar chlorite analyses from Aljustrel Volcanic rocks.

Unit Sample No. of anal.	QET 1-GF 3	QET 3-GF 5	QET 4-GFM 2	QET GF-A 3	QET GF-15.8 3	QET 6-GF-17 3	QET GF-50 6	QET 2-GF-87 3	QET MIDAF 4	QET(*) PMTV-1 6	MT(*) bis 330.25 6	MT(*) bis-341.8 4
SiO ₂	24.04	24.16	24.58	24.08	23.82	23.06	24.49	23.54	24.36	26.51	27.68	27.93
TiO ₂	0.01	0.02	0.00	0.00	0.06	0.01	0.00	0.02	0.00	0.00	0.00	0.00
Al ₂ O ₃	19.80	19.81	19.04	19.87	19.05	20.75	19.62	19.87	21.26	21.74	19.61	19.07
Cr ₂ O ₃	38.86	36.49	36.33	35.64	40.82	37.22	35.90	40.74	30.69	18.03	20.14	20.17
FeO	0.27	0.60	0.47	0.27	0.27	0.29	0.50	0.38	0.43	0.16	0.40	0.71
MnO	5.54	6.84	7.17	7.87	5.77	5.54	7.92	4.71	10.37	19.12	19.30	19.38
MgO	0.00	0.02	0.01	0.02	0.01	0.06	0.00	0.02	0.02	0.00	0.02	0.00
CaO	0.07	0.04	0.04	0.05	0.05	0.05	0.04	0.04	0.00	0.00	0.00	0.06
Na ₂ O	0.01	0.00	0.03	0.01	0.00	0.00	0.00	0.06	0.00	0.03	0.00	0.00
K ₂ O	0.01	0.00	0.00	0.00	0.01	0.00	0.00	0.00	0.00	0.01	0.01	0.00
TOTAL	88.61	87.98	87.67	87.81	89.81	86.98	87.57	89.38	87.13	85.60	87.16	87.32
Number of ions on the basis of 14.0												
Si	2.712	2.714	2.767	2.695	2.681	2.635	2.752	2.663	2.668	2.745	2.849	2.876
Ti	0.000	0.002	0.000	0.000	0.005	0.001	0.000	0.002	0.000	0.000	0.000	0.000
Al	2.632	2.623	2.527	2.621	2.527	2.794	2.598	2.649	2.745	2.653	2.379	2.314
Cr	3.666	3.428	3.421	3.336	3.842	3.556	3.374	3.855	2.811	1.561	1.734	1.737
Fe ²⁺	0.026	0.057	0.045	0.026	0.026	0.028	0.048	0.036	0.040	0.014	0.035	0.062
Mn	0.931	1.145	1.203	1.313	0.968	0.943	1.176	0.794	1.693	2.951	2.961	2.975
Mg	0.000	0.002	0.001	0.000	0.001	0.007	0.000	0.002	0.002	0.000	0.002	0.000
Ca	0.003	0.002	0.002	0.002	0.002	0.002	0.002	0.002	0.000	0.000	0.000	0.002
Ba	0.000	0.000	0.007	0.002	0.000	0.000	0.000	0.013	0.000	0.006	0.000	0.000
Na	0.001	0.000	0.000	0.000	0.000	0.000	0.000	0.000	0.000	0.001	0.001	0.000
K	0.001	0.000	0.000	0.000	0.000	0.000	0.000	0.000	0.000	0.000	0.000	0.000

(*) Green facies rocks

Table II-6. Analyses of sericites from the Aljustrel Volcanic rocks.

Sample Ana. no.	GFA 6	GFA 8	1-GF 73	1-GF 73	4-GFM 66	4-GFM 67	MDAF 19	MDAF 20	MDAE 21
SiO ₂	51.70	52.52	50.33	50.35	49.44	48.20	50.12	51.54	53.82
TiO ₂	0.00	0.00	-	-	-	-	0.00	0.00	0.00
Al ₂ O ₃	28.09	28.68	28.57	28.69	28.37	27.91	31.20	30.92	30.50
FeO	4.54	4.27	4.29	4.78	4.97	4.75	1.80	1.73	1.61
MnO	0.00	0.00	0.06	0.00	0.00	0.00	0.00	0.00	0.00
MgO	2.18	2.25	1.64	1.61	1.82	1.72	1.54	1.63	1.86
CaO	0.00	0.00	0.00	0.00	0.00	0.00	0.20	0.01	0.00
BaO	0.00	0.00	0.12	0.13	0.35	0.31	0.09	0.07	0.05
Na ₂ O	0.00	0.05	0.00	0.00	0.05	0.02	0.09	0.16	0.07
K ₂ O	10.80	10.68	10.09	10.45	10.29	10.67	9.73	9.58	10.74
TOTAL	97.32	98.45	95.13	96.02	95.30	93.59	94.77	95.64	98.65
Number of ions on the basis of 22 O									
Si	6.811	6.816	6.763	6.732	6.685	6.660	6.653	6.752	6.859
Ti	0.000	0.000	-	-	-	-	0.000	0.000	0.000
Al	4.361	4.387	4.524	4.521	4.521	4.545	4.881	4.774	4.581
Fe	0.500	0.463	0.482	0.535	0.562	0.549	0.200	0.190	0.172
Mn	0.000	0.000	0.007	0.000	0.000	0.000	0.000	0.000	0.000
Mg	0.428	0.435	0.328	0.321	0.367	0.354	0.305	0.318	0.353
Ca	0.000	0.000	0.000	0.000	0.000	0.000	0.028	0.001	0.000
Ba	0.000	0.000	0.006	0.007	0.019	0.017	0.005	0.004	0.002
Na	0.000	0.013	0.000	0.000	0.013	0.005	0.023	0.041	0.017
K	1.815	1.768	1.729	1.782	1.775	1.881	1.648	1.601	1.746

Table II-6. Continued (Sericitites)

Sample Anal. no.	6-GF-17-22	6-GF-17-23	6-GF-17-24	6-GF-17-25	6-GF-17-26	2-GF-87-39	2-GF-87-40	2-GF-87-41	2-GF-87-44	2-GF-87-45
SiO ₂	50.43	48.73	51.19	51.67	47.43	49.26	49.23	52.23	50.71	51.77
TiO ₂	0.00	0.00	0.00	0.00	0.00	0.00	0.00	0.01	0.00	0.00
Al ₂ O ₃	27.04	24.47	31.55	28.69	29.73	33.54	34.00	26.92	28.33	29.27
FeO	5.70	4.71	3.66	5.13	3.99	1.37	1.15	5.96	5.37	5.57
MnO	0.00	0.00	0.00	0.00	0.00	0.00	0.00	0.02	0.04	0.00
MgO	3.79	2.75	1.14	1.43	1.00	0.69	0.75	1.45	1.45	1.50
CaO	0.04	0.23	0.00	0.00	0.00	0.00	0.00	0.00	0.00	0.00
BaO	0.00	0.00	0.00	0.00	0.00	0.00	0.00	0.00	0.00	0.00
Na ₂ O	0.04	0.00	0.02	0.04	0.04	0.12	0.04	0.10	0.10	0.29
K ₂ O	8.44	9.50	9.60	9.40	10.02	11.37	10.37	10.74	10.96	10.03
TOTAL	95.49	90.42	97.16	96.35	92.21	96.35	95.59	97.44	96.95	98.43
Number of ions on the basis of 22 O										
Si	6.743	6.914	6.661	6.827	6.576	6.475	6.470	6.915	6.750	6.745
Ti	0.000	0.000	0.000	0.000	0.000	0.000	0.000	0.001	0.000	0.000
Al	4.261	4.092	4.839	4.467	4.858	5.196	5.274	4.200	4.444	4.495
Fe	0.637	0.559	0.398	0.567	0.463	0.151	0.126	0.660	0.598	0.607
Mn	0.000	0.000	0.000	0.000	0.000	0.000	0.000	0.002	0.005	0.000
Mg	0.755	0.582	0.221	0.282	0.207	0.135	0.147	0.286	0.288	0.291
Ca	0.006	0.035	0.000	0.000	0.000	0.000	0.000	0.000	0.000	0.000
Ba	0.000	0.000	0.000	0.000	0.000	0.000	0.000	0.000	0.000	0.000
Na	0.010	0.000	0.005	0.010	0.011	0.031	0.010	0.026	0.026	0.073
K	1.439	1.718	1.594	1.584	1.772	1.907	1.739	1.814	1.861	1.667

Table II-6. Continued (Sericitites)

Sample Anal. no.	3-GF 8	3-GF 9	PMTV-1 32	PMTV-1 33	bis-315.15 37	bis-315.15 38	bis-315.15 39	bis-315.15 40	bis-315.15 41	
SiO ₂	51.84	51.95	46.52	50.80	47.01	48.05	47.93	47.73	47.79	
TiO ₂	0.00	0.00	0.00	0.00						
Al ₂ O ₃	28.99	28.49	33.82	31.64	29.97	30.58	30.76	30.89	30.82	
FeO	4.23	3.82	2.57	1.96	1.28	1.10	1.24	1.38	1.02	
MnO	0.02	0.00	0.00	0.00	0.00	0.04	0.00	0.02	0.02	
MgO	2.05	1.98	1.56	1.46	2.04	2.24	2.15	2.01	2.25	
CaO	0.00	0.00	0.00	0.00	0.41	0.00	0.00	0.00	0.00	
BaO	0.09	0.01	0.00	0.00	0.22	0.30	0.37	0.30	0.21	
Na ₂ O	0.00	0.00	0.65	0.61	0.24	0.26	0.29	0.24	0.28	
K ₂ O	10.16	10.20	7.50	8.89	10.93	11.19	10.99	11.11	11.25	
TOTAL	97.37	96.45	92.63	95.36	92.14	93.84	93.81	93.76	93.71	
	Number of ions on the basis of 22-O									
Si	6.786	6.847	6.290	6.668	6.509	6.523	6.507	6.491	6.494	
Ti	0.000	0.000	0.000	0.000						
Al	4.473	4.425	5.389	4.895	4.890	4.892	4.922	4.951	4.936	
Fe	0.463	0.421	0.291	0.215	0.148	0.125	0.141	0.157	0.116	
Mn	0.002	0.000	0.000	0.000	0.000	0.005	0.000	0.002	0.002	
Mg	0.400	0.389	0.314	0.286	0.421	0.453	0.435	0.407	0.456	
Ca	0.000	0.000	0.000	0.000	0.061	0.000	0.000	0.000	0.000	
Ba	0.005	0.001	0.000	0.000	0.012	0.016	0.020	0.016	0.011	
Na	0.000	0.000	0.170	0.155	0.064	0.068	0.076	0.063	0.074	
K	1.697	1.715	1.294	1.488	1.930	1.938	1.903	1.927	1.950	

Table II-7. Analyses of epidotes from the Aljustrel Volcanic rocks.

Sample Anal. no.	PMTV-1 29	PMTV-1 34	bis-341.8 41	bis-341.8 42	bis-341.8 43	3-GF 7	GF-50 55	GF-50 56
SiO ₂	37.55	37.66	38.10	38.61	38.95	33.55	34.60	34.41
TiO ₂	0.12	0.16	0.05	0.00	0.07	0.14	0.07	0.07
Al ₂ O ₃	24.50	25.23	23.08	22.83	23.20	21.78	22.26	22.68
Fe ₂ O ₃	10.38	9.60	12.61	12.09	11.84	9.66	9.81	9.37
MnO	0.16	0.14	0.20	0.37	0.48	0.41	0.24	0.23
MgO	0.02	0.01	0.01	0.00	0.01	0.07	0.11	0.06
CaO	23.30	23.76	24.72	23.66	24.80	18.09	18.16	19.07
BaO	0.02	0.04	0.14	0.15	0.10	0.13	0.14	0.08
Na ₂ O	0.02	0.00	0.00	0.00	0.00	0.04	0.09	0.12
K ₂ O	0.00	0.00	0.00	0.00	0.04	0.00	0.00	0.00
TOTAL	96.05	96.00	98.91	97.71	99.49	83.83	85.48	86.09
Number of ions on the basis of 12.5 O								
Si	3.016	3.015	3.010	3.072	3.050	3.066	3.093	3.059
Ti	0.007	0.010	0.003	0.000	0.004	0.010	0.005	0.005
Al	2.319	2.381	2.149	2.141	2.141	2.346	2.345	2.377
Fe ³⁺	0.627	0.578	0.750	0.724	0.698	0.664	0.660	0.627
Mn	0.011	0.009	0.013	0.025	0.032	0.032	0.018	0.017
Mg	0.002	0.001	0.001	0.000	0.001	0.010	0.015	0.008
Ca	2.005	1.987	2.093	2.017	2.081	1.771	1.739	1.817
Ba	0.001	0.001	0.004	0.005	0.003	0.005	0.005	0.003
Na	0.003	0.000	0.000	0.000	0.000	0.007	0.016	0.021
K	0.000	0.000	0.000	0.000	0.004	0.000	0.000	0.000
Whole rock Fe ²⁺ /ΣFe	0.44		0.52			0.69		0.76

Table II-7. Continued (Epidotes)

Sample Anal. no.	GF-50 57	GF-50 58	MD4F 22	(a) bis-315.15 34	(a) bis-315.15 35	(a) bis-315.15 36	bis-315.15 42	bis-315.15 43
SiO ₂	36.07	37.63	36.43	38.18	37.90	37.91	39.82	36.87
TiO ₂	0.04	0.15	0.01	0.05	0.08	0.05	0.07	0.09
Al ₂ O ₃	24.35	25.12	25.45	28.20	27.26	27.66	26.89	24.57
Fe ₂ O ₃	8.73	8.67	10.39	6.19	6.43	6.88	7.50	9.17
MnO	0.25	0.12	0.14	0.50	0.19	0.11	0.20	0.17
MgO	0.08	0.07	1.06	0.07	0.02	0.06	0.25	0.09
CaO	20.18	22.73	21.28	23.34	24.01	23.62	21.30	21.42
BaO	0.09	0.03	0.00	0.14	0.10	0.10	0.22	0.25
Na ₂ O	0.01	0.00	0.01	0.02	0.04	0.02	0.30	0.07
K ₂ O	0.00	0.00	0.00	0.00	0.00	0.00	0.75	0.00
TOTAL	89.80	94.52	94.77	96.69	96.03	96.41	97.30	92.70
Number of ions on the basis of 12.5 O								
Si	3.062	3.046	2.952	3.001	3.007	2.994	3.109	3.048
Ti	0.003	0.009	0.001	0.003	0.005	0.003	0.004	0.006
Al	2.436	2.397	2.431	2.612	2.549	2.575	2.474	2.394
Fe ³⁺	0.558	0.528	0.634	0.366	0.384	0.409	0.441	0.570
Mn	0.018	0.008	0.010	0.033	0.013	0.007	0.013	0.012
Mg	0.010	0.008	0.128	0.008	0.002	0.007	0.029	0.011
Ca	1.836	1.971	1.848	1.965	2.041	1.999	1.782	1.897
Ba	0.003	0.001	0.000	0.004	0.003	0.003	0.007	0.008
Na	0.002	0.000	0.002	0.003	0.006	0.003	0.045	0.011
K	0.000	0.000	0.000	0.000	0.000	0.000	0.076	0.000
Whole rock Fe ²⁺ /ΣFe	0.76		0.77	0.97				

Table II-8. Analyses of carbonates from the Aljustrel Volcanic rocks.

Sample Anal. no.	(a) GF-15.8 3	(b) 6-GF-17 27	(b) GF-50 54	(b) MD4F 14	(b) bis-303.3 38	(b) bis-303.3 37	(a) bis-303.3 41	(a) bis-303.3 34
MgO	0.43	0.00	0.05	0.00	0.11	0.36	0.96	1.32
CaO	51.41	56.21	56.02	55.97	55.40	54.77	53.17	52.30
FeO	3.83	0.00	0.00	0.05	0.15	0.25	1.40	2.02
MnO	0.53	0.00	0.13	0.16	0.25	0.27	0.23	0.23
BaO	-	-	-	-	0.00	0.03	0.00	0.00
TOTAL	56.20	56.21	56.20	56.18	55.91	55.68	55.76	55.88
MgCO ₃	0.90	0.00	0.10	0.00	0.23	0.75	2.01	2.77
CaCO ₃	91.77	100.33	100.00	99.91	98.89	97.76	94.91	93.36
FeCO ₃	6.18	0.00	0.00	0.08	0.24	0.40	2.26	3.26
MnCO ₃	0.86	0.00	0.21	0.26	0.41	0.44	0.37	0.39
BaCO ₃	-	-	-	-	0.00	0.04	0.00	0.00
Σ	99.70	100.33	100.31	100.25	99.77	99.40	99.55	99.77
Number of ions on the basis of 2 cations								
Mg	0.022	0.000	0.002	0.000	0.005	0.018	0.048	0.066
Ca	1.855	2.000	1.994	1.994	1.983	1.967	1.906	1.871
Fe	0.108	0.000	0.000	0.001	0.004	0.007	0.039	0.056
Mn	0.015	0.000	0.004	0.005	0.007	0.008	0.007	0.007
Ba	-	-	-	-	0.000	0.000	0.000	0.000

(a) Ferroan calcites

(b) Calcites

APPENDIX III

WHOLE ROCK GEOCHEMICAL DATA
ON THE ALJUSTREL VOLCANICS

III-1. Quartz eye Tuff

III-2. Miné Tuff

Table III-1. Major and selected trace element abundances in Quartz-eye Tuff Formation rocks.

	(a) 7-GF-19	1-GF	ND4F-A	(a) GF-A	6-GF-17	GF-53B	GF-53	ND4F-B	(a) GF-50M	GF-50C
SiO ₂	64.68	70.91	68.20	69.10	72.94	72.35	72.00	69.07	70.64	70.70
TiO ₂	0.62	0.51	0.53	0.50	0.45	0.44	0.44	0.55	0.50	0.42
Al ₂ O ₃	17.70	14.37	15.70	15.06	13.75	14.12	14.26	14.84	15.07	15.30
Fe ₂ O ₃	0.90	0.74	0.80	0.84	0.47	0.75	0.80	1.04	0.81	0.75
FeO	3.68	2.84	3.95	2.67	1.47	2.35	2.36	3.09	2.25	1.95
MnO	0.03	0.02	0.05	0.03	0.02	0.04	0.04	0.05	0.04	0.04
MgO	1.01	0.71	1.30	1.07	0.37	0.62	0.69	1.42	0.64	0.63
CaO	0.80	0.88	1.83	1.16	0.70	0.85	0.83	1.75	1.13	1.05
NaO	0.05	0.07	0.04	0.07	0.09	0.15	0.13	0.04	0.09	0.10
Na ₂ O	3.21	3.47	4.45	2.00	2.19	3.09	3.19	3.46	4.22	4.57
K ₂ O	5.08	3.88	1.47	4.95	6.79	3.01	2.81	1.68	2.30	2.23
P ₂ O ₅	0.30	0.28	0.25	0.33	0.24	0.19	0.18	0.25	0.21	0.18
LOI	1.73	1.42	1.87	1.69	1.03	1.37	1.52	1.94	1.40	1.25
TOTAL	99.79	100.10	99.44	99.47	100.11	99.33	99.24	99.23	99.30	99.17
SS	ND	ND	0.01	ND	ND	0.28	0.24	0.01	0.01	0.01
Nb	190	146	91	163	156	137	135	104	128	118
Sr	91	92	216	89	75	113	108	181	114	115
Ba	464	608	328	586	789	1384	1196	367	785	853
Sc	-	-	15.0	-	-	10.0	11.0	14.0	11.0	11.0
Y	46	50	61	52	-	39	40	58	44	40
Zr	287	256	286	222	215	211	218	289	239	207
Hf	-	-	7	-	-	6	6	8	7	6
Hb	-	-	27	-	-	18	19	27	25	26
Ta	-	-	11	-	-	3	5	8	12	12
Cr	17	12	11	18	11	7	17	17	15	15
Co	20	24	36	24	3	26	29	30	36	33
Ni	ND	6	13	ND	ND	23	21	12	27	27
Cu	ND	ND	ND	ND	ND	ND	ND	15	ND	ND
Zn	45	29	55	47	28	45	45	64	55	42
Pb	ND	ND	41	ND	ND	32	29	33	27	39
Th	-	-	15.0	-	-	13.0	13.0	14.0	15.0	14.0
La	-	-	-	-	-	30.9	-	-	-	-
Ce	-	-	-	-	-	63.7	-	-	-	-
Mn	-	-	-	-	-	34.7	-	-	-	-
Sm	-	-	-	-	-	8.0	-	-	-	-
Eu	-	-	-	-	-	2.1	-	-	-	-
Gd	-	-	-	-	-	7.6	-	-	-	-
Dy	-	-	-	-	-	7.1	-	-	-	-
Er	-	-	-	-	-	4.2	-	-	-	-
Yb	-	-	-	-	-	3.9	-	-	-	-
Fe ²⁺ /ΣFe	0.62	0.81	0.84	0.78	0.78	0.78	0.77	0.77	0.76	0.74

* Total Iron
(a) Alkali feldspar megacrysts absent
(b) Gneiss facies
(c) After Schumaker (1976)

Table III-1: Continued (Quartz eye Tuffs)

	2-GF-87	4-GF-88	6F-68	3-GF	GF-84	GF-84B	(a) GF-23	(a) GF-43	(a,b) PMTV-2H	(b) PMTV-2C
SiO ₂	71.57	67.46	69.94	70.00	73.08	72.27	72.27	71.63	60.01	65.34
TiO ₂	0.46	0.50	0.56	0.50	0.44	0.46	0.48	0.47	0.73	0.55
Al ₂ O ₃	14.70	17.17	15.47	15.50	13.78	14.09	13.62	12.76	20.61	18.10
Fe ₂ O ₃	0.61	1.15	1.14	1.11	1.17	3.59*	1.26	1.21	3.02	2.52
FeO	1.54	2.65	2.52	2.26	2.18		2.17	1.63	2.70	2.09
MnO	0.02	0.04	0.04	0.04	0.05	0.05	0.05	0.04	0.04	0.03
MgO	0.41	0.86	1.20	0.86	0.63	0.62	0.75	0.58	3.37	2.68
CaO	1.11	1.27	0.45	1.06	0.67	0.74	1.53	2.35	1.02	1.08
BaO	0.07	0.12	0.04	0.14	0.05	0.06	0.03	0.06	0.04	0.03
Na ₂ O	2.18	3.88	3.03	2.40	3.97	3.56	4.01	4.48	2.24	2.93
K ₂ O	5.62	3.03	2.79	3.95	1.91	2.10	1.48	1.56	2.61	1.82
P ₂ O ₅	0.24	0.26	0.18	0.24	0.17	0.18	0.24	1.25	0.11	0.12
LOI	1.24	1.70	1.96	1.64	1.49	1.39	1.38	1.27	4.21	3.17
TOTAL	98.77	100.09	99.32	99.70	99.56	99.11	99.27	99.25	100.91	100.46
Sr	ND	0.08	ND	0.03	0.01	ND	ND	0.03	ND	ND
Rb	209	157	192	191	120	127	94	83	110	83
Sr	101	104	52	63	95	98	225	132	217	194
Ba	595	1064	385	1282	478	523	305	549	342	261
Sc	-	-	11.0	-	9.3	9.9	12.0	9.4	-	-
Y	30	44	43	-	36	41	51	58	61	49
Zr	212	237	244	227	201	211	253	207	304	251
Hf	-	-	7	-	5	6	8	5	-	-
Nb	-	-	22	-	21	20	24	18	-	-
Ta	-	-	5	-	7	5	7	6	-	-
Cr	32	6	16	-	12	12	12	20	22	26
Co	36	20	19	28	23	17	25	15	36	39
Ni	ND	ND	21	ND	21	22	25	11	12	8
Cu	ND	ND	ND	ND	ND	ND	ND	ND	ND	ND
Zn	46	48	46	49	38	41	24	35	161	116
Pb	17	16	16	17	35	30	20	23	28	18
Th	-	-	14.0	-	12.0	13.0	14.0	12.0	-	-
U	-	-	-	-	-	26.7	-	-	-	-
Ca	-	-	-	-	-	60.3	-	-	-	-
Mg	-	-	-	-	-	32.7	-	-	-	-
W	-	-	-	-	-	7.6	-	-	-	-
Er	-	-	-	-	-	1.77	-	-	-	-
Sm	-	-	-	-	-	7.4	-	-	-	-
Pr	-	-	-	-	-	7.3	-	-	-	-
Yb	-	-	-	-	-	6.4	-	-	-	-
Fe ²⁺ /ΣFe	0.74	0.72	0.71	0.68	0.67		0.66	0.60	0.50	0.48

TABLE III-1. Continued (Quartz eye tuffs)

	(a,b) PMTV-1M	(b) PMTV-1C	(b,c) RES-7
SiO ₂	67.04	69.12	66.6
TiO ₂	0.57	0.46	0.50
Al ₂ O ₃	17.35	16.73	15.4
Fe ₂ O ₃	2.50	2.00	7.56*
FeO	1.76	1.31	-
MnO	0.03	0.03	-
MgO	2.39	1.88	4.62
CaO	1.15	1.16	2.03
BaO	0.03	0.03	-
Rb ₂ O	2.48	3.41	1.23
K ₂ O	2.04	1.72	2.40
P ₂ O ₅	0.12	0.12	0.07
LOI	3.38	2.88	-
TOTAL	100.84	100.84	-
SE	ND	ND	-
Rb	93	77	-
Sr	205	198	-
Ba	303	257	-
Sc	-	-	-
Y	49	39	-
Zr	258	211	-
Hf	-	-	-
Nb	-	-	-
Ta	-	-	-
Cr	31	6	-
Co	29	36	-
Ni	13	10	-
Cu	ND	ND	-
Zn	96	66	-
Pb	19	21	-
Th	-	-	-
La	85.1	81.2	-
Ce	118.6	210.9	-
Nd	102.1	98.1	-
Sm	26.2	25.5	-
Eu	24.2	23.5	-
Gd	24.2	23.5	-
Dy	20.1	20.1	-
Er	9.2	8.3	-
Yb	7.1	6.5	-
Fe ²⁺ /ΣFe	0.44	0.42	-

Table III-2. Major selected trace element abundances in Mine Tuff formation rocks.

	bis- 283.5	bis- 289	bis- 291.15	bis- 296.5	bis- 303.3	bis- 309.6	bis- 310.8	bis- 330.25	bis- 341.2	bis- 341.8
SiO ₂	69.11	75.16	72.15	78.26	69.29	74.64	65.68	76.45	74.86	66.68
TiO ₂	0.91	0.13	0.16	0.11	0.19	0.12	0.06	0.10	0.15	0.21
Al ₂ O ₃	15.92	12.52	14.95	11.35	17.20	11.72	15.09	12.27	13.15	17.46
Fe ₂ O ₃	0.21	ND	2.18*	0.07	2.53*	1.79*	0.63	0.08	0.67	1.35
FeO	2.02	1.51		1.53			1.01	1.40	1.13	1.37
MnO	0.04	0.02	0.03	0.03	0.02	0.03	0.04	0.03	0.03	0.04
MgO	2.23	0.56	1.50	0.71	2.03	1.48	2.12	1.06	1.02	1.80
CaO	0.80	0.88	0.45	0.27	ND	2.79	1.40	0.29	0.17	0.34
BaO	0.10	0.00	0.09	0.01	0.13	0.01	0.06	0.01	0.04	0.11
Na ₂ O	1.95	6.55	1.79	5.67	1.93	4.80	3.19	5.57	3.65	1.29
K ₂ O	2.90	0.19	3.56	0.30	3.71	0.25	2.11	0.91	2.48	6.63
P ₂ O ₅	ND	ND	ND	ND	ND	ND	ND	ND	ND	ND
LOI	3.56	1.08	2.32	0.81	2.86	1.45	2.77	1.02	1.56	2.36
TOTAL	99.03	98.61	99.18	99.12	99.89	99.08	99.52	99.19	98.88	98.63
ΣΣ	0.41	0.31	0.12	0.21	0.50	0.15	0.25	0.16	0.23	0.21
Rb	198	22	301	31	285	32	163	63	156	366
Sr	74	187	90	142	67	194	160	124	82	83
Ba	884	77	807	104	1124	105	509	129	323	981
Sc	15.0	11.0	12.0	8.8	11.0	10.0	13.0		13.0	
Y	81	63	73	49	64	66	93	54	79	103
Zr	257	178	211	152	252	173	217	148	217	282
Hf	10	7	8	5	9	6	8		8	
Nb	24	25	21	25	24	23	23	23	20	21
Ta	6	7	5	12	5	7	4		5	
Cr	13	9	12	5	3	7	8	8	6	9
Co	38	55	26	58	24	35	19	63	30	38
Ni	12	6	23	7	14	5	15	16	10	20
Cu	ND	ND	ND	ND	ND	ND	ND	32	19	31
Zn	71	33	42	37	54	38	48	43	42	73
Pb	ND	ND	21	ND	44	21	23	37	ND	43
Th	17.0	13.0	15.0	11.0	18.0	12.0	16.0		15.0	
La	79.5	42.7		37.1			108.2		20.0	
Ce	153.1	85.9		76.6			200.5		43.9	
Nd	70.6	42.0		36.2			95.6		24.3	
Sm	14.7	9.8		8.0			21.4		6.4	
Eu	2.0	1.53		1.1			3.2		1.1	
Gd	13.7	10.3		8.0			22.4		7.5	
Dy	14.4	11.8		9.4			22.1		10.5	
Er	9.3	8.5		7.0			12.5		8.1	
Yb	8.3	8.9		8.0			9.4		8.7	
Fe ²⁺ /ΣFe	0.92	1.00		0.96			0.64	0.99	0.65	0.53

* Total Fe expressed as Fe₂O₃.

Table III-2. Continued (Mine tufts)

	6-145.2	7-249.85	8-533.8	21-607.2	21-621.3	21-642	21-648.4	GF-89.50	GF-90	GF-93
SiO ₂	61.91	70.96	55.03	72.06	72.92	63.73	70.92	69.06	59.04	73.02
TiO ₂	0.25	0.18	0.27	0.27	0.22	0.21	0.18	0.18	0.24	0.19
Al ₂ O ₃	20.10	15.20	23.24	14.21	13.42	19.19	16.05	16.06	19.51	14.66
Fe ₂ O ₃	2.36*	0.32	3.01	1.37	2.52	1.14	0.69	1.81	2.89	1.03
FeO		2.15	1.94	0.99	0.25	1.64	1.28	0.51	0.25	0.70
MnO	0.06	0.03	0.04	0.03	0.02	0.02	0.01	0.17	0.17	0.05
MgO	5.49	3.25	4.18	2.34	3.26	4.35	3.01	5.07	5.69	2.36
CaO	1.43	ND	ND	1.60	0.16	0.94	0.25	0.70	3.90	2.11
BaO	0.04	0.06	0.04	0.04	0.04	0.03	0.02	0.27	0.38	0.04
Na ₂ O	2.45	1.00	ND	1.18	1.22	3.45	2.66	2.18	2.45	3.15
K ₂ O	1.13	2.58	6.80	2.31	2.15	1.88	2.01	0.85	1.22	0.80
P ₂ O ₅	0.01	ND	0.02	ND	ND	ND	ND	ND	ND	0.01
LOI	4.66	3.95	5.40	2.42	2.50	3.54	3.96	3.97	5.55	2.38
TOTAL	99.91	99.67	99.97	98.82	98.68	99.96	100.04	100.83	101.27	100.49
SX	ND	1.36	ND	ND	ND	ND	ND	ND	0.01	ND
Rb	91	166	354	171	165	133	128	81	110	85
Sr	385	90	22	132	50	151	110	207	250	460
Ba	356	504	372	329	347	300	199	2487	3391	357
Sc	10.0	12.0	19.0		5.5		13.0	7.7	9.3	7.0
Y	77	72	119		43	114	98	50	106	61
Zr	211	248	341	262	225	281	238	164	209	164
Hf	9	9	12		7		8	6	7	6
Nb	22	22	24	15	16	22	24	17	14	17
Ta	4	3	3		6		5	2	2	4
Cr	8	8	1	1	2	8	3	3	ND	13
Co	16	9	14	21	25	15	17	11	6	25
Ni	23	11	23	11	9	10	15	13	24	5
Cu	ND	ND	ND	ND	ND	ND	ND	ND	ND	ND
Zn	69	38	176	31	47	81	35	59	64	36
Pb	28	18	32	21	10	25	18	15	31	25
Th	20.0	14.0	23.0		10.0		16.0	15.0	19.0	14.0
La			33.9		16.4			45.4		
Ce			72.8		33.9			97.0		
Nd			41.9		18.7			51.4		
Sm			10.8		4.6			12.2		
Eu			1.73		0.86			1.71		
Gd			12.7		5.7			12.9		
Dy			17.4		7.4			16.3		
Er			12.5		5.6			10.9		
Yb			13.1		5.6			9.8		
Fe ²⁺ /ΣFe		0.88	0.42	0.44	0.10	0.62	0.67	0.24	0.09	0.43

Table III-2. Continued (Mine tuffs)

	GF-100	GF-113	SM-11	SM-12
SiO ₂	72.13	75.66	66	72.09
TiO ₂	0.19	0.15	0.32	0.23
Al ₂ O ₃	15.01	13.13	18.25	15.12
Fe ₂ O ₃	1.34	1.04	0.98	2.21*
FeO	0.84	0.72	2.27	
MnO	0.04	0.03	0.06	0.02
MgO	1.97	1.65	5.81	1.03
CaO	0.86	1.00	0.62	ND
BaO	0.05	0.06	0.04	0.03
Na ₂ O	1.60	2.08	2.54	4.09
K ₂ O	3.40	2.14	0.74	2.22
P ₂ O ₅	ND	ND	ND	ND
LOI	2.39	1.86	4.86	2.23
TOTAL	99.71	99.51	100.15	99.27
Si	0.10	ND	ND	ND
Rb	241	145	68	153
Sr	130	156	373	88
Ba	460	551	365	308
Sc	11.0	10.0	10.0	
Y	89	77	83	
Zr	253	212	240	232
Hf	7	7	9	
Nb	21	22	22	18
Ta	4	7	3	
Cr	4	8	4	6
Co	9	5	20	15
Ni	17	11	15	7
Cu	ND	15	ND	ND
Zn	48	65	86	56
Pb	17	17	17	18
Th	13.0	12.0	22.0	
La		32.4	54.8	
Ce		71.5	103.3	
Nd		39.9	52.7	
Sm		9.7	1.76	
Eu		1.44	1.76	
Gd		10.8	12.0	
Dy		14.0	13.8	
Er		10.1	7.8	
Yb		6.8	6.5	
Fe ²⁺ /ΣFe	0.64	0.43	0.22	

APPENDIX IV

REPRESENTATIVE MICROPROBE ANALYSES OF MINERALS
FROM THE FEITAIS-ESTACAO ORE ENVIRONMENT

- IV-1. Chlorites
- IV-2. Sericite and Ba-sericite
- IV-3. Spessartine garnet
- IV-4. Carbonates
- IV-5. Sphalerites

Table IV - 1a) Averages of closely similar chlorite analyses from footwall stockwork rocks and from massive sulphide ores.

Sample no. of anal.	(a)		(a)		(a)		(b)		(b)		(b)	
	bis-234.3 5	bis-240.6 7	bis-249.1 3	8-511.3 18	15.330.2 9	bis-246 5	8-460.2 8	8-466 3	8-479 6	8-502.8 16	21-716.3 6	(b)
SiO ₂	27.28	23.13	23.00	23.27	23.87	23.01	23.77	26.25	26.03	24.19	26.27	
TiO ₂	0.01	0.05	0.05	0.06	0.04	0.05	0.05	0.00	0.00	0.03	0.02	
Al ₂ O ₃	21.29	21.98	21.73	23.41	19.41	21.22	22.68	21.53	21.55	23.23	20.53	
Cr ₂ O ₃		0.07										
FeO	19.17	37.62	38.63	37.31	39.44	38.56	34.22	28.65	28.50	38.30	27.71	
MnO	0.55	0.47	0.42	0.45	0.36	0.45	0.32	0.08	0.27	0.33	0.10	
MgO	19.32	5.53	5.27	4.75	6.13	4.84	6.63	11.69	11.32	9.51	13.52	
CaO	0.00	0.03	0.00	0.01	0.07	0.00	0.01	0.01	0.02	0.02	0.00	
BaO												
Na ₂ O	0.00	0.00	0.08	0.00	0.00	0.00	0.00	0.05	0.01	0.05	0.00	
K ₂ O	0.00	0.03	0.05	0.02	0.00	0.01	0.02	0.03	0.01	0.11	0.00	
Total	87.61	86.91	89.23	89.28	89.32	88.14	87.69	88.30	87.71	87.78	88.14	

Sample no. of anal.	(a)		(a)		(a)		(b)		(b)		(b)	
	bis-234.3 5	bis-240.6 7	bis-249.1 3	8-511.3 18	15.330.2 9	bis-246 5	8-460.2 8	8-466 3	8-479 6	8-502.8 16	21-716.3 6	(b)
Si	2.778	2.583	2.574	2.571	2.682	2.609	2.630	2.782	2.779	2.616	2.780	
Ti	0.001	0.004	0.004	0.005	0.003	0.004	0.004	0.000	0.000	0.003	0.001	
Al	2.554	2.893	2.866	3.048	2.569	2.836	2.958	2.699	2.710	2.961	2.561	
Cr		0.007										
Fe ²⁺	1.632	3.514	3.615	3.448	3.705	3.657	3.167	2.539	2.545	2.741	2.453	
Mn	0.048	0.044	0.040	0.042	0.034	0.043	0.030	0.007	0.025	0.030	0.009	
Mg	2.932	0.921	0.879	0.782	1.026	0.818	1.093	1.846	1.801	1.532	2.133	
Ca	0.000	0.004	0.000	0.001	0.008	0.000	0.001	0.002	0.001	0.003	0.000	
Ba												
Na	0.000	0.000	0.017	0.000	0.001	0.000	0.000	0.011	0.002	0.010	0.000	
K	0.000	0.004	0.007	0.003	0.000	0.001	0.002	0.004	0.002	0.016	0.000	

Number of idhs on the basis of 14.0

(a) Outer stockwork rocks, dominantly sericitic
 (b) Stockwork rocks (Chlorite + quartz + sulphides)

Table IV - 1a) Continued (Ore zone chlorites)

Sample No. of Anal.	(b) 21-722.8 7	(b) 21-735.9 6	(b) 21-738 5	(b) 21-761.2 5	(b) 21-800.5 5	(c) 10.350 9	(d) bis-168.5 7	(e) bis-187.2 2	(e) 7-225.6 4	(e) 8.446 3
	SiO ₂	24.73	23.51	23.44	23.84	29.28	23.14	25.21	25.46	25.46
TiO ₂	0.00	0.03	0.02	0.01	0.00	0.07	0.02	0.04	0.04	0.03
Al ₂ O ₃	21.12	22.29	21.38	21.59	21.43	20.30	19.63	22.09	21.93	21.56
Cr ₂ O ₃	31.77	35.55	35.02	33.44	7.78	0.10			0.05	
FeO _x	0.26	0.74	0.61	0.27	0.30	0.32	0.86	0.79	0.89	0.71
MgO	9.33	6.65	7.33	9.04	27.54	4.35	10.16	10.33	12.82	4.14
CaO	0.00	0.01	0.01	0.00	0.00	0.04	0.00	0.00	0.02	0.06
BaO	0.00	0.00	0.00	0.00	0.00	0.01	0.03	0.07	0.00	0.03
Na ₂ O	0.01	0.00	0.00	0.00	0.00	0.02	0.00	0.09	0.01	0.02
Total	87.22	88.78	87.81	88.19	86.33	88.57	88.89	90.46	87.88	88.76

	Number of ions on the basis of 14 O									
Si	2.715	2.597	2.616	2.617	2.842	2.623	2.744	2.687	2.702	2.663
Ti	0.000	0.002	0.002	0.001	0.000	0.006	0.001	0.003	0.003	0.002
Al	2.733	2.902	2.812	2.793	2.451	2.793	2.517	2.748	2.743	2.853
Cr						0.009			0.004	
Fe ²⁺	2.917	3.284	3.268	3.070	0.631	3.766	3.002	2.788	2.366	3.615
Mn	0.024	0.069	0.058	0.025	0.025	0.031	0.080	0.071	0.080	0.068
Mg	1.527	1.095	1.219	1.479	3.984	0.735	1.648	1.625	2.028	0.694
Ca	0.000	0.001	0.001	0.000	0.000	0.005	0.000	0.000	0.002	0.008
Ba										
Na	0.000	0.000	0.000	0.000	0.000	0.002	0.005	0.014	0.000	0.007
K	0.001	0.000	0.000	0.000	0.000	0.003	0.000	0.012	0.001	0.003

(c) Cu rich massive sulphide ore
 (d) Zn-Pb rich massive sulphide ore
 (e) Zn-rich massive sulphide ore

Table IV - 1 b). Averages of closely similar(*) chlorite analyses from hanging wall rocks.

Sample no. of anal.	(a)	(a)	(b)	(b)	(b)	(c)	(c)	(d)	(d)	(d)	(d)	
	7-159 3	7-161.8 11	8-358 5	11-322 11	15-319.3 12	19-200 7	6-103 6	6-106.9 11	b15-158.6 5	6-105 8	15-285.6 7	15-305-8 6
SiO ₂	25.66	26.11	27.73	25.07	24.76	24.21	23.81	23.58	24.29	24.40	24.48	23.55
TiO ₂	0.00	0.00	0.00	0.06	0.08	0.05	0.02	0.06	0.04*	0.03	0.09	0.05
Al ₂ O ₃	20.83	20.85	18.16	20.98	17.83	19.76	19.73	19.61	21.25	20.81	20.02	20.48
Cr ₂ O ₃								0.11				
FeO	27.98	28.57	23.99	33.86	33.89	41.50	38.22	35.08	31.15	31.97	30.39	36.44
MnO	0.59	0.61	2.57	1.95	1.97	0.69	1.22	2.30	0.62	2.38	1.60	1.14
MgO	11.83	13.20	14.48	5.56	9.11	2.76	6.04	6.05	9.56	8.82	10.29	5.97
CaO	0.02	0.00	-0.03	0.01	0.00	0.02	0.20	0.13	0.02	0.02	0.00	0.41
BeO									0.10			
Na ₂ O	0.00	0.00	0.04	0.02	0.02	0.05	0.06	0.00	0.00	0.02	0.07	0.00
K ₂ O	0.00	0.00	0.22	0.00	0.00	0.00	0.00	0.01	0.00	0.00	0.00	0.01
TOTAL	86.91	89.34	87.21	87.51	87.66	89.03	89.29	86.92	87.03	88.44	86.94	88.05
Ions on the basis of 14 O												
Si	2.769	2.745	2.950	2.794	2.778	2.758	2.671	2.695	2.676	2.678	2.706	2.655
Ti	0.000	0.000	0.000	0.005	0.007	0.004	0.002	0.005	0.003	0.003	0.007	0.004
Al	2.650	2.583	2.277	2.755	2.258	2.652	2.608	2.642	2.759	2.691	2.607	2.721
Cr								0.009				
Fe ²⁺	2.526	2.512	2.134	3.156	3.179	3.953	3.585	3.353	3.870	3.934	2.809	3.436
Mn	0.054	0.054	0.231	0.184	0.187	0.067	0.116	0.223	0.058	0.221	0.150	1.109
Mg	1.903	2.068	2.297	0.924	1.523	0.469	1.010	1.031	1.570	1.443	1.695	1.003
Ca	0.002	0.000	0.003	0.001	0.000	0.002	0.023	0.016	0.002	0.002	0.000	0.050
Be									0.004			
Na	0.000	0.000	0.007	0.005	0.004	0.010	0.013	0.000	0.000	0.004	0.015	0.000
K	0.000	0.000	0.030	0.000	0.000	0.000	0.000	0.001	0.000	0.000	0.000	0.001

(*) Except for sample 6-106.9. Individual analyses in table IV-1 c).

(a) Hanging wall Mine tufts depicting stockwork type alteration.

(b) Cherts and jaspers.

(c) Metalliferous sediments

(d) Deeply altered Ps Fm aluminous rocks

Table IV - 1c). Representative chlorite analyses from metalliferous sediment 6-106.9 (*)

Anal. No.	61	66	67	68	69	70	71	72	73	75	77
SiO ₂	24.44	23.58	22.89	23.90	23.51	24.68	23.73	22.58	23.37	23.45	23.28
TiO ₂	0.02	0.10	0.09	0.05	0.08	0.06	0.04	0.06	0.05	0.08	0.04
Al ₂ O ₃	20.59	17.52	19.34	20.39	19.97	19.58	20.34	18.98	20.02	19.91	19.07
Cr ₂ O ₃	0.11	0.11	0.17	0.13	0.13	0.07	0.05	0.06	0.06	0.08	0.12
FeO	36.19	37.12	37.07	35.66	35.35	34.68	34.57	32.27	33.44	34.08	35.40
MnO	0.98	2.75	2.42	1.30	1.31	1.61	1.02	5.33	4.18	3.09	1.29
MgO	5.83	5.11	5.77	5.89	6.14	7.35	5.30	6.38	6.26	6.02	6.51
CaO	0.07	0.20	0.19	0.07	0.06	0.07	0.09	0.37	0.13	0.09	0.13
Nb ₂ O ₅	0.00	0.00	0.00	0.00	0.00	0.00	0.00	0.00	0.00	0.00	0.00
K ₂ O	0.02	0.00	0.02	0.01	0.00	0.01	0.02	0.01	0.00	0.01	0.02
TOTAL	88.25	86.50	87.96	87.50	86.55	88.09	85.21	86.07	87.50	86.79	85.84

Ions on the basis of 14 O											
Si	2.730	2.758	2.621	2.699	2.688	2.754	2.723	2.629	2.656	2.680	2.691
Ti	0.004	0.008	0.008	0.004	0.008	0.004	0.004	0.004	0.004	0.004	0.004
Al	2.711	2.418	2.613	2.711	2.691	2.574	2.750	2.602	2.680	2.684	2.602
Cr ³⁺	0.012	0.012	0.016	0.012	0.012	0.008	0.004	0.008	0.004	0.008	0.012
Fe ²⁺	3.379	3.633	3.551	3.367	3.379	3.234	3.30	3.141	3.176	3.258	3.426
Mn	0.094	0.273	0.234	0.125	0.129	0.152	0.098	0.523	0.402	0.301	0.125
Mg	0.973	0.891	0.984	1.008	1.047	1.223	0.906	1.105	1.059	1.027	1.121
Ca	0.008	0.027	0.023	0.008	0.008	0.008	0.012	0.047	0.016	0.012	0.016
Na	0.000	0.000	0.000	0.000	0.000	0.000	0.014	0.000	0.000	0.000	0.000
K	0.004	0.000	0.004	0.004	0.000	0.000	0.004	0.004	0.000	0.004	0.004

(*) The only sample where significant variations in chlorite composition were found.

Table IV-2. Analyses of sericites and Barium-sericites.

Sample Anal. no.	(a) 8-511.3		(a) 8-511.3		(b) 8-511.3		(b) 8-511.3		(b) 8-365.4		(b) 8-365.4	
	49	50	53	52	40	42	43	46	47	48	47	48
SiO ₂	46.32	44.57	46.13	45.23	43.64	43.94	44.87	45.12	46.35	44.85	46.35	44.85
Al ₂ O ₃	39.02	38.71	37.81	39.61	37.54	38.30	38.69	36.22	36.95	36.16	36.95	36.16
Cr ₂ O ₃	0.00	0.01	0.18	0.19	0.11	0.00	0.00	0.00	0.00	0.00	0.00	0.00
FeO	0.71	1.43	0.65	0.61	0.86	1.04	0.81	0.27	0.33	0.51	0.33	0.51
MnO	0.00	0.11	0.07	0.17	0.10	0.00	0.00	0.16	0.13	0.35	0.13	0.35
MgO	0.21	0.21	0.26	0.09	0.77	0.71	0.74	2.02	1.90	1.91	2.02	1.91
CaO	0.00	0.06	0.00	0.00	0.00	0.00	0.00	0.00	0.00	0.00	0.00	0.00
BaO	0.11	0.10	0.03	0.11	3.55	3.25	3.60	3.45	3.61	3.29	3.45	3.29
Na ₂ O	0.94	2.32	1.06	0.49	0.65	0.61	0.53	0.66	0.52	0.66	0.52	0.66
K ₂ O	8.95	7.77	8.01	9.16	8.49	8.29	8.41	7.93	7.97	8.00	7.97	8.00
TOTAL	96.26	95.24	94.20	95.67	95.71	96.14	97.64	95.84	97.77	95.74	97.77	95.74
Number of ions on the basis of 22 O												
Si	6.023	5.891	6.098	5.926	5.883	5.871	5.902	6.027	6.059	6.008	6.059	6.008
Al	6.980	6.031	5.891	6.117	5.965	6.031	6.000	5.703	5.695	5.707	5.695	5.707
Cr	0.000	0.000	0.020	0.020	0.012	0.000	0.000	0.000	0.000	0.000	0.000	0.000
Fe	0.078	0.160	0.070	0.066	0.098	0.117	0.090	0.031	0.035	0.059	0.035	0.059
Mn	0.000	0.012	0.008	0.020	0.012	0.000	0.000	0.020	0.016	0.039	0.016	0.039
Mg	0.043	0.043	0.051	0.020	0.156	0.145	0.145	0.402	0.371	0.363	0.402	0.371
Ca	0.000	0.000	0.000	0.000	0.000	0.000	0.000	0.000	0.000	0.000	0.000	0.000
Ba	0.004	0.004	0.000	0.004	0.188	0.172	0.188	0.180	0.184	0.172	0.180	0.172
Na	0.238	0.598	0.273	0.125	0.172	0.156	0.137	0.172	0.133	0.172	0.133	0.172
K	1.484	1.309	1.352	1.531	1.461	1.414	1.410	1.352	1.328	1.367	1.328	1.367

(a) Sericite-chlorite-quartz-sulphide stockwork rock 30 m below massive sulphide ore.
 (b) Sericite-quartz-sulphide outer stockwork rocks near the contact with massive sulphide ore.

Table IV-2. Continued (Sericites and Ba-sericites)

Sample Anal. no.	(c)	(c)	(c)	(c)	(c)	(c)	(c)	(c)	(c)	(d)	(d)	(d)	(d)
	8-369 23	8-369 26	8-369 27	8-369 28	8-369 29	8-446 30	8-446 32	8-446 33	7-159 8	7-159 12	7-159 12	7-159 17	7-159 17
SiO ₂	40.28	41.59	42.45	41.29	42.11	41.82	42.08	40.34	45.36	44.97	44.97	47.16	47.16
Al ₂ O ₃	32.70	36.71	36.14	33.63	34.74	37.99	35.21	39.81	36.20	36.63	36.63	37.70	37.70
Cr ₂ O ₃	0.00	0.09	0.00	0.00	0.08	0.04	0.00	0.00	0.00	0.00	0.00	0.00	0.00
FeO	1.82	1.64	1.47	1.67	1.20	3.01	5.55	2.36	1.20	1.29	1.29	1.20	1.20
MnO	0.17	0.13	0.00	0.04	0.17	0.05	0.13	0.04	0.18	0.00	0.00	0.13	0.13
MgO	1.89	1.66	1.80	1.96	2.27	0.81	0.74	0.57	1.14	1.21	1.21	1.15	1.15
CaO	0.11	0.07	0.00	0.04	0.04	0.00	0.03	0.00	0.03	0.41	0.41	0.00	0.00
BaO	8.06	9.19	8.52	8.86	8.18	7.87	6.05	7.27	4.69	3.98	3.98	4.20	4.20
Na ₂ O	0.46	0.54	0.57	0.33	0.32	0.06	0.25	0.24	0.24	0.07	0.07	0.23	0.23
K ₂ O	6.69	6.45	6.68	6.35	6.80	7.41	6.11	7.39	7.99	8.18	8.18	7.98	7.98
TOTAL	92.19	98.07	97.64	94.17	95.90	99.05	97.15	97.11	97.02	96.74	96.74	99.74	99.74
Number of ions on the basis of 22 O													
Si	5.875	5.703	5.805	5.887	5.859	5.664	5.801	5.543	6.055	6.000	6.000	6.074	6.074
Al	5.621	5.930	5.824	5.652	5.695	6.063	5.719	6.301	5.695	5.762	5.762	5.727	5.727
Cr	0.000	0.008	0.000	0.000	0.008	0.004	0.000	0.000	0.000	0.000	0.000	0.000	0.000
Fe	0.223	0.188	0.168	0.199	0.141	0.340	0.754	0.270	0.133	0.145	0.145	0.129	0.129
Mn	0.020	0.016	0.000	0.004	0.020	0.004	0.016	0.004	0.020	0.000	0.000	0.016	0.016
Mg	0.410	0.340	0.367	0.418	0.469	0.164	0.152	0.117	0.227	0.242	0.242	0.223	0.223
Ca	0.016	0.012	0.000	0.008	0.008	0.000	0.004	0.000	0.004	0.059	0.059	0.000	0.000
Ba	0.461	0.492	0.457	0.496	0.445	0.418	0.328	0.391	0.246	0.207	0.207	0.211	0.211
Na	0.129	0.145	0.152	0.090	0.086	0.016	0.066	0.066	0.063	0.020	0.020	0.059	0.059
K	1.246	1.129	1.168	1.156	1.207	1.281	1.074	1.297	1.359	1.395	1.395	1.313	1.313

(c) massive sulphide ores.

(d) altered Paraiso formation phyllite.

Table IV-3. Spessartine garnet analyses.

Anal. no.	1	2	3	6	7	13	14	15	16	AVERAGE
SiO ₂	35.78	35.28	36.66	36.22	36.18	35.57	35.72	35.76	36.04	35.91
TiO ₂	0.23	0.32	0.25	0.27	0.32	0.29	0.28	0.31	0.33	0.29
Al ₂ O ₃	18.63	18.76	18.67	19.33	19.14	19.29	19.09	18.96	19.22	19.01
Fe ₂ O ₃	1.06	1.84	0.77	1.50	1.68	1.56	1.38	1.53	1.65	1.49
FeO	2.84	1.86	4.03	2.40	2.26	2.71	2.45	2.56	2.22	2.53
MnO	33.50	34.59	33.66	35.20	35.35	35.43	35.00	34.66	35.57	34.77
MgO	0.07	0.07	0.10	0.05	0.06	0.07	0.07	0.04	0.06	0.07
CaO	5.28	5.45	5.26	5.58	5.32	5.37	5.19	5.44	5.25	5.35
TOTAL	97.39	98.47	99.40	100.78	100.66	101.02	99.42	99.45	100.63	99.55
Number of ions on the basis of 24 O										
Si	6.024	5.877	6.076	5.905	5.919	5.768	5.898	5.908	5.881	5.928
Ti	0.029	0.040	0.031	0.033	0.039	0.035	0.035	0.039	0.040	0.036
H ₄	0.000	0.083	0.000	0.062	0.042	0.197	0.067	0.053	0.079	0.036
Al	3.697	3.683	3.647	3.714	3.690	3.686	3.715	3.692	3.696	3.699
Fe ³⁺	0.135	0.231	0.096	0.184	0.207	0.191	0.172	0.190	0.203	0.185
Fe ²⁺	0.440	0.260	0.559	0.305	0.309	0.368	0.339	0.353	0.303	0.349
Mn	4.777	4.880	4.655	4.861	4.898	4.866	4.895	4.851	4.916	4.862
Mg	0.018	0.017	0.025	0.012	0.015	0.017	0.017	0.010	0.015	0.017
Ca	0.952	0.973	0.934	0.975	0.932	0.933	0.918	0.963	0.918	0.946
Andrad.										4.62%
Pyrope										0.51%
Spess.										83.59%
Hydrogross.										0.51%
Gross.										10.77%
Almandine										

Sample 8-358.1

Table IV-3. Continued (Spessartine garnet)

Anal. no.	19	30	32	33	34	11.343.7 AVERAGE
SiO ₂	37.11	36.24	35.78	37.16	36.08	36.32
TiO ₂	0.54	0.25	0.28	0.27	0.29	0.27
Al ₂ O ₃	18.07	19.68	20.16	18.89	20.03	19.69
Fe ₂ O ₃	1.86	0.00	0.00	0.00	0.00	0.00
FeO	3.25	4.46	4.85	4.58	5.06	4.74
MnO	33.31	34.95	34.43	33.04	35.16	34.40
MgO	0.33	0.07	0.09	0.04	0.05	0.06
CaO	4.98	4.14	4.04	4.23	4.32	4.18
TOTAL	99.45	99.79	99.63	98.21	101.45	99.66
Number of ions on the basis of 24 O						
Si	6.107	5.977	5.856	6.171	5.841	5.990
Ti	0.067	0.031	0.034	0.034	0.035	0.033
H ₄	0.000	0.000	0.110	0.000	0.124	0.000
Al	3.505	3.825	3.889	3.697	3.822	3.827
Fe ³⁺	0.230	0.000	0.000	0.000	0.000	0.000
Fe ²⁺	0.447	0.616	0.664	0.636	0.685	0.654
Mn	4.643	4.882	4.773	4.647	4.821	4.805
Mg	0.081	0.017	0.022	0.010	0.012	0.015
Ca	0.878	0.732	0.708	0.753	0.749	0.739
Andrad.	6.32%					
Pyrope	1.58%					0.26%
Spess.	82.63%					83.73%
Hydrogross						
Gross.	9.47%					12.85%
Almandine						3.16%

(19) Dark spessartine in sample 8-358.1
(30,32,33,34) sample 11-343.7

Table IV-4a) Analyses of calcites from stockwork and massive sulphide ores.

Sample Anal. no.	(a)					
	bis-228.6 29	bis-228.6 28	bis-228.6 22	bis-228.6 19	bis-228.6 20	8-425 30 47
MgO	0.09	0.08	0.12	0.10	0.06	0.19
CaO	53.86	53.63	52.42	52.59	50.41	54.05
FeO	0.78	0.93	1.39	1.25	1.33	0.45
MnO	1.59	1.62	1.80	1.63	1.73	1.34
BaO	0.02	0.01	0.00	0.45	0.09	0.14
ZnO	0.00	0.00	0.14	0.11	2.02	0.00
TOTAL	56.34	56.27	55.87	56.13	55.64	56.17
MgCO ₃	0.19	0.17	0.25	0.21	0.13	0.40
CaCO ₃	96.14	95.73	93.57	93.82	89.98	96.48
FeCO ₃	1.26	1.50	2.24	2.02	2.15	0.73
MnCO ₃	2.58	2.62	2.92	2.64	2.80	2.17
BaCO ₃	0.03	0.01	0.00	0.14	0.12	0.18
ZnCO ₃	0.00	0.00	0.22	0.69	3.11	0.00
Σ	100.19	100.03	99.20	99.57	98.28	99.95
Number of ions on the basis of 2 cations						
Mg	0.004	0.004	0.006	0.005	0.003	0.009
Ca	1.928	1.924	1.900	1.900	1.856	1.938
Fe	0.022	0.026	0.039	0.035	0.038	0.013
Mn	0.045	0.046	0.052	0.047	0.050	0.038
Ba	0.000	0.000	0.000	0.001	0.001	0.002
Zn	0.000	0.000	0.003	0.011	0.051	0.000

Table IV-4a) Continued (Calcites)

Sample Anal. no.	(a)		(a)		(a)		(a)	
	8-425 63	8-425 50	8-425 55	8-425 51	8-446 9	8-446 16	8-446 31	
MgO	0.30	0.13	0.22	0.27	0.13	0.00	0.14	
CaO	53.34	51.71	52.35	49.78	53.16	54.34	52.84	
FeO	0.53	1.10	0.58	1.35	0.78	0.02	1.71	
MnO	1.38	1.44	1.27	1.57	2.55	1.93	2.20	
BaO	0.10	0.13	0.13	0.10	0.00	0.00	0.00	
ZnO	0.54	1.60	2.14	3.67	-	-	-	
TOTAL	56.19	56.11	56.69	56.74	56.62	56.29	56.89	
MgCO ₃	0.63	0.27	0.46	0.57	0.27	0.00	0.29	
CaCO ₃	95.21	92.30	93.44	88.86	94.89	97.00	94.32	
FeCO ₃	0.85	1.77	0.94	2.18	1.26	0.03	2.76	
MnCO ₃	2.24	2.33	2.06	2.54	4.13	3.13	3.56	
BaCO ₃	0.13	0.17	0.17	0.13	0.00	0.00	0.00	
ZnCO ₃	0.83	2.47	3.30	5.66	-	-	-	
Σ	99.89	99.31	100.36	99.93	100.55	100.16	100.94	

Number of ions on the basis of 2 cations.	
Mg	0.015
Ca	1.916
Fe	0.015
Mn	0.039
Ba	0.001
Zn	0.013
Mg	0.011
Ca	1.882
Fe	0.016
Mn	0.036
Ba	0.002
Zn	0.053
Mg	0.006
Ca	1.900
Fe	0.022
Mn	0.072
Ba	0.000
Zn	0.092
Mg	0.000
Ca	1.945
Fe	0.001
Mn	0.055
Ba	0.000
Zn	0.000

(a) Zincian calcites

Table IV-4b) Analyses of carbonates scattered in cherts.

Sample Anal. no.	(a) S1-328.7 9	(b) S1-328.7 8	(c) S1-328.7 15	(d) S1-229.1
MgO	0.14	2.23	3.88	1.71
CaO	52.64	13.86	2.61	3.10
FeO	3.06	41.27	52.41	50.56
MnO	0.51	2.51	1.43	5.46
TOTAL	56.35	59.87	60.33	60.83
MgCO ₃	0.29	4.67	8.13	3.58
CaCO ₃	93.96	24.74	4.66	5.53
FeCO ₃	4.96	66.57	84.54	81.55
MnCO ₃	0.83	4.07	2.32	8.85
Σ	100.02	100.05	99.65	99.52

Ions on the basis of 2 cations

Mg	0.007	0.121	0.216	0.097
Ca	1.893	0.542	0.104	0.126
Fe	0.086	1.259	1.635	1.602
Mn	0.014	0.078	0.045	0.175

- (a) Calcite
 (b) Ca-siderite
 (c) Mg-siderite (sideroplesite)
 (d) Siderite

Table IV-4c) Analyses of coexisting carbonates in metalliferous sediments above the feitais orebody.

Anal. no.	(a) 99	(a) 103	(a) 101	(a) 100	(b) 92	(b) 89	(b) 91	(c) 98	(c) 97	(c) 95
MgO	0.37	0.59	0.54	0.49	0.56	0.57	0.56	0.71	0.35	0.43
CaO	42.98	36.65	31.42	29.85	23.03	22.70	22.49	3.47	3.71	3.77
FeO	3.23	4.01	1.37	0.86	1.01	0.50	0.51	6.16	2.16	1.73
MnO	10.35	17.04	25.55	27.31	34.44	35.67	35.92	51.01	54.80	55.14
BaO	0.27	0.01	0.10	0.05	0.16	0.21	0.16	0.36	0.14	0.11
TOTAL	57.20	58.30	58.98	58.56	59.20	59.65	59.74	61.71	61.16	61.18
MgCO ₃	0.78	1.24	1.13	1.03	1.17	1.19	1.38	1.49	0.73	0.90
CaCO ₃	76.72	65.42	56.08	53.28	41.11	40.52	40.14	6.19	6.62	6.73
FeCO ₃	5.21	6.47	2.21	1.39	1.63	0.81	0.82	9.94	3.48	2.79
MnCO ₃	16.77	27.60	41.39	44.24	55.79	57.79	58.19	82.64	88.78	89.33
BaCO ₃	0.35	0.01	0.13	0.06	0.21	0.27	0.21	0.46	0.18	0.14
Σ	99.82	100.74	100.95	100.00	99.91	100.58	100.75	100.72	99.80	99.89
Number of ions on the basis of 2 cations										
Mg	0.019	0.030	0.028	0.026	0.030	0.030	0.035	0.040	0.020	0.024
Ca	1.583	1.356	1.175	1.130	0.888	0.870	0.861	0.140	0.151	0.153
Fe	0.093	0.116	0.040	0.025	0.030	0.015	0.015	0.193	0.068	0.055
Mn	0.301	0.498	0.755	0.818	1.050	1.081	1.087	1.622	1.759	1.767
Ba	0.004	0.000	0.001	0.001	0.002	0.003	0.002	0.005	0.002	0.002

(a) Manganocalcite

(b) Kutnohorite CaMn(CO₃)₂

(c) Rhodochrosite

(a,b,c) sample 9-285

Table IV-4c) Continued (Carbonates in metalliferous sediments)

Anal. no.	(d) 80	(d) 58	(d) 81	(d) 67	(d) 76	(d) 84	(e) 54	(f) 53	(f) 86
MgO	0.40	0.42	0.44	0.30	0.30	0.22	3.28	3.40	3.66
CaO	45.75	46.42	44.45	47.98	44.50	45.79	30.46	29.21	29.72
FeO*	3.16	3.53	3.63	3.88	3.95	5.39	9.88	13.92	15.25
MnO	7.69	6.48	8.30	4.52	8.46	4.84	13.75	11.03	9.22
BaO	0.18	0.21	0.21	0.21	0.20	0.16	0.16	0.09	0.14
TOTAL	57.18	57.06	57.03	56.89	57.41	56.40	57.53	57.65	57.99
MgCO ₃	0.84	0.88	0.92	0.63	0.63	0.46	6.87	7.13	7.67
CaCO ₃	81.67	82.86	79.34	85.64	79.43	81.74	54.37	52.14	53.05
FeCO ₃	5.10	5.69	5.86	6.26	6.37	8.69	15.94	22.45	24.60
MnCO ₃	12.46	10.50	13.45	7.32	13.71	7.84	22.28	17.87	14.94
BaCO ₃	0.23	0.27	0.27	0.27	0.26	0.21	0.21	0.12	0.18
	100.30	100.20	99.84	100.12	100.40	98.94	99.66	99.70	100.44
Number of ions on the basis of 2 cations									
Mg	0.020	0.021	0.022	0.015	0.015	0.011	0.170	0.177	0.188
Ca	1.666	1.689	1.630	1.742	1.625	1.690	1.135	1.091	1.100
Fe	0.090	0.100	0.104	0.110	0.113	0.155	0.287	0.406	0.440
Mn	0.221	0.186	0.241	0.130	0.244	0.141	0.405	0.326	0.270
Ba	0.002	0.003	0.003	0.003	0.003	0.002	0.002	0.001	0.002

(d) Manganoan-ferroan calcite

(d,e,f) sample 9-285 (in vein)

(e) Manganoan ankerite

(f) Ferroan ankerite

Table IV-4c) Continued (Carbonates in metalliferous sediments)

Anal. no.	(g) 42	(g) 72	(g) 52	(g) 82	(g) 51	(h) 65	(h) 87	(h) 64	(h) 66
MgO	1.94	1.65	1.59	1.81	1.13	2.20	1.43	1.61	1.37
CaO	2.27	2.46	2.04	2.54	2.29	1.23	2.80	0.91	0.88
FeO	32.79	33.35	33.54	34.71	35.10	43.95	46.37	47.84	49.19
MnO	24.02	23.51	23.96	21.67	23.08	14.08	10.86	10.54	9.36
BaO	0.19	0.20	0.16	0.18	0.17	0.16	0.16	0.18	0.23
TOTAL	61.21	61.17	61.29	60.91	61.77	61.62	61.62	61.08	61.03
MgCO ₃	4.07	3.46	3.33	3.79	2.37	4.61	3.00	3.37	2.87
CaCO ₃	4.05	4.39	3.64	4.53	4.09	2.20	5.00	1.62	1.57
FeCO ₃	52.89	53.79	54.10	55.99	56.62	70.89	74.79	77.17	79.34
MnCO ₃	38.91	38.09	38.82	35.11	37.39	22.81	17.59	17.07	15.16
BaCO ₃	0.24	0.26	0.21	0.23	0.22	0.21	0.21	0.23	0.30
Σ	100.17	99.99	100.10	99.65	100.68	100.71	100.59	99.47	99.25
Number of ions on the basis of 2 cations									
Mg	0.109	0.093	0.089	0.102	0.063	0.123	0.080	0.092	0.078
Ca	0.091	0.100	0.083	0.103	0.092	0.049	0.113	0.037	0.036
Fe	1.032	1.053	1.059	1.098	1.105	1.378	1.459	1.528	1.578
Mn	0.765	0.752	0.766	0.694	0.736	0.447	0.346	0.341	0.304
Ba	0.003	0.003	0.002	0.003	0.003	0.002	0.002	0.003	0.003

(g) Manganosiderite

(h) Oligonite

(d,e,f,g,h) in vein, sample 9-285

Table IV-4c) Continued (Carbonates in metalliferous sediments)

Anal. no.	(l) 126	(l) 124	(l) 127	(l) 122	(l) 121	(j) 107	(j) 113	(j) 116	(j) 105	(j) 115	(k) 102	(l) 105
MgO	0.29	0.32	0.48	0.20	0.25	0.51	0.54	0.38	0.41	0.38	0.19	0.43
CaO	41.45	40.52	40.03	40.13	40.56	12.67	11.66	11.84	11.50	11.63	8.73	30.89
FeO	1.45	1.64	0.84	0.78	0.20	0.64	0.29	0.33	0.58	0.31	1.03	1.90
MnO	14.50	15.47	15.94	16.81	16.93	46.64	47.78	48.23	48.30	48.42	50.93	25.29
BaO	0.00	0.01	0.00	0.00	0.00	0.06	0.07	0.09	0.13	0.07	0.20	0.05
TOTAL	57.69	57.96	57.29	57.92	57.94	60.52	60.34	60.87	60.92	60.81	61.08	58.56
MgCO ₃	0.61	0.67	1.01	0.42	0.52	1.07	1.13	0.80	0.86	0.80	0.40	0.90
CaCO ₃	73.99	72.33	71.45	71.63	72.40	22.62	20.81	21.13	20.53	20.76	15.58	55.14
FeCO ₃	2.34	2.65	1.35	1.26	0.32	1.03	0.47	0.53	0.94	0.50	1.66	3.06
MnCO ₃	23.49	25.06	25.82	27.23	27.43	75.56	77.40	78.13	78.25	78.44	82.51	40.97
BaCO ₃	-	0.01	-	-	-	0.08	0.09	0.12	0.17	0.09	0.26	0.06
Σ	100.42	100.72	99.64	100.54	100.67	100.35	99.91	100.71	100.74	100.59	100.41	100.14

Number of ions on the basis of 2 cations

Mg	0.015	0.016	0.025	0.010	0.013	0.028	0.030	0.021	0.022	0.021	0.011	0.023
Ca	1.523	1.488	1.484	1.478	1.490	0.499	0.462	0.466	0.453	0.459	0.348	1.116
Fe	0.042	0.047	0.024	0.022	0.006	0.020	0.009	0.010	0.018	0.010	0.032	0.056
Mn	0.421	0.449	0.467	0.489	0.492	1.452	1.498	1.501	1.505	1.510	1.606	0.755
Ba	-	0.000	-	-	-	0.001	0.001	0.001	0.002	0.001	0.003	0.001

(l) Manganocalcite
(j) Calcic rhodochrosite
(l,j) Sample 6-103.1

(k) Calcic rhodochrosite
(l) Manganocalcite, nearly kutnohorite
(k,l) Sample 11-343.7

Table IV-4d) Analyses of carbonates in deeply altered PS phyllites and tuffs above the Feitais orebody.

Sample Anal. no.	(a) 15,285.6 76	(a) 15,285.6 77	(a) 15,285.6 91	(b) 15,285.6 74	(c) 15,285.6 94	(c) 15,285.6 73	(c) 15,285.6 90	(d) 15,285.6 95
MgO	14.64	14.53	13.60	9.35	5.58	7.07	5.53	11.73
CaO	29.42	30.01	29.41	26.66	7.17	5.64	6.32	29.12
FeO	3.83	4.00	4.58	12.33	45.50	46.48	46.58	4.18
MnO	6.82	6.55	7.11	7.33	1.72	1.56	1.09	10.50
BaO	0.00	0.00	0.00	0.00	0.16	0.07	0.09	0.01
TOTAL	54.71	55.09	54.70	55.67	60.13	59.82	59.89	55.54
MgCO ₃	30.69	30.45	28.51	19.60	11.70	14.82	11.59	24.59
CaCO ₃	52.61	53.57	52.20	47.59	12.80	10.07	11.28	51.98
FeCO ₃	6.18	6.45	7.39	19.89	73.39	73.36	75.59	6.74
MnCO ₃	11.05	10.61	11.52	11.87	2.79	2.53	1.77	17.01
BaCO ₃	-	-	-	-	0.21	0.09	0.12	0.01
Σ	100.43	101.09	99.91	98.95	100.88	100.86	100.34	100.33
Number of ions on the basis of 2 cations								
Mg	0.700	0.691	0.658	0.472	0.299	0.377	0.299	0.573
Ca	1.012	1.026	1.023	0.969	0.276	0.216	0.246	1.022
Fe	0.103	0.107	0.124	0.349	1.369	1.259	1.421	0.114
Mn	0.185	0.177	0.195	0.210	0.052	0.047	0.033	0.291
Ba	0.000	0.000	0.000	0.000	0.002	0.001	0.001	0.000

(a,d) Ankerite

(b) Ferroan ankerite

(c) Mg-Ca-Mn siderite

(a,b,c) replacing albite

(c,d) replacing chlorite

Table IV-4d) Continued (Carbonates in PS phyllites and tuffs)

2

Sample Anal. no.	(d) 15-285.6 96	(e) 15-285.6 48	(e) 15-285.6 51	(e) 15-285.6 52	(f) 15-285.6 55	(f) 15-285.6 56	(g) 8-358.1 18	(g) 8-358.1 19
MgO	12.45	12.53	12.21	12.68	0.09	0.11	0.50	0.38
CaO	29.58	29.19	29.08	29.19	54.07	55.25	44.13	46.21
FeO	3.60	3.91	3.71	3.83	0.20	0.20	0.09	0.56
MnO	9.48	9.43	10.42	9.47	0.25	0.32	12.04	9.98
BaO	0.00	0.00	0.01	0.00	0.07	0.02	0.00	0.12
TOTAL	55.11	55.06	55.43	55.17	54.68	55.90	56.76	57.25
MgCO ₃	26.10	26.26	25.29	26.58	0.19	0.23	1.05	0.80
CaCO ₃	52.80	52.10	51.91	52.10	96.51	98.62	77.87	82.48
FeCO ₃	5.81	6.31	5.98	6.18	0.32	0.32	0.15	0.90
MnCO ₃	15.36	15.28	16.88	15.34	0.41	0.52	19.50	16.17
BaCO ₃	0.00	-	0.01	-	0.09	0.03	0.00	0.15
Σ	100.06	99.95	100.38	100.20	97.52	99.72	99.47	100.51
Number of ions on the basis of 2 cations								
Mg	0.606	0.610	0.594	0.616	0.005	0.005	0.026	0.019
Ca	1.034	1.022	1.017	1.019	1.962	1.980	1.622	1.677
Fe	0.089	0.107	0.101	0.104	0.006	0.006	0.003	0.016
Mn	0.262	0.261	0.288	0.261	0.007	0.009	0.350	0.286
Ba	0.000	0.000	0.000	0.000	0.001	0.000	0.000	0.002

(d,e) Ankerite

(f) (Rare) calcite

(g) Manganocalcite

Table IV-4d) Continued (Carbonates in altered PS phyllites and tuffs)

Sample Anal. no.	(g) 8-358.1 23	(g) 8-358.1 20	(h) 6-105.1 66	(i) 6-105.1 70	(j) 6-105.1 92	(k) 6-105.1 74	(k) 6-105.1 93	(k) 6-105.1 73
MgO	0.44	0.55	11.88	5.10	2.86	1.71	1.44	1.80
CaO	44.46	43.74	30.96	1.65	3.50	6.46	5.95	3.90
FeO	0.64	0.95	2.89	22.02	13.10	6.56	6.89	8.55
MnO	11.38	12.11	9.32	31.48	40.35	45.77	46.06	46.57
BaO	0.05	0.15	0.01	0.16	0.04	0.07	0.08	0.16
ZnO	-	-	0.00	0.05	0.04	0.20	0.00	0.14
TOTAL	56.97	57.50	55.06	60.46	59.89	60.77	60.42	61.12
MgCO ₃	0.92	1.15	24.90	10.69	5.99	3.58	3.02	3.77
CaCO ₃	79.36	78.08	55.26	2.95	6.25	11.53	10.62	6.96
FeCO ₃	1.03	1.53	4.66	35.52	21.13	10.58	11.11	13.79
MnCO ₃	18.44	19.62	15.10	51.00	65.37	74.15	74.62	75.44
BaCO ₃	0.06	0.19	0.01	0.21	0.05	0.31	0.10	0.21
ZnCO ₃	-	-	0.00	0.08	0.06	0.09	0.00	0.22
Σ	99.82	100.57	99.94	100.43	98.85	100.24	99.47	100.39
Number of ions on the basis of 2 cations								
Mg	0.022	0.028	0.579	0.279	0.160	0.095	0.080	0.100
Ca	1.629	1.594	1.084	0.065	0.141	0.257	0.239	0.156
Fe	0.018	0.027	0.079	0.675	0.412	0.204	0.216	0.267
Mn	0.330	0.349	0.258	0.978	1.285	1.439	1.463	1.471
Ba	0.001	0.002	0.000	0.002	0.001	0.001	0.001	0.002
Zn	-	-	0.000	0.001	0.001	0.005	0.000	0.004

(g) Manganocalcite

(h) Ankerite

(i) Fe-Mg rhodochrosite

(j) Fe-rhodochrosite

(k) Rhodochrosite

Table IV-4d) Continued (Carbonates in altered PS phyllites and tuffs)

Sample Anal. no.	(1) 15-330.2 129	(1) 15-330.2 130	(1) 15-330.2 134	(1) 15-330.2 136	(1) 15-330.2 138	(1) 15-330.2 139	(1) 15-330.2 141	(1) 15-330.2 142
MgO	0.18	0.14	0.20	0.16	0.18	0.16	0.40	0.09
CaO	53.69	54.79	51.59	54.50	54.83	54.77	53.06	54.97
FeO	0.53	0.56	0.20	0.62	0.44	0.53	1.27	0.98
MnO	1.30	1.13	4.83	1.06	0.86	0.77	1.57	0.75
BaO	0.00	0.00	0.00	0.00	0.00	0.00	0.01	0.00
TOTAL	55.70	56.62	56.82	56.34	56.31	56.23	56.31	56.79
MgCO ₃	0.38	0.29	0.42	0.34	0.38	0.34	0.84	0.19
CaCO ₃	95.84	97.80	92.09	97.28	97.87	97.76	94.71	98.12
FeCO ₃	0.85	0.90	0.32	1.00	0.91	0.85	2.05	1.58
MnCO ₃	2.11	1.83	7.82	1.72	1.39	1.25	2.54	1.22
BaCO ₃	-	-	-	-	-	-	0.01	-
Σ	99.17	100.83	100.65	100.34	100.35	100.20	100.16	101.11
Number of ions on the basis of 2 cations								
Mg	0.008	0.007	0.010	0.008	0.009	0.008	0.020	0.004
Ca	1.939	1.946	1.848	1.945	1.955	1.956	1.900	1.947
Fe	0.015	0.016	0.006	0.017	0.012	0.015	0.035	0.027
Mn	0.037	0.032	0.137	0.030	0.024	0.022	0.044	0.021
Ba	0.000	0.000	0.000	0.000	0.000	0.000	0.000	0.000

(1) Calcite in PS Formation tuff.

Table IV-5. Analyses of sphalerites from the Faltals ore environment.

Sample Anal. no.	bfs-161(a)					bfs-163.3(a)			11-351.9(a)	
	19	20	21	22	23	11	12	13	14	15
S	32.42	33.43	33.46	33.46	33.31	33.09	33.16	33.04	33.49	33.11
Mn	0.00	0.00	0.00	0.00	0.00	0.00	0.00	0.00	0.00	0.01
Fe	4.61	4.27	4.43	4.20	4.44	2.02	2.11	2.60	0.89	0.72
Zn	61.86	62.09	61.51	61.67	62.31	64.69	64.87	64.53	66.78	66.62
Cd	0.00	0.06	0.00	0.02	0.02	0.02	0.06	0.15	0.08	0.00
TOTAL	98.89	99.84	99.38	99.34	100.07	99.82	100.20	100.32	101.24	100.46
FeS mole %	8.02	7.46	7.77	7.38	7.70	3.63	3.67	4.50	1.53	1.25

Sample Anal. no.	11-351.9(a)		bfs-168.5(b)						bfs-180(c)	
	16	17	5	11	12	13	85	86	66	71
S	33.61	33.18	32.90	33.08	33.27	33.31	34.19	34.26	33.26	33.21
Mn	0.00	0.02	0.00	0.00	0.00	0.00	0.00	0.00	0.00	0.00
Fe	1.40	1.38	1.86	2.09	1.75	1.68	2.21	2.12	3.72	4.05
Zn	64.36	64.98	64.41	64.00	64.36	64.58	64.06	62.91	62.50	62.64
Cd	0.00	0.07	0.02	0.10	0.10	0.16	0.00	0.00	0.00	0.01
TOTAL	99.37	99.60	99.18	99.27	99.52	99.78	100.46	99.28	99.48	99.91
FeS mole %	2.48	2.42	3.25	3.66	3.08	2.96	3.88	3.79	6.51	7.03

Sample Anal. no.	bfs-180(c)			bfs-187.2(b)						
	73	74	75	9	11	19	24	25	17	18
S	33.63	33.37	33.82	33.32	34.09	33.63	33.63	33.30	33.38	33.15
Mn	0.01	0.88	6.00	0.00	0.09	0.00	0.00	0.00	0.01	0.00
Fe	4.04	3.67	3.34	1.71	1.98	2.14	1.95	1.78	3.41	3.86
Zn	62.94	62.27	63.20	64.49	64.27	64.86	64.75	64.07	62.42	63.01
Cd	0.00	0.00	0.02	0.10	0.00	0.00	0.00	0.02	0.02	0.00
TOTAL	100.62	99.71	100.38	99.62	100.29	100.63	100.22	99.17	99.21	99.72
FeS mole %	6.99	6.24	5.82	3.01	3.60	3.72	3.61	3.15	6.01	6.20

Table IV-5. Continued (Sphalerites)

Sample Anal. no.	bis-187.2		bis-220.55		B-389.25(b)				B-418.7(c)	
	22(b)	(20(d)	42	41	44	45	46	47	27	30
S	33.89	33.49	33.41	33.46	33.14	33.60	33.24	33.53	33.34	33.48
Mn	0.00	0.00	0.00	0.00	0.00	0.00	0.00	0.00	0.00	0.02
Fe	3.80	2.05	0.57	0.50	0.77	0.86	0.72	0.52	3.79	3.64
Zn	63.35	63.84	65.16	65.87	65.40	64.53	65.23	66.55	63.16	62.64
Cd	0.02	0.05	0.23	0.06	0.00	0.00	0.03	0.11	0.00	0.00
TOTAL	100.57	99.43	99.36	99.88	99.31	98.98	99.23	100.71	100.28	99.90
FeS mole %	6.56	3.62	1.01	0.88	1.36	1.52	1.28	0.91	6.56	6.40

Sample Anal. no.	B-418.7(c)				B-425(c)					
	33	37	40	42	15	21	23	25	26	27
S	33.59	32.11	33.31	33.72	33.89	33.77	33.68	33.67	34.02	33.98
Mn	0.00	0.02	0.02	0.03	0.00	0.04	0.09	0.00	0.03	0.01
Fe	3.81	3.57	5.64	5.64	6.29	5.99	6.08	5.75	5.90	6.27
Zn	63.15	63.54	61.86	61.66	60.24	60.66	59.52	60.21	60.06	60.34
Cd	0.00	0.00	0.00	0.00	0.07	0.00	0.00	0.15	0.04	0.00
TOTAL	100.56	99.23	100.83	101.05	100.49	100.46	99.25	99.79	100.05	100.60
FeS mole %	6.60	6.17	9.64	9.67	10.88	10.35	10.63	10.04	10.30	10.84

Sample Anal. no.	B-425		B-446.85(d)				bis-228.6(e)			
	32(g)	50	51	52	53	55	59	70	80	81
S	33.68	34.01	33.38	34.15	33.87	33.69	34.04	33.38	33.53	33.39
Mn	0.00	0.00	0.00	0.00	0.00	0.00	0.00	0.00	0.00	0.00
Fe	6.07	4.79	5.01	4.88	4.79	4.48	4.83	2.34	2.43	2.48
Zn	60.32	60.94	61.07	61.88	60.78	61.04	61.51	64.01	63.88	63.16
Cd	0.15	0.00	0.00	0.00	0.00	0.00	0.00	0.00	0.00	0.00
TOTAL	100.24	99.74	99.43	100.52	99.43	99.20	100.08	99.74	99.63	98.98
FeS mole %	10.52	8.43	8.78	8.15	8.46	7.91	7.94	4.18	4.28	4.34

Table IV-5. Continued (Sphalerites)

Sample Anal. no.	bfs-228.6(e)			bfs-234.3(e)			21-761.2(e)		
	82	83	84	28	29	30	31	6	7
S	34.03	33.52	33.21	33.66	33.27	33.55	33.21	33.51	32.89
Mn	0.00	0.00	0.00	0.00	0.02	0.00	0.01	0.00	0.00
Fe	2.54	2.38	2.39	1.75	1.81	1.38	1.59	2.11	2.01
Zn	63.46	63.18	63.15	64.52	64.54	64.65	63.93	64.23	64.09
Cd	0.09	0.00	0.04	0.18	0.16	0.23	0.17	0.15	0.13
TOTAL	100.13	99.07	99.29	100.10	99.80	99.81	98.92	100.01	99.14
FeS mole %	4.47	4.22	4.24	3.07	3.17	2.43	2.82	3.70	3.54

Sample Anal. no.	21-800.5(e)			
	32	33	34	35
S	33.30	33.44	33.30	33.33
Mn	0.10	0.05	0.01	0.04
Fe	1.48	1.19	1.12	1.04
Zn	64.52	65.80	64.69	65.89
Cd	0.15	0.15	0.09	0.12
TOTAL	99.55	100.63	99.20	100.42
FeS mole %	2.61	2.07	1.98	1.81

- (a) In cherts and jaspers
- (b) In medium grade Zn-Pb massive ore (Zn+Pb>7%)
- (c) In high grade Zn-Pb massive ore (Zn+Pb>7%)
- (d) In copper rich massive ore
- (e) In stockwork ores

APPENDIX V

WHOLE ROCK GEOCHEMICAL DATA
ON ORE ZONE ROCKS INCLUDING HANGING WALL
CULM GROUP SEDIMENTS

- V-1. Stockwork zone rocks and massive sulphide ores
- V-2. Siliceous and metalliferous sediments (Jasper unit)
- V-3. PS Formation phyllites, tuffites and tuffs
- V-4. Culm Group greywackes and shales

Table V - (a) - Weekly ore zone altered Mine tuffs.

	bis-262	15-412	bis-306.1	8-363.3	8-363.4	bis-254.5	8-499.7	8-487.1	8-365.4
SiO ₂	67.38	63.69	69.19	37.77	49.67	58.90	47.88	64.14	57.31
TiO ₂	0.10	0.21	0.10	0.36	0.32	0.04	0.06	0.10	0.27
Al ₂ O ₃	11.01	16.20	9.96	17.11	25.89	3.78	5.88	7.88	22.57
Fe ₂ O ₃	7.55*	4.84*	1.34*	19.60*	4.60*				0.30
FeO						21.72*	21.60*	14.70*	2.66
MnO	0.05	0.03	0.07	0.10	0.05	0.01	0.14	0.01	0.05
MgO	0.50	2.86	0.88	3.22	2.71	0.10	1.42	ND	2.92
CaO	0.67	0.80	6.80	ND	0.30	ND	2.30	ND	ND
BaO	0.09	0.09	0.21	1.17	2.22	0.18	0.05	0.05	2.40
Na ₂ O	6.83	3.09	1.68*	1.86	1.91	0.25	0.23	0.36	0.96
K ₂ O	0.09	2.46	1.91	2.91	5.15	0.82	1.00	1.64	4.91
P ₂ O ₅	ND	ND	ND	ND	0.02	ND	ND	ND	0.03
LOI	1.73	4.52	5.98	14.84	6.03	15.73	15.25*	9.79	4.73
TOTAL	96.00	98.79	98.12	98.64	98.87	98.53	95.91	98.68	98.71
Si	5.69	3.08	0.32	14.64	2.58	16.79	16.77	11.29	1.82
Rb	14	155	140	179	293	47	50	72	315
Sr	127	74	129	178	288	7	25	34	186
Ba	810	766	1869	10538	19916	1596	464	527	17972
Sc	7.7	15.0	-	11.0	11.0	-	-	6.5	12.0
Y	41	80	69	40	33	21	29	34	62
Zr	151	264	53	252	225	68	93	131	356
Hf	5	9	-	7	10	-	-	4	9
Nb	16	17	17	9	ND	12	30	21	6
Ta	24	5	-	3	3	-	-	42	11
Cr	2	5	4	10	9	4	11	6	5
Co	93	22	36	46	12	96	56	72	14
Ni	5	10	18	5	17	1	ND	2	13
Cu	28	ND	ND	43	27	66	87	1569	41
Zn	93	21	36	151	53	967	27	197	69
Pb	43	33	19	62	ND	93	41	142	ND
Th	11.0	23.0	-	14.0				7.6	22.0
La		71.5							
Ce		142.7							
Nd		72.9							
Sm		15.9							
Eu		2.5							
Gd		14.7							
Dy		18.7							
Er		10.6							
Yb		8.7							

* Total Iron

Table V - 1b) - Outer stactwork rocks (Quartz-sericite-sulphides)

	8-508	18-376.6	9-824.7	bis-259.2	bis-239.5	bis-236.3	bis-229	8-367.9	8-617	bis-230.5
SiO ₂	79.07	73.48	68.62	74.53	61.57	69.35	30.40	66.00	54.53	17.88
TiO ₂	0.10	0.14	0.18	0.14	0.08	0.29	0.27	0.17	0.30	0.17
Al ₂ O ₃	8.44	6.98	15.27	12.08	8.12	15.30	14.68	15.44	25.91	9.68
Fe ₂ O ₃	0.54		ND							
FeO	5.73	5.97*	1.59	3.89*	14.90*	2.98*	19.41*	5.14*	4.00*	40.44*
MnO	0.06	0.25	0.07	0.02	0.01	0.02	0.27	0.01	0.06	0.02
MgO	1.06	1.18	2.05	0.47	ND	0.49	0.48	0.93	1.77	0.25
CaO	ND	1.89	1.70	ND	ND	ND	7.69	ND	ND	ND
BaO	0.10	1.06	0.30	0.34	0.46	0.93	1.23	1.68	0.07	0.50
Na ₂ O	0.19	0.21	0.43	0.32	0.21	0.42	0.29	0.34	0.34	0.13
K ₂ O	1.33	1.17	4.57	3.11	1.84	3.83	3.24	3.77	6.86	7.19
P ₂ O ₅	ND	ND	0.01	ND	ND	ND	ND	0.02	0.01	ND
LOI	2.19	6.67	4.96	4.01	9.98	3.98	19.14	4.34	6.38	28.59
TOTAL	98.81	98.66	99.52	98.91	97.16	97.59	97.10	97.84	100.22	99.84
Si	1.70	3.30	0.63	2.77	11.59	2.42	13.10	3.68	3.25	28.90
Rb	62	58	210	141	84	151	131	231	317	93
Sr	21	39	30	33	32	73	190	96	40	37
Ba	869	9482	267	3078	4004	8298	11012	15078	646	4534
Sc	-	-	-	-	-	-	6.6	7.5	22.0	-
Y	52	25	80	57	26	42	49	25	99	26
Zr	146	190	238	211	138	287	296	227	387	170
Hf	-	-	-	-	-	-	7	6	15	-
Nb	23	1	22	16	10	5	5	ND	29	17
Ta	-	-	-	-	-	-	6	6	10	-
Cr	ND	2	16	10	2	7	14	8	ND	9
Co	43	56	17	49	96	37	55	18	13	82
Ni	4	6	3	16	7	46	13	11	9	1
Cu	39	84	16	43	386	88	62	57	7	438
Au(ppb)	-	-	-	-	-	-	-	-	-	-
Zn	20	413	263	680	576	6102	372	23	106	265
Pb	9	103	28	693	59	1328	896	8	42	1049
Th	-	-	-	-	-	-	13.0	14.0	25.0	-
La									66.8	
Ce									138.6	
Nd									71.6	
Sm									14.7	
Eu									2.1	
Gd									12.0	
Dy									11.9	
Er									7.5	
Yb									7.2	
Fe ²⁺ /ΣFe	0.93		1.00							

* Total Iron

Table V - 1b) - Continued (Outer stockwork rocks)

	11-422.2	8-370	MF-5	21-696.1	21-689.2	15-409.3	21-793.2	bis-230.5
SiO ₂	55.39	74.91	60.78	68.74	73.64	60.18	74.77	57.11
TiO ₂	0.41	0.06	0.23	0.14	0.16	0.18	0.15	0.06
Al ₂ O ₃	18.92	4.81	12.21	11.88	13.49	16.71	13.20	6.29
Fe ₂ O ₃	ND	ND			0.33		0.72	
FeO	6.77	2.44	11.66*	7.80*	1.97	3.18*	2.82	21.07*
MnO	0.18	0.22	0.06	0.06	0.03	0.07	0.04	0.07
MgO	1.77	1.09	0.58	0.72	2.33	3.63	1.44	0.81
CaO	0.22	5.36	ND	ND	ND	3.44	ND	ND
BaO	2.88	1.21	2.13	0.27	0.11	0.19	0.06	0.11
Na ₂ O	0.15	ND	ND	ND	ND	ND	ND	ND
K ₂ O	3.42	0.79	2.10	3.16	3.54	4.26	3.13	0.54
P ₂ O ₅	0.04	ND	ND	ND	ND	ND	ND	ND
LOI	8.13	7.33	8.26	5.87	3.26	7.41	2.58	12.33
TOTAL	98.26	98.22	95.88	98.64	98.66	99.25	98.88	89.38
SS	1.79	2.01	7.96	3.30	0.62	1.68	0.70	13.15
Rb	127	59	92	160	191	237	131	31
Sr	51	176	56	16	13	36	16	12
Ba	25830	10903	19036	2413	1017	1667	572	1020
Sc	-	2.8	-	-	12.0	14.0	-	-
Y	64	ND	22	68	72	81	76	29
Zr	629	100	186	198	219	233	206	90
Hf	-	2	-	-	8	8	-	-
Nb	ND	ND	ND	15	21	17	21	10
Ta	-	7	-	-	6	5	-	-
Cr	4	11	3	13	8	8	5	9
Co	46	62	31	43	16	13	27	181
Ni	12	13	32	8	13	17	8	ND
Cu	41	30	40	25	ND	ND	69	1106
As(ppb)	-	140	-	-	-	-	-	-
Zn	2122	389	32	119	49	80	47	272
Pb	711	148	42	59	17	32	49	96
Th	-	5.8	-	-	16.0	16.0	-	-
La								
Ce								
Nd								
Sm								
Eu								
Gd								
Dy								
Er								
Yb								
Fe ²⁺ /ΣFe	1.00	1.00			0.96		0.81	

* Total Iron

Table V - 1c) Stockwork rocks (Quartz-chlorite-sulphides).

	21-775.6	21-711.5	8-506.3	18-382	21-735.9	8-511.1	21-721.2	bis-240.6	15-390	bis-248.35
SiO ₂	72.94	75.88	66.50	25.82	52.82	75.15	83.29	44.61	69.18	69.94
TiO ₂	0.11	0.07	0.11	0.48	0.13	0.08	0.05	0.09	0.11	0.04
Al ₂ O ₃	9.84	7.45	10.66	22.72	11.95	7.39	4.34	8.17	10.45	4.89
Fe ₂ O ₃	0.73	0.62	1.05		ND	0.86	0.07		0.91	
FeO	6.44	8.14	10.82	19.69*	22.20	11.22	6.83	29.69*	6.70	15.76*
MnO	0.09	0.08	0.13	0.45	0.40	0.14	0.04	0.16	0.16	0.08
MgO	5.96	3.10	5.37	17.12	3.50	1.24	2.04	1.60	5.38	0.64
CaO	ND	ND	ND	ND	ND	ND	ND	ND	0.25	ND
BaO	0.13	0.11	0.05	0.19	0.04	ND	0.04	0.05	0.01	0.03
Na ₂ O	ND	ND	ND	ND	ND	ND	ND	ND	ND	ND
K ₂ O	0.54	0.27	0.24	0.39	0.13	0.07	ND	ND	0.05	ND
P ₂ O ₅	ND	ND	ND	ND	ND	ND	ND	ND	ND	ND
LOI	3.59	2.58	3.95	11.60	8.42	2.49	1.82	12.76	4.88	6.78
TOTAL	100.27	98.30	98.88	98.46	99.59	98.64	98.52	97.14	100.09	97.16
Si	0.11	0.40	1.39	1.58	4.27	0.48	0.51	13.29	0.41	7.13
Rb	31	22	18	27	13	10	6	14	5	12
Sr	3	3	10	13	6	4	1	4	4	6
Ba	1123	999	463	1687	317	57	392	522	72	306
Sc	-	-	-	10.0	11.0	5.6	-	6.7	-	-
Y	59	32	34	100	65	37	28	40	65	24
Zr	158	109	161	419	185	125	88	136	184	84
Hf	-	-	-	14	7	4	-	3	-	-
Nb	16	10	13	16	17	16	15	12	14	21
Ta	-	-	-	2	1	12	-	7	-	-
Cr	ND	ND	10	9	3	13	3	11	7	3
Co	37	56	64	54	69	81	81	116	28	93
Ni	ND	ND	ND	11	ND	ND	ND	ND	ND	ND
Cu	27	33	2766	97	153	37	121	1028	37	563
Au (ppb)	-	-	-	-	-	-	-	-	-	-
Zn	172	377	91	2686	251	46	98	231	543	91
Pb	26	68	ND	237	45	ND	17	37	46	57
Th	-	-	-	19.0	12.5	-	-	8.2	-	-
La				53.4	15.9					
Ce				114.3	36.0					
Nd				61.6	21.1					
Sm				13.3	4.7					
Eu				1.76	0.71					
Gd				12.6	3.7					
Dy				14.5	-					
Er				10.19	2.8					
Yb				9.1	3.6					
Fe ²⁺ /ΣFe	0.91	0.94	0.92		1.00	0.94	0.99		0.88	

* Total iron expressed as FeO

Table V - 1c) Continued (Stockwork rocks)

	21-738	21-756.5	8-504.4	b1s-246.5	8-466.1	8-479.5	8-483.5	21-734	21-778	21-800.5
SiO ₂	76.77	61.32	68.11	69.55	44.38	52.18	35.52	67.94	63.48	30.08
TiO ₂	0.04	0.14	0.10	0.09	0.10	0.14	0.14	0.09	0.11	0.26
Al ₂ O ₃	5.33	11.59	8.73	8.87	8.04	11.18	13.08	7.96	10.53	21.17
Fe ₂ O ₃	0.28	1.07		0.97					0.71	1.62
FeO	8.74	13.98	11.92*	15.08	28.33*	20.91*	27.64*	14.86*	10.66	6.49
MnO	0.43	0.14	0.12	0.13	0.12	0.26	0.34	0.27	0.21	0.47
MgO	1.72	6.86	4.73	1.73	3.79	4.96	5.23	3.13	8.76	27.72
CaO	1.77	ND	0.04	ND	ND	ND	ND	ND	ND	0.56
BaO	0.02	0.04	0.01	ND	ND	ND	ND	ND	ND	ND
Na ₂ O	ND	ND	ND	ND	ND	ND	ND	ND	ND	ND
K ₂ O	ND	ND	ND	ND	ND	ND	ND	ND	ND	ND
F ₂ O ₅	ND	ND	ND	ND	ND	ND	ND	ND	ND	ND
LOI	4.21	4.33	3.69	3.63	12.69	6.94	9.21	4.93	5.36	12.12
TOTAL	99.31	99.47	97.46	99.26	97.46	96.57	91.16	98.78	99.82	100.49
SK	0.87	ND	2.13	1.44	13.96	4.27	8.62	2.47	1.70	ND
Rb	5	7	7	5	7	5	5	3	ND	ND
Sr	29	2	4	1	2	ND	3	ND	3	12
Ba	158	371	129	50	ND	49	31	19	11	ND
Sc	-	-	6.7	6.8	6.6	8.1	-	-	-	18.0
Y	27	67	47	46	37	51	53	43	60	132
Zr	72	202	148	144	143	188	143	134	170	314
Hf	-	-	5	5	5	6	-	-	-	10
Nb	7	16	14	12	18	17	23	11	5	24
Ta	-	-	15	12	17	15	-	-	-	3
Cr	4	1	11	14	10	9	12	2	ND	16
Co	96	66	71	93	96	84	90	77	42	25
Ni	ND	ND	ND	ND	ND	ND	ND	ND	ND	3
Cu	120	ND	3214	407	431	4818	17299	971	46	ND
Au(ppb)	-	-	32	-	-	100	-	-	-	-
Zn	188	319	98	128	100	119	237	251	1022	1096
Pb	16	23	19	ND	67	42	67	38	246	740
Th	-	-	8.3	7.9	7.0	10.0	-	-	-	21.0
La			38.9			46.9				163.8
Ce			73.7			86.7				290.3
Nd			36.1			41.9				133.0
Sm			7.9			9.1				25.2
Eu			1.03			1.24				2.3
Gd			7.3			8.5				16.5
Dy			5.8			7.5				10.3
Er			3.6			4.7				7.1
Yb			4.0			5.0				9.6
Co ²⁺ /Zn	0.97	0.94		0.96					0.94	0.82

Table V - 1d) Massive sulphide ores.

(*)	bis 166.5	bis 180	bis 187.2	bis 196.7	bis 201.7	8-369.25	8-369.8	8-371.1	8-384.5	8-397.2
CuS	0.52	0.19	0.16	0.22	0.12	0.12	0.12	0.13	0.13	0.11
Zn	3.79	10.24	2.60	4.53	2.03	3.56	3.56	4.02	0.36	2.83
Pb	3.07	4.79	0.63	2.23	0.15	2.90	2.90	1.82	0.15	1.66
As	1.05	0.27	0.41	1.09	0.14	0.88	0.88	1.05	0.88	1.17
SZ	35.05	36.56	19.86	44.16	52.00	39.11	26.00	36.57	50.46	30.39
Sr ppm	4	13	112	23	7	5	129	20	27	221
Ba	567	368	2546	<1	<1	326	1229	2300	2730	59300
Sc	<0.5	<0.5	-	-	0.2	0.4	<0.1	-	0.2	<0.1
Y	52	98	44	26	2	8	96	19	17	31
Zr	66	106	101	45	21	32	78	34	31	90
Hf	<5	<5	-	-	<1	<1	<5	-	<5	<5
Ta	<5	<5	-	-	2	5	<5	-	10	<5
Cr	<5	<5	6	6	5	<5	<5	<5	<5	<5
Co	74	48	54	83	121	76	21	83	71	25
Ni	8	23	9	7	<5	<5	24	7	<5	18
Th	<0.5	1.5	-	-	0.9	1.5	<0.1	-	<0.1	<0.1
La	10.8									
Ce	25.9									
Md	11.7									
Sm	3.1									
Eu	1.63									
Gd	3.1									
Dy	3.3									
Er	2.3									
Yb	2.7									

(*) Cu, Zn, Pb and As are drillhole assays of 1 metre long intervals (Pirites Alentejans, unpublished data).

Table V - 1d) Continued (Massive sulphide ores)

	8-404.6	8-413	8-414	8-425	8-436	8-446.86	8-464.4	8-466.7
Cu%	0.24	0.20	0.25	0.39	0.64	0.72	1.81	2.98
Zn	5.45	5.16	7.50	11.24	1.68	3.27	2.13	2.99
Pb	3.17	3.12	3.33	2.62	0.62	0.90	0.86	0.73
As	1.75	1.08	0.77	0.61	0.55	1.10	0.50	0.80
Si	41.40	43.25	40.49	36.23	45.52	42.98	36.88	38.74
Sr ppm	<2	31	11	<2	17	15	26	15
Ba	119	147	73	103	26	6	516	171
Sc	-	-	0.3	<0.5	-	0.7	-	3.6
Y	63	46	44	59	15	38	69	25
Zr	71	61	56	66	29	57	75	70
Hf	-	-	<1	<2	-	-	-	4
Ta	-	-	9	6	-	-	-	20
Cr	<5	<5	<5	<5	<5	<5	7	11
Co	55	60	63	40	93	88	73	97
Ni	13	7	5	12	<5	9	<5	<5
Th	-	-	0.1	0.6	-	-	-	5.0
La						7.5		
Ce						15.6		
Nd						6.3		
Sm						1.58		
Eu						0.51		
Gd						1.48		
Dy						1.44		
Er						0.91		
Yb						0.73		

Table V-2a) Cherts and jaspers

	bis-100.2	bis 161	bis 166	LC5 243.8	8-361.1	11-322	11-351.9	14-129.5	14-133.4	15-315
SiO ₂	84.94	81.84	97.17	81.37	59.09	91.66	75.98	83.83	89.27	86.47
TiO ₂	ND	ND	ND	ND	0.01	ND	ND	ND	ND	ND
Al ₂ O ₃	0.06	0.29	0.01	2.66	1.27	1.50	0.26	0.25	0.06	0.37
Fe ₂ O ₃	5.67	0.20	1.10*	9.53*	10.29*	0.26	17.27*	9.86*	1.89	6.53
FeO	5.39	2.09				3.31			5.22	3.96
MnO	0.09	0.38	0.02	0.33	0.24	0.69	0.24	0.72	0.29	0.59
MgO	ND	0.02	ND	0.88	0.18	0.51	0.07	0.14	0.01	0.18
CaO	0.97	7.97	0.30	0.93	6.78	ND	3.22	ND	ND	ND
BaO	ND	0.46	ND	ND	4.52	ND	ND	ND	ND	0.01
Na ₂ O	ND	ND	ND	ND	ND	ND	ND	ND	ND	ND
K ₂ O	ND	ND	ND	ND	ND	ND	ND	ND	ND	ND
P ₂ O ₅	0.07	0.08	ND	0.04	ND	ND	0.21	0.09	0.02	0.12
LOI	2.08	6.87	0.98	3.83	13.57	1.55	1.15	5.36	2.16	1.06
TOTAL	99.27	100.20	99.58	99.57	95.95	99.46	98.40	100.25	99.00	99.29
SS	0.64	0.61	0.83	2.95	11.25	0.06	0.08	3.19	0.81	0.10
Rb	3	3	3	2	10	2	5	3	1	3
Sr	32	93	2	17	484	3	129	5	3	6
Ba	68	4103	11	10	40600	5	14	4	30	104
Sc	0.4	0.5	<0.1	-	-	-	-	-	-	0.3
Y	2	10	ND	10	6	ND	9	3	3	9
Zr	25	22	16	18	80	19	27	21	21	25
Hf	<1	<1	<1	-	-	-	-	-	-	<1
Nb	ND	9	17	5	ND	14	ND	9	10	11
Ta	8	5	14	-	-	-	-	-	-	11
Cr	17	8	5	18	6	11	41	9	13	17
Co	135	79	203	118	43	148	93	151	148	121
Ni	33	28	8	21	149	48	7	16	17	17
Cu	82	33	90	81	53	56	31	59	48	58
Au (ppb)	11	14	15	-	-	-	51	-	110	20
Zn	36	237	33	71	129	30	21	298	20	51
Pb	ND	36	ND	ND	33	ND	25	127	ND	ND
Th	0.4	0.2	0.2	-	-	-	-	-	-	0.3
La							14.7			7.0
Ce							15.7			7.7
Nd							9.8			6.5
Sm							2.5			1.76
Eu							0.57			0.38
Gd							3.3			2.3
Dy							4.1			2.3
Er							2.7			1.46
Yb							2.8			1.25
Fe ²⁺ /ΣFe	0.81	0.82				0.83			0.75	0.80

* Total iron

(a) Major element abundances estimated from metal analysis

(b) Cherts and jaspers >500 m away from known sulphide mineralization. All others above Feltita-Estaca massive sulphide orebody.

Table V-2a) Continued (Cherts and jaspers)

	15-319.3	15-329	16-252	11-341NV	(a) S1-328.7	(a) S2-430B	(a) S2-430	(a,b) S2-377.8	(a,b) S3-380	(a,b) JR-38-R
SiO ₂	83.69	89.64	90.19	91.41	82	85	85	85	86	96
TiO ₂	ND	ND	ND	ND						
Al ₂ O ₃	0.28	0.10	0.11	0.07						
Fe ₂ O ₃	10.67	7.48	2.84	1.71	15	10	10	10	10	2
FeO	3.43	0.69	2.12	3.87						
MnO	0.10	0.21	1.34	0.57	1					
MgO	ND	ND	ND	0.01						
CaO	0.48	0.49	0.90	0.64	2	1	1	1	1	
BaO	ND	ND	ND	0.01						
Na ₂ O	0.07	ND	ND	ND						
K ₂ O	ND	ND	ND	ND						
P ₂ O ₅	0.67	ND	ND	ND						
LOI	ND	0.90	2.07	0.74						
TOTAL	99.39	99.49	99.55	99.12						
Sr	0.22	0.11	0.07	ND	-	-	-	-	-	-
Rb	1	2	2	1	5	ND	3	3	3	ND
Sr	10	11	29	49	298	28	30	4	3	3
Ba	32	3	19	862	111	211	210	ND	ND	2
Sc	<0.1	0.3	-	-	-	-	-	-	-	-
Y	14	4	2	6	19	6	6	9	9	4
Zr	23	21	25	22	27	21	21	20	24	21
Hf	<1	<1	-	-	-	-	-	-	-	-
Nb	6	11	10	15	3	4	2	9	18	16
Ta	14	7	-	-	-	-	-	-	-	-
Cr	11	20	11	9	7	14	12	11	ND	ND
Co	208	113	88	152	64	101	180	120	135	73
Ni	20	16	18	31	12	10	7	23	-	ND
Cu	54	45	23	63	114	37	33	12	-	11
Au (ppb)	29	-	-	-	-	-	-	-	-	-
Zn	15	8	19	ND	23	ND	ND	23	ND	5
Pb	13	ND	ND	17	20	28	20	ND	ND	ND
Th	<0.1	<0.1	-	-	-	-	-	-	-	-
La	14.9	5.8	4.9							
Ce	9.7	4.6	3.5							
Md	14.4	3.8	3.9							
Sm	3.4	0.86	1.06							
Eu	0.82	0.22	0.39							
Gd	-	-	1.33							
Dy	4.6	1.49	1.64							
Er	2.6	1.04	1.12							
Yb	2.2	1.62	1.28							
Fe ²⁺ /ΣFe	0.26	0.09	0.46							

(a) Major element abundances estimated from modal analysis

(b) Ajpy from sulphide mineralization

Table Y-2a) Continued (Cherts and jaspers)

	(b) JR-34	(b) JR-35	(a,b) SF-11	(a,b) SF-12	(a,b) SF-31	(a,b) SF-41	(a,b) SF-42	(a,b) SN-13A	(a,b) SN-13B	(a,b) SN-13C
SiO ₂	97.88	79.10	90	90	95	97	98	90	90	97
TiO ₂	ND	ND								
Al ₂ O ₃	0.03	ND								
Fe ₂ O ₃	1.99*	20.55*	5	2	3	0.5	0.5	2	5	0.5
FeO										
MnO	0.01	0.06	3	1	0.5	0.5	0.1	1	5	0.5
HgO	ND	ND								
CaO	ND	ND								
BaO	ND	ND								
Nb ₂ O ₅	ND	ND								
K ₂ O	ND	ND								
P ₂ O ₅	ND	0.02								
LOI	0.09	ND								
TOTAL	100.00	99.73								
Si	ND	ND	-	-	-	-	-	-	-	-
Rb	ND	3	ND	ND	ND	ND	ND	ND	ND	ND
Sr	2	3	95	158	20	21	133	12	19	74
Ba	ND	ND	10	9	17	11	ND	6	209	30
Sc	-	-	-	0.9	-	0.2	-	-	-	0.2
Y	7	9	7	7	8	8	5	3	7	6
Zr	26	25	23	24	22	24	18	14	23	20
Hf	-	-	-	1	-	1	-	-	-	1
Nb	17	7	10	11	12	-	13	4	9	17
Ta	-	-	-	8	-	8	-	-	-	14
Cr	9	11	3	15	7	8	ND	19	5	7
Co	65	98	82	72	70	66	101	65	49	63
Ni	ND	ND	ND	ND	11	ND	11	ND	6	ND
Cu	ND	23	91	17	29	15	29	29	33	ND
Au (ppb)	-	-	-	-	-	<1	-	-	-	8
Zn	ND	ND	16	ND	9	ND	ND	17	20	11
Pb	ND	16	ND	ND	ND	21	15	ND	ND	18
Th	-	-	-	0.5	-	0.2	-	-	-	0.2
La										
Ce										
Nd										
Sm										
Eu										
Gd										
Dy										
Er										
Yb										
Fe ²⁺ /ΣFe										

(a) Major element abundances estimated from modal analysis

(b) Assay from sulphide mineralization

Table V-2a) Continued (Cherts and jaspers)

	(a,b) SM-1300	(a,b) SM-1303	(b) SM-14	(a,b) SM-140
SiO ₂	90	90	86.92	86
TiO ₂			ND	
Al ₂ O ₃	5	5	13.24*	5
FeO				
MnO	5	5	0.01	10
MgO			ND	
CaO			ND	
BaO			ND	
Na ₂ O			ND	
K ₂ O			ND	
P ₂ O ₅			ND	
LOI			0.38	
TOTAL			99.55	
Si	-	-	ND	-
Rb	3	3	ND	2
Sr	10	8	6	83
Ba	ND	10	ND	45
Sc	-	-	-	1.6
Y	16	11	7	9
Zr	17	13	25	22
Hf	-	-	-	81
Nb	10	13	6	11
Ta	-	-	-	10
Cr	21	20	16	130
Co	118	122	68	96
Ni	ND	ND	ND	ND
Cu	ND	ND	ND	30
Mn (ppb)	-	-	-	-
Zn	486	178	32	74
Pb	90	ND	22	149
Th	-	-	-	0.4
La				
Ce				
Pr				
Nd				
Sm				
Eu				
Gd				
Dy				
Er				
Tb				
Fe ²⁺ /ΣFe				

Table V-2b) Metalliferous sediments

	LCS-240	6-103.4	6-106.9	9-285	11-343.7	16-253.4	51-229.7	(a) SF-6	(a) SF-21	(a) SF-22	(a) SM-138
SiO ₂	47.19	36.06	17.15	12.96	13.56	31.23	21.26	[2]	[2]	[2]	[2]
TiO ₂	0.09	0.03	0.37	0.04	0.19	0.04	0.13				
Al ₂ O ₃	2.53	1.72	6.49	2.34	3.92	2.78	6.54				
Fe ₂ O ₃	2.79*	0.88	12.75	15.20	32.35*	13.91*	15.67	[3]	[0.5]	[1]	[0.5]
FeO		6.15	23.86	12.99			36.56				
MnO	18.31	18.14	10.21	11.16	12.96	17.14	1.44	[86]	[96]	[90]	[96]
MgO	1.70	1.09	2.07	0.58	1.63	1.70	1.61				
CaO	7.72	13.66	5.20	18.49	16.97	10.07	0.75				
BaO	0.08	ND	ND	2.18	0.53	ND	0.06				
Na ₂ O	ND	ND	ND	ND	ND	ND	ND				
K ₂ O	0.40	ND	ND	ND	ND	ND	0.01				
P ₂ O ₅	ND	0.02	0.92	0.12	0.26	ND	0.30				
LOI	18.73	22.79	19.43	23.48	18.38	12.29	14.80				
TOTAL	99.54	99.51	96.46	99.53	100.73	89.16	98.13				
SS	0.16	0.30	0.21	0.27	0.17	5.80	1.37				
Rb	29	7	11	16	11	7	29	10	17	18	19
Sr	157	161	111	609	433	122	113	41	894	586	537
Ba	745	ND	5	19600	4713	44	573	74	2006	4623	12300
Sc		1.4	6.8	1.6			6.5	0.7	9.1		0.7
Y	15*	21	145	28	47	25	38	21	102	76	46
Zr	37	52	109	64	78	70	58	48	96	21	22
Hf		1	2	<1			1	<1	1		<1
Nb	ND	9	22	5	34	9	36	48	31	25	27
Ta		3	2	<1			1	3	2		2
Cr	20	14	64	19	27	10	34	21	28	24	22
Co	19	34	90	43	43	40	127	6	41	33	19
Ni	31	171	399	51	200	133	13	49	961	636	5
Cu	370	581	61	43	ND	96	ND	ND	500	257	ND
As (ppb)		15	63	21						380	240
Zn	70	101	493	325	376	297	247	166	584	475	732
Pb	33	17	ND	30	33	31	54	34	44	24	21
Th		0.6	5.8	1.3			2.6	0.7	2.0		<0.1
La		118.0	152.1					31.5			
Ce		152.5	138.6					36.3			
Nd		66.8	80.3					16.3			
Sm		13.2	13.9					2.9			
Eu		4.2	3.1					0.86			
Gd		12.1	12.8					3.0			
By		17.4	10.3					7.5			
Er								1.69			
Yb		13.3	4.7								
Fe ²⁺ /ΣFe		0.88	0.88	0.49			0.72				

* Total iron

(a) Major element abundances estimated from model analysis; these samples >400 m may be from sulphide mineralization.

FEITA

ALJUSTREL MINES

ALJUSTREL OREBODIES

GEOLOGY of LEVEL 200

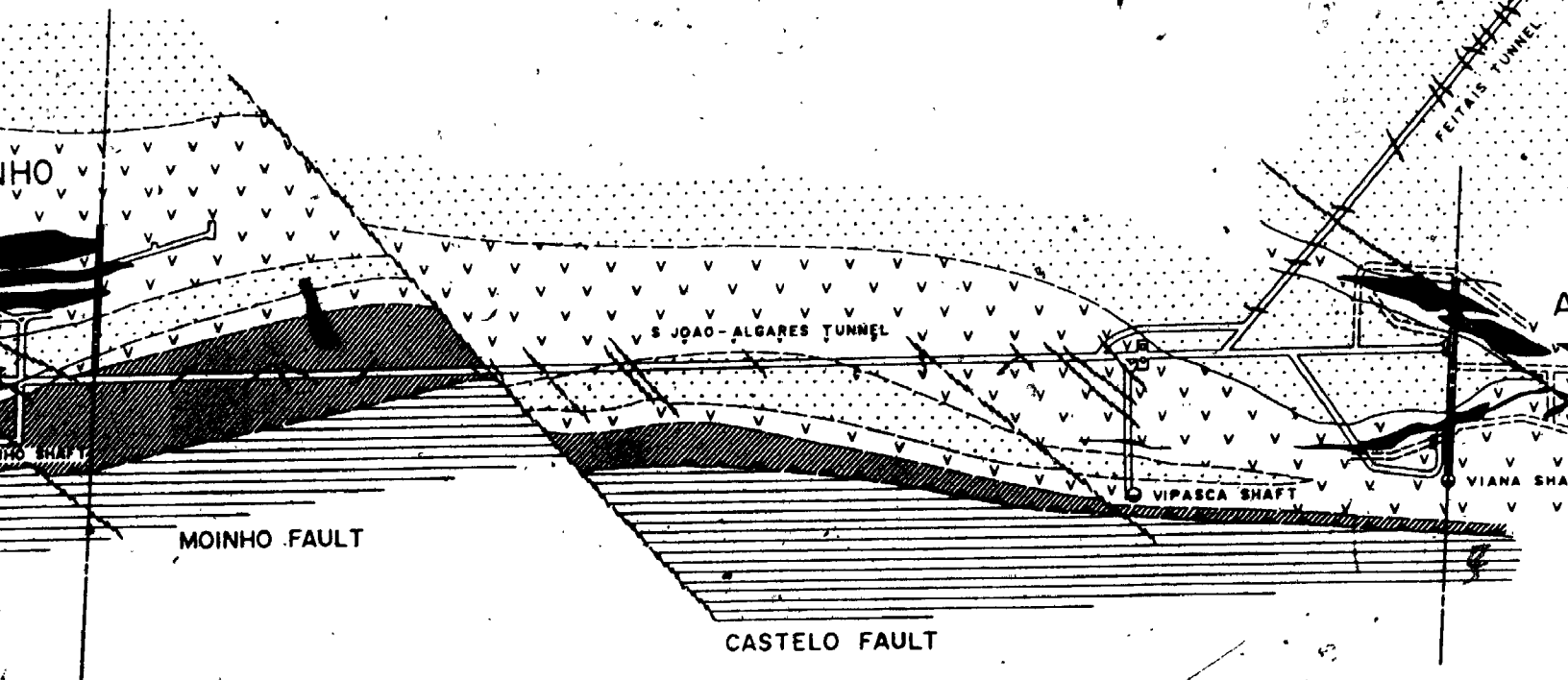
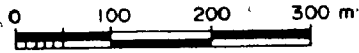


Table V-3b)- Continued (PS Fm phyllites)

	(b) 8-346	(b) 8-355.7	(b) S2-425.3
SiO_2	70.18	61.75	69.00
TiO_2	0.67	0.71	0.66
Al_2O_3	14.82	15.59	15.39
Fe_2O_3	1.03		
FeO	3.04	10.40	5.43
MnO	0.17	0.49	0.06
MgO	1.43	2.59	1.87
CaO	0.64	ND	ND
NaO	0.29	0.22	0.34
Ni_2O	1.17	0.89	ND
K_2O	3.30	2.96	3.61
P_2O_5	0.02	0.09	0.03
LOI	3.33	3.67	3.22
TOTAL	100.31	99.25	99.26
SS	0.03	0.02	ND
Rb	220	230	277
Sr	88	59	34
Ba	2636	1976	3090
Sc	13.0	-	13.0
Y	33	39	28
Zr	141	154	155
Hf	4	-	4
Nb	21	15	23
Ta	2	-	4
Xe	85	76	80
Co	21	51	34
Ni	52	71	170
Cu	119	20	49
Au (ppb)	30	-	-
Zn	54	196	140
Pb	ND	ND	14
Th	9.0	-	8.9
La			
Ce			
Nd			
Sm			
Eu			
Gd			
Dy			
Er			
Tb			
$\text{Fe}^{2+}/\text{zFe}$	0.77		

Table V-3b) Little altered and unaltered PS rocks.

	(a) 15-330.2	(a) 15-283.5	(a) GF-86	(b) b15-134	(b) b15-143.1	(b) b15-150.2	(b) LCS-242.6	(b) 8-291.25	(b) 8-308.5	(b) 8-310.6
SiO ₂	47.77	59.01	56.46	80.93	52.90	80.34	39.40	60.29	79.11	74.59
TiO ₂	0.30	0.19	0.86	0.26	0.74	0.34	1.19	0.63	0.47	0.56
Al ₂ O ₃	23.58	23.76	23.37	7.86	20.51	8.91	29.96	16.94	10.63	12.61
Fe ₂ O ₃	1.60		1.25		1.66	0.57		1.20	0.93	
FeO	11.03	2.09*	5.24	2.19*	7.46	3.06	8.63*	6.30	1.88	2.37*
MnO	0.26	0.10	0.29	0.40	0.63	0.21	0.14	0.34	0.07	0.04
MgO	3.09	1.65	1.95	0.99	2.31	1.16	1.77	1.40	0.93	1.04
CaO	0.86	ND	0.86	0.38	0.31	0.31	0.07	2.64	ND	0.73
BaO	0.09	0.93	0.07	0.18	0.62	0.19	1.99	0.06	0.06	0.04
Na ₂ O	3.34	1.94	2.41	0.26	0.64	0.38	0.15	1.75	0.39	0.08
K ₂ O	1.01	6.07	2.77	1.67	4.24	1.74	7.15	2.99	2.62	3.35
P ₂ O ₅	0.05	ND	0.09	0.04	0.02	0.02	0.27	0.07	ND	ND
LOI	4.72	3.10	5.10	4.42	6.49	2.45	7.13	5.44	2.86	4.14
TOTAL	97.70	98.84	100.72	99.56	98.43	99.67	97.86	100.04	99.93	99.55
Si	0.06	ND	0.03	0.33	1.08	0.03	2.04	0.02	0.11	0.06
Rb	87	567	183	84	212	92	372	156	159	186
Sr	346	133	326	46	91	48	78	241	37	39
Ba	810	8367	601	1614	4675	1686	17800	444	401	376
Sc	9.3	-	16.0	-	19.0	-	-	13.0	9.3	-
Y	36	8	49	11	31	17	61	38	24	23
Zr	235	148	370	84	166	77	283	248	117	104
Hf	8	-	10	-	3	-	-	7	3	-
Nb	15	6	29	17	13	15	15	51	26	24
Ta	2	-	3	-	2	-	-	4	4	-
Cr	32	ND	37	59	84	53	118	66	47	64
Co	64	14	23	113	51	86	43	56	34	34
Ni	88	164	27	184	161	86	179	90	64	33
Cu	ND	ND	ND	130	55	39	59	-	595	75
Au (ppb)	-	-	-	-	19	-	-	-	-	-
Zn	250	33	121	136	93	55	75	-	29	26
Pb	42	ND	24	46	19	27	ND	41	81	ND
Th	24.0	-	22.0	-	13.0	-	-	11.0	6.4	-
La					20.8			41.3		
Ce					42.3			96.9		
Nd					18.9			40.5		
Sm					3.5			8.4		
Eu					0.82			2.4		
Gd					2.7			7.2		
Dy					2.1			7.5		
Er					1.40			3.7		
Tb					1.28			4.1		
Fe ²⁺ /TFe	0.88		0.82		0.83		0.86	0.88	0.89	

* Total Iron

(a) Tuffs

(b) Tuffites, phyllites

Table V-4. Major and selected trace element abundances in Culin Group rocks.

	(a) bits 109.1	(a) 11-251.9	(a) 10-250.9	(a) 16-233.7	(b) bits 119.7
SiO ₂	64.80	66.94	67.23	67.06	59.91
TiO ₂	0.70	0.67	0.67	0.78	0.75
Al ₂ O ₃	14.49	13.86	15.57	15.14	15.25
Fe ₂ O ₃ *	5.64	5.20	5.86	5.92	8.69
MnO	0.15	0.09	0.08	0.06	0.12
MgO	2.58	1.49	1.98	1.96	2.25
CaO	1.82	1.58	0.54	0.60	0.98
BaO	0.03	0.04	0.04	0.07	0.07
Na ₂ O	2.55	2.42	2.07	2.72	1.07
K ₂ O	1.42	1.61	2.09	1.39	2.33
P ₂ O ₅	0.10	0.12	0.09	0.10	0.08
LOI	5.27	5.22	3.00	2.75	8.31
TOTAL	99.56	99.24	99.22	98.54	99.81
SE	0.15	0.76	0.63	0.06	1.38
Rb	64	73	96	65	101
Sr	178	173	185	187	104
Ba	304	330	367	639	650
Sc	12.0	10.0	11.0	12.0	-
Y	27	22	23	27	27
Zr	137	138	138	149	142
Hf	4	3	4	4	-
Nb	18	15	11	12	13
Ta	3	5	4	5	-
Cr	76	53	60	75	90
Co	47	28	32	33	63
Ni	38	13	21	30	47
Cu	31	12	26	10	82
Zn	63	30	50	54	62
Pb	16	15	16	18	88
Th	7.5	6.2	7.6	7.5	-
La	29.7				
Ce	41.4				
Nd	24.1				
Sm	4.9				
Eu	1.66				
Gd	4.1				
Dy	3.7				
Er	2.1				
Yb	2.3				

* Total Iron expressed as Fe₂O₃

(a) Greywackes

(b) Black shale

APPENDIX VI

UNDERGROUND GEOLOGY

AND KEY TO SAMPLE LOCATIONS

- VI-1. Geology of level 200 of the Aljustrel mines
(After Freire d'Andrade and Schermerhorn, 1971)
- VI-2. Geologic cross section 2-2' across the Feitais
orebody (ibid.)
- VI-3. Projection of the Feitais orebody and surface
drill holes on a horizontal plane (Pirites
Alentejanas, unpublished)
- VI-4. Key to sample locations

Figure VI-1. Geology of level 200 of the Aljustrel mines.

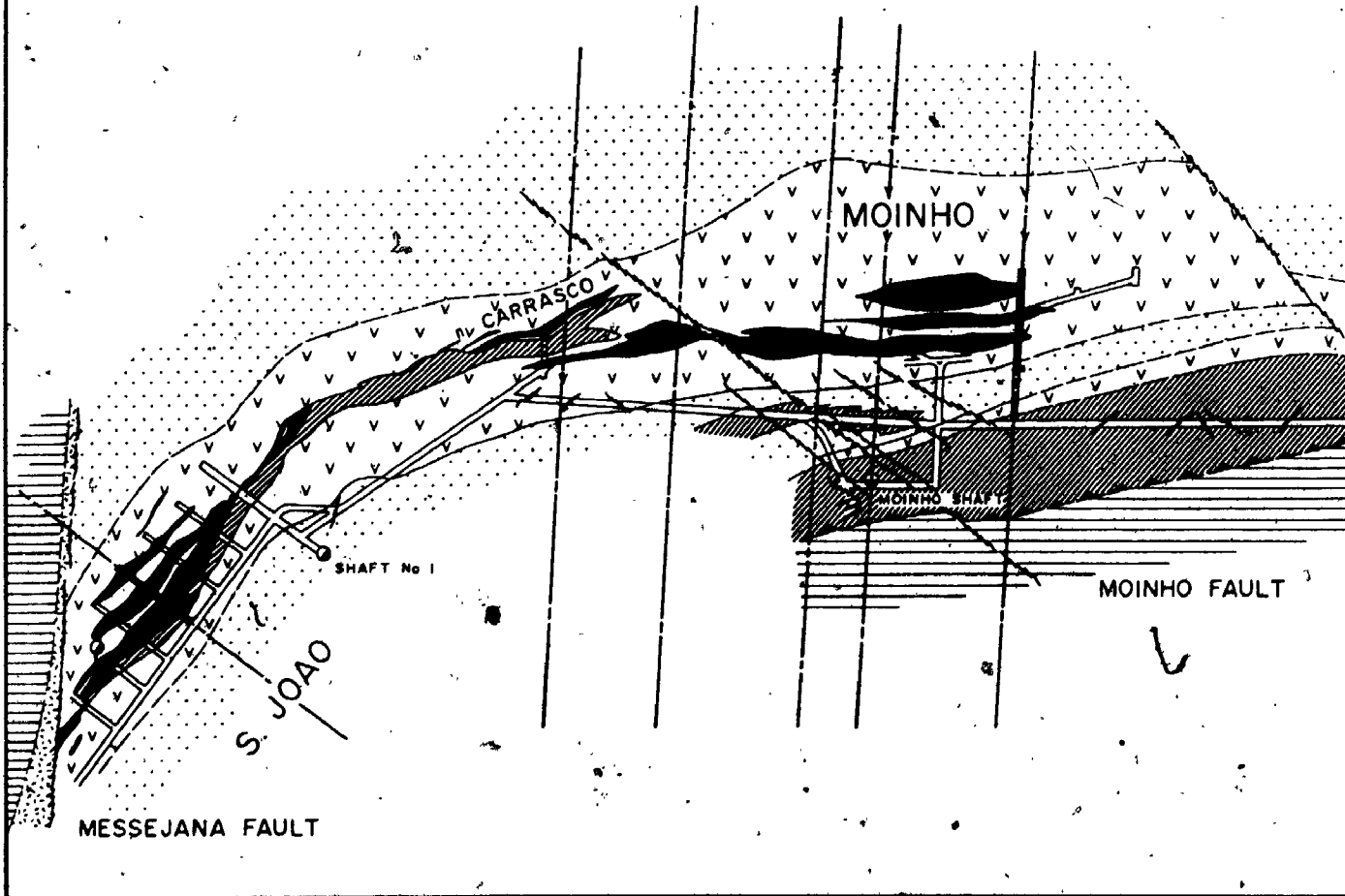
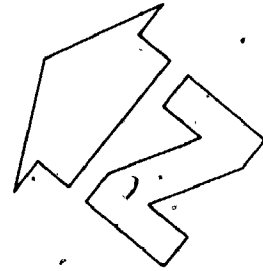
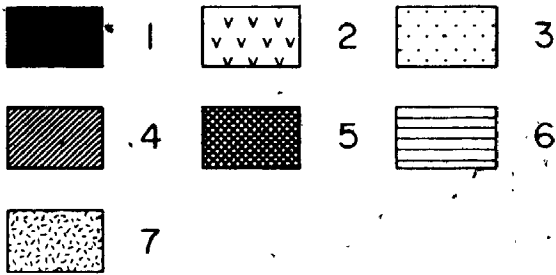
1, massive sulphide orebodies; 2, upper tuffs (mostly Green facies of both the Quartz-eye Tuff and the Mine Tuff; 3, lower tuffs (QET and MT); 4, phyllites, tuffites and tuffs of the Paraiso Siliceous Formation; 5, Jasper unit; 6, Culm Group; 7, Messejana dolerite.

After Freire d'Andrade and Schermerhorn (1971).

ALJ

ALJ

GEOL



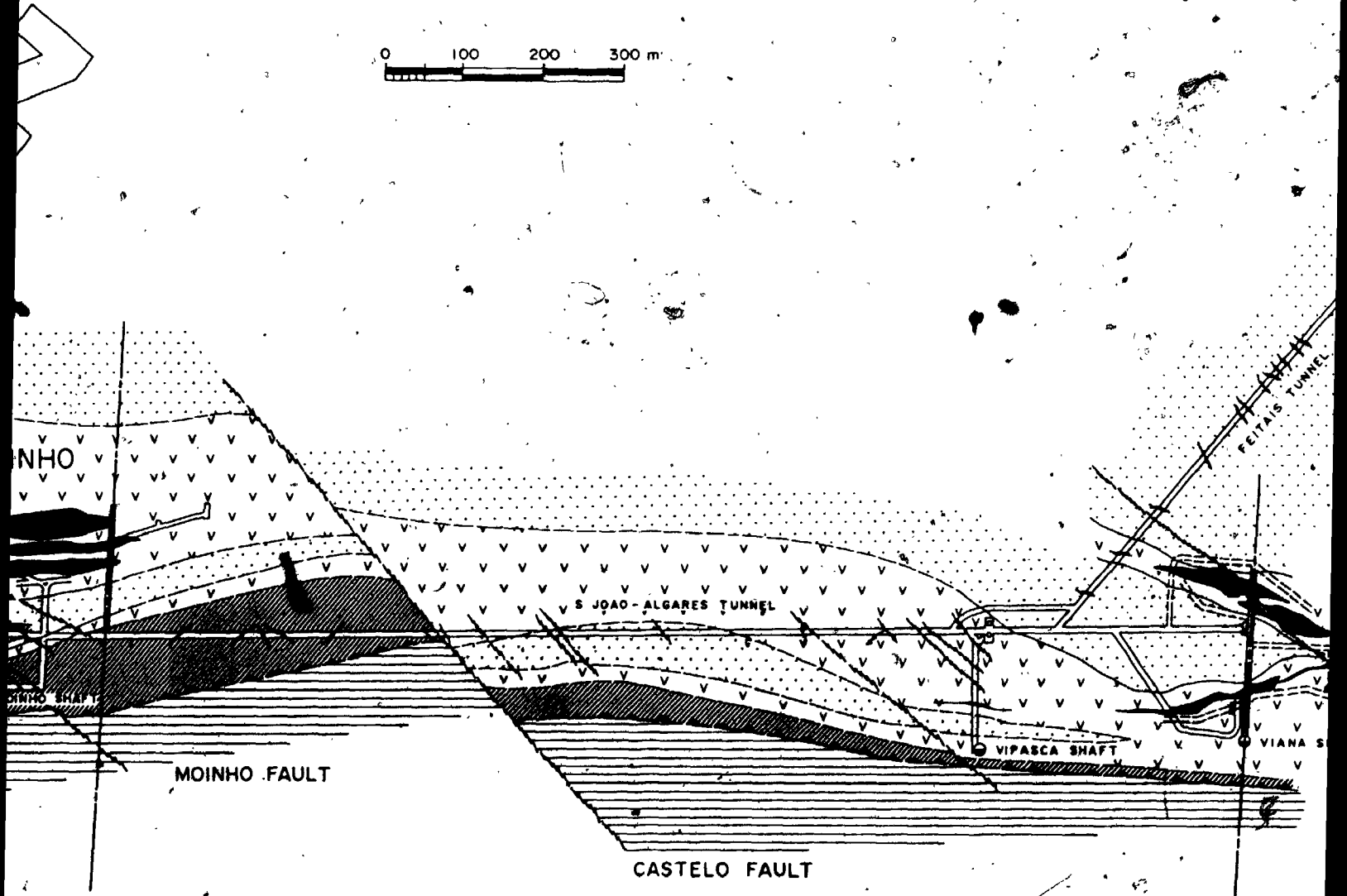
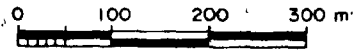
1 of

FEIT

ALJUSTREL MINES

ALJUSTREL OREBODIES

GEOLOGY of LEVEL 200



207

EL MINES

OREBODIES

LEVEL 200

200 300.m

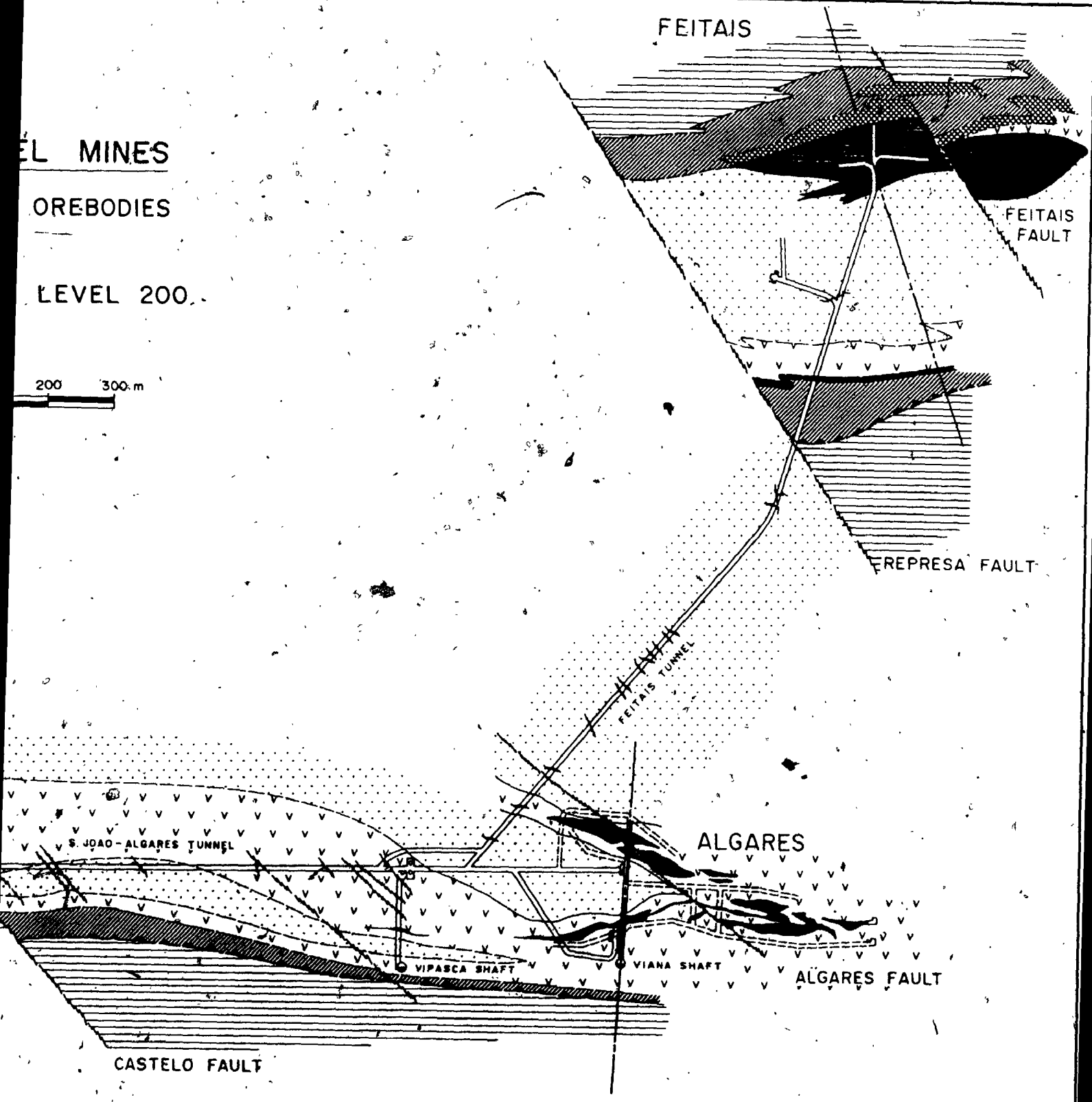


Figure VI - 1

3 of 3

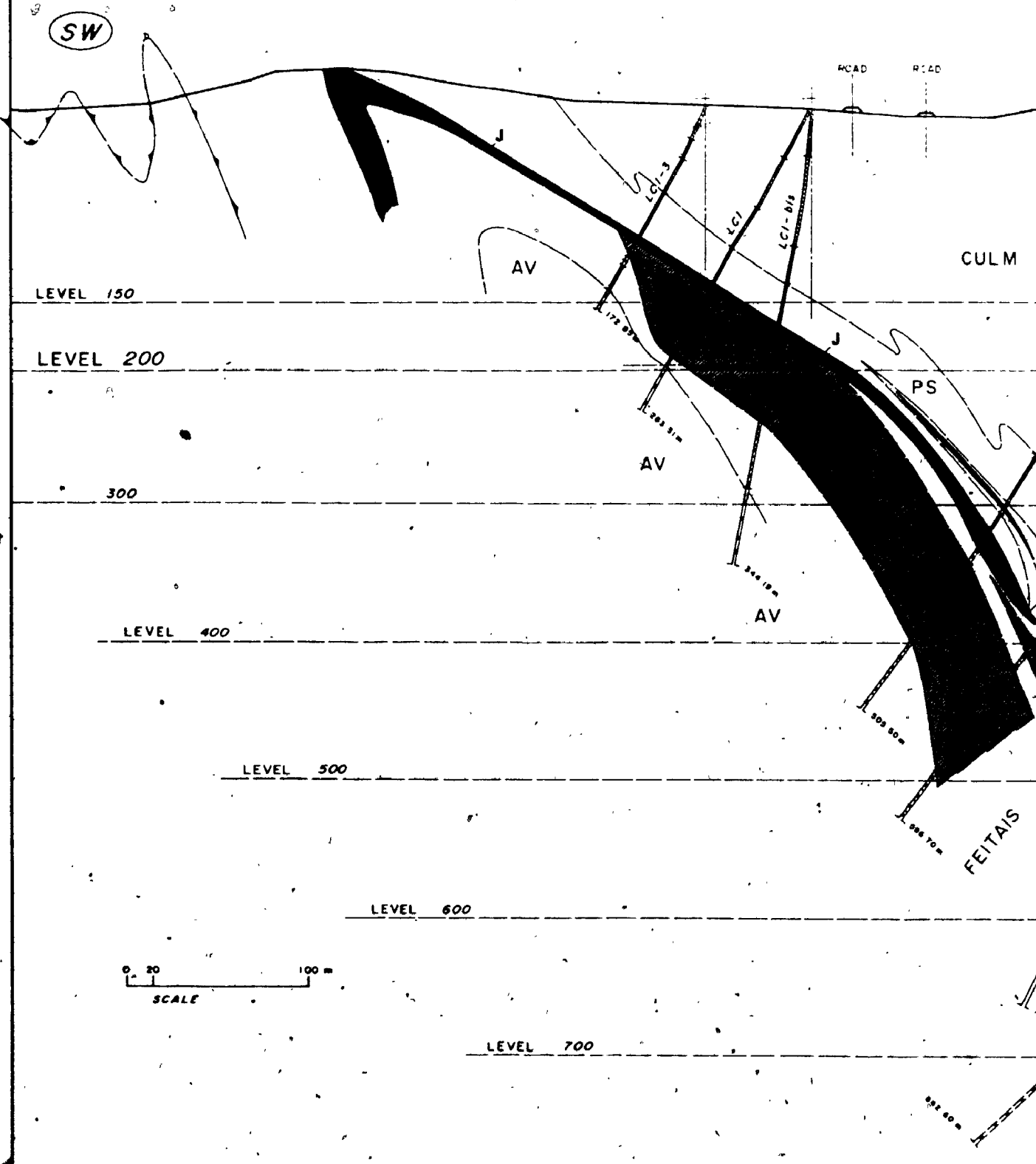
Figure VI-2. Geologic cross section 2-2' across the Feitais orebody.

PS, Paraiso Siliceous Formation; J, Jasper unit;

AV, Aljustrel Volcanics; shaded area, massive sulphide

ore. After Freire d'Andrade and Schermerhorn (1971).

FEITAIS 2-2' CROSS SECTION



106

FEITAIS 2-2' CROSS SECTION

NE

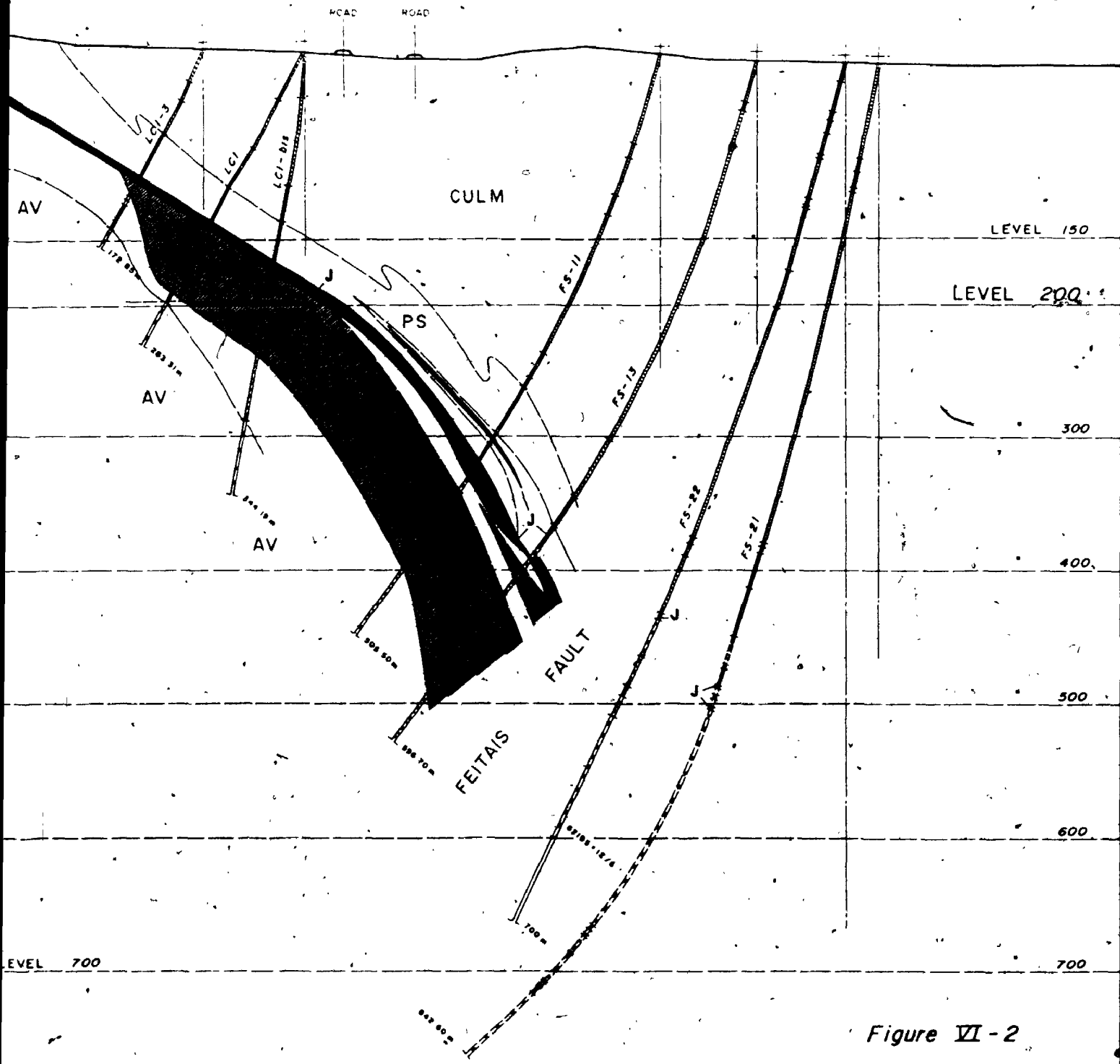


Figure VI-2

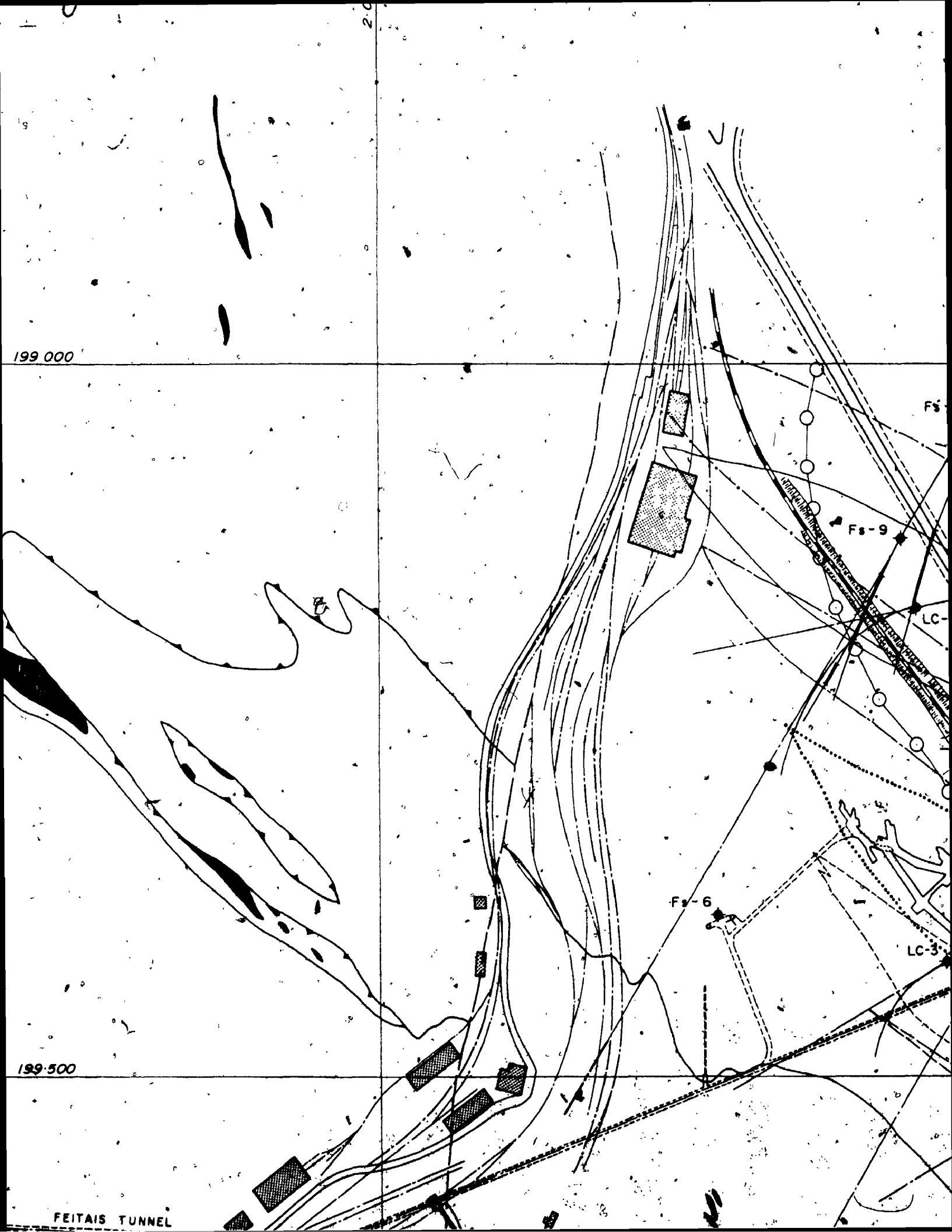
Figure VI-3. Projection of the Feitais orebody and surface drill holes on a horizontal plane (Pirites Alentejanas, unpublished).

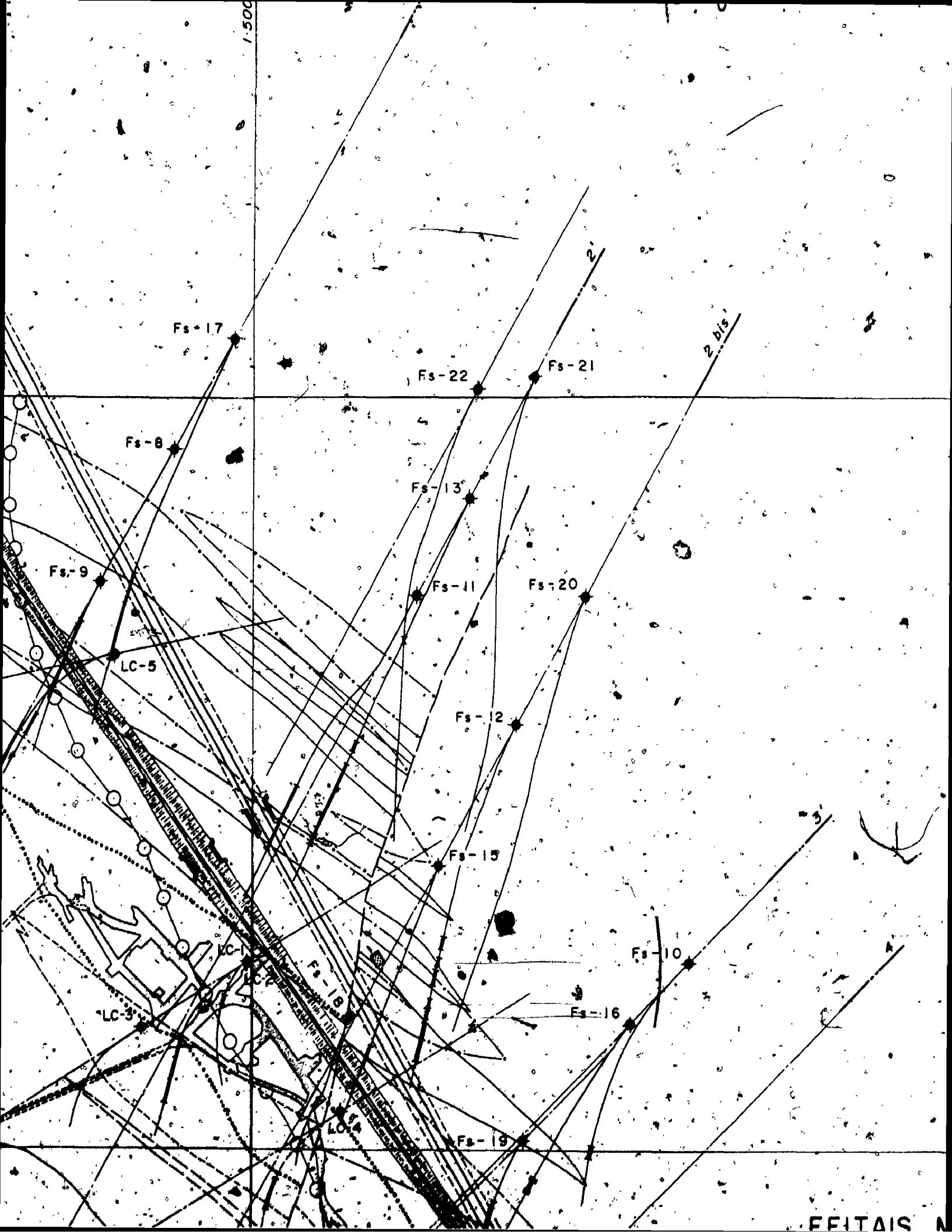
200

199 000

199 500

FEITAIS TUNNEL





1.500

Fs-17

Fs-22

Fs-21

Fs-8

Fs-13

Fs-9

Fs-11

Fs-20

LC-5

Fs-12

Fs-15

Fs-10

Fs-16

Fs-18

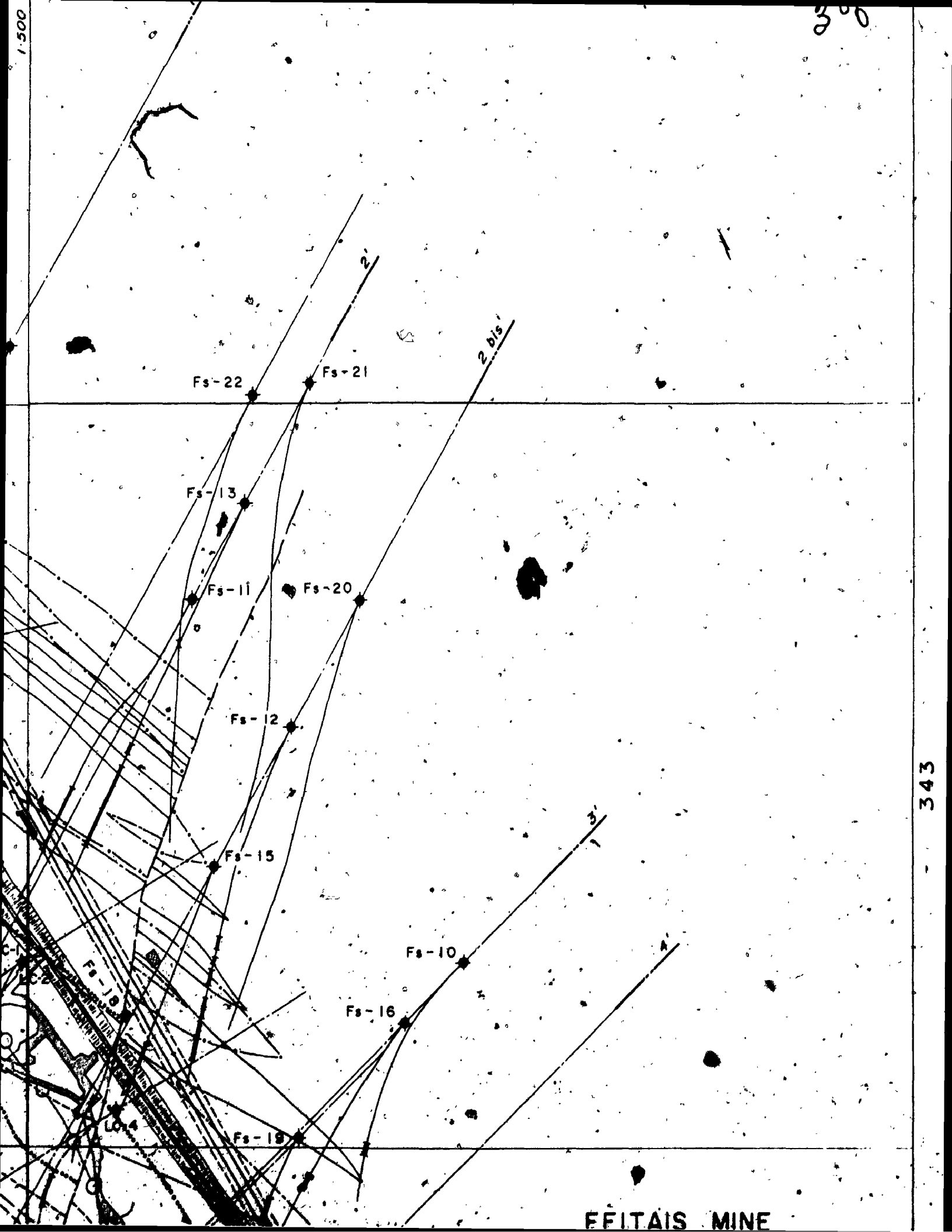
Fs-19

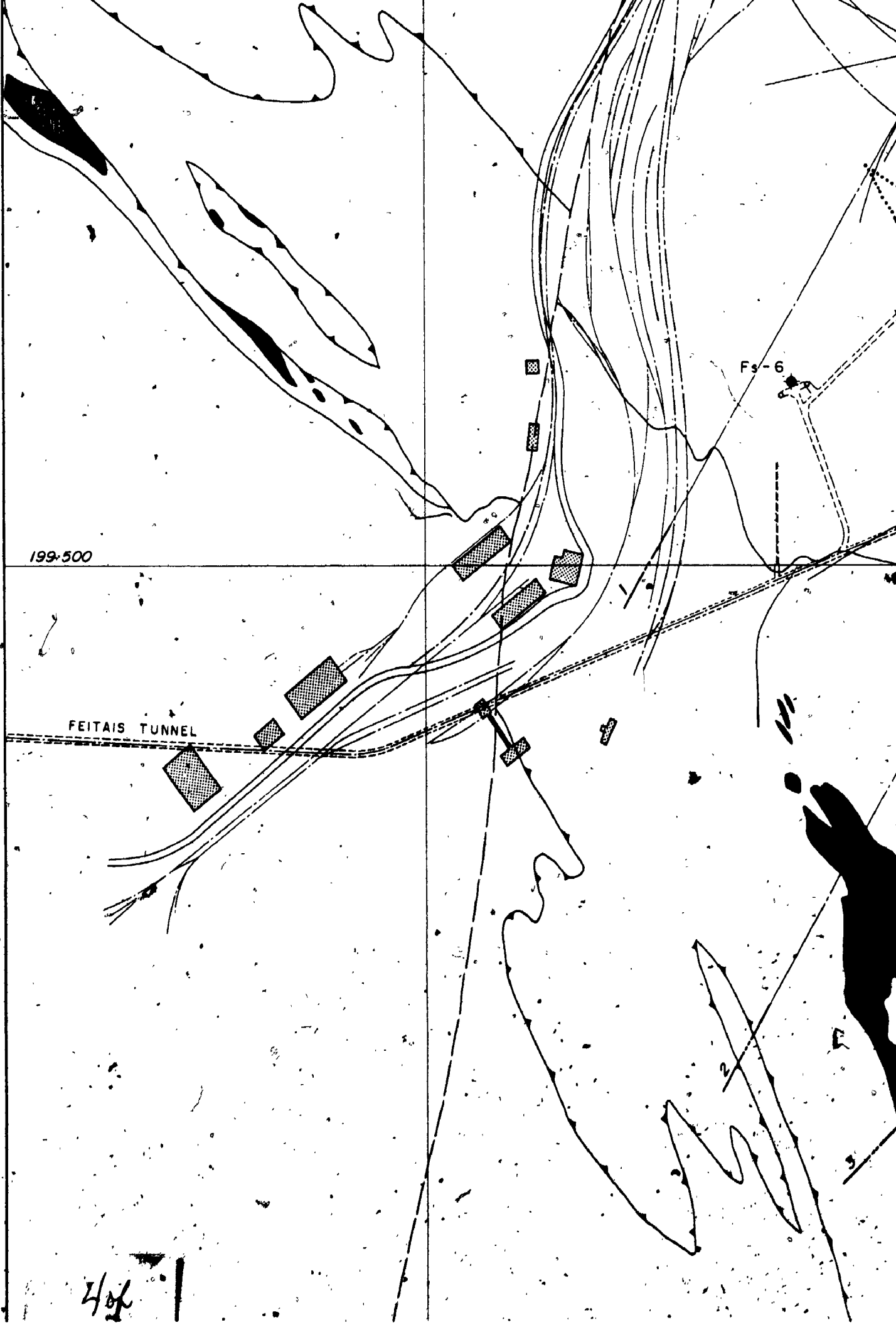
LC-3

LC-4

LC-5

FEITAIS M



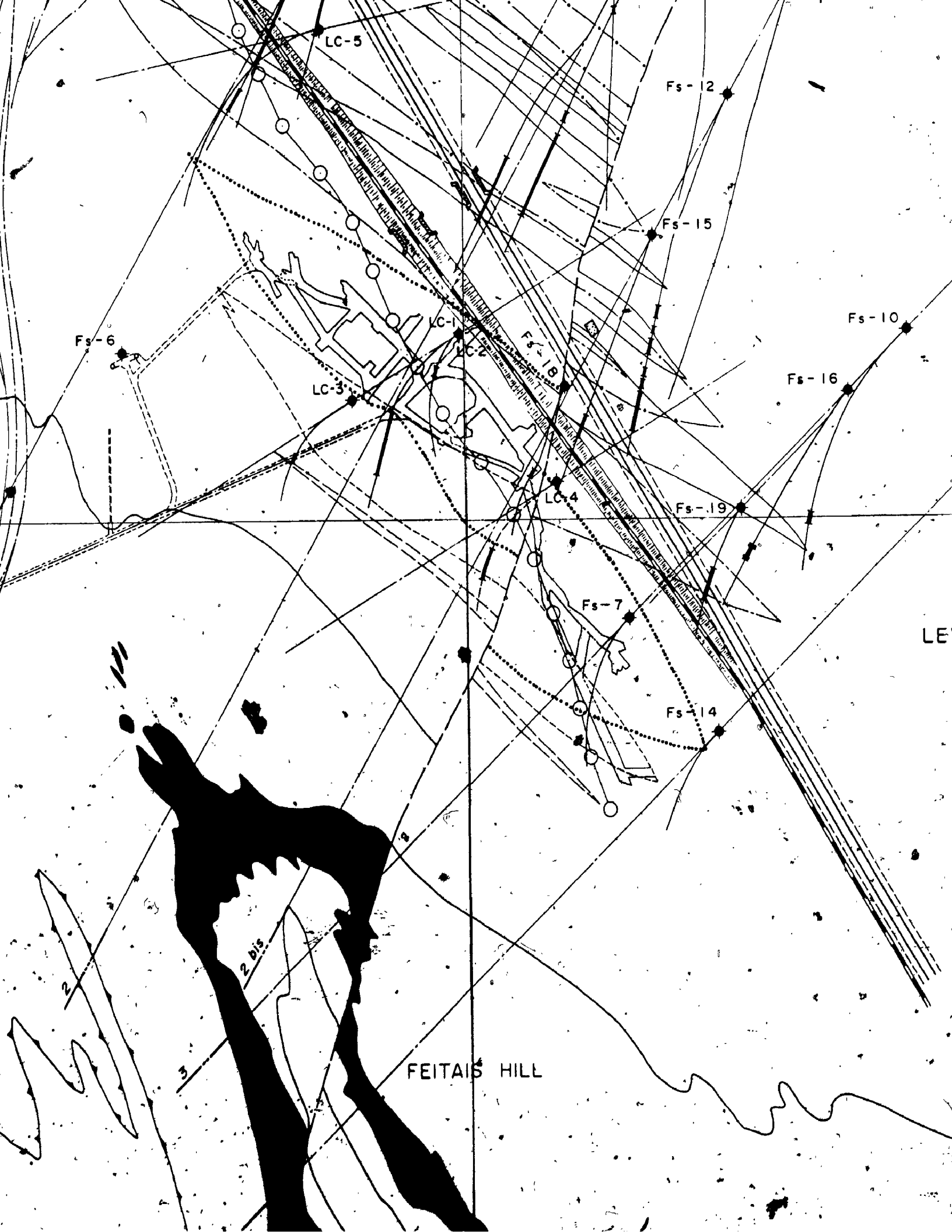


199-500

FEITAIS TUNNEL

Fs-6

404



LC-5

Fs-2

Fs-15

Fs-10

Fs-6

Fs-16

LC-3

Fs-18

LC-1

LC-2

LC-4

Fs-19

Fs-7

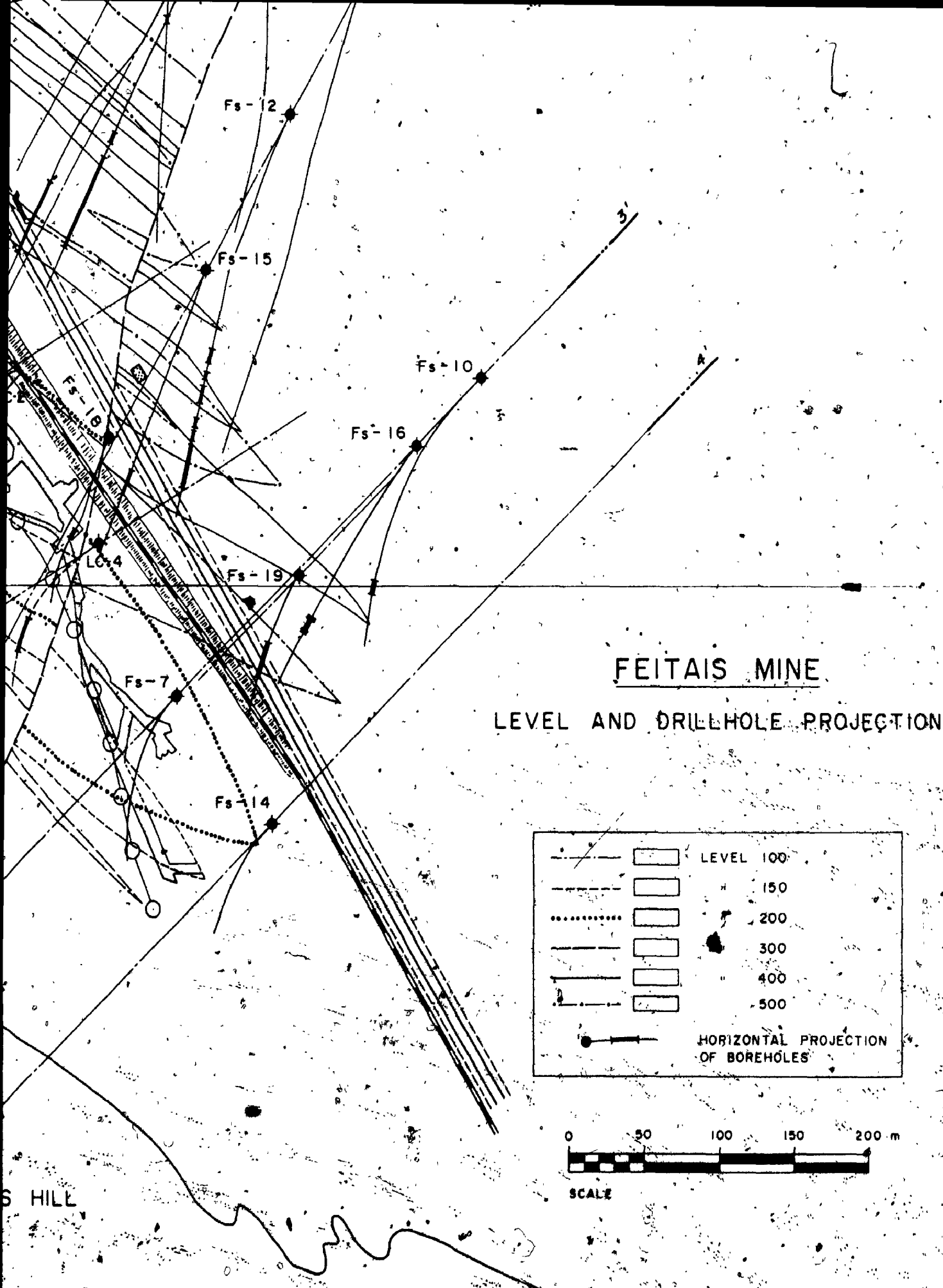
Fs-14

2 bis

3

FEITAI'S HILL

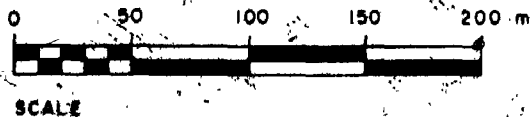
LE



FEIT AIS MINE

LEVEL AND DRILLHOLE PROJECTION

		LEVEL 100
		" 150
		" 200
		" 300
		" 400
		" 500
	HORIZONTAL PROJECTION OF BOREHOLES	



S HILL

VI-4. Key to sample locations

All sample numbers starting with numerals refer to FS drill holes; the number after the hyphen represents metres from surface (e.g. sample 15-315 was collected in drillcore FS-15, 315 metres below surface). 'bis' and LC5 refer to drill holes LC1-bis and LC5, respectively. For drill hole locations see figures VI-2 and VI-3. Samples MD4F were collected from that drillcore (see Fig. 3.4b).

Samples labelled GF were collected in the Feitais tunnel (Fig. VI-1). Surface samples were collected on hills where the Jasper unit outcrops (see Figs. 3-2 and VI-3). FS means surface in Feitais anticline; MS surface in the Moinho area; JR, jaspers remote from sulphide mineralization; PM, Moinho quarry.

REFERENCES

- Addy, S. K. (1979). Rare earth element patterns in manganese nodules and micronodules from Northwest Atlantic. *Geochim. Cosmochim. Acta* 43: 1105-1116.
- Albouy, L., Conde, L. N., Foglierini, F., Leca, X., Morikis, A., Callier, L., Carvalho, P., and Songy, J. C. (1981). Le gisement de sulfures massifs polymétalliques de Neves-Corvo (Baixo Alentejo, Sud Portugal). *Chr. Res. Miniere* 460: 5-27.
- Alderton, D.H.M., Pearce, J. A. and Potts, P. J. (1980). Rare earth element mobility during granite alteration; evidence from Southwest England. *Earth. Planet. Sci. Lett.* 49: 149-165.
- Anderson, R. N., Hobart, M. A. and Langseth, M. G. (1979). Convective heat transfer in oceanic crust and sediment in the Indian Ocean. *Science* 204: 828-832.
- Anderson, R. N., Honnorez, J., Becker, K., Adamson, A. C., Alt, J. C., Emmermann, R., Kempton, P. D., Kinoshita, H., Laverne, C., Mottl, M. J. and Newmark, R. L. (1982). DSDP hole 504B, the first reference section over 1 km through layer 2 of the oceanic crust. *Nature* 300: 589-598.
- Anderson, R. N., Langseth, M. G., and Sclater, J. G. (1977). The mechanism of heat transfer through the floor of the Indian Ocean. *J. Geophys. Res.* 82: 3391-3409.
- Anderson, R. N. and Skilbeck, J. N. (1981). Oceanic heat flow. In Emiliani, C., ed., *The Sea*, vol. 7, *The Oceanic Lithosphere*: New York, Wiley-Interscience, p. 489-524.
- Andrews, A. J. and Fyfe, W. S. (1976). Metamorphism and massive sulphide generation in oceanic crust. *Geosci. Can.* 3: 84-94.
- Appleyard, E. C. (1980). Mass balance computations in metasomatism: Metagabbro/nepheline syenite pegmatite interaction in Northern Norway, *Contrib. Mineral. Petrol.* 73: 131-144.
- Arrhenius, G. and Bonatti, E. (1965). Neptunism and volcanism in the ocean. In *Progress in Oceanography*, vol. 3, M. Sears, ed., Pergamon Press, New York, p. 7-21.

- Aye, F. and Strauss, G. K. (1975). Identification de cymerite (Ba, Al, Si₃O₈ OH) dans la province pyritense sub-iberique. Mineraux associés (La Zarza, Huelva, Espagne). C.R. Acad. Sci. Paris, T.281, Ser.D, p. 1935-1938, Paris.
- Bacon, C. R., Macdonald, R., Smith, R. L. and Baedecker, P. A. (1981). Pleistocene high-silica rhyolites of the Coso volcanic field, Inyo County, California. J. Geophys. Res., 86: B10223-B10241.
- Ballard, R. D. and Grassle, J. F. (1979). Return to Oases of the Deep. Nat. Geogr. Mag. 156: 690-705.
- Bard, J. P. (1969). Metamorphisme regional progressive des Sierras d'Aracena en Andalousie Occidentale (Espagne); sa place dans le segment Hercynien Sub-Iberique. Thesis, Fac. Sci. Montpellier, 397 p.
- Barnes, H. L. and Czamanske, G. K. (1967). Solubilities and transport of ore minerals. In Barnes, H. L., ed., Geochemistry of hydrothermal ore deposits. Holt, Rinehart and Winston, N.Y., p. 334-381.
- Barriga, F.J.A.S. and Carvalho, D. (1983). Carboniferous volcanogenic sulphide mineralizations in South Portugal (Iberian Pyrite Belt). In The Carboniferous of Portugal (in press).
- Barriga, F.J.A.S., Fyfe, W. S., Haq, Z., Macdonald, A. M. and Yifun, Z. (1983). Sea floor metamorphism. In press.
- Barriga, F.J.A.S. and Kerrich, R. (1981). High ¹⁸O fluids, circulation regimes, and mineralization at Aljustrel, Iberian Pyrite Belt. Geol. Soc. Am. Abs. W. Pgs. 13(7): 403-404.
- Battey, H. M. (1955). Alkali metasomatism and the petrology of some keratophyres from New Zealand. Geol. Mag. 92: 104-126.
- Bear, J. (1972). Dynamics of fluids in porous media. American Elsevier, New York, 764 p.
- Beaty, D. W. and Taylor, Jr. H. P. (1982). Some petrologic and Oxygen isotopic relationships in the Amulet Mine, Noranda, Quebec, and their bearing on the origin of Archean massive sulphide deposits.. Econ. Geol. 77: 95-108.

- Beaty, D. W., Taylor, Jr. H. P. and Coad, P. (1980). The Oxygen isotope geochemistry of the Kidd Creek Mine: evidence for a high ^{18}O ore-forming solution and implications regarding the genesis of volcanogenic massive sulphide deposits. Geol. Soc. Am. Abs. W. Pgs. 61: 384.
- Berner, R. A. (1969). The synthesis of framboidal pyrite. Econ. Geol. 64: 383-384.
- Bertine, K. K. and Keene, J. B. (1975). Submarine barite-opal rocks of hydrothermal origin. Science 18: 150-152.
- Bishoff, J. L. and Dickson, F. W. (1975). Seawater-basalt interaction at 200°C and 500 bars: implications for origin of sea floor heavy metal deposits and regulation of sea water chemistry. Earth Planet. Sci. Lett. 25: 385-397.
- Bjornsson, S., Arnorsson, S. and Tomasson, T. (1972). Economic evaluation of Reykjanes thermal brine area, Iceland. Am. Assoc. Pet. Geol. Bull. 56: 2380-2391.
- Blatt, H., Middleton, G. V. and Murray, R. C. (1980). Origin of sedimentary rocks, 2nd edition. Prentice Hall, Englewood Cliffs, N. J., 782 p.
- Bonatti, E. (1981). Metal deposits in the oceanic lithosphere. In Emiliani, C., ed., The Sea, vol. 7, The Oceanic Lithosphere: New-York, Wiley Interscience, p. 639-686.
- Bonatti, E., Guerstein-Honnorez, B. M. and Honnorez, J. (1976). Copper-iron sulfide mineralizations from the equatorial Mid-Atlantic Ridge. Econ. Geol. 71: 1515-1525.
- Bonatti, E. and Joensuu, O. (1966). Deep sea iron deposits from the South Pacific. Science 154: 643-645.
- Bonatti, E., Kraemer, T. and Rydell, H. S. (1972). Classification and genesis of submarine iron-manganese deposits. In Ferromanganese Deposits on the Ocean Floor. IDOE, Columbia University, New York, p. 149-166.
- Boogaard, M. Van den (1967). Geology of the Pomarao region (Southern Portugal). Univ. Amsterdam, Rotterdam Delko, 113 p.

- Bostrom, K. (1970). Submarine volcanism as a source for iron. *Earth Planet. Sci. Lett.* 9: 348-354.
- Bostrom, K. and Peterson, M.N.A. (1966). Precipitates from hydrothermal exhalations on the East Pacific Rise. *Econ. Geol.* 61: 1258-1265.
- Caltagirone, J.-P., Cloupeau, M. and Combarous, M. (1971). Convection naturelle fluctuante dans une couche poreuse horizontale. *C.R. Acad. Sc. Paris* 273: B833-B836.
- Campbell, I. H., Franklin, J. M., Gorton, M. P., Hart, T. R. and Scott, S. D. (1981). The role of subvolcanic sills in the generation of massive sulphide deposits. *Econ. Geol.* 76: 2248-2253.
- Carron, M. K., Mrose, M. E. and Reiser, A. N. (1964). New data on cymrite, a hydrated silicate of barium and aluminum (abs.). *Geol. Soc. Am. Spec. Pap.* 82: 26.
- Carvalho, D. (1974). Lineament patterns and hypogene mineralization in Portugal, - Problems of Ore Deposition. Fourth IAGOD Symp. V.II, p. 444-453, Varna.
- Carvalho, D. (1976). Consideracoes sobre o vulcanismo da regio de Cercal-Odemira. Suas relacoes com a Faixa Piritosa. *Commun. Serv. Geol. Port.* 60: 216-238, Lisboa.
- Carvalho, D. (1979). Geologia, metalogenia e metodologia da investigacao de sulfuretos polimetalicos do Sul de Portugal. *Commun. Serv. Geol. Port.* 65: 169-191.
- Carvalho, D. (1982). Pirites - Novos rumos para a prospeccao. *Geonovas* 1: 11-21.
- Carvalho, D., Correia, H.A.C. and Inverno, C.M.C. (1976a). Contribuicao para o conhecimento geologico do Grupo de Ferreira-Ficalho. Suas relacoes com a Faixa Piritosa e Grupo do Pulo do Lobo. *Mem. Not. Publ. Mus. Lab. Mineral. Geol. Univ. Coimbra* 82: 145-169.
- Carvalho, D., Conde, L., Enrile, J., Oliveira, V. and Schermerhorn, L.J.G. (1976b). Livro guia das excursoes geograficas na Faixa Piritosa Iberica. *Com. Serv. Geol. Portugal* 60: 271-315.
- Carvalho, D., Goinhas, J., Oliveira, V. and Ribeiro, A. (1971a). Observacoes sobre a geologia do sul de

Portugal e consequencias metalogeneticas. Est. Not. Trab. Serv. Fom. Min. 20(1-2): 153-199.

- Carvalho, D., Goinhas, J.A.C. and Schermerhorn, L.J.G. (1971b). Principais jazigos minerais do Sul de Portugal. I. Congresso Hispano-Luso-Americano de Geologia Economica (Livro Guia da Excursao no. 4). Serv. Geol. Portugal, Special Publ., 94 pp.
- Chilingar, G. V. (1963). Relationship between porosity, permeability, and grain-size distribution of sands and sandstones. Proc. Intern. Sedimentol. Congr., Amsterdam, Antwerp.
- Clayton, R. N. and Mayeda, T. K. (1963). The use of bromine pentafluoride in the extraction of Oxygen from oxides and silicates for isotopic analysis. Geochim. Cosmochim. Acta 27: 43-52.
- Clayton, R. N., O'Neil, J. R. and Mayeda, T. K. (1972). Oxygen isotope exchange between quartz and water. J. Geophys. Res. 77: 3057-3067.
- Cogne, J. (1976). La chaine Hercynienne Quest-Europeene correspond-elle a un orogene par collision? Propositions pour une interpretation geodynamique globale. Coll. Int. C.N.R.S. 268: 111-129.
- Combarrous, M. and Le Fur, B. (1969). Transfert de chaleur par convection naturelle dans une couche poreuse horizontale. C.R. Acad. Sc. Paris 269: B1009-B1012.
- Corliss, J. B., Lyle, M., Dymond, J. and Crane, K. (1978). The chemistry of hydrothermal mounds near the Galapagos Rift. Earth Planet. Sci. Lett. 40: 12-24.
- Corliss, J. B., Dymond, J., Gordon, L. I., Edmond, J. M., Von Herzen, R. P., Ballard, R. D., Green, K., Williams, D., Bainbridge, A., Crane, K. and Van Andel, T. H. (1979). Submarine thermal springs on the Galapagos Rift. Science 203: 1073-1083.
- Costa, U. R. (1980). Hydrothermal footwall alteration and ore formation at Mattagami Lake mine, Mattagami, Quebec. Ph.D. thesis, Univ. Western Ontario, 288 p.
- Costa, U. R., Barnett, R. L. and Kerrich, R. (1983). The Mattagami Lake mine Archean Zn-Cu massive sulphide: coprecipitation of talc and sulphides in a sea floor brine pool. Econ. Geol. (in press).

- Costa, U. R., Fyfe, W. S., Kerrich, K. and Nesbitt, H. W. (1980). Archean hydrothermal talc evidence for high ocean temperatures. *Chem. Geol.* 30: 341-349.
- Cox, K. G., Bell, J. D. and Pankurst, R. J. (1979). The interpretation of igneous rocks. George, Allen and Untwin, Boston, 450 p.
- Craig, H. (1966). Isotopic composition and origin of the Red Sea and Salton Sea geothermal brines. *Science* 154: 1544-1548.
- Crerar, D. A., Namson, J., So Chyi, M., Williams, L. and Feigenson, M. D. (1982). Manganiferous cherts of the Franciscan assemblage. I. General geology, ancient and modern analogues, and implications for hydrothermal convection at oceanic spreading centers. *Econ. Geol.* 77: 519-540.
- Davis, E. E. and Lister, C.R.B. (1977). Heat flow measured over the Juan de Fuca ridge: evidence for widespread hydrothermal circulation in a highly heat transportative crust. *J. Geophys. Res.* 82: 4845-4860.
- Deer, W. A., Howie, R. A. and Zussman, J. (1963). *Rock Forming Minerals*. John Wiley and Sons, Inc.
- Eby, G. N. (1972). Determination of rare earth, yttrium, and scandium abundances in rocks and minerals by an ion-exchange-X-ray fluorescence procedure. *Anal. Chem.* 44: 2137-2143.
- Edmond, J. M. and Von Damm, K. L. (1983). Ridge crest hydrothermal activity in the Eastern Pacific (Abs.). *Geodynamics Symposium on Oceanic Lithosphere*, Texas A&M Univ., April, College Station, Texas.
- Elder, J. (1965). Physical processes in geothermal areas. In Lee, W.H.K. (ed.), *Terrestrial heat flow*. Am. Geophys. Union, Washington, D.C. 211 p.
- Elder, J. (1967). Steady free convection in a porous medium heated from below. *J. Fluid Mech.* 27: 29-48.
- Ellis, A. J. (1968). Natural hydrothermal systems and experimental hot water/rock interaction: Reactions with NaCl solutions and trace metal extraction. *Geochim. Cosmochim. Acta* 32: 1356-1363.
- Ellis, A. J. (1979). Explored geothermal systems. In Barnes, H. L. (ed.), *Geochemistry of hydrothermal ore*

deposits, 2nd ed. Holt, Rinehart and Winston, p. 632-683.

Essene, E. J. (1967). An occurrence of cymrite in the Franciscan Formation, California. *Am. Min.* 52: 1885-1890.

Ethier, V. G., Campbell, F. A., Both, R. A., Krouse, H. R. (1976). Geological setting of the Sullivan orebody and estimates of temperatures and pressure of metamorphism. *Econ. Geol.* 71: 1570-1588.

Farrand, M. (1970). Framboidal sulfides precipitated synthetically. *Miner. Deposita* 5: 237-247.

Ferry, J. M. (1978). Reaction mechanisms, physical conditions, and mass transfer during hydrothermal alteration of mica and feldspar in granitic rocks from South-Central Maine, U.S.A. *Contrib. Mineral. Petrol.* 68: 125-140.

Fiske, R. S. and Matsuda, T. (1964). Submarine equivalents to ash flows in the Tokiwa Formation, Japan. *Am. J. Sci.* 262: 76-106.

Francheteau, J., Needham, H. D., Choukroune, P., Juteau, T., Seguret, M., Ballard, R. D., Fox, P. J., Normark, W., Carranza, A., Cordoba, D., Guerrero, J., Rangin, C., Bougault, H., Cambon, P. and Hekinian, R. (1979). Massive deep sea sulphide ore deposits discovered on the East Pacific Rise. *Nature* 277: 523-528.

Franklin, J. M., Lydon, J. W. and Sangster, D. F. (1981). Volcanic-associated massive sulphide deposits. *Econ. Geol.*, 75th Ann. Vol.: 485-627.

Freeze, R. A. and Cherry, J. A. (1979). *Groundwater*. Prentice Hall, Englewood Cliffs, N.J., 604 p.

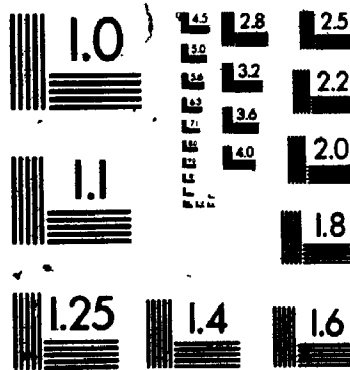
Froelich, F. and Sandrea, A. (1973). Presence de cymrite dans les mineralizations devoniennes stratiformes a blende-galene-barytine d'Arrens (Hautes-Pyrenees). *C.R. Acad. Sci. Paris* 277: D2445-D2448.

Freire d'Andrade, R. and Schermerhorn, L.J.G. (1971). Aljustrel e Góvilao. In Carvalho, D. and Goinhas, J.A.C. (eds.), *Principais jazigos minerais do Sul de Portugal*. Livro-Guia exc. 4, I Congr. Hispano-Luso Americano Geol. Econ.: 32-59. Madrid-Lisboa.

- Fryer, B. (1977). Rare earth evidence in iron formations for changing Precambrian oxidation states. *Geochim. Cosmochim. Acta* 41: 361-367.
- Fyfe, W. S. (1973). The generation of batholiths. *Tectonophysics* 17: 273-283.
- Fyfe, W. S. (1974). *Geochemistry*. Clarendon Press, Oxford, 107 p.
- Fyfe, W. S. and Henley, R. W. (1973). Some thoughts on the chemical transport processes, with particular reference to gold. *Miner. Sci. Engng.* 5: 295-303.
- Fyfe, W. S. and Kerrich, R. (1976). Geochemical prospecting: extensive versus intensive factors. *J. Geoch. exploration* 6: 177-192.
- Fyfe, W. S. and Lonsdale, P. (1981). Ocean floor hydrothermal activity. In Emiliani, C. (ed.), *The Sea*, vol. 7, *The Oceanic Lithosphere*. New York, Wiley-Interscience, p. 589-638.
- Fyfe, W. S., Price, N. J. and Thompson, A. B. (1978). *Fluids in the Earth's Crust*. Elsevier, Amsterdam, 383 p.
- Garrels, R. M. and Christ, C. L. (1965). *Minerals, solutions, and equilibria*. Harper & Row Publ., New York, 541 p.
- Gaspár, O. and Conde, L. (1978). A caracterizacão dos sulfuretos de Aljustrel com vista ao seu aproveitamento integral. *Congr. O. Eng. Portugal* 3(12), 17 p., Porto.
- García Palomero, F. (1977). Caracteres geológicos y relaciones morfológicas y genéticas de las mineralizaciones del anticlinal de Rio Tinto. *Acta Salmanticensis, Tesis de Ciencia*.
- Gresens, R. L. (1967). Composition-volume relationships of metasomatism. *Chem. Geol.* 2: 47-65.
- Guichard, F., Church, J. M., Treuil, M. and Jaffrézic, H. (1979). Rare earths in barites: distribution and effects on aqueous partitioning. *Geochim. Cosmochim. Acta* 43: 983-998.
- Hajash, A. Jr. (1975). Hydrothermal processes along mid-ocean ridges: an experimental investigation. *Contrib. Mineral. Petrol.* 53: 205-226.

55

OF / DE



- Hajash, A. and Archer, P. (1980). Experimental sea water/basalt interactions: the effect of cooling. *Contrib. Mineral. Petrol.* 75: 1-13.
- Hamet, J. and Delcey, R. (1972). Age, synchronisme et affiliation des roches rhyolitiques de la province pyrítico-cuprifere du Baixo-Alentejo (Portugal): mesures isotopiques par la methode $87\text{Rb}/87\text{Sr}$. *C.R. Acad. Sci. Paris*, 272, Ser. D., 2143-2146.
- Haskin, L. A. and Haskin, M. A. (1968). Rare earth elements in the Skaergaard intrusion. *Geochim. Cosmochim. Acta* 32: 433-447.
- Haskin, L. A., Haskin, M. A., Frey, F. A. and Wildeman, T. R. (1968). Relative and absolute abundances of the rare earths. In Ahrens, L. H. (ed.), *Origin and distribution of the elements*, 889-912, Pergamon Press.
- Hattori, K. and Muehlenbachs, K. (1980). Marine Hydrothermal alteration at a Kuroko ore deposit, Kosaka, Japan. *Contrib. Mineral. Petrol.* 74: 285-292.
- Hattori, K. and Sakai, H. (1979). D/H ratios, origins and evolution of the ore-forming fluids for the Neogene veins and Kuroko deposits of Japan. *Econ. Geol.* 74: 535-555.
- Hattori, K. and Sakai, H. (1980). Implications of D/H and $18\text{O}/16\text{O}$ ratios of ore fluids for Neogene vein-type and Kuroko mineralization of Japan. In Ridge, J. D. (ed.), *IAGOD Symposium, 5th Proc.: Stuttgart, E. Schweizerbart'sche Verlagsbuchhandlung*, p. 325-336.
- Haymond, R. M. and Kastner, M. (1981). Hot spring deposits of the East Pacific Rise at 21°N : preliminary descriptions of mineralogy and genesis. *Earth Planet. Sci. Lett.* 53: 363-381.
- Heaton, T.H.E. and Sheppard, S.M.F. (1977). Hydrogen and Oxygen isotope evidence for sea water-hydrothermal alteration and ore deposition, Troodos, Cyprus. In *Volcanic Processes and Ore genesis*, London: Inst. Min. Metall. and Geol. Soc., p. 42-57.
- Helgeson, H. C. (1970). A chemical and thermodynamic model of ore deposition in hydrothermal systems. *Min. Soc. Am. Spec. Paper* 3: 155-186.
- Hellman, P. L. and Henderson, P. (1977). Are rare earths mobile during spilitization? *Nature* 267: 38-40.

- Henley, R. W. (1973). Some fluid dynamics and ore genesis. Trans. Inst. Min. Metall. 82: B1.
- Herzberg, C. T., Fyfe, W. S. and Carr, M. J. (1983). Density constraints on the formation of the continental Moho and crust. In press.
- Hildreth, W. (1979). The Bishop Tuff: evidence for the origin of compositional zonation in silicic magma chambers. In Chapin, C. E. and Elston, W. E. (eds.), Ash-flow tuffs. Geol. Soc. Am. Spec. Paper 180: 43-75.
- Hildreth, W. (1981). Gradients in silicic magma chambers: implications for lithospheric magmatism. J. Geophys. Res. 86: B10153-B10192.
- Hoefs, J. (1980). Stable Isotope Geochemistry. Springer-Verlag, Berlin-Heidelberg, 208 p.
- Hogdahl, O. T., Melson, S. and Bowen, V. T. (1968). Neutron activation analysis of lanthanide elements in sea water. Am. Chem. Soc. Advances in Chemistry Series 73: 308-325.
- Humphris, S. E. and Thompson, G. (1978a). Hydrothermal alteration of oceanic basalts by seawater. Geochim. Cosmochim. Acta 42: 107-125.
- Humphris, S. E. and Thompson, G. (1978b). Trace element mobility during hydrothermal alteration of oceanic basalts. Geochim. Cosmochim. Acta 42: 127-136.
- Hutchinson, R. W. (1973). Volcanogenic sulphide deposits and their metallogenic significance. Econ. Geol. 68: 1223-1246.
- Hutchinson, R. W., Fyfe, W. S. and Kerrich, R. (1980). Deep fluid penetration and ore deposition. Minerals Sci. Engng. 12: 107-120.
- Hutchinson, R. W. and Searle, D. L. (1971). Stratabound pyrite deposits in Cyprus and relations to other sulphide ores. Soc. Mining Geologists Japan, Spec. Issue 3: 198-205.
- Iijima, A. (1972). Argillaceous and zeolitic alteration zones surrounding Kuroko (Black Ore) deposits in Odate district of Akita Prefecture. Mining Geology 22: 1-20. (in Japanese)

- Iijima, A. (1974). Clay and zeolitic alteration zones surrounding Kuroko deposits in the Hokuroku district, Northern Akita, as submarine hydrothermal-diagenetic alteration products. Soc. Mining Geologists of Japan, Spec. Issue 6: 267-290.
- Jahn, B.-M., Auvray, B., Blais, S., Capdevilla, R., Cornichet, J., Vidal, F. and Hameurt, J. (1980). Trace element geochemistry and petrogenesis of Finnish Greenstone Belts. J. Petrol. 21: 201-244.
- Jambor, J. L. (1979). Mineralogical evaluation of proximal-distal features in New Brunswick massive sulfide deposits. Canadian Mineralogist, v. 17: 649-664.
- Jones, B. J. and Segnit, E. R. (1971). The nature of opal. I. Nomenclature and constituent phases. J. Geol. Soc. Aust. 18: 57-68.
- Kastner, M. (1981). Authigenic silicates in deep-sea sediments: formation and diagenesis. In Emiliani, C. (ed.), The Sea, vol. 7, The Oceanic Lithosphere, New York, Wiley Interscience, p. 915-980.
- Keays, R. R. and Scott, R. B. (1976). Precious metals in ocean-ridge basalts: Implications for basalts as source rocks for gold mineralization. Econ. Geol., 71: 705-720.
- Klockmann, F. (1894). Ueber die lagartige Natur der Kiesvorkommen des sudlichen Spareiens und Portugals. Sber. preuss. Akad. Wiss. 46: 1173-1181.
- Knauth, L. P. and Lowe, D. R. (1978). Oxygen Isotope geochemistry of cherts from the Onverwacht Group (3.4 billion years), Transvaal, South Africa, with implications for secular variations in the isotopic composition of cherts. Earth Planet. Sci. Lett. 41: 209-222.
- Krauskopf, B. K. (1957). Separation of Manganese from Iron in sedimentary processes. Geochim. Cosmochim. Acta 12: 61-84.
- Krauskopf, B. K. (1967). Introduction to geochemistry. McGraw-Hill, New York.
- Lambert, I. B. and Sato, T. (1974). The Kuroko and associated ore deposits of Japan: a review of their features and metallogenesis. Econ. Geol. 69: 1215-1236.

- Lapwood, E. R. (1948). Convection of a fluid in a porous medium. Proc. Cambridge Phil. Soc. 44: 508-521.
- Large, D. (1979). Proximal and distal stratabound ore deposits. A discussion of the paper by I. R. Plimer, Mineralium Deposita 13: 345-353 (1978). Mineral. Deposita 14: 123-124.
- Large, R. R. (1977). Chemical evolution and zonation of massive sulfide deposits in volcanic terrains. Econ. Geol. 72: 549-572.
- Lawrence, J. R. and Glekes, J. M. (1981). Constraints on water transport and alteration in the oceanic crust from the isotopic composition of pore water. J. Geophys. Res. 86: 7924-7933.
- Lecolle, M. (1974). Presence de tufs soudés dans le volcanisme de Huelva (Espagne). C.R. Acad. Sci. Paris 287: 839-842.
- Lecolle, M. (1977). La ceinture sud-iberique: un exemple de province a amas sulfures volcano-sedimentaires (tectonique, metamorphisme, stratigraphie, volcanisme, paleogeographie et metallogenie). Thesis, Univ. Pierre et Marie Curie, Paris, 609 p.
- Liou, J. G. (1973). Synthesis and stability relations of epidote, $\text{Ca}_2\text{Al}_2\text{FeSi}_3\text{O}_{12}(\text{OH})$. J. Petrology 14: 381-413.
- Lister, C.R.B. (1972). On the thermal balance of a mid-ocean ridge. Geophys. J. R. Astr. Soc. 26: 515-535.
- Lister, C.R.B. (1977). Qualitative models of spreading-center processes, including hydrothermal penetration. In Uyeda, S. (ed.), Subduction zones, mid-ocean ridges, oceanic trenches and geodynamics. Tectonophysics 37: 203-218.
- Lister, C.R.B. (1981b). Rock and water histories during sub-oceanic hydrothermal events. Oceanologica Acta, Proc. 26th Int. Geol. Congress, Paris, p. 41-46.
- Lonsdale, P. (1977). Deep tow observations at the mounds abyssal hydrothermal field, Galapagos Rift. Earth Planet. Sci. Lett. 36: 92-110.
- Lotze, F. (1945). Zur gliederung der Varisziden der Iberischru Meseta. Geotekt. Forsch. 6: 78-92.

- Love, L. G. and Amstutz, G. C. (1966). Review of microscopic pyrite. *Fortschr. Mineral.* 43: 273-309.
- Lovering, T. S. (1961). Sulfide ores formed from sulfide-deficient solutions. *Econ. Geol.* 56: 68-99.
- Ludden, J. N. and Thompson, G. (1977). Behaviour of rare earth elements during submarine weathering of submarine basalt. *Nature* 274: 147-149.
- Lydon, J. W. (1981). An addendum. *Geosci. Can.* 8: 101-103.
- MacGeehan, P. J. and MacLean, W. H. (1980). Tholeiitic basalt-rhyolite magmatism and massive sulphide deposits at Matagami, Quebec. *Nature* 283: 153-157.
- Mahood, G. and Hildreth, W. (1983). Large partition coefficients for trace elements in high silica rhyolites. *Geochim. Cosmochim. Acta* 47: 11-30.
- McCulloch, M. T., Gregory, R. T., Wasserburg, C. J. and Taylor, Jr. H. P. (1980). A Neodymium, Strontium and Oxygen isotopic study of the Cretaceous Samail ophiolite and implications for the petrogenesis and seawater hydrothermal alteration of oceanic crust. *Earth Planet. Sci. Lett.* 46: 201-211.
- Meagher, E. P. (1980). Silicate Garnets. In P. H. Ribbe (ed.), *Orthosilicates*. *Min. Soc. Am. Rev. Min.* 5: 25-66.
- Madel, J. and Lopera, E. (1976). Geologia de la zona minera de tharsis. Livro guia das excursões geológicas na Faixa Piritosa Iberica. *Com. Serv. Geol. Portugal.* 60: 288-295.
- Montès, F. L. and Silva, J.M.L. (1979). O programa de aproveitamento integrado das pirites. *SINACT*, Lisbon, 35 p.
- Moody, J. B. (1979). Serpentinites, spilites and ophiolite metamorphism. *Can. Min.* 17: 871-887.
- Mottl, M. J. (1976). Chemical exchange between seawater and basalt during hydrothermal alteration of the oceanic crust. Ph.D. thesis, Harvard Univ., 188 p.
- Mottl, M. J. and Holland, H. D. (1978). Chemical exchange during hydrothermal alteration of basalt by seawater. I. Experimental results for major and minor components of seawater. *Geochim. Cosmochim. Acta* 42: 1103-1115.

- Mottl, M. J., Holland, H. D. and Corr, R. F. (1979). Chemical exchange during hydrothermal alteration of basalts by seawater. II. Experimental results for Fe, Mn, and sulfur species. *Geochim. Cosmochim. Acta* 43: 869-884.
- Mottl, M. J. and Seyfried, W. E. (1980). Sub-seafloor hydrothermal systems rock-vs. seawater-dominated. In Rona, P. A. and Lowell, R. P. (eds.), *Seafloor Spreading Centers: Hydrothermal Systems*. Dowden, Hutchinson and Ross, Stroudsburg, p. 66-82.
- Mueller, S. T., Prodehl, C. L., Mendes, A. and Sousa Moreira, V. (1973). Crustal structure in the southwestern part of the Iberian Peninsula. *Tectonophysics* 20: 307-318.
- Munha, J. (1976). Nota preliminar sobre o metamorfismo na Faixa Piritosa Portuguesa. *Com. Serv. Geol. Portugal*. 60: 151-161.
- Munha, J. (1979). Blue amphiboles, metamorphic regime and plate tectonic modelling in the Iberian Pyrite Belt. *Contrib. Mineral. Petrol.* 69: 279-289.
- Munha, J. (1981). Igneous and metamorphic petrology of the Iberian Pyrite Belt volcanic rocks. Ph.D. thesis, Univ. Western Ontario, 711 p.
- Munha, J. (1983). Low grade regional metamorphism in the Iberian Pyrite Belt. *Commun. Serv. Geol. Port.* (in press).
- Munha, J., Fyfe, W. S. and Kerrich, R. (1980). Adularia, the characteristic mineral of felsic spilites. *Contrib. Mineral. Petrol.* 75: 15-19.
- Munha, J. and Kerrich, R. (1980). Sea Water Basalt interaction in spilites from the Iberian Pyrite Belt. *Contrib. Mineral. Petrol.* 73: 191-200.
- Munha, J. and Kerrich, R. (1981). High temperature (>400°C) equilibrium of marine water with ocean floor: evidence from ¹⁸O enriched fluids of the Iberian Pyrite Belt. *Am. Geophys. Union Fall Meet.* 1981.
- Nance, W. B. and Taylor, S. R. (1977). Rare earth element patterns and crustal evolution. II. Archean sedimentary rocks from Kalgoorlie, Australia. *Geochim. Cosmochim. Acta* 41: 225-231.

- Nesbitt, H. W. (1979). Mobility and fractionation of rare earth elements during weathering of a granodiorite. *Nature* 279: 206-210.
- Normark, W. R., Morton, J. L., Koshi, R. A., Clague, D. A. and Delaney, J. R. (1983). Active hydrothermal vents and sulphide deposits on the southern Juan de Fuca Ridge. *Geology* 11: 158-163.
- Norrish, K. and Hutton, J. T. (1969). An accurate X-ray spectrographic method for the analysis of a wide range of geological samples. *Geochim. Cosmochim. Acta* 33: 431-451.
- Ofstedal, C. (1958). A theory of exhalative-sedimentary ores. *Geol. Foren. Stockholm Forth.* 80: 1-19.
- Ohmoto, H. and Rye, O. R. (1974). Hydrogen and Oxygen isotope composition of fluid inclusions in the Kuroko deposits, Japan. *Econ. Geol.* 69: 947-953.
- Oliveira, J. T. (in press). The Devonian-Carboniferous stratigraphy and geodynamics of Southern Portugal: some comments. *Neues Jahrb. Geol. Palaeont. Abh.*
- Oliveira, J. T., Horn, M. and Paproth, E. (1979). Preliminary note on the stratigraphy of the Baixo Alentejo Flysch Group, Carboniferous of Southern Portugal, and on the paleogeographic development, compared to corresponding units in Northwest Germany. *Commun. Serv. Geol. Port.* 65: 151-168.
- Oliveira, V.M.J. (1971). Breve nota sobre a alteracao meteorica do grande filao doleritico do Alentejo e paleogeografia das formacoes encaixantes. I *Chillage, Seccao* 4(2): 781-786.
- O'Neil, J. R. and Taylor, H. P. (1967). The oxygen isotope and cation exchange chemistry of feldspars. *Am. Mineral.* 52: 1414-1437.
- Ostwald, J. and England, B. M. (1977). Notes on framboidal pyrite from Allandale New South Wales, Australia. *Mineral Deposita* 12: 111-116.
- Ostwald, J. and England, B. M. (1979). The relationship between euhedral and framboidal pyrite in base-metal sulphide ores. *Min. Mag.* 43: 297-300.
- Pearce, J. A. and Norry, M. J. (1979). Petrogenetic implications of Ti, Zr, Y and Nb variations in volcanic rocks. *Contrib. Mineral. Petrol.* 69: 33-48.

- Pfefferkorn, H. W. (1968). Geologie des gebietes zwischen Serpa und Mertola (Baixo Alentejo, Portugal).
Münst. Forsch. Geol. Palont., p. 9-143.
- Piper, D. Z. (1974). Rare earth elements in ferromanganese nodules and other marine phases. *Geochim. Cosmochim. Acta* 38: 1007-1022.
- Pisutha-Arnond, V. and Ohmoto, H. (1980). Chemical and isotopic compositions of the Kuroko ore-forming fluids. *Geol. Soc. Am. Abs. W. Pgs.* 61: 500.
- Plimer, I. R. and Carvalho, D. (1982). The geochemistry of hydrothermal alteration at the Salgado copper deposit, Portugal. *Mineral. Deposita* 17: 193-211.
- Príem, H.N.A., Boelrijk, N.A.I.M., Hebeda, E. H., Schermerhorn, L.J.G., Erdurmen, E.A.T. and Verschure, R. H. (1978). Sr isotopic homogenization through whole rock systems under low-greenschist facies metamorphism in Carboniferous pyroclastics at Aljustrel (South Portugal). *Chem. Geol.* 21: 307-314.
- Prodehl, C. L., Sousa Moreira, V., Müller, S. T. and Mendes, A. (1975). Deep seismic sounding experiments in central and southern Portugal. XIVth General Assembly of the European Seismol. Comm., p. 261-266, DDR Nat-Komitee Geodasie und Geophysik, Berlin.
- Rambaud Perez, F. (1969). El sinclinal Carbonifero de Rio Tinto y sus mineralizaciones asociadas. *Mem. Inst. Geol. Miner. Espana* 71: 229.
- Rast, N. and Grant, R. (1973). Transatlantic correlation of the Variscan-Appalachian Orogeny. *Am. J. Sci.* 273: 572-579.
- Ribando, R. J., Torrance, K. E. and Turcotte, D. L. (1976). Numerical models for hydrothermal circulation in the oceanic crust. *J. Geophys. Res.* 81: 3007-3012.
- Ribeiro, A. (1981). A geotraverse through the Variscan Fold Belt in Portugal. *Geol. en. Mijbouw* 60: 41-44.
- Ribeiro, A. (in press). Noticia explicativa da carta geologica 1/50,000 - Bordeira. *Serv. Geol. Port., Lisbon.*
- Ribeiro, A., Antunes, M. T., Ferreira, M. P., Rocha, R. B., Soares, A. F., Zbyszewski, G., Moifinho de Almeida, F., Carvalho, D. and Monteiro, J. H. (1979). Introduction a la Geologie generale du Portugal. *Serv. Geol. Portugal. Special publication*, 114 p.

- Ribeiro, A., Oliveira, J. T. and Silva, J. B. (1982). La estructura de la zona Surportuguesa. Libro de homenaje a J.M. Rios. Inst. Geol. Min. Espana (in press).
- Ribeiro, A., Ribeiro, L. and Iglesias, M. (1983). Collision tectonics in the Iberian segment of the Variscan Fold Belt (abs.). Quarterly J. Geol. Soc. L., spec. iss. William Smith meet. Collis. Tectonics (in press).
- Rickard, D. T. (1970). The origin of framboids. Lithos 3: 269-293.
- Rickwood, P. C. (1968). On recasting analyses of garnet into end-member molecules. Contrib. Mineral. Petrol. 18: 175-198.
- Ripley, E. M. and Ohmoto, H. (1979). Oxygen and Hydrogen isotopic studies of ore deposition and metamorphism at the Raul Mine, Peru. Geochim. Cosmochim. Acta 43: 1633-1643.
- RISE Project Group (1980). East Pacific Rise: hot springs and geophysical experiments. Science 207: 1421-1433.
- Riverin, G. and Hodgson, C. J. (1980). Wall rock alteration at the Millenbach Cu-Zn mine, Noranda, Quebec. Econ. Geol. 75: 424-444.
- Roberts, R. G. and Reardon, E. J. (1978). Alteration and ore-forming processes at Mattagami Lake mine, Quebec. Canadian Jour. Earth Sci. 15: 1-21.
- Robertson, A.H.F. (1977). The origin and diagenesis of cherts from Cyprus. Sedimentology 24: 11-30.
- Rockingham, C. J. and Hutchinson, R. W. (1980). Metamorphic textures in Archean copper-zinc massive sulphide deposits. CIM Bulletin, April, 1980, pp. 104-112.
- Roedder, E. (1968). The noncolloidal origin of "colloform" textures in sphalerite ores. Econ. Geol. 63: 451-471.
- Ross, C. S. and Smith, R. L. (1961). Ash-flow tuffs: their origin, geologic relations and identification. U.S. Geol. Surv. Prof. Paper 366, 81 p.
- Routhier, P., Aye, F., Boyer, C., Lecolle, M., Moliere, P., Picot, P. and Roger, G. (1980). La Ceinture Sud-

Iberique a amas sulfures dans sa partie espagnole mediane. Mem. B.R.G.M. 94, 265 p.

- Runnels, D. D. (1964). Cymrite in a copper deposit, Brooks Range, Alaska. Am. Min. 49: 158-165.
- Salpeteur, I. (1976). Etude structural et petrographique de la zona de Paymogo (Nord de la Province d'Huelva). Metallogenese des amas sulfures associes. These Universite de Nancy I. 234 p.
- Sakai, H. and Matsubaia, O. (1974). Isotopic geochemistry of the thermal waters of Japan and its bearing on the Kuroko ore solutions. Econ. Geol. 69: 974-991.
- Sato, T. (1972). Behaviours of ore-forming solutions in seawater. Mining Geol. 22: 31-42.
- Schermerhorn, L.J.G. (1970a). Mafic geosynclinal volcanism in the lower Carboniferous of South Portugal. Geol. Mijnb. 46(9): 439-450.
- Schermerhorn, L.J.G. (1970b). The deposition of volcanics and pyritite in the Iberian Pyrite Belt? Mineral. Deposita. 5: 273-279.
- Schermerhorn, L.J.G. (1971a). An outline stratigraphy of the Iberian Pyrite Belt. Bol. Geol. Minero. LXXX-III-IV: 239-268.
- Schermerhorn, L.J.G. (1971b). Pyrite emplacement by gravity flow. Bol. Geol. Minero. 82(III-IV): 304-308.
- Schermerhorn, L.J.G. (1973). What is keratophyre? Lithos. 6: 1-11.
- Schermerhorn, L.J.G. (1975). Spilites, regional metamorphism and subduction in the Iberian Pyrite Belt: some comments. Geol. Mijnb. 54(1): 23-35.
- Schermerhorn, L.J.G. (1976). The Aljustrel volcanics: Megacryst tuff and green tuff (Aljustrel and Gavião pyrite deposits, South Portugal). Mem. Not. Publ. Mus. Lab. Minerol. Geol. Univ. Coimbra 82: 41-60.
- Schermerhorn, L.J.G. (1978). Epigenetic magnesium metasomatism or syngenetic chloritite metamorphism at Falun and Orifervi. Trans. Inst. Mineral. Metall. 87: B161-B167.

- Schermerhorn, L.J.G. and Stanton, W. I. (1969). Folded overthrusts at Aljustrel (South Portugal). *Geol. Mag.* 106: 130-141.
- Seyfried, W. E. and Bischoff, J. L. (1977). Hydrothermal transport of heavy metals by seawater: the role of seawater/basalt ratio. *Earth Planet. Sci. Lett.* 34: 71-77.
- Shirozu, H. (1974). Clay minerals in altered wall rocks of the Kuroko-type deposits. *Soc. Mining Geologists Japan, Spec. Issue 6*: 303-311.
- Sigvaldson, G. E. (1959). Mineralogische untersuchungen über gesteinszersetzung durch postvulkanische aktivität in island. *Beitr. Mineralogie Petrologie* 6: 405-427.
- Smith, I.E.M. and Johnson, R. W. (1981). Contrasting rhyolite suites in the late Cenozoic of Papua New Guinea. *J. Geophys. Res.* 86: B10257-B10272.
- Smith, J. V. (1974). Feldspar minerals, vol. 2. Springer-Verlag, Berlin, 690 p.
- Smith, W. C., Barnister, F. A. and Hey, M. H. (1949). Cymrite, a new barium mineral from the Benallt manganese mine, Rhiw, Carnarvonshire. *Min. Mag.* 28: 676-681.
- Soler, E. (1969). L'association spilites-keratophyres de la province de Huelva (Espagne). Thesis, Univ. Paris, 105 p.
- Solomon, M. (1976). "Volcanic" massive sulphide deposits and their host rocks - a review and an explanation. In Wolf, K. A. (ed.), *Handbook of stratabound and stratiform ore deposits, II, Regional studies and specific deposits*. Amsterdam, Elsevier, p. 21-50.
- Solomon, M. and Walshe, J. L. (1979). The formation of massive sulfide deposits on the sea floors. *Econ. Geol.* 74: 797-813.
- Soong, R. and Olivecrona, J. A. (1975). An occurrence of cymrite in black shale, north-west Nelson, South Island, New Zealand. *Min. Mag.* 40: 311-312.
- Sparks, R.S.J., Sigurdsson, H. and Carey, S. N. (1980). The entrance of pyroclastic flows into the sea. I. Oceanographic and geologic evidence from Dominica, lesser Antilles. *J. Volc. Geoth. Res.* 7: 87-96.

- Sparks, R.S.J., Sigurdsson, H. and Carey, S. N. (1980). The entrance of pyroclastic flows into the sea. II. Theoretical considerations on subaqueous emplacement and welding. *J. Volc. Geoth. Res.* 7: 97-105.
- Spooner, E.T.C. (1977). Hydrodynamic model for the origin of the ophiolitic cupriferous pyrite ore deposits of Cyprus. In *Volcanic processes in ore genesis*. London, Inst. Mining Metall. and Geol. Soc., p. 58-71.
- Spooner, E.T.C., Beckinsale, R. D., England, P. C., and Senior, A. (1977a). Hydration, ^{18}O enrichment and oxidation during ocean floor hydrothermal metamorphism of ophiolitic metabasic rocks from E. Liguria, Italy. *Geochim. Cosmochim. Acta* 41: 857-871.
- Spooner, E.T.C., Beckinsale, R. D., Fyfe, W. S. and Smewing, J. D. (1974). ^{18}O enriched ophiolitic metabasic rocks from E. Liguria (Italy), Pindos (Greece), and Troodos (Cyprus). *Contrib. Mineral. Petrol.* 47: 41-62.
- Spooner, E.T.C., Chapman, H. J. and Smewing, J. D. (1977b). Strontium isotopic contamination and oxidation during ocean floor hydrothermal metamorphism of the ophiolitic rocks of the Troodos Massif, Cyprus. *Geochim. Cosmochim. Acta* 41: 873-890.
- Spooner, E.T.C. and Fyfe, W. S. (1973). Sub-sea-floor metamorphism, heat and mass transfer. *Contrib. Mineral. Petrol.* 42: 287-304.
- Straus, J. M. (1974). Large amplitude convection in porous media. *J. Fluid Mech.* 64: 51-63.
- Strauss, G. K. (1965). Zur Geologie der SW-iberischen kiesprovinz und ihrer lager-statten, mit besonderer Berucksichtigung der Pyritgrube Lousal, Portugal. Thesis, Univ. Munich, 152 p.
- Strauss, G. K. and Madel, J. (1974). Geology of massive sulphide deposits in the Spanish-Portuguese Pyrite Belt. *Geol. Bunds.* 63(1): 191-211.
- Strauss, G. K., Madel, J. and Alonso, F. F. (1977). Exploration practice for strata-bound volcanogenic sulphide deposits in the Spanish-Portuguese Pyrite Belt. In D. B. Klemm and H. Y. Schneider (eds.), *Time-and-Strata-Bound Ore Deposits*. Springer, 56-91.

- Sweeney, R. E. and Kaplan, I. R. (1973). Pyrite framboid formation: laboratory synthesis and marine sediments. *Econ. Geol.* 68: 618-634.
- Taylor, Jr. H. P. (1974). The application of Oxygen and Hydrogen isotope studies to problems of hydrothermal alteration and ore deposition. *Econ. Geol.* 69: 843-883.
- Taylor, Jr. H. P. (1978). Oxygen and Hydrogen isotope studies of plutonic granitic rocks. *Earth Planet. Sci. Lett.* 38: 177-210.
- Thurston, D. (1973). Studies on bedded cherts. *Contrib. Mineral. Petrol.* 36: 329-334.
- Toth, J. R. (1980). Deposition of submarine crusts rich in manganese and iron. *Geol. Soc. Am. Bull.* 91(1): 44-54.
- Turner, J. S. and Gustafson, L. B. (1978). The flow of hot saline solutions from vents in the sea floor - some implications for exhalative massive sulfide and other deposits. *Econ. Geol.* 73: 1082-1100.
- Walker, R. R., Matulich, A., Amos, A. C., Watkins, J. J. and Mannard, G. W. (1975). The geology of the Kidd Creek mine. *Econ. Geol.* 70: 80-89.
- Webb, J. S. (1958). Observations on the geology and origin of the San Domingos pyrite deposits. *Comun. Serv. Geol. Port.* 62: 129-143.
- Wedepohl, K. H. (Ed., 1978). *Handbook of Geochemistry*. Springer Verlag, Berlin.
- Weiser, H. B. (1949). *A textbook of colloid chemistry*. John Wiley & Sons, New York, 2nd ed., 444 p.
- Wenner, D. B. and Taylor, Jr. H. P. (1971). Temperatures of serpentinization of ultramafic rocks based on $^{18}O/^{16}O$ fractionation between co-existing serpentine and magnetite. *Contrib. Mineral. Petrol.* 32: 165-185.
- White, D. W., Anderson, E. T. and Grubbs, D. K. (1963). Geothermal brine well: mile deep hole may tap ore-bearing magmatic water and rocks undergoing metamorphism. *Science* 139: 919.
- Whitehead, R. D. (1973). Environment of stratiform sulphide deposition; variation in Mn:Fe ratio in host

rocks at Heath Steele mine, New Brunswick, Canada.
Mineral. Deposita 8: 148-160.

- Williams, H. and McBirney, A. R. (1979). Volcanology.
Freeman, Cooper & Co., San Francisco, 397 p.
- Wilson, A. D. (1955). A new method for the determination
of ferrous iron in rocks and minerals. Bull. Geol.
Surv. Gt. Britain 9: 56-58.
- Wright, I. L. (1968). X-ray and optical study of alkali
feldspar: an X-ray method for determining the
composition and structural state from measurement of
28 values for three reflections. Am. Min. 53:
88-104.
- Wright, I. L. and Stewart, D. B. (1968). X-ray and optical
study of alkali-feldspar. I. Determination of
composition and structural state from refined unit
cell parameters and 2V. Am. Min. 53: 38-87.
- Yamada, E. (1973). Subaqueous pumice flow deposits in the
Onikobe caldera, Miyagi Prefecture, Japan. J. Geol.
Soc. Japan 79: 585-597.

END

20103184

FIN